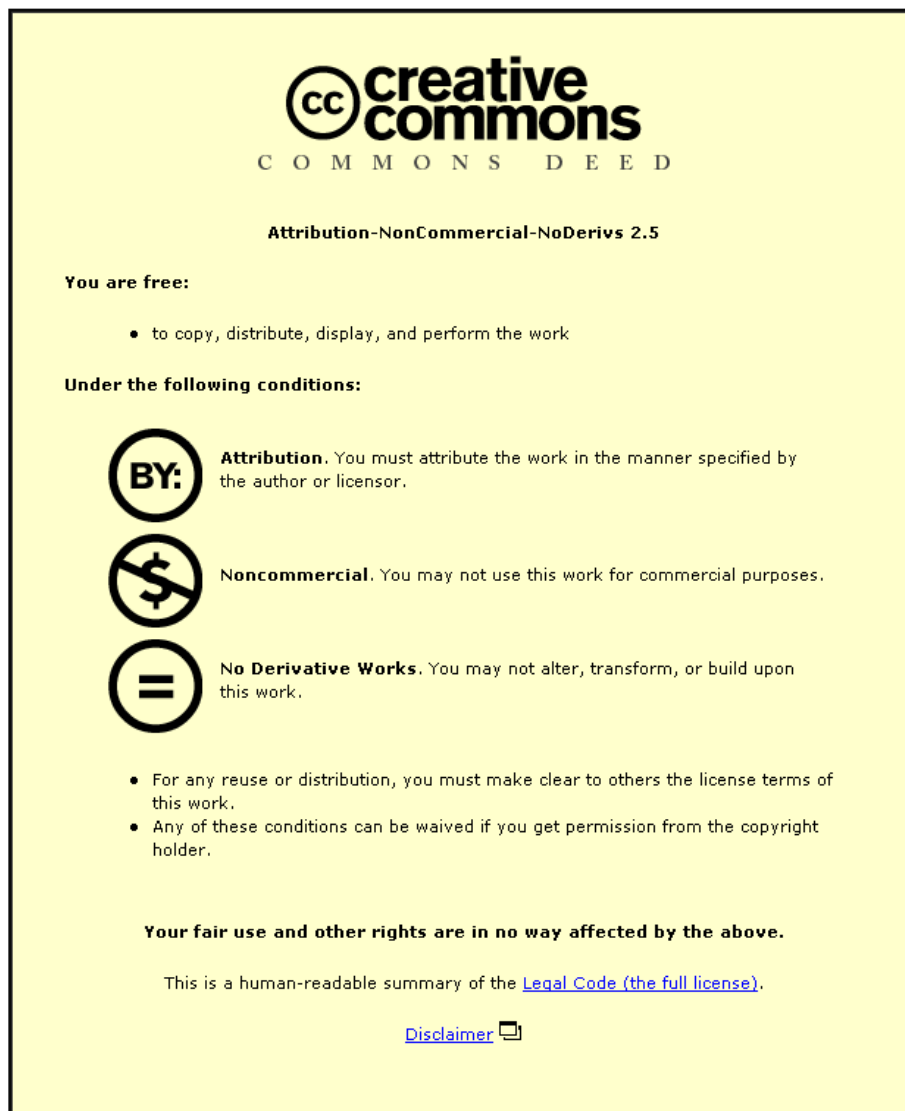


This item was submitted to Loughborough University as a PhD thesis by the author and is made available in the Institutional Repository (<https://dspace.lboro.ac.uk/>) under the following Creative Commons Licence conditions.



For the full text of this licence, please go to:
<http://creativecommons.org/licenses/by-nc-nd/2.5/>

**LOUGHBOROUGH
UNIVERSITY OF TECHNOLOGY
LIBRARY**

AUTHOR/FILING TITLE		
MEHTA, PS		
ACCESSION/COPY NO.		
152257/02		
VOL. NO.	CLASS MARK	
<p>25 NOV 83</p> <p>6 JUL 1984</p> <p>date due for return:-</p> <p>14 MAY 1984</p> <p>No Renewal</p> <p>1 JUL 1988</p> <p>5 JUL 1985</p> <p>5 JUL 1985</p>	<p>LOAN COPY</p> <p>4 JUL 1986</p> <p>21 DEC 88</p> <p>1 JUL 1988</p> <p>28 JUN 1996</p> <p>22 MAR 1996</p>	<p>27 JUN 1997</p> <p>26 JUN 1998</p> <p>25 JUN 1999</p> <p>14 JAN 2000</p>

0815 152257 02





PHENOMENOLOGICAL COMBUSTION MODEL
FOR
DIRECT INJECTION DIESEL ENGINE

by

PRAMOD SHANKAR MEHTA

A Doctoral Thesis
submitted in partial fulfilment of the
requirements for the award of
Doctor of Philosophy of
Loughborough University of Technology

December 1981

Supervisor: Professor J C Dent, PhD, CEng
Department of Mechanical Engineering

© by Pramod Shankar Mehta

Loughborough University of Technology Library	
Date	Mar 82
Class	
Acc. No.	152257/02

SUMMARY

In the present investigation a new phenomenological model for Quiescent and Swirl Type Direct Injection Diesel Engines has been developed.

The model enables prediction of engine cylinder pressure, fuel injection and evaporation rates, air entrainment rate into fuel sprays, heat release rate, heat transfer and mean cylinder gas temperatures and exhaust smoke level.

A soot model is proposed based on chemical kinetics and a turbulent mixing rate concept. The model predictions are verified with several experimental data.

The predictions are made over a range of engine speed, load, injection timing, boost pressure and intake swirl level.

Comparison with available engine experiments is in general good.

ACKNOWLEDGEMENTS

The author wishes to express his grateful appreciation to the following:

Professor J C Dent for his untiring guidance and supervision throughout this work.

Ruston Diesels Ltd (UK) for scholarship support to carry out this investigation.

Cummins Engine Co. Inc. (USA) and AVL (Austria) for providing experimental data to test the model.

The University of Roorkee (India) for granting of study leave.

Dr P A Lakshminarayanan, Mr S P Kagoda and other friends for their inspirations and help during this work.

Mr G P Gerard and the staff of the Computer Centre, Loughborough University for providing help at time of difficulties.

PUBLICATIONS

The following papers have been published based on the work reported in Chapters II and VI at SAE.

1. J C Dent and Pramod S Mehta, '*Phenomenological Combustion Model for a Quiescent Chamber Diesel Engine*', Presented at Fuels and Lubricants Meeting, Tulsa, Oklahoma, October, 1981.

NOTATION

A	=	Area	(m^2)
A_c	=	Total cylinder surface area	(m^2)
A_o	=	Nozzle orifice area	(m^2)
$b_{\frac{1}{2}}$	=	Half width	(m)
B	=	Transfer number	$(-)$
C	=	Concentration	(kg/m^3)
C_d	=	Nozzle orifice discharge coefficient	$(-)$
CN	=	Fuel cetane number	$(-)$
C_p, C_v	=	Thermal capacity	$(J/kg K)$
D	=	Cylinder bore	(m)
d_o	=	Nozzle orifice diameter	(m)
d_o'	=	Nozzle orifice equivalent diameter	(m)
d_p	=	Droplet diameter	(m)
D_p	=	Normalised droplet diameter	$(-)$
E	=	Activation energy	$(J/kg \text{ mole})$
f	=	Mass concentration of fuel, mixture fraction	$(-)$
g^*	=	Mass transfer conductance	(kg/m^2s)
G	=	Momentum	$(kg \text{ m/s})$
H	=	Distance of wall from the nozzle	(m)
h_{fg}	=	Enthalpy of vaporisation	(J/kg)
h_i	=	Instantaneous heat transfer coefficient	(W/m^2K)
H_o	=	Enthalpy of reaction	(J/kg)
J	=	Momentum flux	$(kg/m s)$
k	=	Specific kinetic energy	(m^2/s^2)

L	=	Stroke	(m)
L_c	=	Connecting rod length	(m)
m	=	Mass	(kg)
M	=	Molecular weight	(kg/kg mole)
\dot{m}	=	Mass flow rate	(kg/s)
\dot{m}''	=	Mass transfer rate	(kg/m ² s)
m_{aa}	=	Available air mass at the end of injection	(kg)
n	=	Number of holes in the nozzle; nuclei concentration of soot	
N	=	Engine speed;	(rpm)
		particle concentration of soot	(part/m ³ s)
N_p	=	Number of droplets	
Nu	=	Nusselt Number	
P_c	=	Cylinder pressure	(Pa)
ΔP	=	Pressure drop across nozzle orifice	(Pa)
P_{fu}	=	Partial pressure of fuel	(Pa)
P_{O_2}	=	Partial pressure of oxygen	(Pa)
Pr	=	Prandtl Number	
q	=	Surface reaction rate	(kg/m ² s)
\dot{Q}	=	Fuel injection rate	(m ³ /s)
Q_{rel}	=	Heat release	(J)
\dot{Q}_{tr}	=	Heat transfer rate	(J/s)
r	=	Radius	(m)
R	=	Gas constant	(J/kg K)
R_u	=	Universal gas constant (= 8314.3 J/kg mole K)	
s	=	Stoichiometric constant	(-)
S	=	Spray penetration	(m)
SR	=	Swirl ratio	(-)
S_w	=	Wall jet penetration	(m)
SMD	=	Sauter Mean Diameter	(m)

t	=	Time	(s)
Δt	=	Time interval	(s)
T	=	Temperature	(K)
T_0	=	Datum temperature	(K)
u	=	Internal energy	(J/kg)
U	=	Velocity	(m/s)
$U_0,$ U_{jet}	=	Jet velocity	(m/s)
V	=	Volume	(m ³)
V_{cf}	=	Cumulative volume fraction	(-)
V_{cl}	=	Clearance volume	(m ³)
V_f	=	Volumetric fuel delivery per stroke	(m ³)
V_{fi}	=	Volume of fuel injected	(m ³)
V_p	=	Mean piston speed	(m/s)
V_s	=	Swept Volume	(m ³)
X	=	Mass fraction	(-)
Y_p	=	Normalised radial position	(-)
Y_w	=	Distance of impingement point from the wall	(m)
Z_w	=	Impingement distance	(m)
ϵ	=	Energy dissipation rate	(m ² /s ³)
θ	=	Crank position	(-)
θ_{ip}	=	Injection period	(^o CA)
ν	=	Kinematic viscosity	(m ² /s)
ω	=	Angular velocity	(rad/s)
ρ	=	Density	(m /s)
τ	=	Mixing time	(s)
ϕ	=	Fuel vapour-air ratio, equivalence ratio	(-)

SUBSCRIPTS

The following subscripts pertain to:

a	air
ac	air consumption during combustion
aE	air entrained into the spray
a _{s,r}	air in the surrounding
ch	condition of the engine cylinder charge
cr	condition at critical point
evo	exhaust valve opening
f	fuel, formation of soot
fl,l	liquid fuel
fu	unburnt fuel
fb	burnt fuel
fv,v	fuel vapour
G	conditions in bulk air in the engine
h	heat transfer
inj	injection
j,jet	jet
m	jet centre line, mass transfer
n	normal
net	net values
o	oxidation, orifice conditions
O ₂	oxygen
s	soot
S	conditions at the droplet surface
st	stoichiometric condition
s _{w,ω}	swirl
t	total or mixture condition, tangential
vb	fuel vapour burned
w	wall

CONTENTS

	Page Nos
SUMMARY	i
ACKNOWLEDGEMENTS	ii
PUBLICATIONS	iii
NOTATION	iv
CHAPTER I: MATHEMATICAL MODELLING OF DIESEL ENGINES - GENERAL DISCUSSION AND LITERATURE SURVEY	1
1.1 Introduction	1
1.2 Quiescent and Swirl Type Engines	1
1.3 Mathematical Modelling of Engines	3
1.3.1 Importance of Modelling	
1.3.2 Types of Model	
1.4 Salient Features and Discussion of the Literature Pertaining to Mathematical Models of the Diesel Engine	5
1.4.1 Phenomenological Models	
1.4.2 Description of Various Models from Literature	
CHAPTER II: BASIS OF THE PROPOSED MODEL	
2.1 Introduction	27
2.2 Physical Basis of Modelling	28
2.2.1 Fuel Injection	
2.2.2 Spray Penetration	
2.2.3 Entrainment	
2.2.4 Jet Structure	
2.2.5 Droplet Size and Distribution	
2.2.6 Droplet Evaporation	
2.2.7 Impingement and Wall Jet Structure	
2.2.8 Ignition Delay	
2.2.9 Combustion	
2.2.10 Heat Transfer	
2.2.11 Turbulent Mixing	

	Page Nos
2.2.12 Thermodynamic Analysis
2.2.13 Low Load Calculation
 CHAPTER III: GENERAL STRUCTURE OF THE COMPUTER PROGRAM	
3.1 Introduction ...	63
3.2 Flow Chart and Program Modules ...	63
3.3 Model Input ...	67
3.4 Model Output ...	67
3.5 Summary ...	69
 CHAPTER IV: SOOT PREDICTION MODEL	
4.1 Introduction ...	70
4.2 Literature on Soot ...	70
4.2.1 Soot Formation
4.2.2 Soot Oxidation
4.2.3 Current Status
4.3 Proposed Model ...	80
4.4 Calculation Procedure for the Net Soot Release	87
4.5 Calculation of Exhaust Soot in Terms of Bosch Number ...	89
 CHAPTER V: MODEL FOR SWIRL IN DIESEL ENGINES	
5.1 Introduction ...	91
5.2 Physical Basis of the Model ...	92
5.2.1 Calculation of Swirl Ratio ...	94
5.3 Modification in Quiescent Chamber Model ...	94
5.3.1 Spray Trajectory
5.3.1.1 Penetration
5.3.1.2 Spray Deflection
5.3.1.3 Jet Width
5.3.2 Air Entrainment
5.3.3 Ignition Delay
5.3.4 Wall Impingement
5.3.5 Turbulent Mixing

				Page Nos
CHAPTER VI:	RESULTS AND DISCUSSION	
6.1	Quiescent Chamber Diesel Engine	105
6.1.1	Results	
6.1.2	Discussion	
6.2	Soot Results	111
6.3	Effect of Swirl	112
CHAPTER VII:	CONCLUSION AND FUTURE WORK	115
7.1	Conclusion	115
7.2	Future Work	115
REFERENCES	117
APPENDIX A:	DETERMINATION OF CENTRELINE CONCENTRATION AND VELOCITY AT ANY AXIAL POSITION	134
APPENDIX B:	DROPLET-SIZE DISTRIBUTION	140
APPENDIX C:	EVALUATION OF MEAN THERMODYNAMIC AND PHYSICAL PROPERTIES	143
APPENDIX D:	CALCULATION OF SHALLOW PISTON GEOMETRY	150
APPENDIX E:	MASS AND ENERGY BALANCE FORMULATION	153
APPENDIX F:	ENGINE SPECIFICATIONS	162

CHAPTER 1

MATHEMATICAL MODELLING OF DIESEL ENGINES - GENERAL DISCUSSION AND LITERATURE SURVEY

1.1 Introduction

The Diesel engine because of its high compression ratio and unthrottled mode of operation, is unrivalled as a power source for heavy duty vehicles and stationary applications in terms of fuel economy.

Intense development at the present time in the light duty Direct Injection Diesel engine field is aimed at improving the speed range of these engines, their smoke limited maximum power output, and reducing combustion generated noise. Wide application of the light duty Diesel engine in the automotive market is imminent.

Diesel engine combustion systems are divided into direct and indirect injection types. Higher air fuel mixing rates in the indirect injection engine gives it a wider operating speed range than the direct injection engine, however the increased heat transfer and delayed heat release in relation to top dead centre (due to the transfer port) result in a fuel consumption penalty relative to the direct injection engine. However, the gaseous emissions characteristic of the direct injection engine are generally inferior to its indirect injection counterpart.

1.2 Quiescent and Swirl Type Engines

For efficient running of diesel engines, an ideal requirement is the rapid injection and mixing of injected fuel with the air in the combustion chamber. These requirements affect combustion chamber design. Based on combustion chamber configuration, diesel engines are classed as either Quiescent or Swirl type.

Quiescent chamber engines are at one extreme where combustion is controlled by the fuel injection process. These include large engines used in industrial or marine applications, where engine speed is low and therefore sufficient time is available for mixing. Also, fuel consumption rather than maximum power tends to be important so that a large amount of excess air is acceptable to effect complete combustion. The combustion chamber is usually compact with minimal surface to volume ratio and is shallow dish shaped. Because the injection process controls the air fuel mixing, the fuel injector nozzle is configured to have the largest number of holes compatible with low maintenance in service and efficient combustion (no interaction between adjacent sprays).

The use of very high line pressures (greater than 600 bars) together with small hole sizes (0.3 mm) are required for ideal performance. However, this imposes severe mechanical stresses on the injection system.

On the other hand, air motion can be used with the injection process to further enhance mixing. This permits the use of lower injection pressures and hence reduced cost of the injection system. This idea is taken to the limit with indirect injection Diesel engines where, in effect, a single orifice pintle type nozzle is used with fuel pressures of the order of 300 bars. Enhanced fuel air mixing can be attained by using 'Air Swirl' and 'Squish'. Air swirl is induced by the flow geometry of the inlet port and enhanced by the conservation of momentum through the combustion chamber bowl, during the compression stroke. Also, in the engine, this primary motion compounds with the 'squish' arising from the radial component of the flow by transferring the fluid from the outer cylinder into the combustion chamber, as the piston approaches top dead centre on the compression stroke.

Small high speed engines used in automotive applications require a high degree of air motion. In indirect injection or direct injection

engines with high swirl the air motion and fuel injection characteristics are matched to yield the desired rate of pressure rise. Swirl engines need a smaller total hole area, leading to fewer holes, compared with the quiescent type engine. The advantages of swirl induced air motion have been achieved at the cost of a loss in volumetric efficiency and increased heat transfer from cylinder walls. However greater research and development effort is now aimed at a better understanding of the intake port flow behaviour and losses, and in reducing cylinder heat transfer by better design and the use of thermal shielding, by employing ceramic coatings on heads and pistons.

1.3 Mathematical Modelling of Engines

1.3.1 Importance of Modelling

In an overview of engine combustion modelling, Heywood (1) summarizes the three important phases of modelling as:

- i) Model development through an analysis of the individual processes which are linked together in the engine operating cycle.
- ii) Exploratory use of the model, its validation, and studies of sensitivity of model predictions to initial assumptions.
- iii) Use of the model in extensive parametric studies which examine the effects of changes in engine operating and design parameters on performance, efficiency and emissions.

In the past few years, diesel engine combustion modelling has attracted many research workers (2-20), however the description of the diesel engine combustion process seems incomplete. The heterogeneous mixture condition and the transient nature of the in-cylinder processes pose major problems in the development of suitable models.

1.3.2 Types of Model

There are two broad approaches to diesel engine combustion modelling - multi-dimensional models and phenomenological models. The former require detailed finite difference formulations of mass, momentum and energy conservation, applied to the cylinder charge and the injected fuel along with mathematical descriptions of the turbulent energy state and chemical state of the system. Solution yields an equally detailed set of information about the combustion process such as spatial and temporal distributions of velocity, temperature, and species concentration.

Phenomenological modelling on the other hand is formulated around empirical or simplified quasi-steady equations describing the individual processes of fuel injection, atomisation and droplet distribution, air entrainment, mixing, combustion and heat transfer. The simplified equations are often characterised by controlling parameters derived from engine design and operating variables. The simplified process equations are arrived at from engine experiments, and also from more fundamental theoretical and experimental studies of particular processes, for example, jet entrainment and mixing.

Following the classifications of Bracco (2), phenomenological models can be placed in two categories - zero-dimensional models and quasi-dimensional models. These models are based on thermodynamic analysis of engine cylinder contents and empirical or semi-empirical process descriptions. In the zero-dimensional models the details of the combustion process are fixed as an input to the calculation in the form of a burning rate law while in quasi-dimensional models attempts are made to couple the combustion process with the conditions inside the engine cylinder.

Apart from these two types, there are many other ways of classifying diesel models. This is illustrated in Figure 1.1 and will be used in the literature survey to follow.

1.4 Salient Features and Discussion of the Literature Pertaining to Mathematical Models of the Diesel Engine

It is of importance to describe the salient details of multi-dimensional and phenomenological models existing in the literature. Multi-dimensional models are useful where details of engine geometry and flow are essential. The coupling of the air motion and injected fuel droplets is an essential feature of these models. They are two- or three-dimensional in nature. However, because of the greater complexity of three-dimensional models and their higher cost, the two-dimensional approach is preferred for assessing the accuracy of computational methods. There are only a few multi-dimensional models (2-5) available in the literature. At this stage, they are explorative in use and are less suited for quantitative parametric studies. However, the following discussion is focussed on the literature pertaining to Direct Injection diesel engine models, and phenomenological models are elaborated on in detail because of their attractiveness as a development tool, through much smaller demands on computational time and facilities.

1.4.1 Phenomenological Models

The apt description of the physical and chemical processes affecting diesel engine combustion is the essence of the phenomenological model. Modelling studies in the literature, can be placed into two categories. Those concerning fundamental non-engine studies to describe processes such as atomisation, penetration, evaporation, mixing, auto-ignition, and spray combustion fall in the first category. The second category includes fundamental studies based on the actual in cylinder engine processes. Therefore, the fundamental non-engine studies will always be of interest in the development of better phenomenological models. In fact, multi-dimensional models also need phenomenological descriptions of some processes such as turbulence, heat transfer and chemical kinetics.

Central to the phenomenological model is the analysis of the first law of thermodynamics. These models are either zero- or quasi-dimensional, expressed as an ordinary differential equation in terms of time as an independent variable. A model with more than one independent variable is made up of partial differential equations. The most general model has four independent variables: time and three space coordinates. The dropping of one or two space coordinates through assumptions of planar symmetry introduces two- or one-dimensionality in the model. An arbitrary relationship between space and time variables through geometric consideration make them pseudo-dimensional in nature.

The early models (6-9) were zero-dimensional in description. They were mainly concerned with basic cycle thermodynamics for evaluating performance as a function of engine operating conditions. The homogeneous mixture condition, thermodynamic equilibrium and absence of flow characterization were the basic assumptions used. One of the major drawbacks of such models is the need for 'a priori' specification of the fuel burning rate. An assumption of satisfactory mixing is inbuilt in a zero-dimensional model. Therefore, the situation of poor mixing and pollutant formation cannot be covered by these models.

Later models (10-20) dealt in greater detail with the heterogeneity of the mixture, and the flow characteristics of the fluid inside the engine cylinder, which are essential for emission predictions. The inclusion of fuel spray and swirl motion brought one- or two-dimensionality into the models. However, simplified assumptions were made such as: conical configuration of the fuel spray, calculation of air entrainment based on spray penetration, droplet evaporation based on isolated droplet behaviour, characterisation of turbulent air-fuel mixing, solid body rotation for describing swirl flow, and calculation of burning rate in terms of local air fuel mixture conditions. In the literature survey to follow, these assumptions will be examined in some detail.

1.4.2 Description of Various Models from the Literature

A list of useful models available from the literature for direct injection diesel engines is given in Table 1.1.

In a very early attempt at phenomenological modelling Lyn (6) established a relationship between the fuel injection rate and the burning rate in a diesel engine assuming uniform mixture condition in the engine cylinder. A schematic of such a relationship is shown in Figure 1.2. A triangular heat release pattern is related to the various packets of injected fuel quantity obtained from needle lift data.

For the first element of fuel injected, this procedure considered an arbitrary base of the triangle equal to 30° crank angles (approximately 3 to 5 percent of the total cycle duration). The height of the triangle was obtained from consideration of equal areas under fuel injection and burning rate curves. For subsequent fuel elements, the burning time (that is, the base of the triangle) was increased by 3° crank angle per degree after beginning of injection. This criterion was suggested in their work (21) on an empirical basis from tests data obtained from a single cylinder direct injection engine.

The fuel packets injected during ignition delay give rise to the first peak in the heat release diagram. Lyn suggested that the total combustion process occurs in three stages as shown in Figure 1.3. From his experiments, he found that the diesel combustion process is very insensitive to the cylinder temperature. It is the mixing process that plays a dominant role. Lyn's burning rate law formed the basis of many subsequent diesel engine models (7,14).

In general, zero-dimensional or thermodynamic models require the following set of equations:

TABLE 1.1

List of Phenomenological Models of Direct Injection Diesel Engines
in Chronological Order

	Author(s)	Year	Purpose	Concept used
1	W T Lyn	1963	Heat release	Burning rate law
2	G L Borman	1964	Performance	Thermodynamic cycle simulation
3	N D Whitehouse and R Way	1969-1970	Heat release	Single-zone burning law
4	J Shipinski P S Myers and O A Uyehara	1969-1970	Heat release	Single droplet, spray burning
5	D Adler and W T Lyn	1969-1970	Evaporation and mixing	Quasi-steady integral approach
6	H C Grigg and M H Syed	1969-1970	Heat release	Fuel-spray air-entrainment
7	E K Bastress K M Chng and D M Dix	1971	Performance and Nitric oxide	Thermodynamic analysis with empirical rate processes
8	I M Khan G Greeves and D M Probert	1971	Nitric oxide and Soot	Spray mixing
9	S M Shahed W S Chiu and V S Yumlu	1973	Nitric oxide	Burning rate law
10	N D Whitehouse and B K Sareen	1974	Heat release	Two-zone spray mixing
11	S M Shahed W S Chiu and W T Lyn	1975	Combustion and Nitric oxide	Spray mixing
12	D Hodgetts and H D Shroff	1975	Nitric oxide	Multi-zone spray mixing
13	H Hiroyasu and T Kadota	1976	Combustion Nitric oxide and Soot	Intermittent spray mixing

/Continued...

Author(s)	Year	Purpose	Concept Used
14 C J Kau T J Tyson and M P Heap	1976	Heat release Nitric oxide and Soot	Spray mixing
15 M Meguerdichian and N Watson	1978	Heat release	Multi-zone spray mixing

- i) Conservation of energy
- ii) Conservation of mass
- iii) Conservation of momentum
- iv) Equation of state for the working fluid
- v) Composition equations

Ideally, the solution of these equations with certain assumptions seems very attractive for engine simulation work. In a real situation, the description of processes such as mass transfer and heat transfer, and their unsteadiness have to be considered. This leads to the need to solve many additional equations for complete and accurate results.

Borman's work (7) is typical of thermodynamic cycle calculation in the diesel engine. He attempted the complete mathematical simulation of the diesel engine by coupling equations describing the thermal and flow behaviour during changes in the engine cycle. He assumed a homogeneous mixture condition, presented a rigorous heat transfer analysis, and accounted for unsteady flow conditions and dissociation in his calculation. In a way, he used Lyn's approach for heat release calculations, but it was based on experimental pressure time diagrams. In the subsequent literature, the procedure of obtaining the heat release diagram from the experimental pressure trace utilized by Borman was termed the 'apparent heat release rate' method. The analysis includes heat transfer and dissociation effects. McAulay et al (22) have presented comprehensive results on engine performance from this model.

Arguing that Lyn's burning rate law does not account for oxygen availability in the engine cylinder, Whitehouse and Way (8) developed a semi-empirical formula for calculating heat release rate in turbocharged direct injection engines.

The generalized forms of their fuel preparation rate (P) and reaction rate (R) equations are:

$$P = K M_i^{(1-x)} M_u^x p_{O_2}^m \quad (1.1)$$

$$R = K' \frac{p_{O_2}}{N\sqrt{T}} e^{-\frac{A}{T}} \int (P-R) d\theta \quad (1.2)$$

where M_i is the mass of fuel injected up to the time under consideration, M_u is the amount of fuel available for preparation, p_{O_2} is the partial pressure of oxygen, N is the engine speed, T is temperature, $d\theta$ is crank interval, and K , K' , x , m and A are various constants. The authors have published values of these constants for specific engines.

The assumption of single droplet behaviour is implicit in their constants in equation (1.1). Figure 1.4 illustrates the results from this model. A single zone model such as those considered cannot indicate the effect of air fuel mixing on the combustion process since it assumes that a single constant controls this process for all engine conditions. Therefore, the prediction of maximum power and emission is not possible.

Shipinski et al (9) utilized single droplet behaviour in their spray burning model. Since their approach did not account for mixing controlled combustion, they used an empirical spray burning coefficient (C_E). This is given by:

$$C_E = \frac{mT^n}{250} \quad (1.3)$$

where m and n are the constants determined from experiments. These constants show the effect of the engine configuration and the conditions inside the engine cylinder on the burning rate.

The one-dimensional model of Adler and Lyn (10) is developed on the basis that transient jet phenomenon can be described by

steady-state conditions, by treating an elemental section of the spray as a quasi-solid body under equilibrium of the inertia and drag forces in the flow field (see Figure 1.5). The equations of continuity, momentum, energy, and diffusion are applied to a differential volume element of the spray. This first attempt, however, was limited to a simple solution of complicated equations for evaporation and mixing processes only. For this purpose, the authors adopted concepts such as equivalent velocity, equivalent temperature, an evaporation function and similarity profiles for solving integral equations. The approximations of rectangular spray cross-section, the arbitrary value of the deflection coefficient representing the gas forces on the spray, and the determination of drag coefficient from the analysis of droplets as solid spheres in clouds were used in their work. These assumptions are simple and far from the real situation. No results regarding effect of combustion are available from the analysis.

Breaking away from the conventional droplet burning approach, Grigg and Syed (11) proposed a model based on the process of air entrainment into the fuel sprays. They assumed two types of spray geometry - conical and doughnut shapes (see Figure 1.6). The air entrainment was computed from Schweitzer's penetration (23) equation. The turbulent mixing in the fuel sprays, and chemical kinetic controlled burning rate in geometrically similar jets were considered. The values of the diffusivity coefficient in turbulent mixing and the steric factor in the Arrhenius type burning rate equations needed adjustment to match the experimental results. The effect of evaporation of droplets was implicit in the constants. They found that the first peak of the heat release diagram is controlled by chemical kinetics due to low temperatures during delay period. After that the air entrainment and turbulent mixing are the controlling factors. Both conical plumes and doughnut models calculated similar entrainment rates (see Figure 1.7). This looks a surprising coincidence which the authors could not explain. The air entrainment was found inadequate in case of naturally aspirated engines (see Figure 1.8).

Other one-dimensional models for direct injection diesel engines include:

- i) NREC model (Bastress et al (12))
- ii) CAV model (Khan et al (13))
- iii) Cummins model (Shahed et al (14,16))
- iv) Two-zone model of Whitehouse and Sareen (15)

The NREC model described six parameters controlling the important engine processes, namely, injection, evaporation, ignition, mixture formation and dilution, heat release, and heat transfer. The parameters are provided as input to the model and need adjustment with experiments. They are not in any way related to the controlling physical processes. This model, therefore, remains difficult to use in practice.

The CAV model is based on the fuel spray model of Grigg and Syed (11). It considers the fuel spray as a gaseous jet. Two empirical constants termed diffusion constant and entrainment ratio are used in the model to calculate the fuel preparation-burning rate and the effect of swirl on the air entrainment respectively. The model considered the wall impingement in an unconfined manner and neglected the cross flow effects of air swirl. At any instant the jet geometry is divided into four zones as shown in Figure 1.9. These are:

- i) the surrounding air zone
- ii) the entrainment zone
- iii) the intense reaction and products zone (the heat release and NO_x -formation zone)
- iv) the fuel rich zone (soot formation zone).

The Zeldovich mechanism is used to predict nitric oxide formation in the intense reaction zone where high temperature favours

its formation. The soot formation in the rich zone is based on an Arrhenius type equation involving an equivalence ratio function. Results of nitric oxide and soot predictions (24) obtained from this model for varying injection timing and fuelling levels are shown in Figures 1.10 and 1.11. The nitric oxide results are reasonable while soot-predictions show considerable scatter (Figure 1.12). The poor predictability for the effect of load, speed and inlet temperature using this model is confirmed by Wilson and Waldman et al (25). Blumberg et al (26) pointed out a possibility of some inherent difficulty in the soot results of the CAV model. The soot burn up calculations of the model showed no alteration in the overall trends of soot formation results, despite the soot combustion being shown to be about half of the formation (see Figure 1.13). The decrease in temperature and partial pressure in the soot combustion region during the expansion period with increasing coagulation diameter of soot particles is probably a reason for constant combustion rate of soot in the model.

The calculation of local equivalence ratio stratification in the regions of soot formation and nitric oxide formation is chosen in a very artificial manner as:

$$\phi_{\text{soot}} = \frac{15 (X - x)}{(A - a)} \cdot \frac{X}{x} \quad (1.4)$$

$$\phi_{\text{NO}} = \frac{15 x'}{M_a} \quad (1.5)$$

where X is the quantity of fuel injected, x is the fuel prepared for heat release, x' is the fuel burned, A is the mass of air entrainment, a is the air consumed and M_a is the micromixed air.

The temperatures in these regions are approximated as the thermodynamic mean temperature in the whole jet for the soot cal-

ulation, and the equilibrium temperature calculated from the heat release for nitric oxide evaluation.

The micromixing is based on the molecular diffusion constant rather than any fundamental mixing length criterion. These calculation procedures and the absence of a proper account of heat losses from the heat release zone may be the contributing factors in the variability of the results. However, the model shows the correct trends.

The chemical kinetically controlled combustion assumption of Grigg and Syed (11) during the early phase of combustion was adopted by Khan et al.

The Cummins model was developed in two stages: preliminary model (14) and spray-mixing model (16). The preliminary model is empirical in nature due to the use of Lyn's burning rate law approach. Subsequently the model has been improved by describing the spray mixing process using turbulent jet theory. The gaseous jet assumption was used but the effect of wall impingement was neglected. The parameters defining the jet were obtained from extensive combustion bomb experiments conducted at elevated pressures with and without swirl. The model schematic is shown in Figure 1.14. The burning zones B_i , limited to a maximum value of ten and bounded by lean and rich limits of combustion $0.3 < \phi < 3$, appear progressively between air zone A and fuel core region C during the combustion period. The assumptions of stoichiometric combustion, the local equilibrium of burned mixture and continuous dilution of burning zones are used in the model. The various thermodynamic parameters and the performance are evaluated using conservation equations. The results concerning performance and nitric oxide predictions are shown in Figures 1.15 and 1.16. Figure 1.17 shows the effects of injector hole size and air swirl on these predictions. The performance results show good agreement while the nitric-oxide predictions were less accurate, differing by a factor of two. However, the results showing the effect of injector hole size, and air swirl agreed well with experiments.

Four recent studies have introduced two-dimensionality in the description of spray behaviour in diesel models.

Hodgetts and Shroff (17) showed the need for more than two zones to predict nitric oxide emissions. They found that the two zone approach is adequate only at full load conditions, but at part load, results are not consistent until at least ten zones are considered. This is because at part load air fuel mixing characterization is critical for combustion calculation. In their multi-zone two-dimensional model the temporal history of temperature, equivalence ratio and air entrainment are considered for each zone, as shown in Figure 1.18. They modified the preparation rate equation from Whitehouse et al (8) by introducing a turbulence factor. The burning rate is controlled by an exponential type equation suggested by Whitehouse et al (8). The jet structure followed from a quasi-steady analysis using the penetration equation given by Oz (28). Contrary to intuition, this work and the work of Whitehouse and Sareen (15) showed a reduction in the air entrainment rate in the wall region. This is explained by reduction in penetration length due to increase in thickness of annular region occupied by the burning zone outside the jet.

Using an axisymmetric spray with 400 isolated packages, Hiroyasu and Kadota (18) developed an intermittent spray-combustion model. They described all major physical processes concerning diesel combustion through their own correlations developed over a period of time and summarized in reference (29). Axial division of the spray coincides with the location of the fuel elements injected during each specified interval of time. The radial division is based on equal solid angles with their vertices at the nozzle orifice. A schematic of their model is shown in Figure 1.19. In the spray, each small isolated zone consisted of liquid fuel, fuel vapour and air. The droplet evaporation is calculated by means of a single droplet analysis and stoichiometric combustion is assumed after the delay period. The mixing between zones, and jet impingement on the wall is neglected. The assumption of adiabatic compression (or expansion)

is used to calculate local temperatures from the original burning temperature of the zone. Therefore, the heat transfer calculation between zones is of no consequence. Overall heat transfer obtained from Woschni's equation (30) is applied in the energy balance so as to arrive at the engine cylinder pressure diagram. Good agreement is reported between computed and experimental pressure time diagrams at different operating conditions.

This model has been used to predict nitric oxide soot and CO emissions. NO_x calculations were carried out using the Zeldovich mechanism. The net soot concentration in the exhaust is computed from the difference of soot formation and combustion rates. The formation rate is based on an Arrhenius type equation by considering liquid and vapour phase pyrolysis. Soot combustion is handled by using the equation of Lee et al (31). Both these rate equations needed empirical constants to be adjusted from engine experiments based on exhaust soot level. CO emissions were calculated by assuming instantaneous equilibrium in each zone. A comparison of predicted and experimental results for exhaust emissions are shown in Figure 1.20 for variations in injection timing and engine speed respectively. Nitric oxide concentration is over-predicted from the model. The CO and soot predictions appear reasonable for the injection timings used. However, soot concentration decreased with speed unlike the experimental results.

The Ultrasystems model was developed in two stages. The first stage carried out by Wilson et al (25), was mainly concerned with engine development work and produced data for pollutant formation studies. A basis for detailed modelling was established by following four activities:

- i) Emission data were correlated with engine parameters.
- ii) Existing models were then assessed.
- iii) A model of heat release was outlined.
- iv) High speed photographic studies were undertaken in a pre-chamber engine to determine combustion development.

Exhaust measurements of NO, soot and hydrocarbons were made on a single cylinder diesel engine. In addition to confirming the effects of air-fuel ratio and injection timing, the effect of engine geometry, mixing parameters (orifice size and air swirl) and the state of the intake mixture (exhaust gas recirculation and water injection) were found to change nitric oxide emissions by 40 percent or more with corresponding changes in soot concentration.

With this experience, the second stage carried out by Kau et al (19) developed a computer model for a direct injection diesel engine. This was based on a two-dimensional spray-mixing approach. The important feature of the model is the modular arrangement of various elements. These elements describe cycle thermodynamics, fuel spray injection, entrainment, vaporization, ignition, mixing, heat release and emission formation, and are built from fundamental and empirical information. In each case empirical constants are put into two categories:

- i) constants affected by gross changes in the engine;
- ii) constants requiring adjustments for different operating conditions (listed in Table 1.2).

The model assumed a quasi-steady, axisymmetric spray and neglected the effect of piston motion, relative motion between droplets and air, transition of free jet to wall jet, effect of fuel volume and the curvature of the piston bowl. A schematic of the model is shown in Figure 1.21. The effect of evaporation, entrainment, impingement and swirl are considered in the calculations. At any instant the total cylinder volume was considered to comprise four hypothetical zones - the air zone, vaporizing liquid fuel zone, fuel vapour zone, and the burning zone. The mass and energy conservation equations were written for these zones. The mechanism of heat release depends on the isolated droplet assumption, which has been modified to provide for flame confinement and vitiation of the atmosphere through boundary conditions at finite distance

TABLE 1.2

Adjustable Empirical Constants in Ultrasystems Model (19)

Constants	Description	Remarks
C_{sef}	Parameter controlling air entrainment into the spray prior to ignition	Shows strong influence on premixed combustion and therefore, on NO level as well
C_{mix}	Parameter controlling random mixing process between the burning zones and the air zones after ignition	Shows strongest effect on NO
C_{vidi}	Parameter controlling vitiation of the air prior to mixing with the burning zone	No strong influence
ϵ_{hu}	Droplet heating up time	Assumed to be equal to a typical physical delay time
A_{ig}	Parameter to match the measured ignition delay data	-
A_{sf}	Parameter to match the measured exhaust soot concentration	-
C_{nor}	Parameter to match exhaust NO value	Same value as assumed by Khan et al (24)

from each droplet. This revision over the classical isolated droplet theory was necessary because the classical approach gave a total flame volume greater than the available cylinder volume. The complex cloud combustion is described by three modes of heat release: homogeneous premixed, homogeneous diffusion and heterogeneous. An empirical ignition criterion for each zone was set from the data of Shipinski et al (9). After ignition, the mixing process is modelled as a completely random process involving only air and burning zones. Thus, the air is continuously vitiated and is proportional to the rate of dilution expressed as:

$$\frac{dm_D}{d\theta} = \frac{1}{\tau_{mix}} \frac{m_{aa} m_{bm}}{(m_{aa} + m_{bm})} \quad (1.6)$$

where τ_{mix} is a characteristic mixing time and is proportional to the ratio of the turbulent length scale squared and the turbulent diffusivity. This random mixing criterion is utilized to calculate nitric oxide formation in two regions:

- i) Spherical diffusion flame around the droplets.
- ii) Homogeneous burned gas away from the droplets.

Except in the early period of combustion, the first region is found to contribute very little to the nitric oxide formed in the engine. Therefore, only the gas phase region is a major contributor of nitric oxide. This fact substantiated the gas jet assumption of the earlier model (14) used for predicting nitric oxide.

Soot formation and oxidation are computed by the relationship of Khan et al (13) and Lee et al (31) respectively.

The model predictions were compared with one experimental data set, subsequently referred to as the baseline condition. The effect of variations in injection timing, speed, load, exhaust gas recirculation, compression ratio, swirl, turbocharging and nozzle hole diameter

were studied with respect to the baseline results. Figure 1.22 shows the corresponding results. The sensitivity of the model to the empirical constants is shown in Figure 1.23. The parameter controlling random mixing has shown the strongest effect on the results. The predictability of this model is summarized in Table 1.3.

TABLE 1.3

Summary of Predictive Capability of Ultrasystems Model (19)

Variable	Exhaust NO _x	Exhaust Soot
Fuel injection timing	Good	Good
Load	Good	Fair
Engine speed	Good	Good
Compression ratio	Poor	Fair
Exhaust gas recirculation	Good	Poor
Swirl	Good	Poor
Turbocharging ratio	Good	Fair
Nozzle holes, number and diameter	Good	Fair

The recent work of Meguerdichian and Watson (20) reports a multi-zone gaseous jet model (Figure 1.24) for prediction of mixing and heat release in diesel engines. The general approach of the model is to apply the first law of thermodynamics, the equation of state and the burning rate equation to small individual zones, within a fuel spray. The burning rate equation is of an exponential type and includes instantaneous values of zone temperature and available unburnt fuel and air. This work avoids use of any ignition delay correlation. Instead, the moment of ignition was predicted through mixture ratio and temperature conditions. The effect of the wall was considered by changing a free jet in cross flowing

stream. At the transition from the free to wall region, the jet cross-sectional area and fuel and air mass flow rates are assumed equal. The zoning pattern in the model is on an equal fuel mass basis. The criterion of stoichiometric combustion in regions within limits of inflammability ($0.378 < \phi_z < 4.54$) is utilised. The burning rate calculations are therefore governed by equivalence ratio and fuel mass burnt fraction in each zone. The simultaneous solution of the energy equation, the equation of state and the burning rate equation in the burning zones yields instantaneous temperature, volume and pressure values. The instantaneous change in the mass of burning zones was due to additional air obtained from the concentration profile used. There is no explicit way of calculating air entrainment in the model.

The effect of swirl is considered assuming that every zone of the non-swirl case possessed a corresponding zone in a jet affected by swirl. This is reflected in higher entrainment rates obtained by modifying local concentration values in swirl. The local concentration of a zone in the presence of swirl (C_{sz}) was given by:

$$C_{sz} = \frac{C_{sm}}{C_m} C_z \quad (1.7)$$

where C_z is the local concentration without swirl and C_{sm} and C_m are the centreline concentrations at any instant with and without swirl. The centreline concentration (C_{sm}) and the deflection of jet is obtained from Patrick's equations (32).

The spatial distribution of temperature and burning rate were plotted and the two variables showed similar patterns except in completely burned zones where subsequent distribution by the concentration profile of air caused a reduction in temperature. The overall heat release predictions showing the effect of injection timing, swirl ratio and inlet air temperature for a turbocharged engine are computed by this model. Figure 1.25 shows these variations.

The authors reported an underestimation of the first pressure peak in the heat release diagrams. They attributed it to the fact that the predicted ignition was earlier than measured. To overcome this difficulty, they adjusted the centreline concentration. This would indicate that the spatial variation of concentration, if plotted, would not be reliable.

A summary of the salient features of the one- and two-dimensional models described above are included in Table 1.4.

In conclusion, therefore, it is felt that a new phenomenological model based on spatial and temporal droplet distribution, droplet evaporation and air entrainment needs to be developed, in which features such as wall impingement, jet interaction and the effect of turbulence on mixing must be considered in a quantitative manner.

Considering the zoning patterns adopted in existing methods, it appears that the solution of the energy equation in a large number of zones would require long computational time. Here, the application of an integral approach using similarity profiles in the jet will enable an economical model to be developed.

It also appears possible that the calculation of jet deflection, air entrainment into the spray and turbulent mixing in presence of swirl will follow the general principles indicated above for the quiescent engine situation.

The existing literature on soot formation and emission from Diesel engines does not appear to be well developed, the basic mechanisms of formation and combustion not being clearly resolved within the engine context.

TABLE 1.4

Summary of the Process Description in Some Useful Phenomenological Models

Process	Grigg and Syed	Bastress et al (NREC model)	Khan et al (CAV model)	Shahed et al (Cummins model)	Whitehouse and Sareen	Hodgetts and Shrof	Hiroyasu and Kadota	Kau et al (Ultra-systems model)	Meguerdichian and Watson
Injection	-	Injection quantity is input as data at each crank angle	-	Uses an injection scheduling	Injection quantity is an arbitrary input data	Uses an experimental injection diagram	Uses an injection scheduling	Assumes uniform injection	-
Penetration	Uses Schweitzer's equation (23)	-	Uses Schweitzer's equation (23)	Uses equation developed by Chiu et al (27)	Uses Dent's equation (33)	Uses Oz's equation (28)	Uses equation developed by Kadota et al and given in Ref. (29)	-	Uses Dent's (33) equation with an impulsive jet factor
Evaporation	Implicit through a constant	Described through constant in evaporation rate equation	Neglected	Neglected	Taken account through a constant in the preparation equation	Same as Whitehouse et al	Considers spray droplet, evaporation through SMD & drop size distribution equations	Considers evaporation using upper limit distribution function and maximum drop size equation	Neglected

Entrainment	Calculated from penetration equation using momentum continuity	-	Considered from conical jet shape and its movement	Through mixture equivalence ratio	In terms of jet shape and its movement	In terms of penetration distance	From spray configuration	Using steady state jet theory along with empirical constant	No explicit expression. implied through concentration value obtained from profile shape
Ignition	Uses experimental value of ignition delay	Uses Tsao's (35) equation for the ignition delay	Uses experimental value of ignition delay	From Lyn-Valdamin's data (36)	-	Uses Wolfer type ignition delay equation	Uses ignition delay equation developed by Kadota et al (34)	Uses Shipinski's ignition delay correlation (9)	Uses a criterion of the mixture condition and the temperature to predict moment of ignition
Heat Release	Uses Arrhenius type burning rate equation	Implicit through a constant	Assuming a triangular burning rate law	Used Lyn's burning law in preliminary model (14) subsequently refined by stoichiometric mixture burning (16)	Considered an Arrhenius type reaction rate equation through mixture preparation term in it	Arrhenius type equation	Stoichiometric combustion in each packet	After delay period fuel vapour in each zone reacts with available air	Uses mixing controlled Arrhenius type equation for burning of fuel in each zone

Heat Transfer	The predicted results are lowered by 10% to account for heat transfer	Through an empirical heat transfer parameter given as an input	-	Uses Annand's equation (37)	Uses Annand's equation (37)	Uses Woschni's equation (30)	Uses Woschni's equation (30)	Uses Annand's equation (37)	Uses Eichelberg's equation
Impingement	Not considered	Not considered	Unconfined wall jet characterised by using Glauert's equations (38)	Not considered	Considers impingement by thickening the outer ring of the spray and decreases air entrainment	Considers momentum loss of normal component of the jet and 50% reduction in air entrainment	Reflected by introducing constant in air entrainment equation	Constant in air entrainment equation is modified	Extends free jet analysis using Glauert's equations (38)
Swirl	Assumes that swirl has no other effect except burning the sprays	Not explicit	Suggests an empirical parameter 'entrainment ratio' to increase air entrainment rate in presence of swirl	Effect of swirl on free jet penetration is considered	Considers the momentum equation for computing penetration and deflection of the spray (39)	Assumes jet distortion in presence of swirl using solid body rotation assumption	Reflected by introducing constant in air entrainment equation	Constant in air entrainment equation is modified	Entrainment in the jet is increased by changing local concentration values compared to quiescent case

Diesel Engine Models

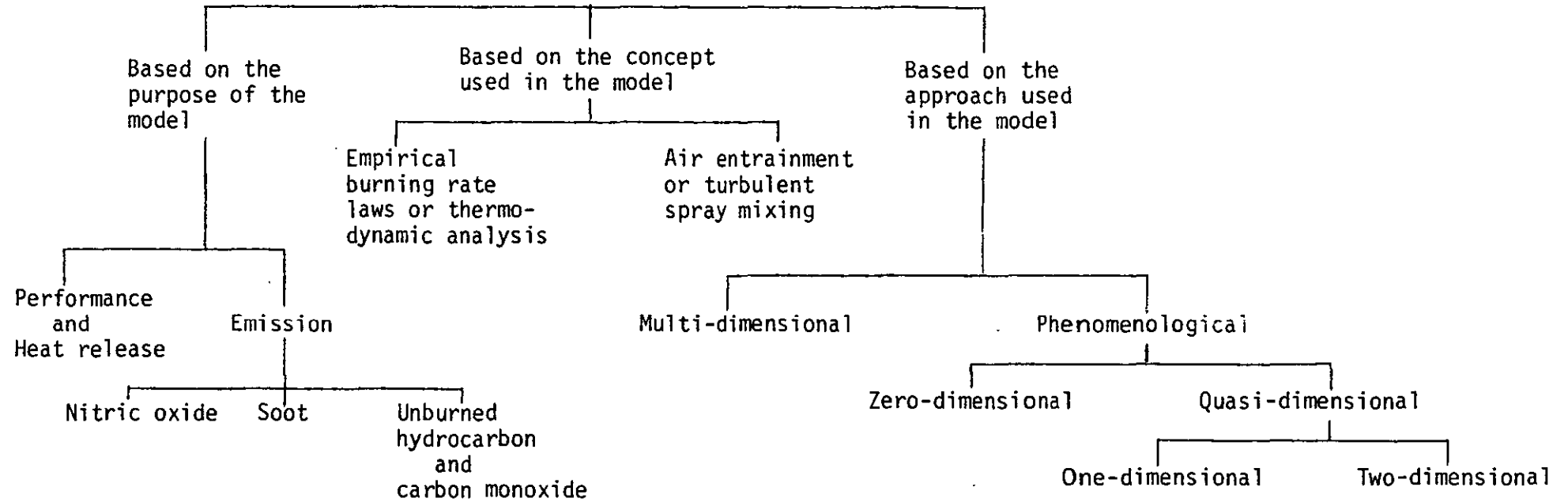


FIG. 1.1 Classification of Diesel Engine Models

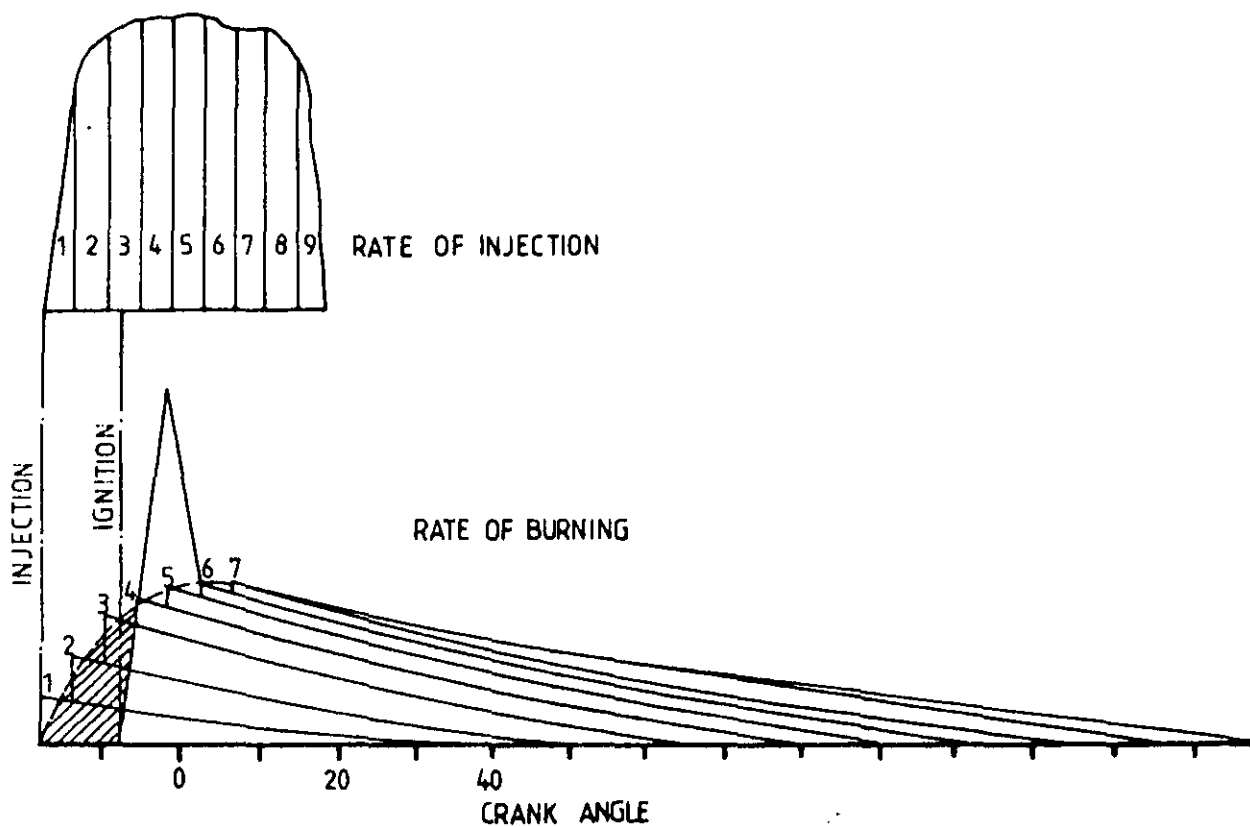


FIG. 1.2 Schematic of Lyn's Triangular Burning Rate Law (6)

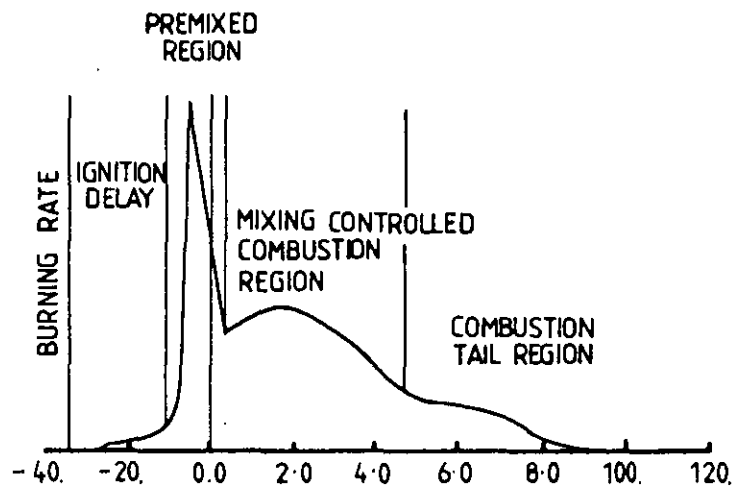


FIG. 1.3 Stages of Diesel Engine Combustion (6)

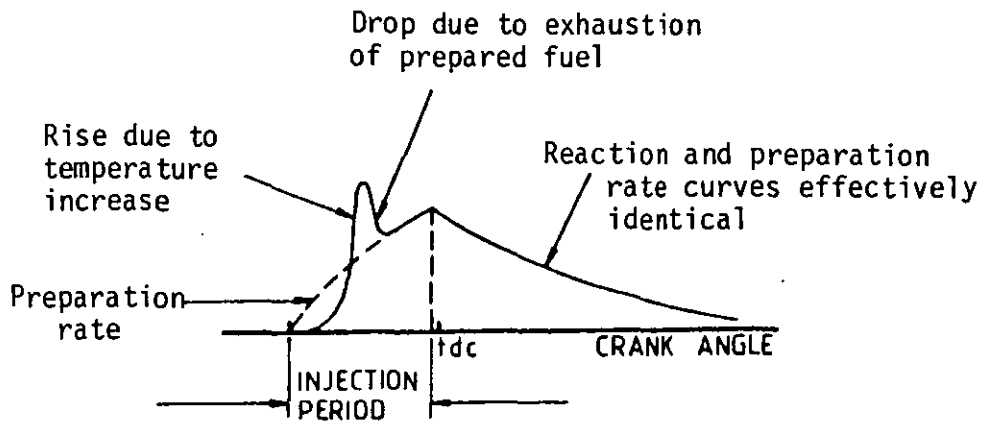


FIG. 1.4 Illustration of Results from which Whitehouse and Way Model (8)

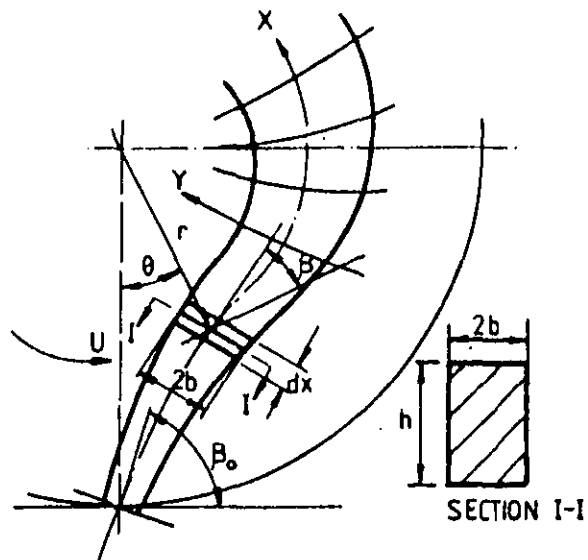


FIG. 1.5 Spray-Geometry in the Model of Adler and Lyn (10)

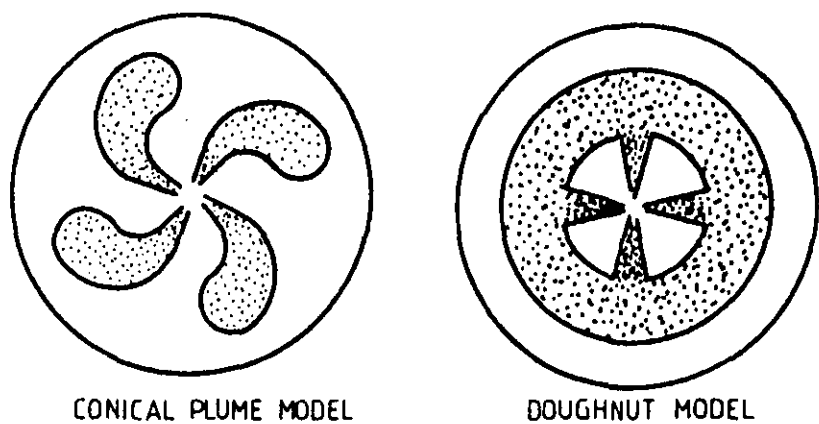


FIG. 1.6 Spray-Geometry for the Air Entrainment Model of Grigg and Syed (11)

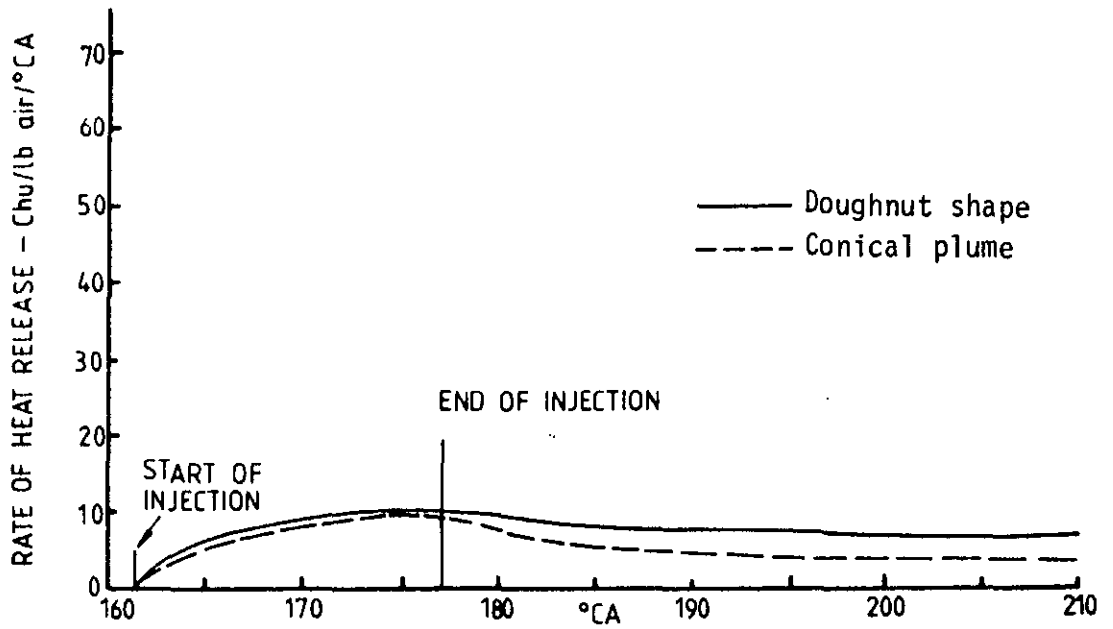


FIG. 1.7 Air Entrainment Rates for Two Spray Configurations (11)

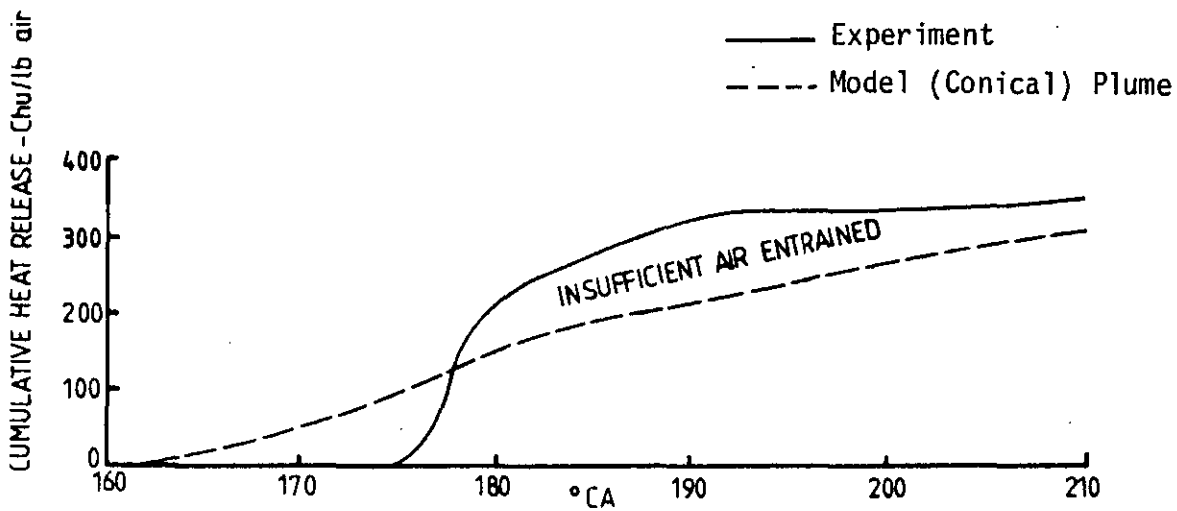
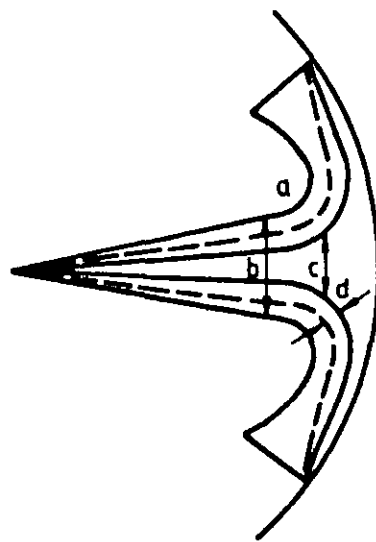


FIG. 1.8 Air Entrainment Rates from Turbocharged and Naturally Aspirated Engines (11)



- a = Surrounding air zone
- b = Entrainment zone
- c = Heat release and NO_x - formation zone
- d = Soot formation zone

FIG. 1.9 Spray Geometry for the CAV Model (13)

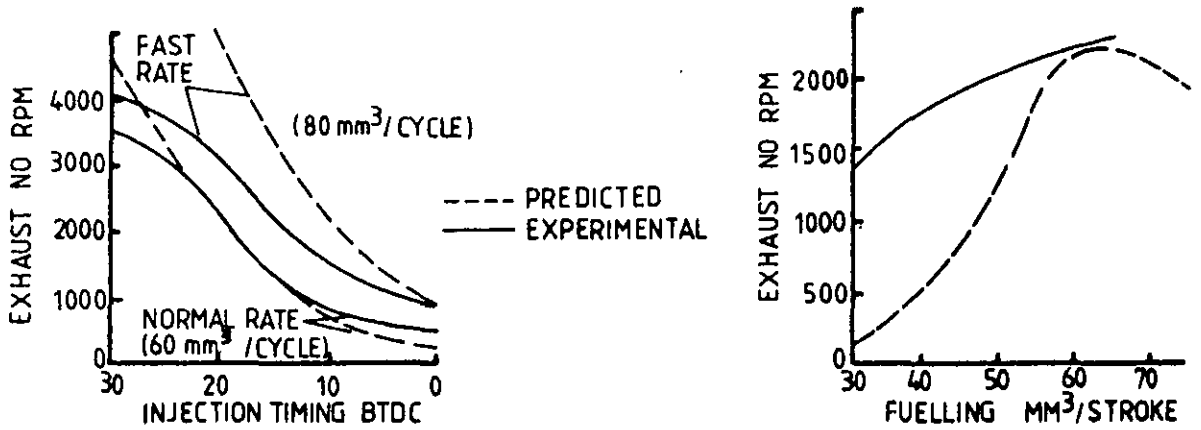


FIG. 1.10 Results of NO_x Predictions from the CAV Model (13)

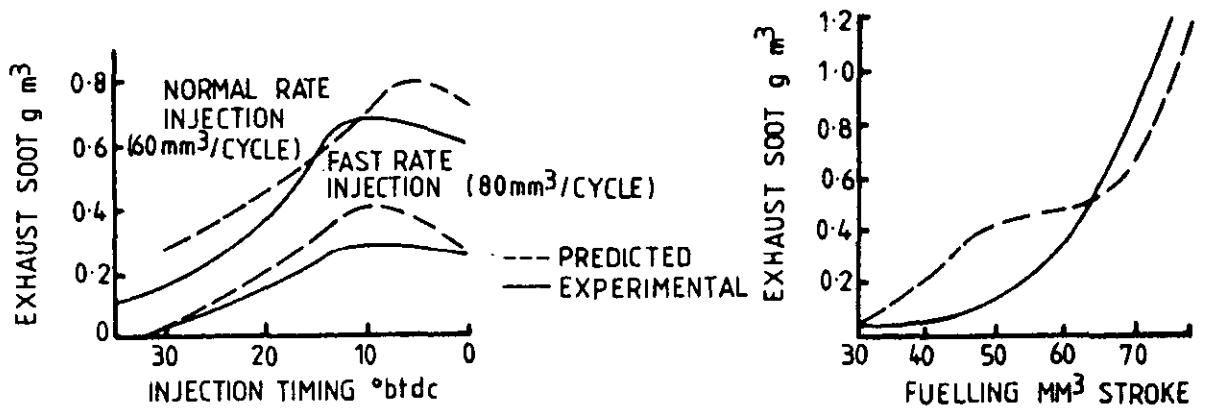


FIG. 1.11 Results of Soot Predictions from the CAV Model (13)

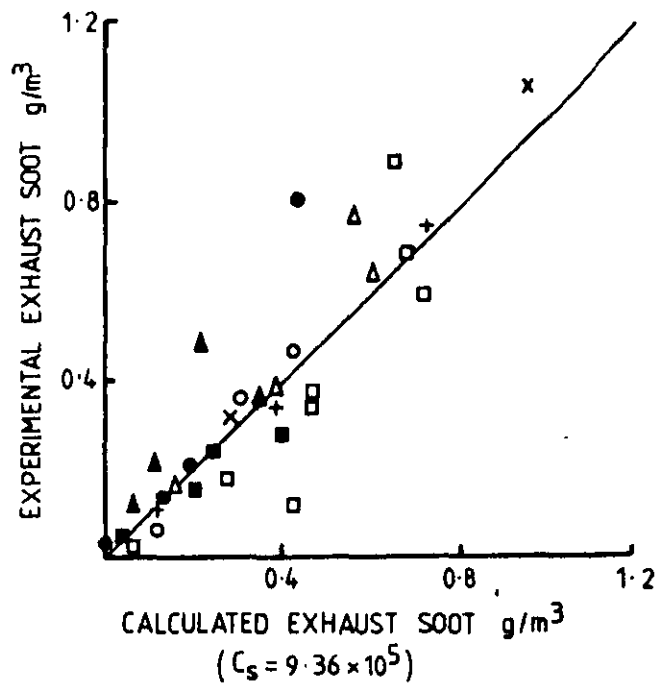


FIG. 1.12 Experimental Versus Calculated Exhaust Soot Values from Khan et al (24)

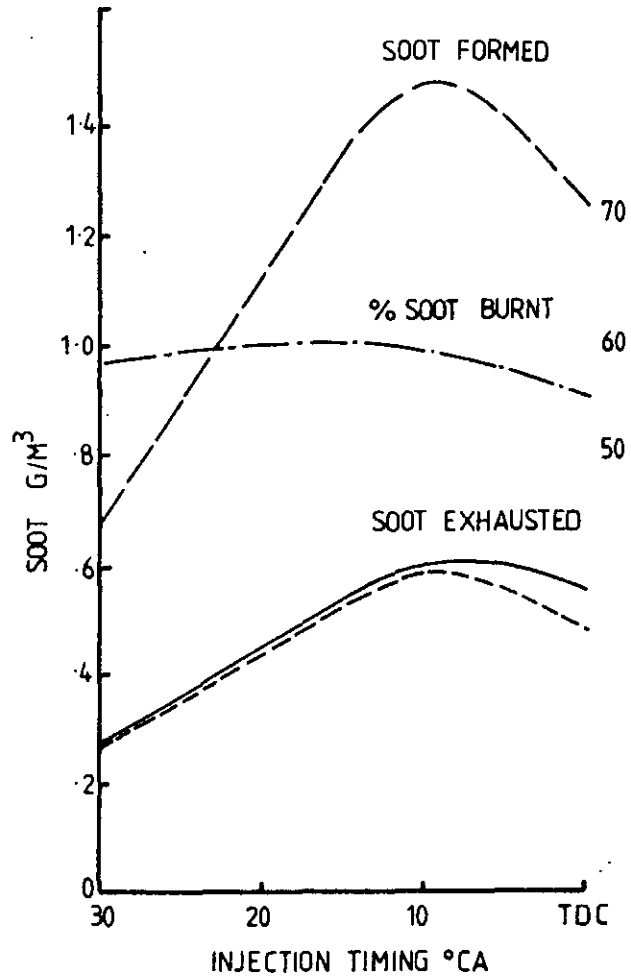


FIG. 1.13 Results of Soot Formation and Oxidation from Khan et al (24)

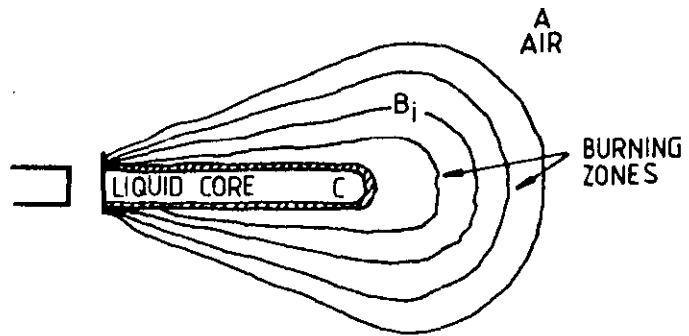


FIG. 1.14 Schematic of Cummins Spray Mixing Model (16)

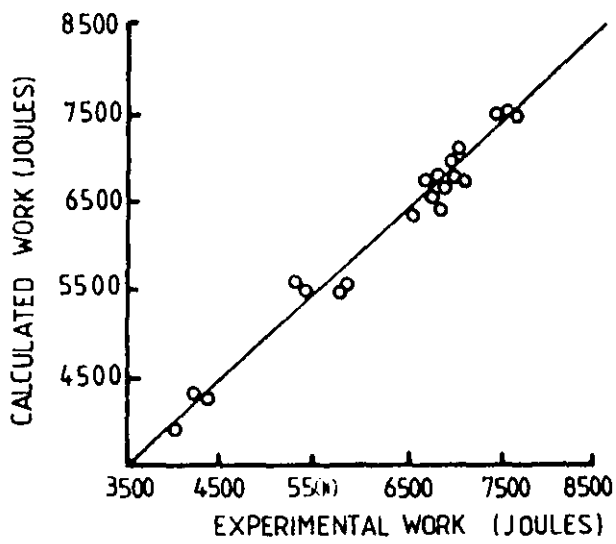


FIG. 1.15 Engine Performance Results from the Cummins Model (27)

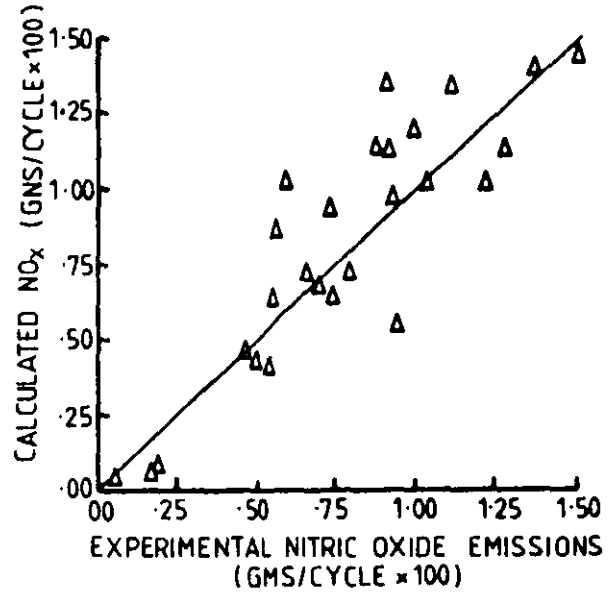


FIG. 1.16 NO_x-Prediction Results from the Cummins Model (27)

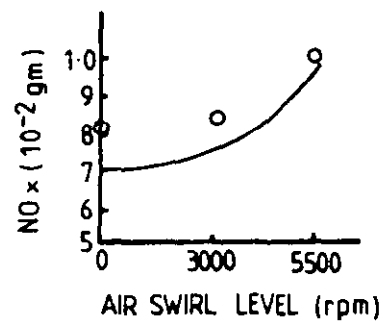
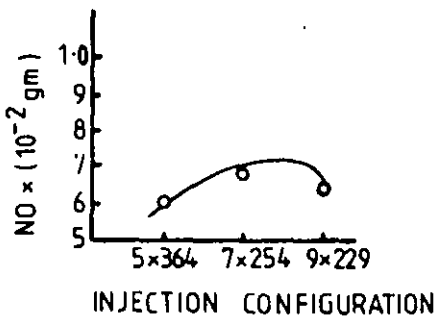
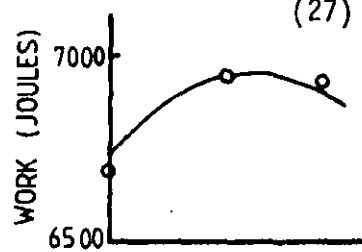
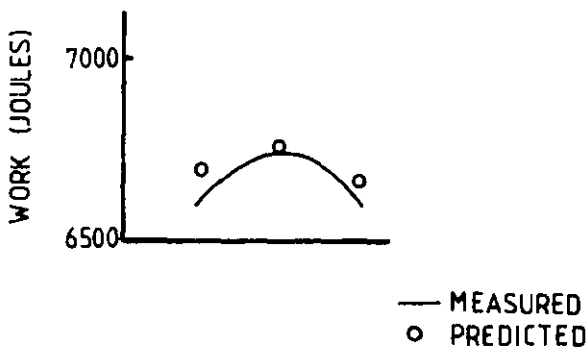


FIG. 1.17 Effect of Injector Hole Size and Air Swirl in the Cummins Model (27)

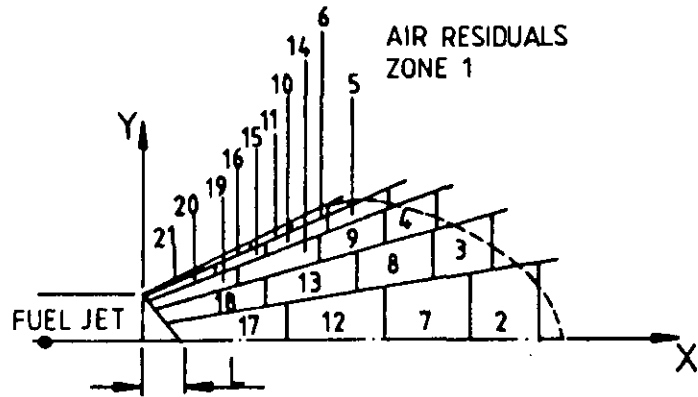


FIG. 1.18 Schematic of Hodgett and Shroff Model (17)

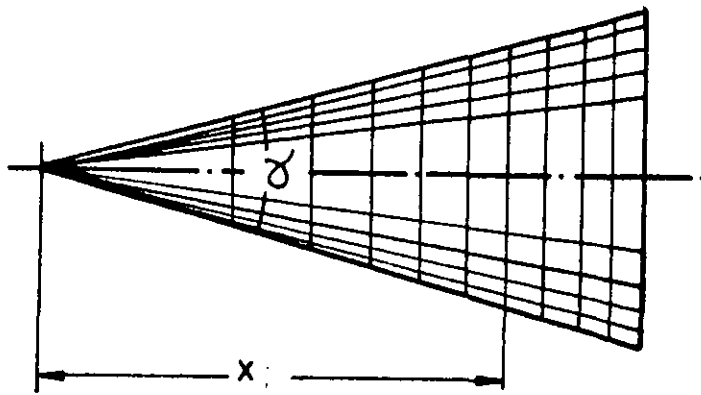


FIG. 1.19 Schematic of Hiroyasu and Kadota's Model (18)

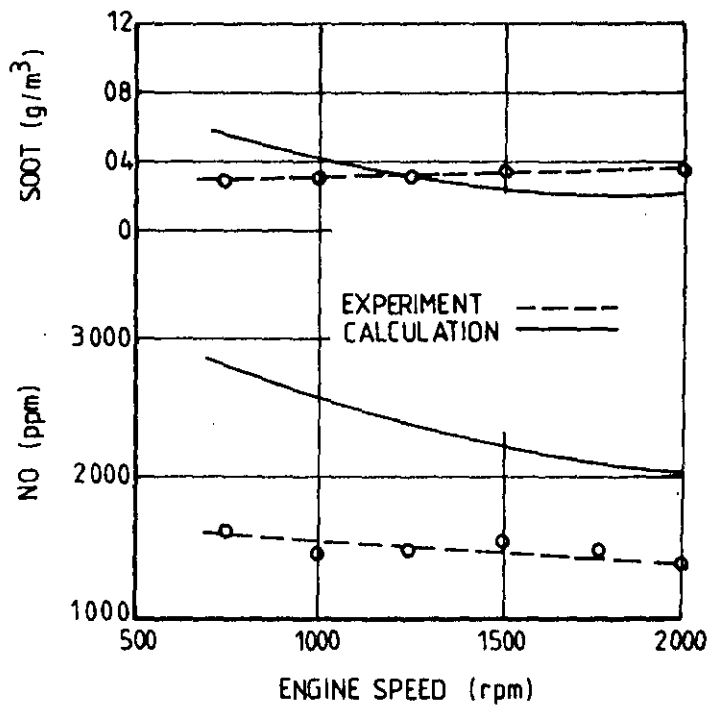
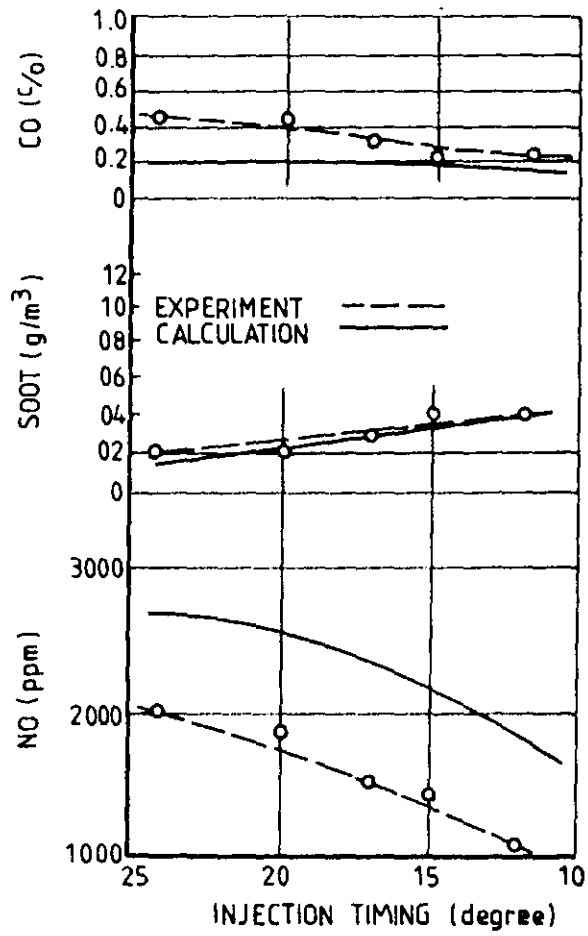


FIG. 1.20 Comparison of Predicted and Experimental Results from Hiroyasu and Kadota (18)

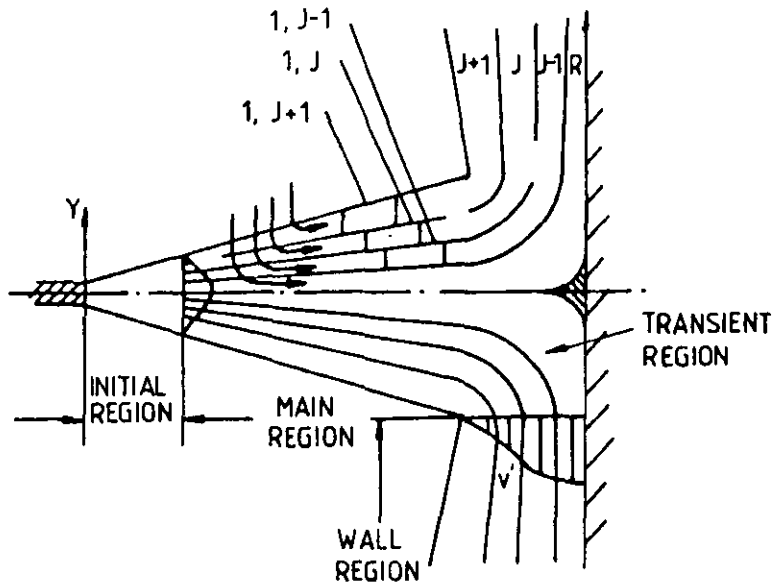


FIG. 1.21 Schematic of the Ultrasystems Model (19)

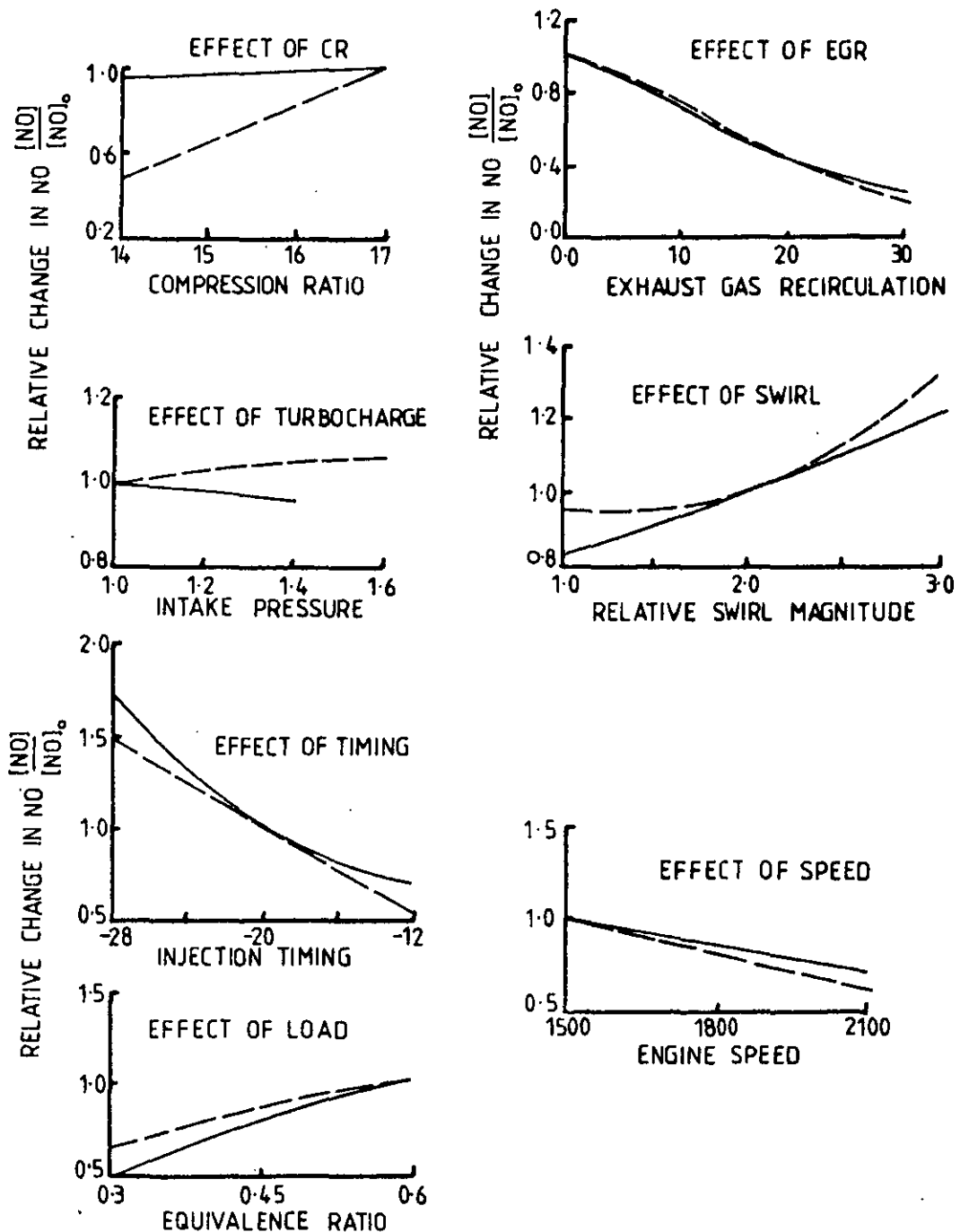


FIG. 1.22 Results from the Ultrasystems Model (19) at Various Operating Conditions

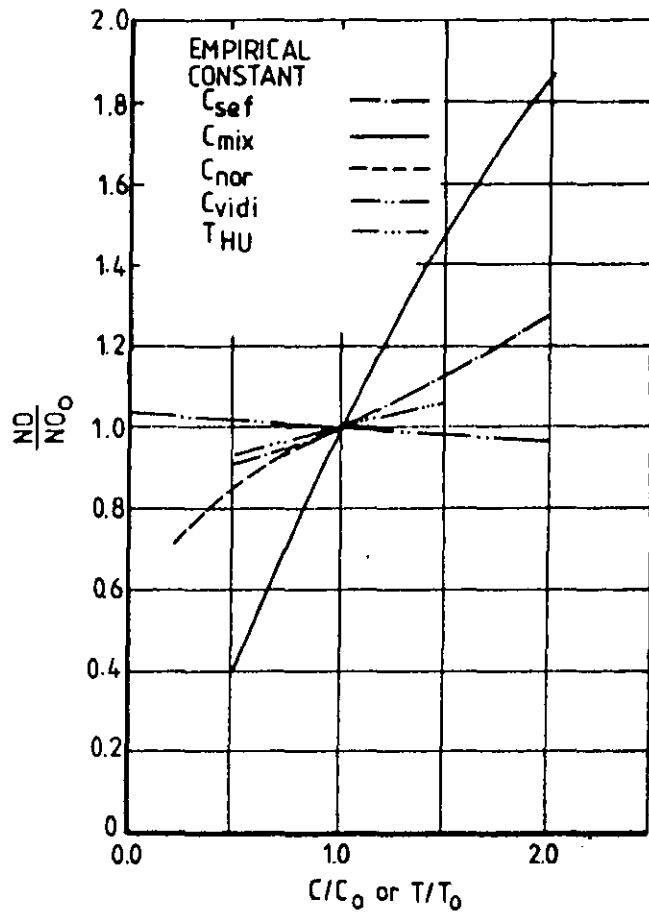


FIG. 1.23 Sensitivity of the Ultrasystems Model (19) to the Empirical Constants

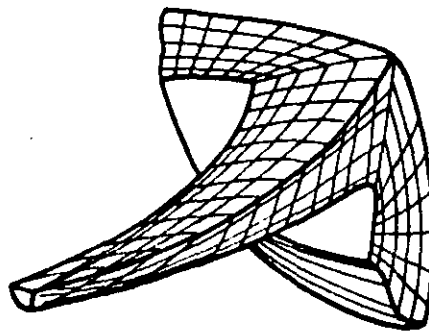


FIG. 1.24 Schematic of the Multi-Zone Model of Meguerdichian and Watson (20)

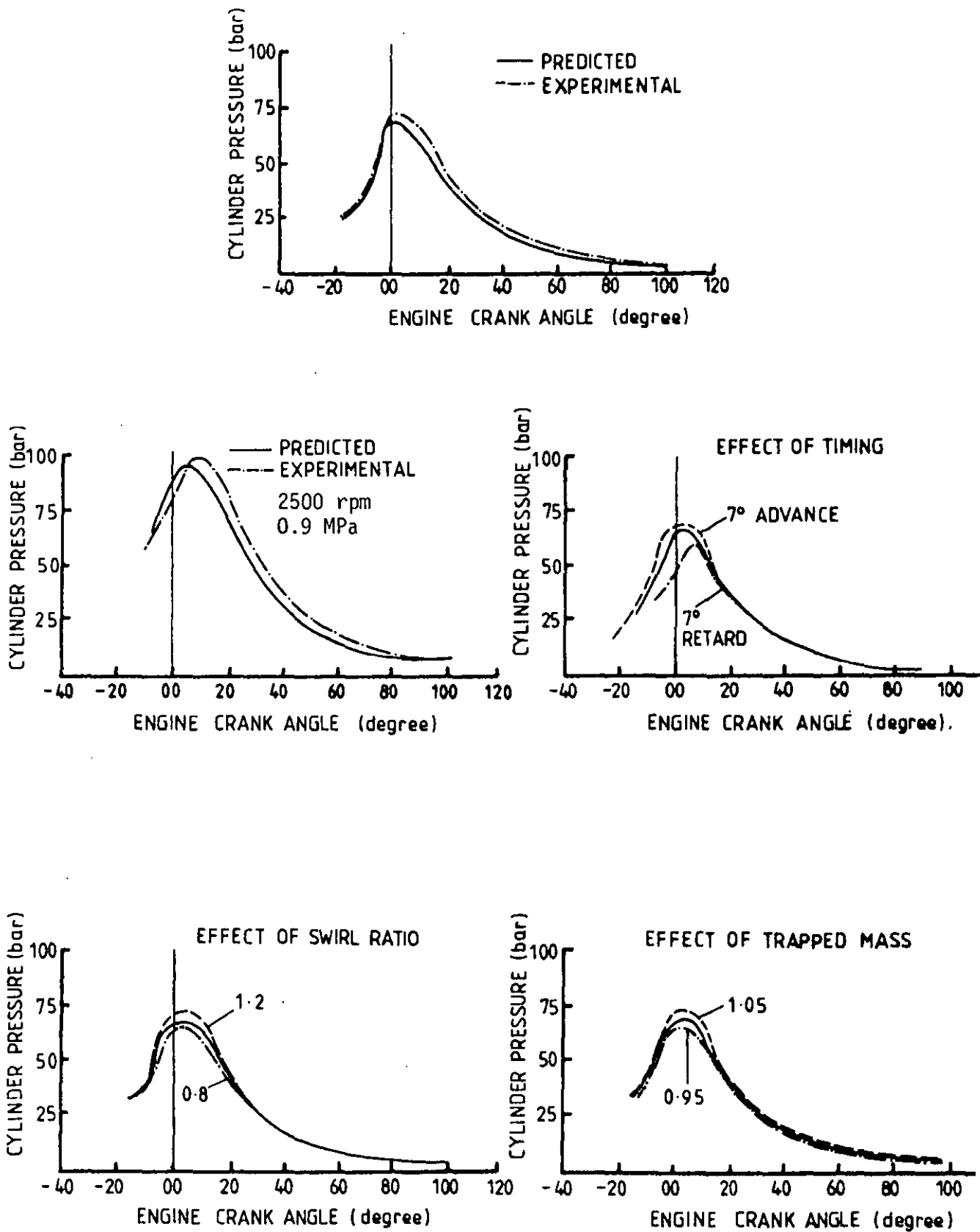


FIG. 1.25 Results of Cylinder Pressure and Parametric Studies from the Multi-Zone Model of Meguerdichian and Watson (20) at speed 1000 rpm and load 0.45 MPa

CHAPTER II
BASIS OF THE PROPOSED MODEL

2.1 Introduction

The proposed model is a synthesis of the equations describing the various engine process mechanisms, in conjunction with a thermodynamic analysis. The simplified process equations are arrived at from the relevant literature. A review of recent studies in related areas enabled better description of the physical and chemical processes of the diesel engine combustion process. The following features are incorporated in the model:

- i) Spray evaporation.
- ii) An air entrainment relationship is used in conjunction with jet penetration, to determine local air fuel ratio in the jet.
- iii) A droplet size distribution is evaluated to account for atomisation.
- iv) The jet structure is decided from two-phase, quasi-steady, turbulent jet theory using similarity profiles for fuel concentration, temperature and velocity in the jet.
- v) Mass transfer theory is used to calculate the vaporisation rate of the fuel with the capability of accounting for the presence of combustion.
- vi) Stoichiometric combustion in regions falling within specified limits of inflammability is postulated.
- vii) The effect of wall impingement is considered.
- viii) Turbulent mixing is characterised in terms of the energy dissipation rate of the injected fuel jets.

The detailed description of the model related to quiescent chamber direct injection diesel engines follows in the next section. However the modifications required for the swirl type engine are described in Chapter V.

The concept of an equivalent diameter (defined as the nozzle diameter through which the fluid is emerging with the same initial momentum and the same velocity, but with the density of the surrounding fluid rather than the nozzle fluid) is given by

$$d_0' = d_0 \sqrt{\frac{\rho_f}{\rho_a}} \quad (2.1)$$

and is consistently used in the model so that the fuel spray in the diesel engine is treated as a confined jet with variable density.

The physical basis of the model is shown schematically in Figure 2.1.

2.2 Physical Basis of Modelling

This section outlines the various elements and the underlying assumptions of the model.

2.2.1 Fuel Injection

Fuel is injected into the high temperature compressed air charge in the engine cylinder. In the absence of a fuel injection model, the complete experimental injection pressure diagram is approximated by straight-line segments.

This is shown in Figure 2.2.

The instantaneous total volume of the engine cylinder is computed from

$$V(\theta) = V_{cl} + \frac{V_s}{2} \left[1 - \cos(\theta) + L_c - \sqrt{L_c^2 - \left(\frac{L \sin\theta}{2}\right)^2} \right] \quad (2.2)$$

where: V_{cl} and V_s are the clearance volume and the swept volume respectively, L and L_c are the stroke and connecting rod length, θ the crank position with respect to top dead centre

The trapped mass and the instantaneous properties of the air in the cylinder are calculated from the slider-crank relationship (equation 2.2), the initial air charge properties, the assumption of a polytropic constant equal to 1.35, and the use of the ideal gas equation of state. The calculation of trapped mass on instantaneous basis as above is found to match within 5 percent of the value obtained from specified experimental results with volumetric efficiency between 85 and 90 percent.

Injected fuel quantity (\dot{Q}) is evaluated from the fuel jet velocity and the nozzle orifice area A_o as indicated below:

$$\dot{Q} = C_d \left(\frac{2 \Delta P}{\rho_f} \right)^{\frac{1}{2}} A_o \quad (2.3)$$

where ΔP is the difference between the fuel line pressure (P_{inj}) and the engine cylinder pressure (P_{cyl}) over the discretised time step, C_d is the orifice discharge coefficient and ρ_f the fuel density.

A suitable mean value of discharge coefficient is adopted in computation such that the quantity of fuel injected over the injection

period attains the prescribed limit. There are two reasons for making such an adjustment, if needed, from a normally recommended (40) value of $C_d = 0.8$. First, the possibility of having lower actual injection pressure than predicted from the simulation of the injector line pressure diagram for the injection system having a long fuel delivery pipe and secondly the error in approximation of the injection diagram itself. A value of the discharge coefficient computed on the basis of local injection conditions will be more representative than adopting a mean value. However, in the absence of a detailed injection pressure simulation in this model, such an assumption is unavoidable.

2.2.2 Spray Penetration

Many expressions are available for the calculation of spray penetration in diesel engines and are reviewed by Hay and Jones (41). They evaluated the twelve of the existing penetration correlations and found that the correlation suggested by Dent (33) covers a wide range of engine conditions. Dent's correlation is based on a large selection of experimental data and is given by the expression:

$$S = (8 U_{\text{jet}} d_o' t)^{\frac{1}{2}} \left(\frac{294.4}{T_a} \right)^{\frac{1}{4}} \quad (2.4)$$

where U_{jet} is the jet velocity $(= (\frac{2 \Delta P}{\rho_f})^{\frac{1}{2}})$, d_o' is the equivalent diameter, ρ_f is the fuel density, t is the time from the start of injection, and T_a is the surrounding air temperature.

The early injection period is outside the range of the above correlation. Hence, for $t < 0.3$ ms, the penetration is calculated using a low value of discharge coefficient ($C_d = 0.39$) following Hiroyasu (29).

$$S = 0.39 \left(\frac{2 \Delta P}{\rho_f} \right)^{\frac{1}{2}} t \quad (2.5)$$

2.2.3 Entrainment

The heat release rate depends on the entrainment of air into the jet. The entrainment process is a consequence of momentum exchange between the fuel spray and its surroundings, hence fluid from the surroundings is drawn radially inward through the jet across its conical surface. The mass flow rate of the injected fluid (\dot{m}_f) across a section at right angles to the jet axis is the function of axial distance (S) from the nozzle.

Air entrainment into the free jet is calculated from the expression of Ricou and Spalding (42). They deduced an expression for mass entrainment rate for axisymmetric turbulent jets from extensive experiments, which has the form:

$$\frac{\dot{m}}{\dot{m}_f} = 0.32 \frac{S}{d_0} \quad (2.6)$$

where \dot{m} ($= \dot{m}_{aE} + \dot{m}_f$) is the total mass flow rate of air entrained (\dot{m}_{aE}) and fuel injected (\dot{m}_f) over the time the jet penetrates to a distance S.

2.2.4 Jet Structure

Since Schweitzer's (23) classical work on spray penetration, many workers (11,13) tended to apply steady state jet theory to attain a simple and more realistic model for diesel engines. An integral solution of mass and momentum equations helped to achieve economy in the computational aspects of the problem. Dent has successfully extended the work of Forstall and Shapiro (43) on co-axial gas jets to the calculation of a penetration formula. It has given adequate support to the use of jet theory in diesel engines. Also, works of Rife and Heywood (44) and Morris (45) established that the description of the fuel spray can be effectively

achieved by jet theory. The assumption of a two-phase quasi-steady jet, and the successful application of fuel mass and momentum conservation equations by Rife and Heywood in rapid compression machine experiments was a useful first step for more elaborate use of this assumption in diesel engine modelling. Successful application of these assumptions to diesel engine combustion models have been discussed by Kau et al (19).

Keeping in mind the fact that droplet behaviour in the jet is to be accounted for, the results of Abramovich (46) for two phase jet growth, and similarity profiles for radial distribution of velocity and mass concentration at any axial position S of the jet are applied in the model. The equations are:

$$\frac{dr_{\text{jet}}}{dS} = 0.11 \left(\frac{\rho_a + \rho_{\text{jet}}}{\rho_{\text{jet}}} \right) \quad (2.7)$$

$$\frac{U}{U_m} = (1 - Y_p^{3/2})^2 \quad (2.8)$$

$$\frac{f}{f_m} = \left(\frac{U}{U_m} \right)^{\frac{1}{2}} \quad (2.9)$$

where r_{jet} is the jet radius, ρ_a the density of air and ρ_{jet} the mean density of fluid within the jet boundary. At any instant, U is the local velocity at the normalised radius $Y_p (= Y/r_{\text{jet}})$, U_m is the jet centreline velocity at penetration S . The fuel mass concentration at Y_p is denoted by f and that at S on the jet centreline by f_m .

The application of mass and momentum conservation equations in conjunction with the entrainment equation (2.6) and similarity profiles for mass concentration and velocity yield f_m and U_m by

the procedure described in Appendix A. The results of the analysis are:

$$f_m = \frac{2 \int_0^{r_{\text{jet}}} \frac{m_{fY_p}}{(1 - Y_p^{3/2})} dY_p}{m_{aE} + m_f} \quad (2.10)$$

and

$$U_m = \frac{P}{R} f_m \quad (2.11)$$

where m_{fY_p} is the mass of fuel at Y_p , and P and R are integral constants defined as:

$$P = 2 \int_0^1 \left(\frac{Y_p}{\beta}\right) \left(\frac{f}{f_m}\right) \left(\frac{U}{U_m}\right) dY_p$$

$$R = 2 \int_0^1 \left(\frac{Y_p}{\beta}\right) \left(\frac{U}{U_m}\right)^2 dY_p$$

β is the density function, expressing the density of the fluid in the jet comprising liquid, vapour and air components, discussed in Appendix A.

Entrainment of heated air from surroundings into the jet requires consideration of jet temperature profiles in a manner similar to that used for velocity and concentration considered above. Thring and Newby (47) and others have shown that mean concentration and temperature profiles are identical, provided the normalised temperature is expressed as follows:

$$\frac{T - T_a}{T_f - T_a} = f \quad (2.12)$$

where T is the local temperature at Y_p , T_a is the surrounding air temperature and T_f is the fuel temperature at the nozzle orifice. The value of fuel temperature is taken between 300-350 K.

The similarity expressed in equation (2.12) is not valid during combustion. Hence, from the start of combustion the local temperatures are computed using the conserved property rule (48) expressed in terms of instantaneous total enthalpy and mass fractions in a simple chemically reacting system (SCRS).

One of the useful conserved properties considered here is the mass fraction of excess fuel defined as:

$$X = \left(X_f - \frac{X_{O_2}}{s} \right) \quad (2.13)$$

where X is the mass fraction of the excess fuel, X_f and X_{O_2} are the fuel and oxidant mass fractions respectively and s is the stoichiometric oxygen-fuel ratio.

With the SCRS model it is assumed that a reaction between two reactants (fuel and oxidant) occurs in fixed proportion by mass to produce a unique product. Also the specific heats of all mixture components and their transport properties are assumed equal at any point in the mixture. Here, these assumptions are applied to the mixture of fuel, air and products in the gaseous state available in radial annular regions considered in the jet. Also, an adiabatic steady-flow mixing process is applied to each of these regions with the stagnation enthalpy term as a conserved property. The contribution of the kinetic energy is neglected to arrive at the stagnation enthalpy:

$$h = C_p T + X_f \cdot H_o \quad (2.14)$$

where C_p is thermal capacity of the mixture and H_o is the enthalpy of reaction.

In Figure 2.3, the fuel vapour stream F_G and the air-products stream A_G flow together to form a mixture M_G . Suffix G indicates the gaseous state of the bulk fluid. An extensive property equation is applied to the system in its general form expressed for any property ψ as

$$f \psi_{f,G} + (1 - f) \psi_{A,G} = \psi_{M,G} \quad (2.15)$$

which leads to

$$f = \frac{\psi_M - \psi_A}{\psi_f - \psi_A} \quad (2.16)$$

Applying conditions prevalent in the combustion situation, that is the F_G stream contains only fuel and A_G stream contains oxidant but no fuel so that

$$X_{f,A_G} = 0, \quad X_{f,F_G} = 1, \quad X_{O_2,F_G} = 0$$

and equating the terms obtained for different mixture stoichiometries in equations (2.13) and (2.14) respectively, we obtain

$$\begin{aligned} \text{i) } \quad f &< f_{st} \\ (T - T_a) / (T_f - T_a + H_o / C_p) &= \\ (-X_{O_2,M_G} / s + X_{O_2,A_G} / s) / (1 + X_{O_2,A_G} / s) & \quad (2.17) \end{aligned}$$

$$\begin{aligned}
 \text{ii)} \quad f &> f_{st} \\
 & \frac{[T - T_a - (X_{O_2, A_G}/s)(H_o/C_p)]}{[T_f - T_a - (X_{O_2, A_G}/s)(H_o/C_p)]} \\
 & = (X_{f, M_G} + X_{O_2, A_G}/s)/(1 + X_{O_2, A_G}/s) \quad (2.18)
 \end{aligned}$$

$$\begin{aligned}
 \text{iii)} \quad f &= f_{st} \\
 & (T - T_a)/(T_f - T_a + H_o/C_p) \\
 & = (X_{O_2, A_G}/s)/(1 + X_{O_2, A_G}/s) \quad (2.19)
 \end{aligned}$$

where X_f and X_{O_2} are local fuel and oxygen mass fractions respectively. H_o is the enthalpy of reaction and C_p is thermal capacity of the mixture. Suffix st represents the stoichiometric condition.

For computing local temperature (T) from the above equations, the value of mass fractions using similarity profiles are used. The value of fuel temperature T_f and thermal capacity C_p are assumed equal to the local saturation temperature (0.9 times the critical temperature for conditions near critical point) and 1100 J/kg K respectively. The effect of heat transfer and dissociation are neglected in the derivation of the above equations.

2.2.5 Droplet Size and Distribution

The atomisation and dispersion characteristics of fuel sprays are of importance in obtaining efficient combustion with low smoke emissions in the direct injection diesel engine. Availability of data on fuel spray atomisation and droplet size distribution are scarce in the literature. However, droplet size distribution correlations can give some indication of the effects of atomisation.

It is assumed here that the quantity of fuel injected over a discretised time interval is atomised and distributed in size around an instantaneous Sauter Mean Diameter (SMD), computed from the relation of Knight (49) which can be written in the form:

$$\text{SMD} = 8.0 \Delta P^{-0.458} \dot{Q}^{0.209} \nu_f^{0.215} \quad (2.20)$$

where ν_f is the kinematic viscosity of the fuel.

The distribution of droplet size as a function of the cumulative volume fraction (V_{cf}) of the injected fuel was obtained from Simmons' (50,51) extensive correlations of gas turbine spray droplet data in the normalised size range $0.082 < (d_p/\text{SMD}) < 3$. The applicability of Simmons' findings to the diesel engine case were verified by comparison with the experimental data of Lee (52) and Retel (53). The comparison obtained over a range of conditions are shown in Figure 2.4. The list of conditions are given in Table 2.1. The cumulative volume fraction (V_{cf}) as a function of the normalised droplet diameter $D_p = d_p/\text{SMD}$ in the range $0.082 < D_p < 3$ is

$$V_{cf} = \exp(0.05328 D_p - 0.54174 D_p^2) \quad (2.21)$$

In the discretised time step it is assumed that the droplets in the normalised size range 0.082 to 3 are distributed radially

TABLE 2.1

Test conditions for atomisation data of Figure 2.4

Test condition	Range	
	Lee (52)	Rete1 (54)
Injection pressure (bars)	30-400	150-450
Air density (kg/m ³)	4.9-25	-
Orifice diameter (mm)	0.2032-0.762	0.4
Orifice length/diameter	0.5-6	1-5
Cylinder pressure (bars)	-	1-30

according to the concentration profile described by equation (2.9) and the cumulative volume fraction equation (2.21) such that the decrease in droplet size with radius is equal to the rate of change of injected fuel volume fraction with radius, divided by the rate of change of cumulative volume fraction with droplet size. Expressed algebraically this is

$$-\frac{dD_p}{dY} = \frac{1}{V_{fi}} \frac{\left(\frac{dV_{fi}}{dY}\right)}{\left(\frac{dV_{cf}}{dD_p}\right)} \quad (2.22)$$

where V_{fi} is the volume of fuel injected.

Simmons, using a binary droplet division model for atomisation, showed that in the normalised droplet diameter range $0.082 < D_p < 3$ there are sixteen classes of droplet size. In the present study it is assumed that the size classification results in a set of radial annular sectors each containing droplets of a particular normalised diameter D_p , with the largest droplets on the jet axis and

the smallest at its edge. This would appear reasonable in the light of the experimental studies of Lee (52).

Simmons suggested the binary division model for atomisation such that each successive division of droplets resulted in two equal size droplets of diameter = $\sqrt[3]{1/2}$ X the diameter of the originating drop. In droplet size range $0.082 < D_p < 3$, this results in 16 classes shown schematically in Figure 2.5. The representation of droplet classes following a geometric progression in normalised diameter can be expressed as:

$$\Delta D_p = \left(\frac{D_{p_{\max}}}{D_{p_{\min}}} \right)^{1/n} \quad (2.23)$$

where ΔD_p is the interval size in normalised droplet diameter and n is the number of droplet classes.

The droplet sizes obtained using this classification coincide with the size classification of Simmons. Further, it was found in the present study that the droplet sizes could conveniently be represented by ten classes following a geometric progression without affecting evaporation results. The droplet sizes in these ten classes are represented in Figure 2.6.

With the specified values of D_p and the use of equations (2.9), (2.21) and (2.22), a numerical solution for Y_p is obtained. The details are outlined in Appendix B.

In the presence of evaporation there will be a reduction in droplet size between successive discretised time intervals, therefore a redistribution of droplet size is carried out at the end of each time interval.

The redistribution procedure is suggested assuming that;

- i) there are j sizes of droplets represented by diameters d_{p_j} ($j = 1, 11$) respectively.

- ii) the new diameters of droplets, on evaporation, are represented by d'_{p_j} for all the classes of droplets,
- iii) the reduced droplet sizes fall within the limits of two specified droplet sizes, say k and $k+1$ respectively, such that

$$d_{p_k} < d'_{p_j} < d_{p_{k+1}}$$

Now redistribution on a weighted volume and surface area basis is represented by

$$N_{p_j} d_{p_j}'^3 = N_{p_k} d_{p_k}^3 + N_{p_{k+1}} d_{p_{k+1}}^3 \quad (2.24)$$

$$N_{p_j} d_{p_j}'^2 = N_{p_k} d_{p_k}^2 + N_{p_{k+1}} d_{p_{k+1}}^2 \quad (2.25)$$

where N_{p_j} , N_{p_k} and $N_{p_{k+1}}$ are the number of droplets in size d_{p_j} ,

after partial vaporisation, and in sizes d_{p_k} and $d_{p_{k+1}}$ after redistribution.

Simultaneous solution of equations (2.24) and (2.25) determines the value of droplet numbers in sizes k and $k+1$ and hence the volume and mass of droplets in these respective classes. These masses are added to the mass available from distribution of injected fuel at any instant during the period of injection.

It should be noted that the redistribution results in a reduced number of droplets in each sector. When evaporation is very rapid, the redistribution will not occur in the immediately adjacent sector. Droplets falling outside the lowest size limit are considered as vapour.

The number of droplets (N_p) in any annular radial sector is obtained from:

$$N_p = \frac{V_p}{\frac{\pi}{6} d_p^3}$$

where V_p is the total volume of droplets of diameter d_p at Y_p .

Figure 2.7 is a schematic of the sequence of events described above.

At the end of injection, this distribution and redistribution procedure becomes inoperative. Instead a mean value of Sauter Mean Diameter is computed following the definition:

$$SMD = \frac{\sum N_p d_p^3}{\sum N_p d_p^2}$$

where N_p and d_p are the number of droplets and their diameter in respective sizes at the last instant of the injection process. Subsequently the evaporation is considered based on this SMD value with reduction in total number of droplets from instant to instant.

2.2.6 Droplet Evaporation

The evaporation of fuel sprays containing droplets of a wide range of sizes is a complex phenomenon. Kamimoto and Matsuoka (54) demonstrate that consideration of fuel evaporation is of importance in diesel engine combustion calculations. In large engines having high injection rates and long injection periods, the heat absorption during evaporation of droplets need consideration in heat release predictions. There are various correlations (55-58) proposed as a

result of experimental studies limited to an isolated droplet at atmospheric or near atmospheric pressure. The spray behaviour based on an isolated droplet assumption has successfully been verified by Kamimoto and Matsuoka (54). Their results have shown reasonable trends using the correlation of Ranz and Marshall (56), which is

$$\text{Nu} = 2 + 0.6 \text{Re}^{1/2} \text{Pr}^{1/3} \quad (2.26)$$

where Reynolds Number (Re) is based on the droplet diameter and local velocity at Y_p . Prandtl number (Pr) is taken equal to 0.7. During evaporation, the effect of relative velocity of the droplets was considered important by Kamimoto and co-worker.

From the onset of combustion, an appreciable reduction of the relative velocity between the droplet and the surrounding atmosphere reduces the drag force on the droplet. Bolt and Saad (59) from experimental studies on various fuels found that the existence of the flame around and in the wake of the droplet tends to decrease the drag force. Hence the assumption of Nusselt number equal to 2 holds for the calculation of mass transfer rate from the droplet surface.

On this basis, the present study includes the isolated droplet model and uses equation (2.26) during evaporation and assumes value of $\text{Nu} = 2$ after the start of ignition.

Calculation of mass transfer rate (\dot{m}'') from the droplet surface follow from the Reynolds Flow model, illustrated in Figure 2.8. According to this model the mass transfer rate per unit surface area is given by

$$\dot{m}'' = g.B \quad (2.27)$$

where g is the conductance, and B is the driving force.

In the case of intense mass transfer situation, it can be shown from Kays (60) that the Reynolds hypothesis can be modified as

$$\dot{m}'' = g^* \ln(1 + B) \quad (2.28)$$

and

$$\frac{g}{g^*} = \frac{\ln(1 + B)}{B} \quad (2.29)$$

where g^* is the convective mass transfer conductance = $\left(\frac{h}{C_p}\right)$.

Assuming Lewis number (Le) equal to unity, g^* is obtained from Nu in equation (2.26) as

$$g^* = \frac{h}{C_p} = \frac{k Nu}{d_p C_p} \quad (2.30)$$

where k is the thermal conductivity, and C_p the specific heat.

The driving force B is a dimensionless quantity and it represents the ratio of conserved properties in the mass-transfer flux and the Reynolds flux. The value of B is evaluated from conservation laws - mass conservation or energy conservation. Hence, the transfer number is represented by

$$B_m = \frac{X_{f,G} - X_{f,S}}{X_{f,S} - 1} = \frac{\dot{m}''}{g} \quad (2.31)$$

and

$$B_h = \frac{C_p (T_G - T_S)}{[h_{fg} + C_{pf} (T_S - T_0)]} = \frac{\dot{m}''}{g} \quad (2.32)$$

respectively, where T_G and T_S are the temperatures of the air vapour mixture surrounding the droplets, and the droplet surface respectively. The corresponding fuel vapour mass fractions are $X_{f,G}$ and $X_{f,S}$. $[h_{fg} + C_{pf} (T_S - T_0)]$ is the specific enthalpy of saturated fuel vapour at T_S relative to a datum temperature T_0 . Equation (2.32) is solved for T_S and B . The evaluation of B is based on an iteration between expressions (2.31) and (2.32) in order to reach a common solution due to intersection of B_m and B_h curves shown in Figure 2.9(a).

Under engine conditions which support rapid evaporation, the possibility exists for the presence of localised saturated air-vapour states (that is $B = 0$). Under these conditions, localised droplet evaporation will cease.

In the presence of combustion, the Transfer Number must be modified (61). Under these conditions, evaporation from a fuel rich surface to an oxygen rich gaseous state results in equations (2.31) and (2.32) taking the form:

$$B_m = \left(\frac{\frac{X_{O_2,G}}{s} + X_{f,S}}{1 - X_{f,S}} \right) \quad (2.33)$$

and

$$B_h = \frac{[C_p (T_G - T_S) + \frac{X_{O_2,G}}{s} H_0]}{[h_{fg} + C_{pf} (T_S - T_0)]} \quad (2.34)$$

respectively,

where T_G and T_S are the temperatures of the air-vapour-product mixture surrounding the droplets, and the droplet surface respectively.

The corresponding oxygen and fuel vapour mass fractions are $X_{O_2,G}$ and $X_{f,S}$. s is the stoichiometric constant for fuel-oxygen mixture and H_0 is the enthalpy of reaction.

Under supercritical conditions, the B_m and B_h curves do not intersect, Figure 2.9(b), hence it is impossible to obtain an iterative solution. Therefore, the evaporation rate is calculated using only equation (2.32) or (2.34) whichever is applicable. This follows from the work of Natarajan and Brzustowski (61). The value of T_S is equal to 0.9 times the critical temperature of the hydrocarbon fuel.

Further, since the mass evaporation rate equals the time rate of change of mass of the droplet, equation (2.27) and (2.30) together can yield an expression for the reduction in droplet diameter which is:

$$-\frac{\Delta d_p}{\Delta t} = 2 \frac{\dot{m}''}{\rho_f} \quad (2.35)$$

The evaluation of mean properties during evaporation and combustion are discussed in Appendix C.

The verification of the evaporation model is carried out using unpublished experimental results (62) obtained in the I.C. Engines Laboratory of the Mechanical Engineering Department, Loughborough University. These experiments were conducted in a combustion bomb using laser interferometric techniques. The comparisons of these results with model predictions are shown in Figure 2.10 for various sets of data given in Table 2.2. A comparison of air-fuel ratio contours with experimental data is also shown in Figure 2.11 for data set B. The good agreement between experimental and model results validates the use of the above calculation procedure.

TABLE 2.2

Experimental conditions for study of transient n-Pentane jet (0.21 mm orifice diameter) in a bomb system

Code	Nozzle opening press bars	Injection quantity mm ³ /injection	Injection duration m sec	Bomb condition	
				press bars	Temp K
A	110	7.0	1.2	3	433
B	110	7.0	1.2	3	403
C	110	11.0	1.5	3	403
D	110	11.0	1.5	6	403
E	110	7.0	1.2	6	403

2.2.7 Impingement and Wall Jet Structure

The position of the jet in the engine cylinder is determined from simple geometric considerations of the piston shape and jet penetration. Figure 2.12 shows that the relative position of the jet tip with respect to the wall distance (H) is considered to decide the impingement on the engine cylinder wall. The spray angle α_0 will control the position of the point of impingement of the jet. The distance along the jet axis from the impingement surface at which the free jet plume begins to diffuse and form a wall jet is computed from Giralt et al (63). The onset of impingement, and the commencement of deflection of the free jet is given by following relationships:

$$Y_w = 1.2 d_0' \quad \text{for} \quad \frac{H}{d_0'} < 6.8 \quad (2.36)$$

or

$$Y_w = 0.153 \frac{H}{d_0'} \quad \text{for} \quad \frac{H}{d_0'} > 6.8 \quad (2.37)$$

where Y_w is the distance of the wall jet from the wall.

Figure 2.13 schematically represents the impingement and wall jet regions.

The wall jet analysis based on a quasi-steady assumption is essentially that described by Rajaratnam (64) with the effects of viscous friction at the wall neglected. The similarity profiles given by equations (2.8) and (2.9) are assumed to hold over the wall jet, the width of the wall jet at any wall penetration distance S_w is denoted by b . This assumption in the present work implies that the effect of the boundary layer adjacent to the wall of thickness δ is neglected and the region further from the wall is essentially that found in a free jet.

In the impinging region, Era and Saima (65) observed that the boundary layer thickness δ is about one-third of the half-velocity width ($b_{1/2}$) of the wall jet and decreases rapidly with increase in nozzle Reynolds number.

The wall jet penetration (S_w) is obtained from the equation for decay of the wall jet maximum velocity U_{m_w} with distance S_w . The wall jet penetration is derived in a similar manner to that for the free jet (33). Rajaratnam (64) showed that the decrease of maximum wall jet velocity U_{m_w} with S_w is directly related to the jet orifice conditions U_o and d_o' by the relation

$$U_{m_w} = 1.03 U_o d_o' / S_w \quad (2.38)$$

but

$$U_{m_w} = \frac{dS_w}{dt} \quad (2.39)$$

hence by substitution for (2.39) in (2.38) and integrating

$$S_w = (2.06 U_{jet} d_o' t_w)^{1/2} + C \quad (2.40)$$

but

$$S_w = 0 \text{ at } t_w = 0$$

resulting in

$$C = 0$$

where t_w is time from commencement of the wall jet.

The air entrainment rate into the wall jet is calculated from the following empirical equation of Hertel (66):

$$\frac{\dot{m}_{aw} + \dot{m}_f}{\dot{m}_f} = 0.865 \frac{S_w}{d_o'} \quad (2.41)$$

The origin of S_w is considered to be the intersection of the jet axis and the impingement surface.

The jet width (b) perpendicular to the wall is expressed in terms of ($b_{\frac{1}{2}}$), the distance between the position of maximum velocity and the point where the velocity has reached half its maximum value at a given S_w from reference (64)

$$b_{\frac{1}{2}} = 0.087 S_w \quad (2.42)$$

The total jet width is assumed equal to three times $b_{\frac{1}{2}}$, this follows from results of reference (65).

The application of similarity profile (equation 2.9) in the outer region of the wall jet is verified from results (62) obtained in our laboratory and is shown in Figure 2.14.

2.2.8 Ignition Delay

There are several empirical ignition delay formulae available in the literature. Most of these relationships show that the ignition delay can be expressed in the form:

$$\text{i.d.} = \frac{A e^{\frac{E/R_u T}}{p^n}} \quad (2.43)$$

where A is the constant specified for each combustion chamber, E is an exponent dependent upon the properties of the fuel, T is the absolute temperature, p is the absolute pressure and n is an exponent determined experimentally.

The commonly used formulae in engine studies include those of Wolfer (67), Tsao (35), Shipinski (9), Sitkei (68), Stringer (69), and Hiroyasu (70). A summary of these equations is given in Table 2.3.

Wolfer's equation is for the pressure rise delay in a constant volume vessel and follows the form of equation (2.43). Hiroyasu calculated ignition delay for various fuels in a constant volume vessel. He introduced the percentage oxygen in the pre-exponential term and gave the values of the constants and exponents. Shipinski's formula includes the fuel cetane number.

Sitkei provided a formula for the illumination delay in a pre-chamber engine. He uses the multiphase character of the hydrocarbon ignition. The equation includes three terms, the first term describes the physical ignition delay due to evaporation, the second due to premixed flame, and the third for the diffusive burning flame.

The equation presented by Tsao et al (35) is for the temperature rise delay in a modified CFR open chamber engine. Stringer proposed another form for the ignition delay from data obtained in a steady flow system

$$\text{i.d.} = \frac{1}{p^{n'} (BT - K)} \quad (2.44)$$

The values of constants B and K , and exponent n' for various fuels are available in his work.

In a recent study, Hardenberg and Hase (71) presented an empirical relationship for the pressure rise delay in direct injection

TABLE 2.3

List of Various Ignition Delay Correlations

Author	Correlation	Remarks
Wolfer	$\text{i.d. (ms)} = 0.398 \times 10^6 P^{-1.19} e^{\left(\frac{4650}{T}\right)}$	P and T are pressure and temperature respectively at the point of ignition
Tsao	$\text{i.d. (ms)} = \left(\frac{8.48 \times 10^5}{P} + 0.415\right) \left\{ \left(1.332 - \frac{1210}{T}\right) \text{RPS} + \left(\frac{26.36 \times 10^3}{T} - 26.66\right) + (1.8 \times 10^{-3} T - 1.45)(16.66 - \text{RPS}) \right\}$	P and T are pressure and temperature respectively at the point of injection, RPS is engine speed (s^{-1}).
Hiroyasu	$\text{i.d. (ms)} = 3.05 \times 10^6 P^{-1.31} \phi^{-2.02} e^{\left(\frac{4350}{T}\right)}$ $\phi = \frac{p_{O_2}}{0.21 P}$	P and T are pressure and temperature respectively at the point of ignition. p_{O_2} is partial pressure of oxygen in the O_2 fuel air mixture at the point of ignition
Shipinski	$\text{i.d. (ms)} = 10.472 P^{-0.386} CN^{-0.69} e^{\left(\frac{4644.4}{T}\right)}$	P and T are mean pressure and temperature respectively during delay period. CN is fuel cetane number
Sitkei	$\text{i.d. (ms)} = 0.5 + (430.86 P^{-0.7} + 4.915 \times 10^9 P^{-1.8}) e^{\left(\frac{3927.5}{T}\right)}$	P and T are mean pressure and temperature respectively during delay period

/Continued...

TABLE 2.3 ... continued

Author	Correlation	Remarks
Stringer	$\text{i.d. (ms)} = 1.428 \times 10^4 \frac{p^{-0.83}}{(0.216 \times 10^{-3} T - 0.1506)}$	P and T are mean pressure and temperature respectively during delay period
Hardenberg and Hase	$\text{i.d. (ms)} = \frac{1000}{\text{RPS}} [(0.36 + 0.22 v_p) e^{\{E_A (\frac{1}{R_u T_i r^{c-1}} - \frac{1}{17190}) + (\frac{21.2}{p_i r^{c-12.4}})^{0.63}\}}]$ $c = k - \frac{k-1}{(F v_p + 1)} ; k_j = 1.4, F = 1.1$ $E_A = (\frac{618840}{\text{CN} + 25}) \text{ J/mole}$	v_p = mean piston speed R_u = universal gas constant T_i & P_i = intake temperature and pressure respectively. r is compression ratio and CN is fuel cetane number

diesel engines. Their analysis was based on a large number of experimental data from naturally aspirated and turbocharged diesel engines. The correlation obtained is a functional relationship of fuel quality and the pressure and temperature in the cylinder during the delay period, and a mean polytropic exponent c was determined as a function of the piston speed, to specify the mean pressure and temperature conditions at the point of ignition calculated from intake manifold conditions. The effect of cetane number is included in finding the activation energy

$$E_A = \frac{618840}{CN + 25} \text{ J/mole} \quad (2.45)$$

An extensive study using about two hundred data points from three engines and the above correlations of the ignition delay showed (see Figure 2.15) that the empirical correlation of Hardenberg and Hase (71) is the most suitable. Table 2.4 shows the value of correlation obtained in each case. The specifications of the engines used for ignition delay are given in Table 2.5. The data points include various conditions of injection pressure, fuelling rate, orifice diameter, turbocharging ratio, intake temperature and engine dimensions.

A comparison between experimental and predicted delay data using Hardenberg and Hase's correlation is shown in Figure 2.16. On rejecting about twenty percent data points which fall beyond twenty percent accuracy of the experimental results, the correlation was further improved. These data points are shown separately on the diagram and are found to be mainly for low load and retarded injection timing conditions. Hardenberg and Hase's equation is, therefore, found unsuitable for these conditions. This is attributed to the fact that the calculation of polytropic exponent c in these two cases will be in error, particularly under the highly retarded injection timings of some of the data used.

TABLE 2.4

Values of correlation coefficient for various ignition delay formulae

Author	Correlation
Wolfer	0.65
Tsao	0.54
Shipinski	0.25
Sitkei	0.21
Stringer	0.10
Hiroyasu	0.66
Hardenberg	0.77

TABLE 2.5

Engine specifications for ignition delay correlation

	Engine 1	Engine 2	Engine 3
Bore (mm)	216	100	140
Stroke (mm)	241	128.6	152
Compression ratio	12.9	18.8/17.26	14.3
Fuel cetane number	47	54.7	43

2.2.9 Combustion

Following the ignition delay period, combustion in the spray occurs in regions where actual fuel vapour to air ratio (ϕ_v) falls within the limits of inflammability. These limits are $0.028 < \phi_v < 0.2$ in accordance with Halstead et al (72).

In each of the burning regions stoichiometric combustion is postulated. In a discretised time step, the mass of fuel burned (dm_{vb}) and the air consumption in burning (dm_{ac}) are calculated depending upon actual mixture conditions in that region at that instant. The calculation of these masses follow from Table 2.6.

TABLE 2.6

Calculation of fuel and air mass consumption during combustion

	Lean region $\phi_v < 1$	Rich region $\phi_v > 1$
Mass of fuel burnt	Total fuel mass available	Stoichiometric fuel vapour-air ratio times the mass of available air
Mass of air consumed	Stoichiometric air-fuel ratio times the mass of fuel available	Total mass of air available

These two masses add up to give the total mass of combustion products in each sector.

In a discretised time interval, the amount of heat release (dQ_{rel}) due to combustion is given by

$$dQ_{rel} = dm_{vb} H_o \quad (2.46)$$

where H_0 is the enthalpy of reaction of fuel.

2.2.10 Heat Transfer

Heat transfer from hot cylinder gas to the wall is given as

$$\dot{Q}_{tr} = h_i A_c (T_{ch} - T_w) \quad (2.47)$$

where A_c is the area of the engine cylinder head, piston and wall surfaces, h_i is the instantaneous heat transfer coefficient, and T_{ch} and T_w are the mean cylinder gas and wall temperatures respectively.

The instantaneous heat transfer coefficient (h_i) is calculated using Woschni's correlation (30)

$$h_i = 0.01279 p^{0.8} D^{-0.2} T^{-0.53} \left[C_1 v_p + C_2 \frac{V_S}{V_1} \frac{T_1}{p_1} (p - p_0) \right]^{0.8} \quad (2.48)$$

where v_p is the mean piston speed, V_S is the swept volume and p_0 is the instantaneous motoring pressure. The constants C_1 and C_2 are assumed to be 2.28 and 0.00324 m/s °C respectively during compression and expansion strokes, as indicated by Woschni. The datum pressure, temperature and volume are p_1 , T_1 and V_1 respectively, and are evaluated at intake valve closure.

The mean wall temperature is assumed to be 550K and the mean cylinder gas temperature is represented as the weighted mean of surrounding gas and jet fluid temperatures by the equation:

$$T_{ch} = \frac{m_{jet} T_{jet} + m_{a,sr} T_a}{m_f + m_a} \quad (2.49)$$

where T_{jet} and T_a are the mean jet and the surrounding air temperatures respectively and $m_{a,sr}$, m_{jet} , m_a , m_f refer to the masses of air in the surroundings, the fuel in the jet, total cylinder air and the total fuel mass respectively.

Total heat transfer is apportioned to the surrounding gas and the jet regions in relation to their mass and temperature as:

$$d\dot{Q}_{tr_{jet}} = \frac{m_{jet} T_{jet}}{m_{jet} T_{jet} + m_{a,sr} T_a} d\dot{Q}_{tr} \quad (2.50)$$

and

$$d\dot{Q}_{tr_s} = \frac{m_{a,sr} T_a}{m_{jet} T_{jet} + m_{a,sr} T_a} d\dot{Q}_{tr} \quad (2.51)$$

These terms are used in the overall energy balance to compute conditions in the engine cylinder at any instant.

The total surface area A_c of the engine cylinder comprises the cylinder head, side walls of the cylinder and the piston surfaces.

For the Shallow-Hesselman geometry the computation of piston surface area is indicated in Appendix D.

2.2.11 Turbulent Mixing

At the end of the injection period, the jet momentum due to fuel injection will be zero, and therefore air entrainment as computed from equation (2.5) and (2.41) will cease to have relevance. The mixing process by which available air continues to be utilised will

now be controlled by the turbulent kinetic energy dissipation in the fuel jets.

The mass transfer rate of air by turbulent mixing into the burning products from the unutilised air available in the jet and the surrounding regions can be expressed as $C_1 (m_a/\tau)$ where m_a is the mass of air, τ is the turbulent mixing time for the breakdown of large scale eddies, and C_1 is a constant to be discussed in detail later. The depletion rate of available air mass is $-\frac{d m_a}{dt}$. Therefore by mass conservation:

$$-\frac{d m_a}{dt} = C_1 \left(\frac{m_a}{\tau}\right) \quad (2.52)$$

Rearrangement of equation (2.52) and integration yields

$$\ln (m_a) = C_1 t/\tau + C_2 \quad (2.53)$$

where t is the cumulative time from the end of the injection process and C_2 is the constant of integration. C_2 can be evaluated using the initial condition at the end of injection. At $t = 0$, $m_a = m_{aa}$ yielding $C_2 = \ln(m_{aa})$, where m_{aa} is the total unutilised air available at the end of injection.

Substitution of the value C_2 in equation (2.53) yields:

$$\frac{m_a}{m_{aa}} = \exp(-C_1 \frac{t}{\tau}) \quad (2.54)$$

The mixing time (τ) is characterised by the following equation for large scale eddy structure

$$\tau = \left(\frac{L^2}{\epsilon}\right)^{1/3} \quad (2.55)$$

where L is the length scale and ϵ is the energy dissipation rate of the eddy structure.

Length scale L is taken to be the nozzle orifice equivalent diameter (d_o'). Dent (73) has characterised the turbulent energy dissipation in a quiescent chamber Diesel engine in terms of injection variables and engine speed by the expression

$$\epsilon = C \left(\frac{N}{\theta_{ip}}\right)^3 \left(\frac{V_f}{nd_o^2}\right)^2 \quad (2.56)$$

where N is the engine speed, θ_{ip} is the injection period, V_f is the volumetric delivery of fuel per stroke of the injection pump, n the number of holes in the injector nozzle, and d_o the injector orifice diameter. C is a known constant ($\sim 4.924 \times 10^5$).

The constant C_1 in equation (2.52) is evaluated by equating the time mean entrainment rate over the whole injection period to the right hand side of equation (2.51). This procedure is justified because it gives a means of relating the turbulent mixing rate due to dissipation to the entrainment of air due to the injection process.

2.2.12 Thermodynamic Analysis

The basis of the analysis follows from Shahed et al (16).

The conservation equations are derived for the whole jet and surrounding gas as:

Mass conservation:

For jet:

$$\text{Rate of change of mass in jet} = \text{Rate of fuel mass injected} + \text{Air entrainment rate into the spray}$$

$$\frac{dm_{jet}}{d\theta} = \frac{dm_{fi}}{d\theta} + \frac{dm_{ac}}{d\theta} \quad (2.57)$$

This can be subdivided further as:

$$\begin{array}{l} \text{Rate of change of} \\ \text{mass of fuel in jet} \end{array} = \begin{array}{l} \text{Rate of fuel} \\ \text{mass injected} \end{array} - \begin{array}{l} \text{Rate of fuel} \\ \text{mass evaporated} \end{array}$$

$$\frac{dm_{fjet}}{d\theta} = \frac{dm_{fi}}{d\theta} - \frac{dm_{fv}}{d\theta} \quad (2.58)$$

$$\begin{array}{l} \text{Rate of change of} \\ \text{air mass in jet} \end{array} = \begin{array}{l} \text{Rate of air} \\ \text{mass entrained} \end{array} - \begin{array}{l} \text{Rate of air mass} \\ \text{consumed during} \\ \text{combustion} \end{array}$$

$$\frac{dm_{ajet}}{d\theta} = \frac{dm_{ae}}{d\theta} - \frac{dm_{ac}}{d\theta} \quad (2.59)$$

$$\begin{array}{l} \text{Rate of change of} \\ \text{fuel vapour in jet} \end{array} = \begin{array}{l} \text{Rate of mass of} \\ \text{fuel evaporated} \end{array} - \begin{array}{l} \text{Rate of mass of} \\ \text{fuel vapour burned} \end{array}$$

$$\frac{dm_{fvjet}}{d\theta} = \frac{dm_{fv}}{d\theta} - \frac{dm_{vb}}{d\theta} \quad (2.60)$$

$$\begin{array}{l} \text{Rate of change of} \\ \text{mass of combustion} \\ \text{products} \end{array} = \begin{array}{l} \text{Rate of mass of} \\ \text{fuel vapour burned} \end{array} + \begin{array}{l} \text{Rate of mass of air} \\ \text{consumed during} \\ \text{combustion} \end{array}$$

$$\frac{dm_{cp}}{d\theta} = \frac{dm_{vb}}{d\theta} + \frac{dm_{ac}}{d\theta} \quad (2.61)$$

The interaction of mass elements is shown in Figure 2.17

For the surroundings:

Rate of change of mass in surroundings = Rate of mass of surrounding medium entrained in the jet

$$\left(\frac{dm_{ae}}{d\theta}\right)_{sr} = \frac{dm_{ae}}{d\theta} \quad (2.62)$$

Each of the energy conservation equations will follow from:

Rate of change of absolute internal energy in the region = - External work done by the region + Heat transfer rate to the region

+ Enthalpy associated with the flow rate of masses across boundary of the region + Heat release rate during combustion

$$\frac{d}{d\theta}(mu)_{region} = -p\left(\frac{dV}{d\theta}\right)_{region} + \left(\frac{dQ_{tr.}}{d\theta}\right)_{region} + \left(\frac{d(M_f H_f)}{d\theta}\right)_{region} + \left(\frac{dQ_{rel}}{d\theta}\right) \quad (2.63)$$

In conjunction with these conservation equations, the equations of state are also written for the jet and surrounding fluid.

Also, at any instant, the total cylinder volume equals the sum of surrounding and jet volumes.

Appendix E gives a detailed derivation of the set of equations used in the thermodynamic analysis carried out in the model.

2.2.13 Low Load Calculation

The overall structure of the model is maintained for low load calculations, however in a large number of cases the injection period is less than the delay period, under these circumstances turbulent mixing is considered as the mechanism for further entrainment of air as discussed earlier for the high load conditions. The structure of the jet is maintained up to the ignition delay period. Photographic studies (62) carried out in the I.C. Engines Laboratory of the Mechanical Engineering Department, seem to justify this assumption. At the point of ignition delay the total air-fuel ratio of the jet plume is considered. Therefore as air is entrained into the mixture by the turbulent mixing process it will immediately burn because of the stoichiometric burning assumption used.

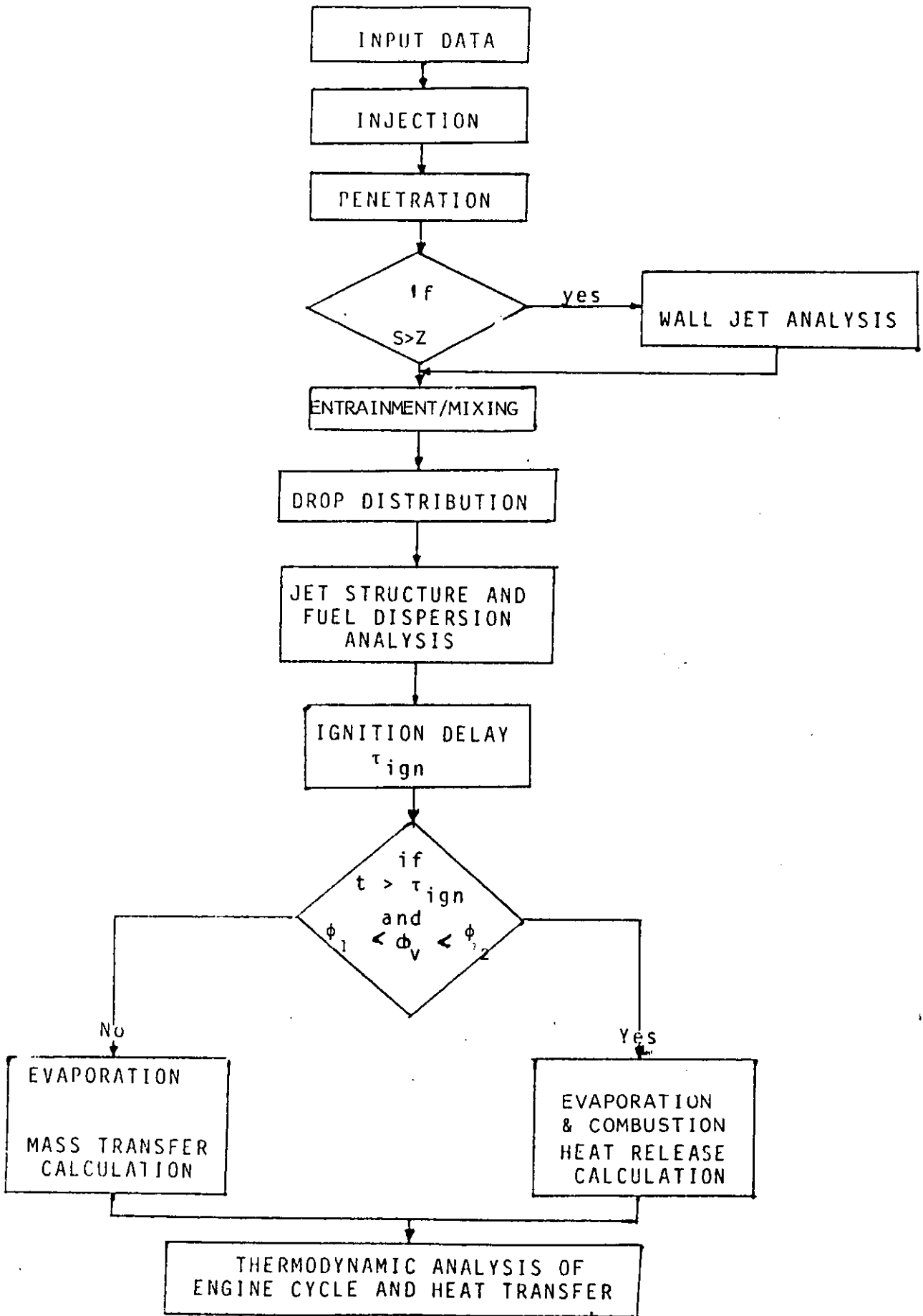


FIG. 2.1 Structure of Simulation Program

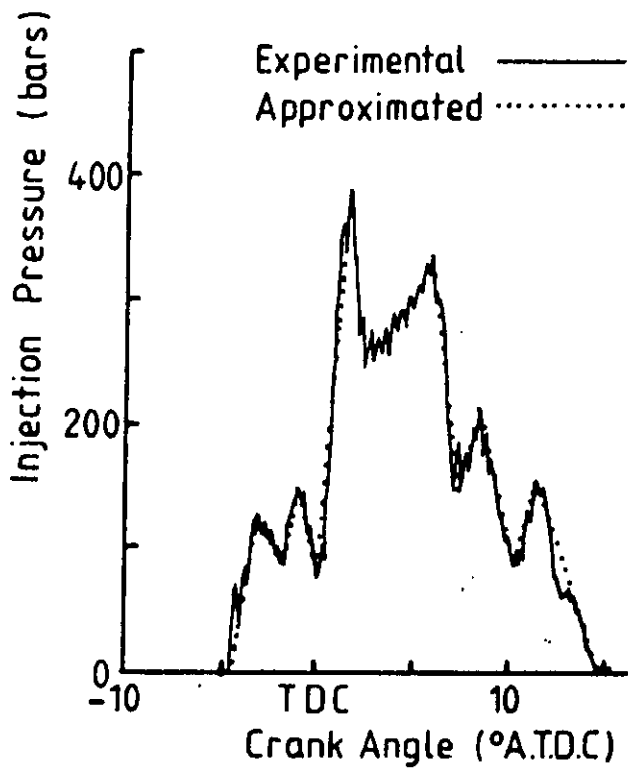


FIG. 2.2 Approximation of Fuel Injection Pressure Diagram

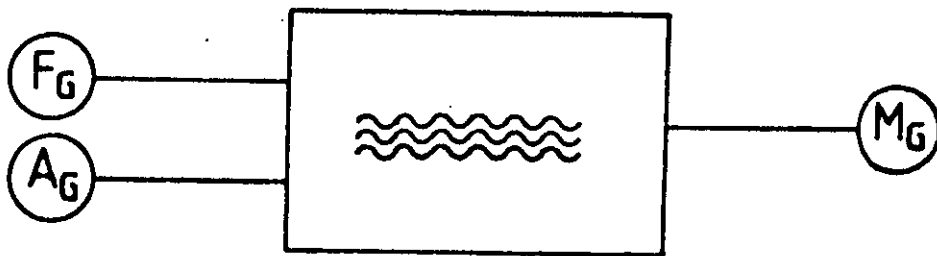


FIG. 2.3 Schematic Representation of Mixing in Chemically Reacting Systems

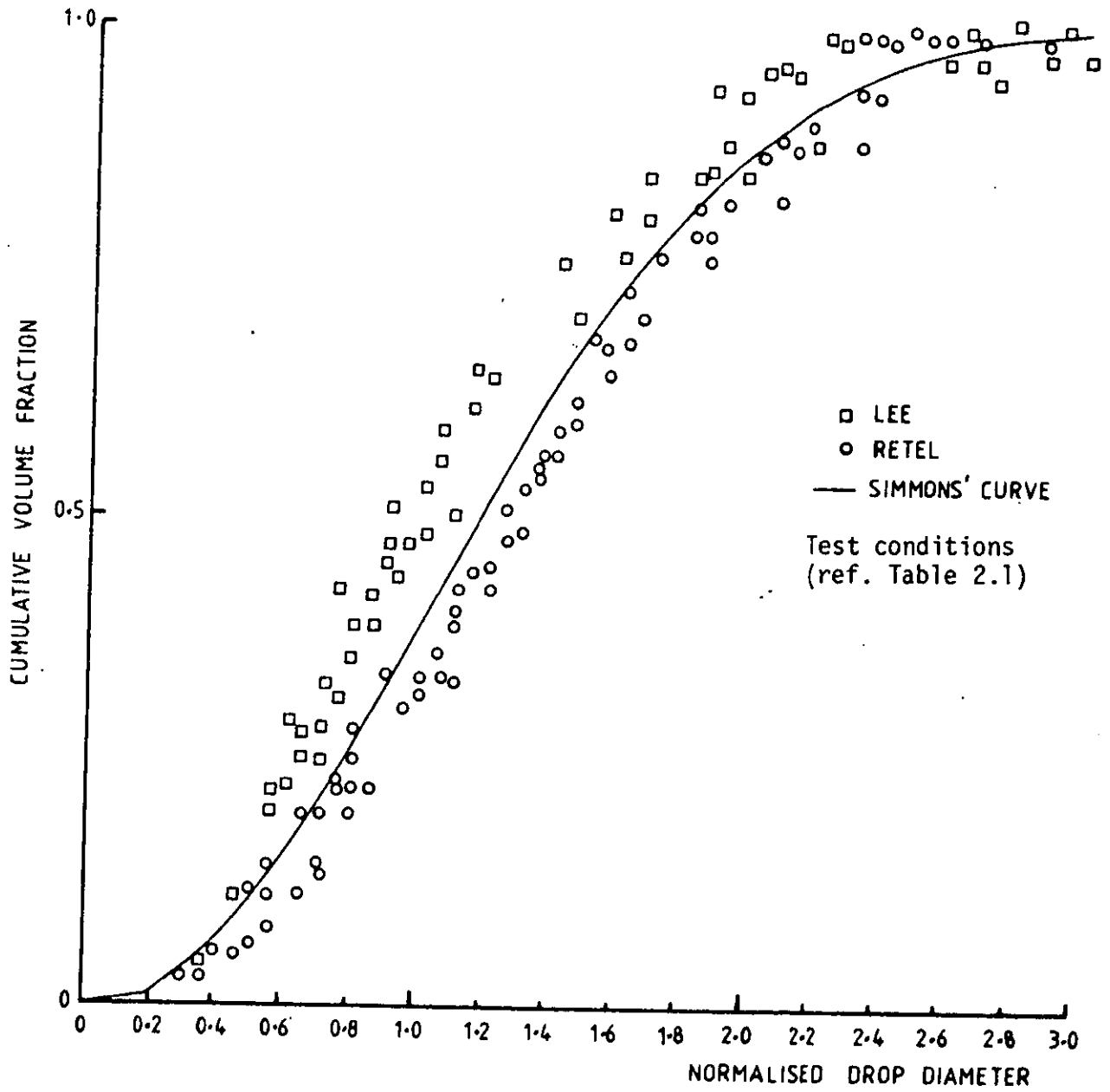


FIG. 2.4 Results of Verification of Droplet Size Relationship of
 Simmons (51) for Data of Lee (52) and Retel (53)

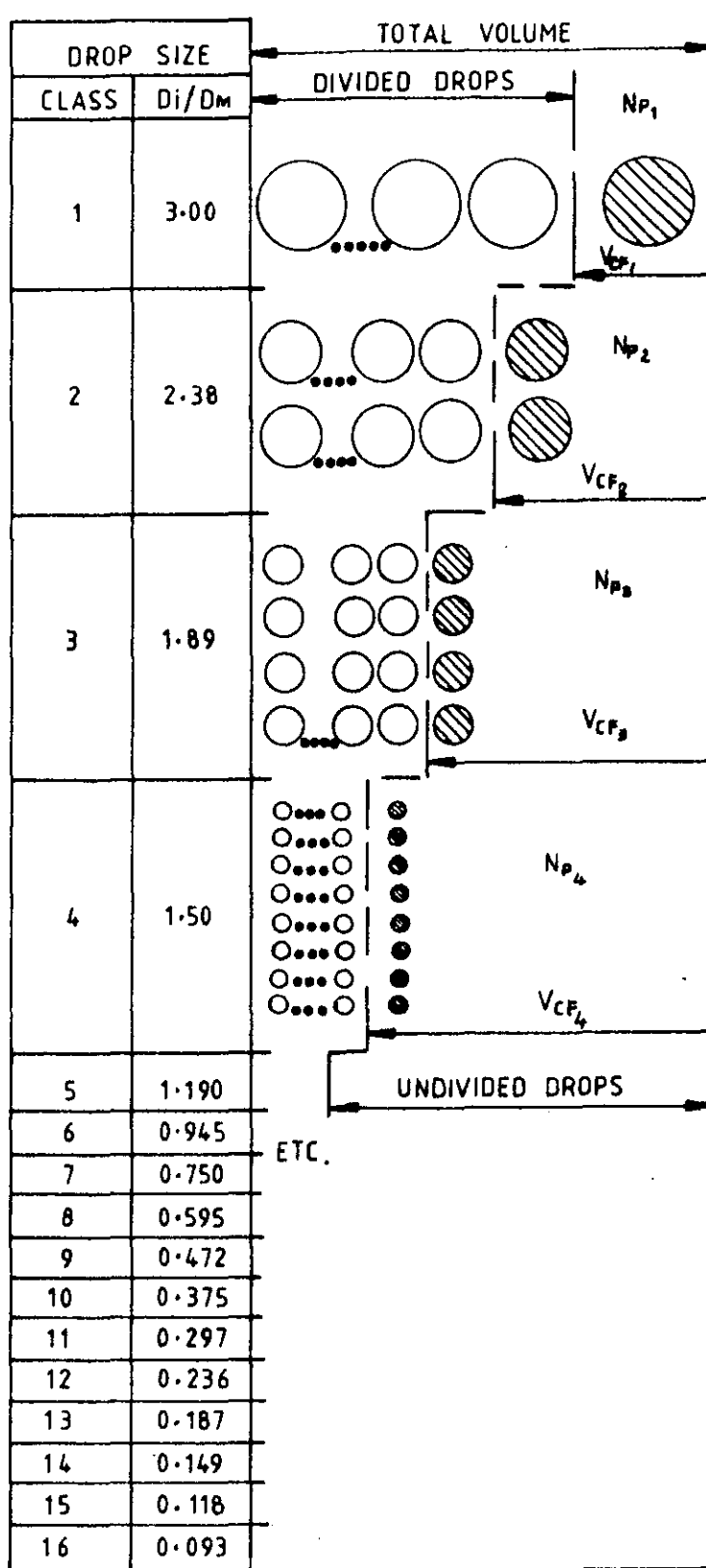


FIG. 2.5 Representation of Droplet Sizes from Simmons Binary Division Model

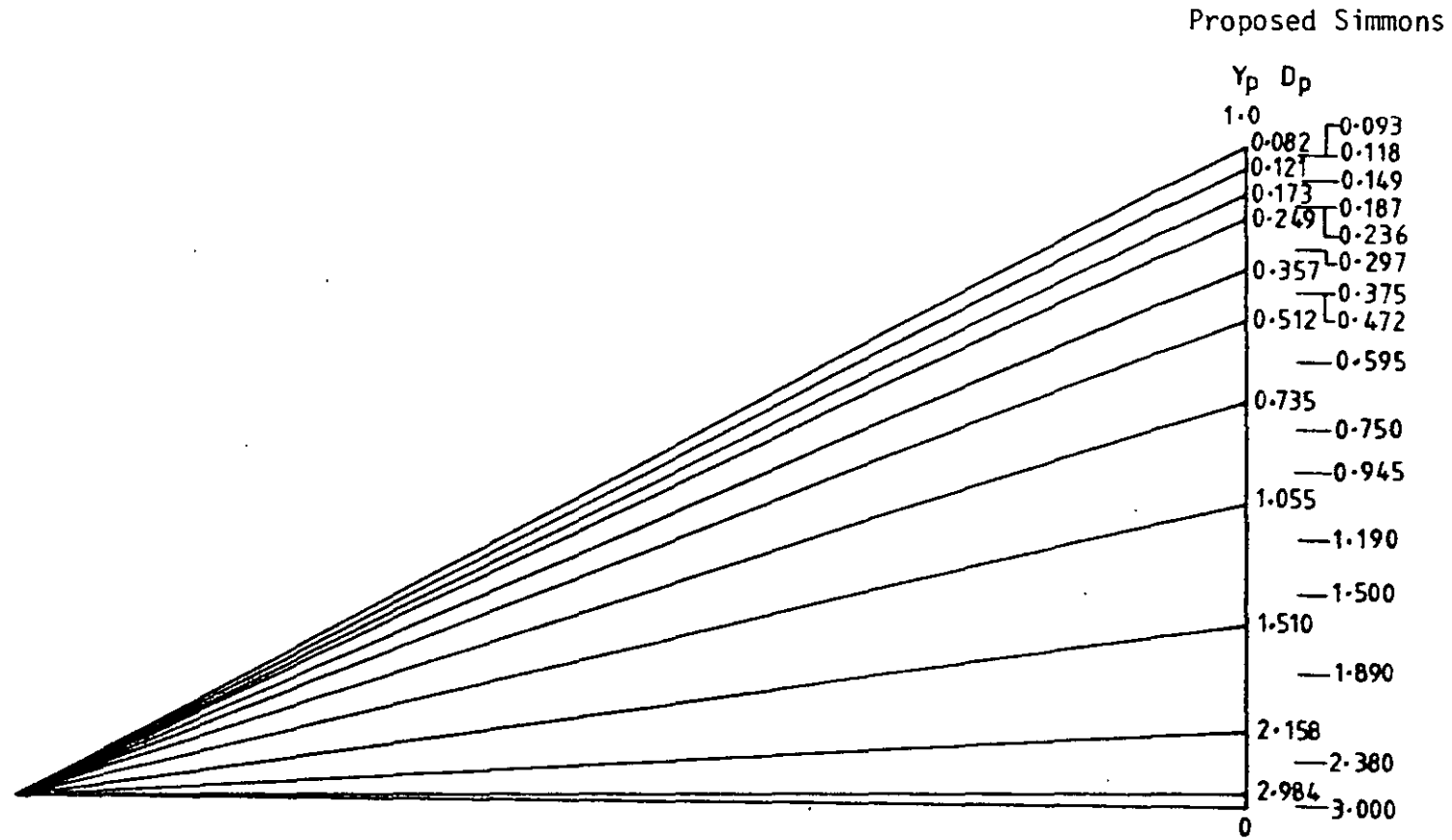


FIG. 2.6 Representation of Proposed and Simmons Droplet Size Distribution

Case i Evaporation
 ii Rapid Evaporation

$$N_{p_j} \cdot d_{p_j}^3 = N_{p_k} \cdot d_{p_k}^3 + N_{p_{k+1}} \cdot d_{p_{k+1}}^3$$

$$N_{p_j} \cdot d_{p_j}^2 = N_{p_k} \cdot d_{p_k}^2 + N_{p_{k+1}} \cdot d_{p_{k+1}}^2$$

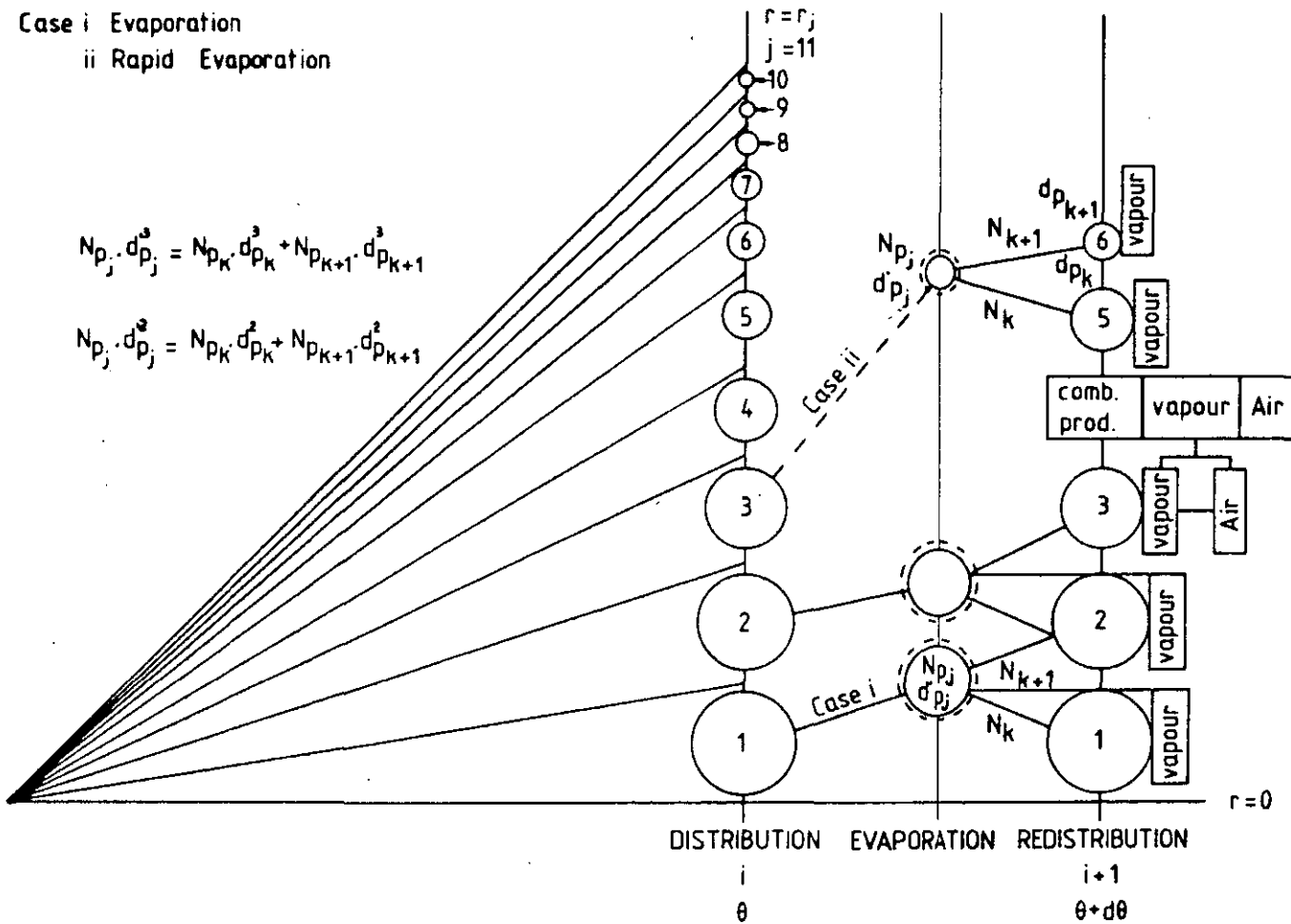


FIG. 2.7 Schematic of Distribution, Evaporation and Redistribution of Droplets in the Proposed Model

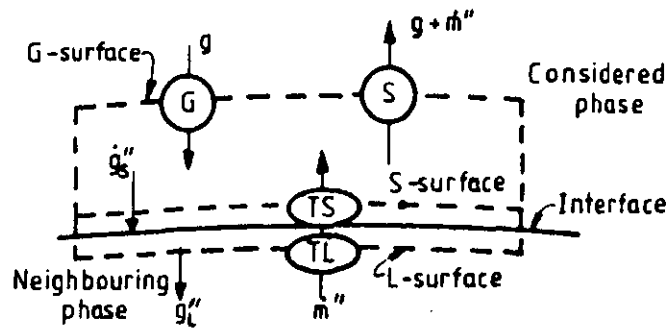


FIG. 2.8 The Reynolds Flow Model

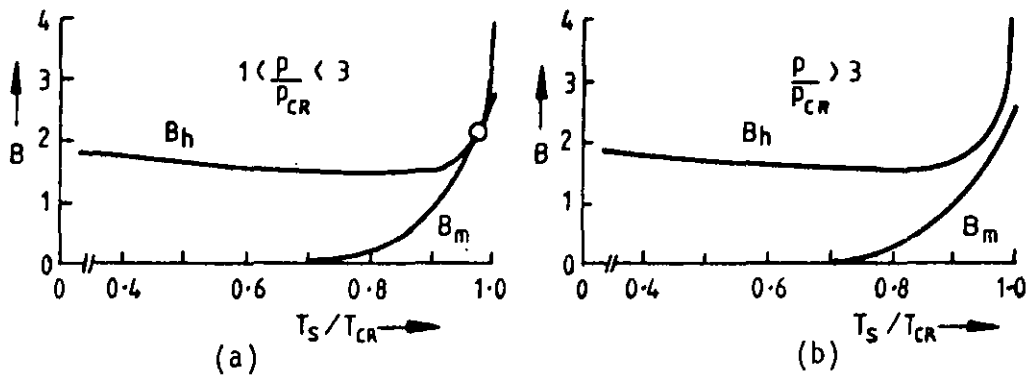


FIG. 2.9 Representation of the Mass Transfer Functions B_m and B_h

FUEL: PENTANE
 FUEL = 0.21mm

● EXPERIMENT
 — MODEL

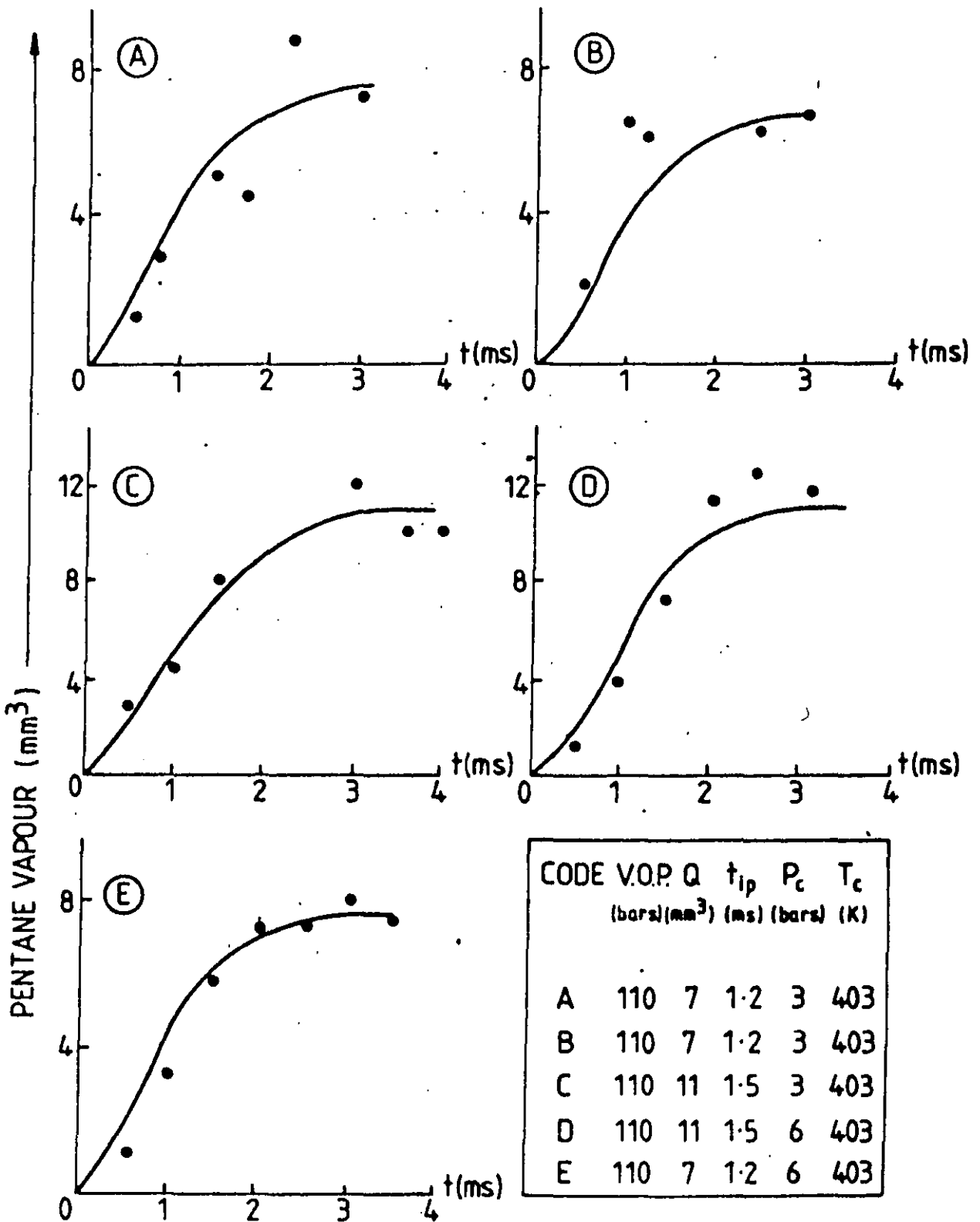


FIG. 2.10 Comparison of Predicted and Experimental Results of Evaporation

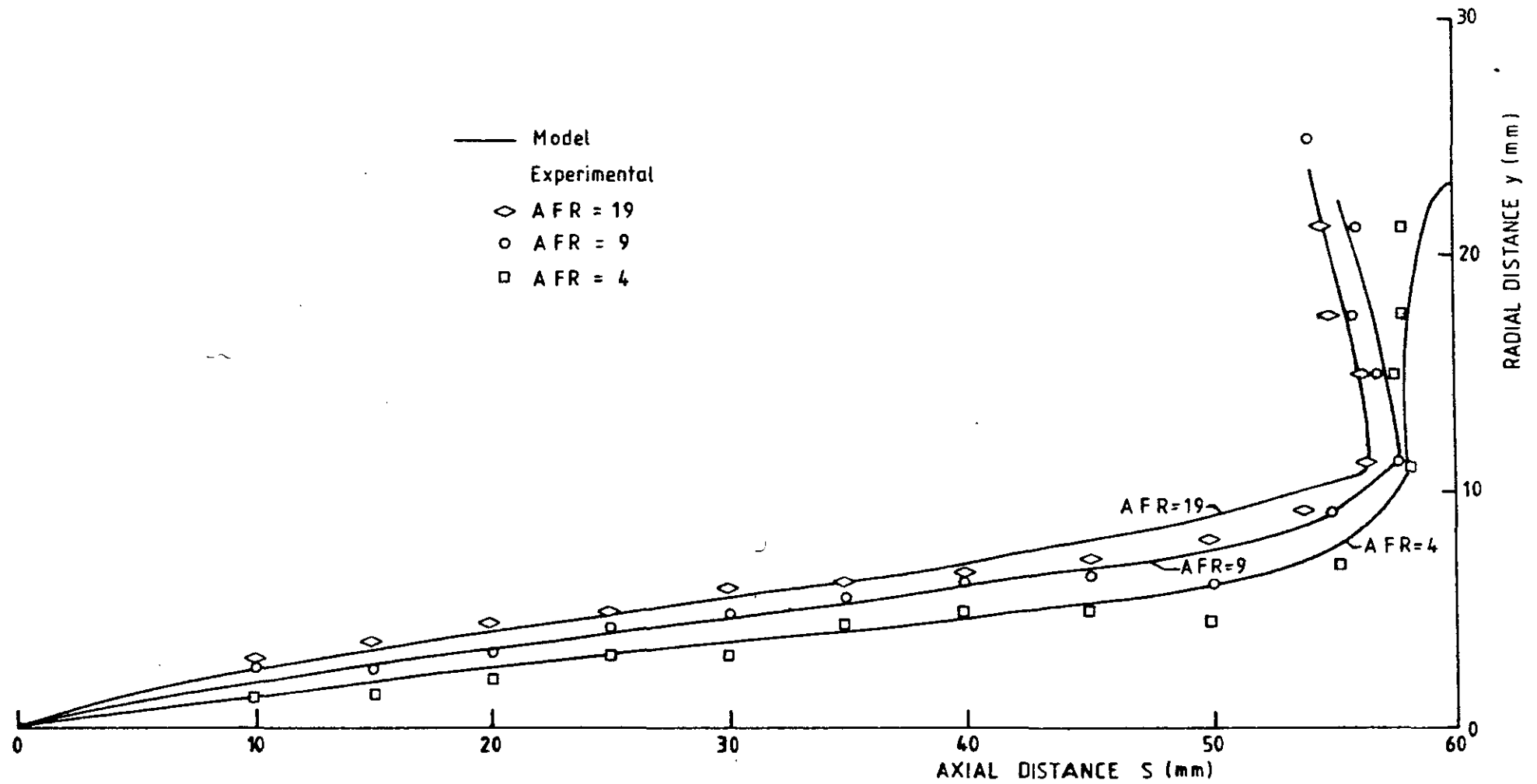


FIG. 2.11 Comparison of Predicted and Experimental Results of Air Fuel Ratio Contours

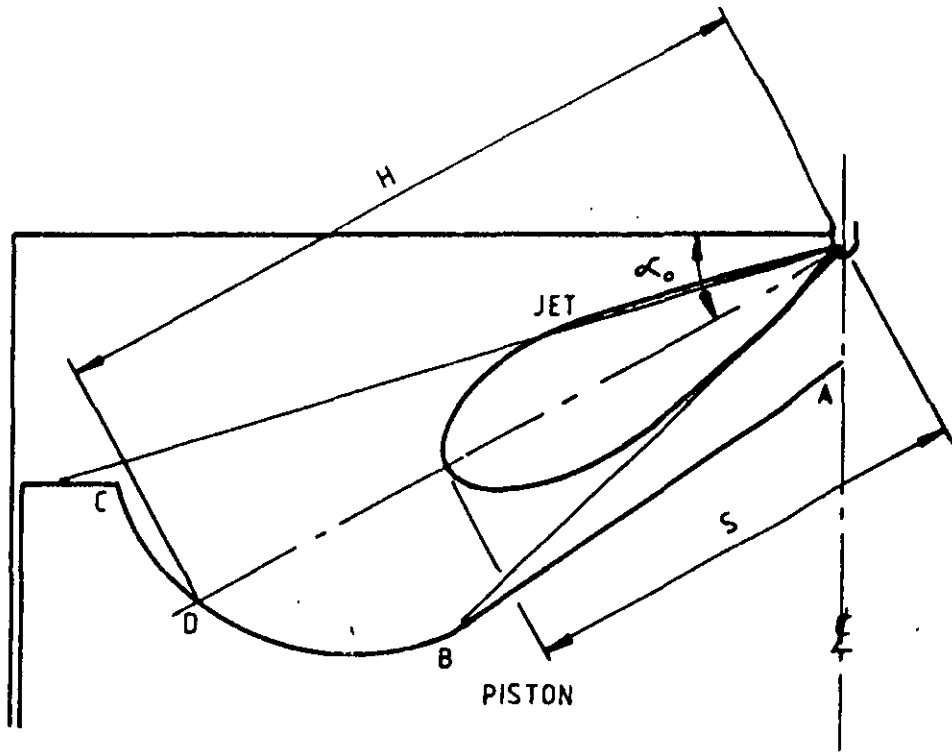


FIG. 2.12 Development of Jet

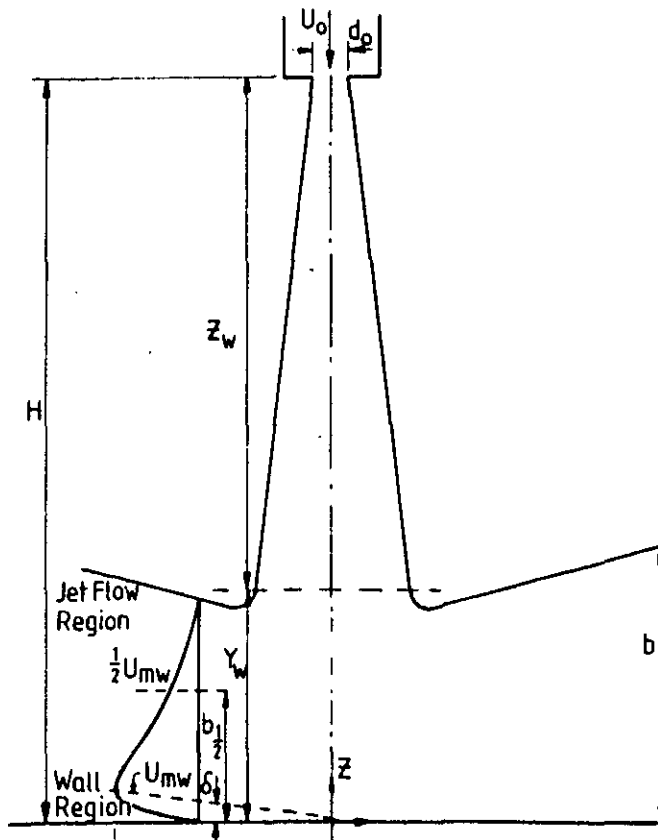


FIG. 2.13 Schematic of Impingement and Wall Jet Regions

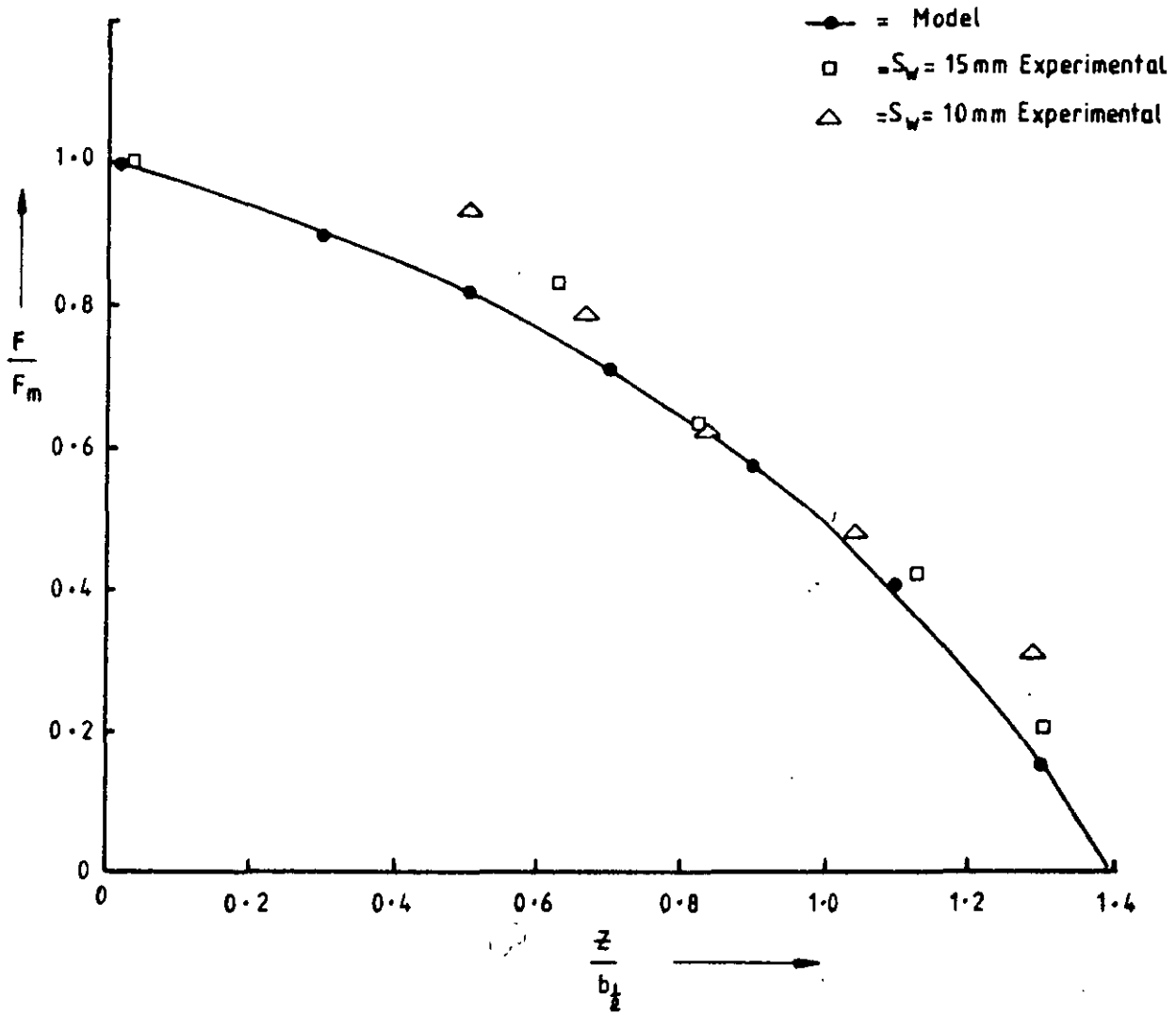


FIG. 2.14 Results for Verification of Concentration Similarity Profile Equation (2.9) in Wall Region

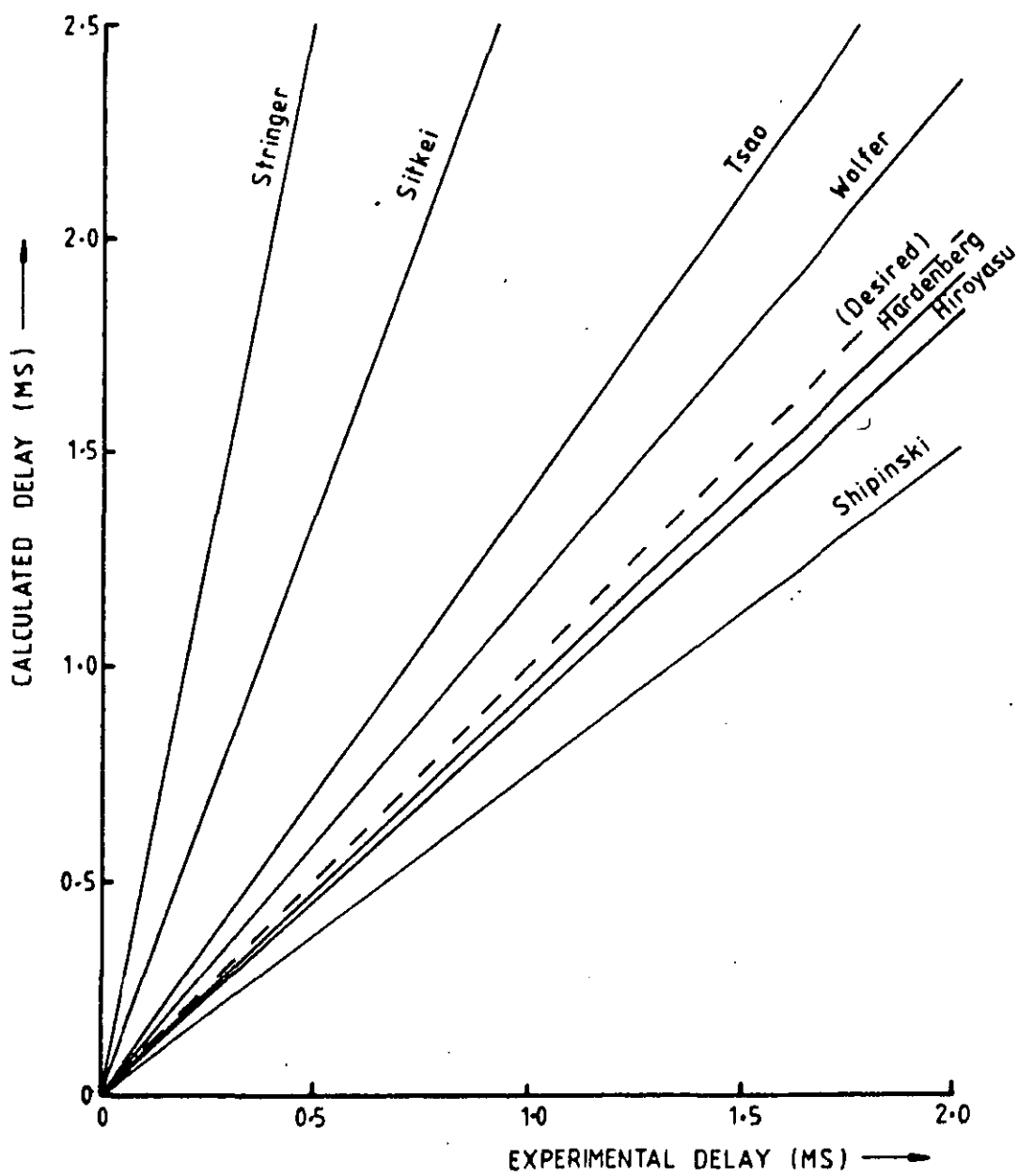


FIG. 2.15 Results of Comparison of Various Ignition Delay Correlations

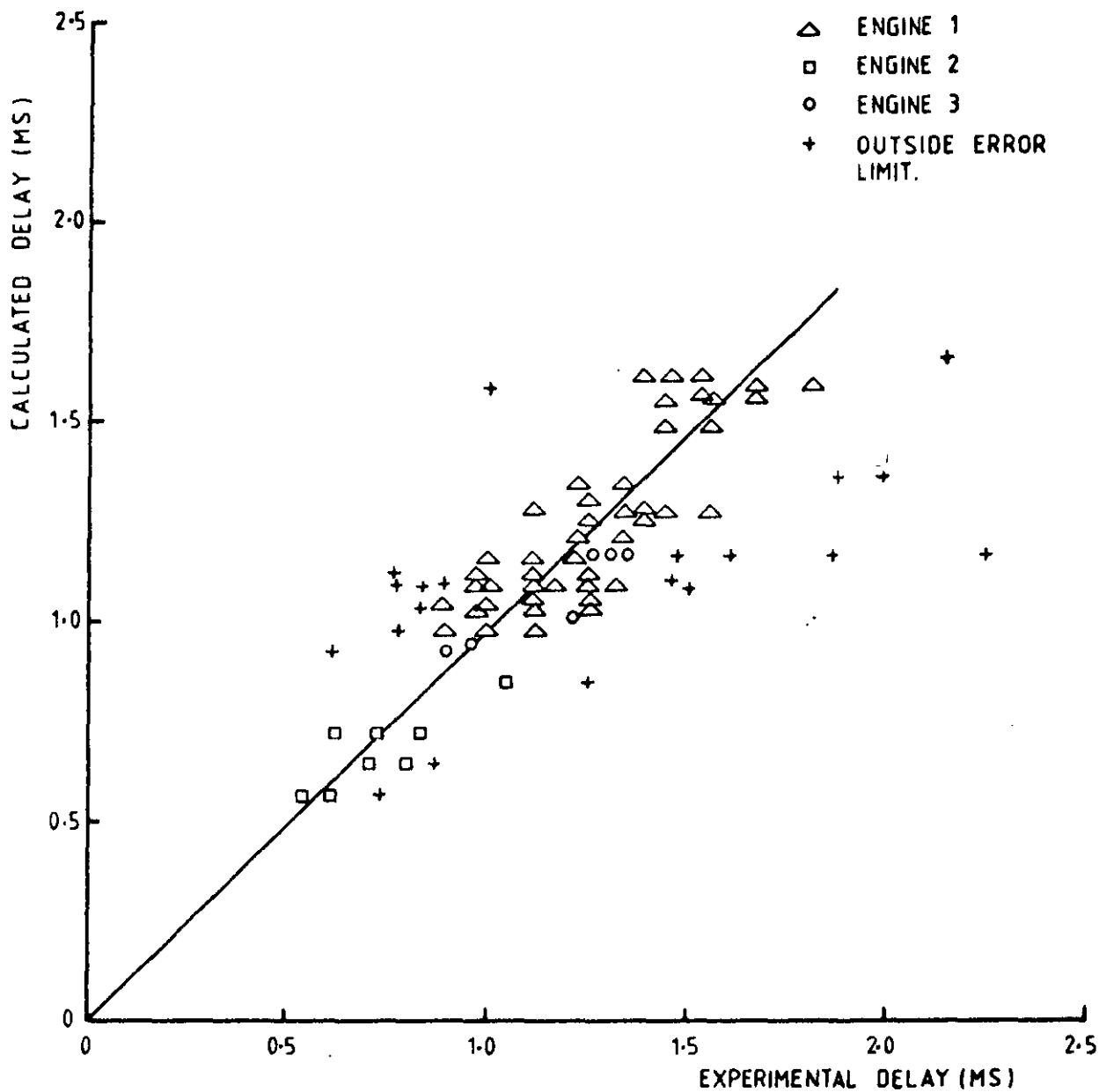
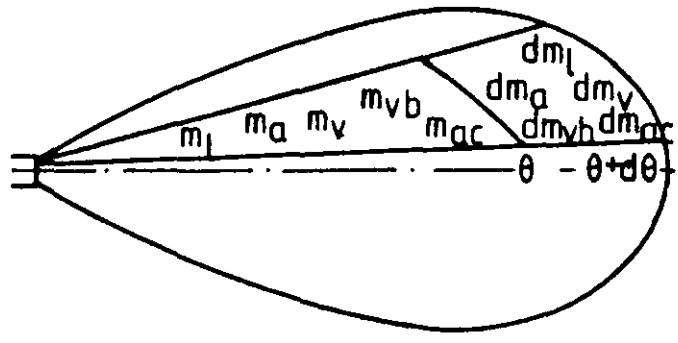
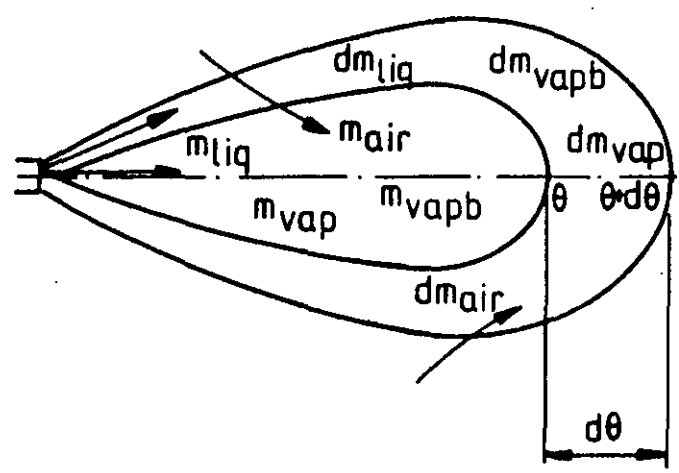


FIG. 2.16 Results of Ignition Delay Data Correlation with Hardenberg and Hase's Equation (71)



(a) sectors



(b) overall

FIG. 2.17 Instantaneous Interaction of Mass Elements

CHAPTER III

GENERAL STRUCTURE OF THE COMPUTER PROGRAM

3.1 Introduction

A computer simulation program is developed using the physical basis described in Chapter II. The phenomenological description of various processes is dealt with in separate subroutines, giving a modular arrangement to the complete simulation program. Fortran language is used in coding the statements and computations are carried out using the ICL 1904S computer available at Loughborough University of Technology.

3.2 Flow Charts and Program Modules

A flow chart of the computer model is shown in Figure 3.1. A connection of the flow chart with the structure of the model is discussed below. The titles of the subprograms used in the model appear in brackets at appropriate locations.

There are ten major subroutines, supported by others, used to describe the processes affecting diesel engine combustion. The lists of these subroutines are given in Table 3.1. The function subprograms are meant to represent various equations used in computation relating the physical processes and the property evaluation of the working substances. The list of these functions are included in Table 3.2.

The principal aim of the model is the accurate performance prediction of an engine at various operating conditions with economic use of computer storage and running time. Also, the prediction of soot emission and the effect of swirl will need additional modules in the program. They are described in subsequent chapters.

The engine geometry and operating conditions including the injection pressure diagram, are assumed as input data read in the

TABLE 3.1
Usage of Subprograms

Processes	Main Subprogram	Supporting Subprogram Subroutine Function
1 Injection	INJSIM	- -
2 Droplet Size Distribution	DVNR	- FDDV
3 Impingement and Wall Jet	IMPING, WALJET	GEOM, VGEOM -
4 Jet Structure	AXLUCT, RDLUCT	- FC, FT, FU
5 Evaporation and Combustion	EVAP	BISECT, BMBH PROP CPA, CPF, CONT2, CONT3 ENL, FUN1, VIST2, VIST3
6 Redistribution	REDIST	- -
7 Turbulent Mixing	MIX	EVAPM -
8 Mass Balance	MASSB	- ENTR, ENTRW
9 Heat Transfer	WOSCH	- HTC
10 Thermodynamic Analysis	CROUT	- CPA, CPF, CPV ENF, ENT, ENV

TABLE 3.2

List of Function Subprograms in Alphabetical Order

Name	Description
CPA(T)	Specific heat polynomial for air at T ⁰ K
CPF(T)	Specific heat of liquid hydrocarbons T ⁰ K
CPV(T)	Specific heat of hydrocarbon fuel vapour at T ⁰ K
CONT2(T)	Conductivity of air at T ⁰ K
CONT3(T)	Conductivity of fuel vapour at T ⁰ K
DVDTH(THR)	Derivative of piston displacement with crank angle
ENF(T)	Enthalpy of liquid hydrocarbon at T ⁰ K
ENL(T)	Enthalpy of vaporisation for hydrocarbon at T ⁰ K
ENT(A,T)	Enthalpy of air at T ⁰ K
ENTR(X,D)	Air entrainment law for free region
ENTRW(X,D)	Air entrainment law for wall region
ENV(A,T)	Enthalpy of hydrocarbon fuel vapour at T ⁰ K
FC(Y)	Similarity profile for concentration at Y
FDV(DR)	Drop-size volume fraction distribution function
FDDV(Q)	First derivative of drop-size volume fraction distribution function
FT(Y)	Similarity profile for temperature at Y
FU(Y)	Similarity profile for velocity at Y
FUN1(T)	Saturation pressure for hydrocarbon at T ⁰ K
FUN2(P)	Saturation temperature for hydrocarbon at P (N/m ²)
FW(YW)	Integral functions of mass and momentum conservation equations
HTC(T)	Heat transfer coefficient
RHOFV(NFAV,T,P)	Density of hydrocarbons in liquid or vapour phase
VIST2(T)	Absolute viscosity of air at T ⁰ K
VIST3(T)	Absolute viscosity of hydrocarbon fuel vapour at T ⁰ K
VOL(THR)	Slider-crank relationship for piston displacement

subprogram READ.

The computation begins at inlet valve closure, and until start of injection the instantaneous cylinder volume, pressure and temperature conditions are computed using subprogram PREINJ and MOTOR.

The synthesis of the injection pressure diagram in subroutine INJSIM allows the calculation of the following quantities in subroutine AUXMN over the discretised time step (Δt):

- Injected fuel quantity
- Spray penetration
- Sauter Mean Diameter of atomised droplets
- Instantaneous engine motoring conditions
- Cylinder trapped mass

The relative position of the jet tip with respect to the piston geometry (subroutines GEOM, VGEOM) allows the consideration of jet impingement (IMPING) and the possibility of their interaction in the wall region (WALJET). The jet structure defined in subroutines AXLUCT and RDLUCT allows the transition from a free to wall jet condition.

The fuel droplet size distribution and air entrainment into the spray is computed for each discretised time interval in subroutines DVNR and MASSB respectively.

Fuel vaporisation rate using mass transfer considerations is evaluated with and without combustion in subroutine EVAP. The ignition delay and inflammability limits are used as criteria for the heat release calculation (EVAP).

The droplet redistribution (REDIST), mass balance (MASSB) and thermodynamic analysis (CROUT) follows the evaporation-combustion calculation in the model.

On completion of fuel injection, the jet analysis is replaced by the turbulent mixing rate calculation (MIX) followed by thermo-

dynamic analysis at each instant until exhaust valve opens. The values are integrated using subroutine EULER.

3.3 Model Input

The data required as inputs to the program are listed in Table 3.3.

Items 7 to 9 in Table 3.3 are stored in block data STOR. All other variables are read in the form of input data cards in the program. The values of pressure, fuel injection rate, angles, orifice hole diameter and enthalpy of reaction are read in bars, $\text{mm}^3/\text{CA}/\text{hole}$, degree, mm and megajoules/kg respectively. However, these values are converted to respective SI units before computation begins. All calculations are consistently carried out using SI units. The interval size for computation can be specified as input which is generally taken as 1° CA.

3.4 Model Output

The various computation results from the model are printed using subroutine WRITE.

The outputs from the model as a function of crank angle are:

- Cylinder pressure
- Rate of heat release
- Air entrainment and mixing rate
- Mass fraction of fuel vaporised
- Mass fraction of fuel burned
- Mean jet and total trapped charge temperatures
- Heat transfer rate from the gaseous charge

TABLE 3.3

Data Input to the Model

Input concerning	Variables
1 Engine dimensions and operating parameters	Engine bore, stroke, speed, compression ratio, and connecting rod length
2 Injector dimension and injection conditions	i) Number of injector holes, orifice diameter, injection timing, duration of injection, angle of spray axis relative to cylinder head, mean injection pressure, and mean fuel injection rate ii) Approximated values for injection pressure diagram in terms of crank position
3 Valve timing	Inlet valve closing and exhaust valve opening time in terms of crank position with respect to the top dead centre at compression
4 Fuel characteristics and other conditions	Inlet fuel temperature, normal boiling point of fuel, critical temperature of fuel, critical pressure of fuel, fuel cetane number, enthalpy of reaction for fuel, intake air temperature and pressure, and mean cylinder wall temperature
5 Specification of engine geometry (Ref: Figure D1 of Appendix D)	Bowl dimensions (height and depth), angle of piston crown, radius of curvature for piston bowl, X and Y coordinates of various location points A, B and C with respect to cylinder head centre and point A respectively, nozzle immersion depth, distance of piston crown from cylinder head at TDC and angle of curved portion of piston bowl (α_B)
6 Physical properties of working fluids	Density, molecular weight, thermal conductivity and viscosity of liquid fuel, air and fuel vapour respectively
7 Empirical and universal constants	Universal gas constant, polytropic index, stoichiometric air-fuel ratio, nozzle discharge coefficient and some conversion factors
8 Coefficients for property polynomials	Coefficients of specific heat, enthalpy and density polynomials for working fluids viz air and fuel
9 Others	Discrete values of radial droplet size distribution with radial position

3.5 Summary

The computer simulation program as designed here, uses 3200 cards. The modular arrangement of the model proves advantageous in updating the process description. Continuing advancement and understanding of related areas demands such flexibility in the model structure. The run time for a job over a closed cycle period is 900 mill units (1 mill unit is about $\frac{1}{2}$ second) for the ICL 1904S computer which is of the order of 5 to 6 seconds on an IBM 370 computer. The memory storage requirement of this program is only 18000 words.

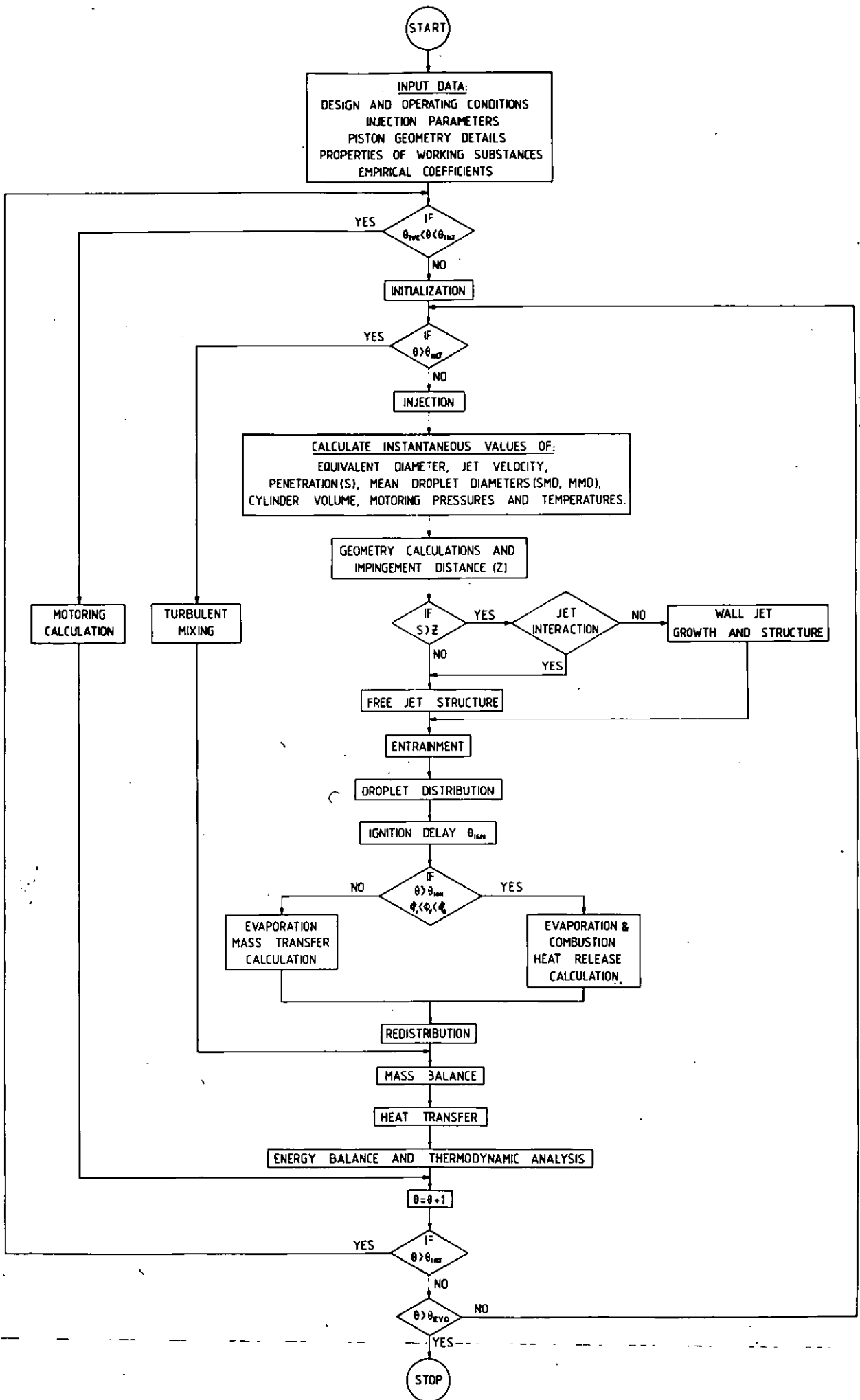


FIG. 3.1 Flow chart of computer model

CHAPTER IV

SOOT PREDICTION MODEL

4.1 Introduction

From an environmental pollution standpoint, the emission of soot particulates from the Diesel engine exhaust is a limiting factor to their wide application. Due to the heterogeneous and mixing controlled nature of combustion in Diesel engines, they emit a greater quantity of soot particulates compared with spark ignition engines. Despite its importance, the emission of soot is one of the least understood aspects of diesel combustion.

A major part of soot particulates is solid carbon generated during combustion. The concentration of soot in diesel exhaust is the net result of its formation and oxidation in the combustion chamber. Therefore, an understanding of soot formation and oxidation mechanisms are required independently. Such studies, however, are difficult to carry out in the engine combustion chamber. Hence most of the available information relates to either open diffusion flame studies, or the oxidation of carbon in air and oxygen/nitrogen mixtures to establish its controlling mechanism.

Considering the volume of literature on soot formation mechanisms, there is little in the literature (13, 18, 19, 79) on the prediction of exhaust soot emission from diesel engines. A brief review of the existing literature on soot emission and the mechanisms of formation and oxidation is presented below. From this an attempt is made to develop a soot emission model applicable to diesel engines.

4.2 Literature on Soot

4.2.1 Soot Formation

Several authors (80-85) have reviewed soot formation phenomena in open flames and/or engines. In an early review for the formation

and combustion of soot in laboratory hydrocarbon flames, Broome and Khan (80) emphasised that the soot results solely from the vapour-phase pyrolysis of fuel molecules in the presence of high temperature and insufficient oxidant. There is the possibility for many routes to be followed by the basic reactions in the formation of soot, depending on different physical and chemical conditions. They presented a simplified qualitative scheme for such reaction paths as shown in Figure 4.1. The effect of operating variables on diesel engine exhaust soot were summarised by them in Figure 4.2.

Essentially Broome and Khan (80) divided the soot formation into three major stages:

- i) Nucleation and formation of precursors.
- ii) Growth of the nuclei into soot particles.
- iii) Coagulation of soot particles into bigger agglomerates.

For the formation of soot, there are two basic mechanisms suggested in the literature - polymerization and thermal decomposition. In general there is agreement about the kinetically controlled nature of soot formation. The former mechanism proposed by Homann (86) considers the nucleation due to the bonding of large molecules produced by simultaneous polymerization and dehydrogenation of the original hydrocarbons. Contrary to this view, Tesner (87) considers that at high temperature, the probability of decomposition processes controlling are greater than that of polymerization. Apart from these two nucleation theories, there are six other theories advanced by various investigators (81). In the face of such uncertainty, the existing soot models (13, 18, 19, 79) have used an Arrhenius type relationship for the soot formation. These are summarised in Table 4.1. Basically these models are developed on the grounds that soot formation is affected by pressure, temperature, and equivalence ratio. Each of these engine studies needed empirical constants to obtain quantitative results at different engine operating conditions.

TABLE 4.1

Summary of Existing Diesel Engine Soot Models

AUTHOR	FORMATION	OXIDATION	REMARKS
Khan et al (13, 92)	$\dot{S}_f = C_s \frac{V}{V_{NTP}} \phi^n P \exp\left(-\frac{E_{sf}}{RT}\right)$ $C_s = 9.36 \times 10^5, n = 3$ $E_{sf} = 40000 \text{ cal/mol}$	$\dot{S}_c = C_o \pi D_p^2 \frac{p_{O_2}}{T^2} \exp\left(-\frac{E_{so}}{RT}\right)$ $C_o = 7.5 \times 10^4$	<p>ϕ, T, P and V are the local unburnt equivalence ratio, temperature and pressure and volume respectively for soot formation zone. V_{NTP} is the volume of cylinder contents at NTP and p_{O_2} is the partial pressure of O_2 oxygen.</p>
Hiroyasu and Kadota (16)	$\dot{S}_f = (C_g \frac{dm_{fi}}{dt} + C_l m_{fl}) P \exp\left(-\frac{E_{sf}}{RT}\right)$ $E_{sf} = 19860 \text{ cal/mole}$	$\dot{S}_c = C_b V_u \frac{6 m_s}{\rho_s d_s} p_{O_2} \exp\left(-\frac{E_{so}}{RT}\right)$	<p>$\frac{dm_{fi}}{dt}$ is the fuel mass injection rate, m_{fl} is the mass of liquid fuel in the package at any instant, P is cylinder pressure, V and T is the package volume and local temperature respectively, m_s is the mass of formed soot S and p_{O_2} is the partial pressure of O_2 oxygen</p>
Kau et al (19)	$\dot{S}_f = A_{sf} \left(\frac{V_{bm,I}}{V}\right)^2 \left(\frac{\bar{T}}{T}\right) \phi^3 P \exp\left(-\frac{E_{sf}}{RT}\right)$ $A_{sf} = 3.52$ $E_{sf} = 40000 \text{ cal/mol}$	$\dot{S}_c = A_{so} \left(\frac{m_s}{\rho_s d_s}\right) \left(\frac{Y_{O_2} P}{T^2}\right) \exp\left(-\frac{E_{so}}{RT}\right)$ $A_{so} = 6.51 \times 10^4$	<p>\bar{T} is average temperature of cylinder contents, V is the local volume, $V_{bm,I}$ is the volume of burning zone, ϕ, P and T are the local equivalence ratio, pressure and temperature, m_s is the mass of soot formed S, and Y_{O_2} is the mass fraction of O_2 oxygen</p>

TABLE 4.1 continued

AUTHOR	FORMATION	OXIDATION	REMARKS
Watson and Janota (79)	$\dot{S}_f = K_f \frac{V}{V_{NTP}} m_{fu} p_f \exp\left(-\frac{E_{sf}}{RT}\right)$	$\frac{S_0 - S_c}{S_0} = \left[1 - K_c \frac{2}{\rho_s d_s} \frac{p_{O_2} \Delta t}{T^2} \exp\left(-\frac{E_{so}}{RT}\right)\right]^3$	<p> S_0 is the initial soot concentration, V is the zone volume, V_{NTP} is the volume of cylinder contents at NTP, m_{fu} is the mass of unburnt fuel in the zone, p_f is the partial pressure of fuel, p_{O_2} is the partial pressure of oxygen, T is the local temperature and ρ_s and d_s are the mean soot density and particulate size respectively </p>

Although successful, these attempts are not fundamentally based and it is difficult to be certain about their generality.

It is reported by Wagner (82) that in any combustion system soot usually forms at temperatures between 1300 and 2800K and at lower C/O ratio (~ 0.5), than would be predicted theoretically. Dyer and Flower (88), through experiments in a combustion bomb, go further to suggest that the experimentally determined threshold for soot formation is related not only to the equivalence ratio but also to the flame temperature as shown in Figure 4.3. This has been confirmed by Plee et al (83).

The review of McArragher and Tan (89) suggests that there are limited studies (90-91) showing the effect of pressure on soot concentration. However, there is a pronounced effect of pressure on soot emission. The soot formation rate increases with pressure depending upon the type of flame and the fuel used. Tesner's experiments (93) in diffusion flames suggest that the formation of soot particle nuclei start from acetylene nuclei. The dominance of acetylene near the surface of a burning droplet within an envelope flame is also shown (Figure 4.4) in the experiments of Gollahali and Brzutowski (94). Tesner (87) has regarded formation of soot as a branched chain process. He also considers the destruction of active nuclei on the soot particle surface as an essential mechanism. In order to relate the rate of formation of active particles with experimental results on soot formation, he considers a two stage formation process:

i) The rate of formation of radical nuclei is written as

$$\frac{dn}{dt} = n_0 + (f - g) n - g_0 n N \quad (4.1)$$

where n_0 is the spontaneous formation rate of particles (particles/m³/s), n is the concentration of the radical nuclei (particles/m³), N is the concentration of soot particles (particles/m³), f is the linear branching coefficient, g is the

linear termination coefficient, and g_0 is the coefficient of linear termination on soot particles. n_0 is expressed by

$$n_0 = a_0 N_0 \exp\left(-\frac{E_{sf}}{RT}\right) \quad (4.2)$$

where N_0 is the concentration of acetylene in molecules/m³.

- ii) The total rate of formation of soot particles by considering termination process at the surface of the soot particles is expressed as

$$\frac{dN}{dt} = (a - bN)n \quad (4.3)$$

where a and b are constants.

A successful application of this scheme in turbulent flames has been demonstrated by Magnussen and Hjertager (95-96). Encouraged with this attempt which relates closely to the engine case, it is thought that Tesner's model should be applied here. Also, as pointed by Ahmad et al (85), the equations of Tesner et al are a unique set describing the important subprocesses involved in soot formation. Ahmad et al have successfully verified a model in steady high pressure turbulent spray and jet flames using Tesner's scheme.

4.2.2 Soot Oxidation

The soot oxidation process depends on the diffusion of the reactants to, and the products from, the reaction sites at the particle surface and also on the kinetics of the reaction itself. In the engine, coagulation and oxidation occur simultaneously.

In all the existing diesel engine soot models at present, the soot oxidation process is defined as kinetically controlled in terms of the local temperature (T) and the partial pressure of the oxygen (p_{O_2}). A semi-empirical equation of Lee et al (52) is adopted in all² the models. The equation of Lee et al for the surface oxidation rate (q) of a soot particle in a hot laminar plume of a gas diffusion flame is expressed as:

$$q = 1.084 \times 10^4 \frac{p_{O_2}}{T^2} \exp\left(-\frac{E_{SO}}{RT}\right) \text{ (g/cm}^2\text{s)} \quad (4.4)$$

They determined a first order dependence on the oxygen concentration and an apparent activation energy of 39300 cal/mol. The measurements of Tesner and Tsibulevsky (97) in diffusion flames and that of Park and Appleton (98) in a shock tube, for conditions given in Table 4.2, show a similar dependence on partial pressure of oxygen. At high oxygen partial pressures (> 4 atm) Park and Appleton confirmed the findings of Nagle and Strickland-Constable (99) regarding the zero order dependence of the rate.

According to the theory of Nagle and Strickland-Constable, there are two types of reaction sites, A and B, on the carbon surface responsible for oxidation. Site A is more reactive than B and they are inter-convertible. On this basis they proposed the following semi-empirical relation.

- i) At low temperature (1050-1700K), the surface is entirely covered by A sites. At low partial pressure (< 0.2 atm) of oxygen

$$q = 2.4 \times 10^2 p_{O_2} \exp\left(-\frac{30000}{RT}\right) \quad (4.5)$$

At higher partial pressures (0.1 - 0.6 atm)

$$q = 11.3 \exp\left(-\frac{34000}{RT}\right) \quad (4.6)$$

- ii) At higher temperatures ($> 1700\text{K}$), where thermal rearrangement produces an increasing proportion of B sites,

$$q = 3.10^{-8} p_{\text{O}_2} \exp\left(\frac{81800}{RT}\right) \quad (4.7)$$

- iii) At still higher temperatures ($> 2500\text{K}$), the A-site oxidation becomes negligibly small compared to the B-site, and

$$q = 5.35 \times 10^{-2} p_{\text{O}_2} \exp\left(-\frac{15200}{RT}\right) \quad (4.8)$$

A summary of these measurements of soot oxidation rates is shown in Figures 4.5 (a) and (b).

TABLE 4.2
Conditions of Soot Oxidation Measurements

AUTHOR	p_{O_2} (atm)	$T^{\circ}\text{K}$	MEAN PARTICLE SIZE A°
Lee, Thring and Beer	0.04-0.1	1300-1700	400
Tesner and Tsibulevsky	0.1	1400-2000	-
Park and Appleton	0.05-13	1700-4000	45-180
Nagle and Strickland-Constable	0.1-0.6	1000-2000	-
Fenimore and Jones	10^{-4} -0.3	1530-1890	-

Fenimore and Jones (100) from their experiments of dry soot oxidation showed a weak dependence on the oxygen concentration in contradiction to the preceding workers. They claimed that the primary agent responsible for soot oxidation was the hydroxyl radical OH. Page and Ates (101) also confirmed the effectiveness of hydroxyl radical in soot oxidation in fuel rich flames.

Radcliffe and Appleton (102) found it unnecessary to involve the hydroxyl radical in an oxidation mechanism. They argue that the rates measured (100,101) in rich flames may be due to traces of oxygen greater than their equilibrium estimates, but still too small to measure. They found that the oxidation rates measured in flames and that of pyrographite are in reasonable agreement. Therefore, the suggestion of Rosner and Allendorf that the OH radical removed a carbon atom less frequently (1 percent) than found (10 percent) by Fenimore and Jones supports the view that the contribution of the OH radical on the rate of soot oxidation is small.

In an early work, Magnussen (103) established a rate equation for oxidation of soot in turbulent flames in the form

$$q = \frac{K_1}{1 + \frac{K_1}{K_2}} \quad (4.9)$$

NO - this laminar.

where K_1 is the rate of adsorption of oxygen and K_2 is the rate of desorption of CO on the soot particle surface. These rates are expressed as

$$K_1 = 3.05 \times 10^6 p_{O_2}^2 \exp\left(-\frac{29200}{RT}\right) \quad (4.10)$$

and

$$K_2 = 9.84 \times 10^{-5} \exp\left(\frac{300}{RT}\right) \quad (4.11)$$

In this study Magnussen found that the calculated oxidation rates are higher than the observed rates. He therefore suggested that the role of turbulence is vital for estimating realistic soot oxidation rates in turbulent flames.

Becker and Yamazaki (104) and Prado et al (105) suggest that any model in a turbulent fuel combustion system has to combine both the mixing of a fuel and air, and the chemistry of soot formation and burnout. Neither of these two processes is well understood and only very approximate global modelling of soot formation is at present possible.

4.2.3 Current Status

At this stage, the soot emission predictions in turbulent flames and engines appear in a state of confusion. As regards chemical kinetics, there have been many studies predicting soot oxidation rate as discussed above. The study of Nagle and Strickland-Constable (99) covers a wide range in terms of temperature and partial pressure of oxygen. They suggested that the soot oxidation rate in high partial pressure regions have zero order dependence with respect to partial pressure of oxygen (Figure 4.5(b)). They presented three equations (4.5) - (4.8) for the four of temperature and oxygen partial pressure regimes, this makes their use cumbersome. Out of these four equations (4.6) and (4.7) will appear suitable for engine conditions. However they bear a different relationship with temperature and varying dependence with partial pressure of oxygen as against equation (4.4) of Lee et al. However the equation of Lee et al is widely applied in existing Diesel soot emission studies. This equation has first order dependence on oxygen concentration. From an engine study (83) there is an evidence of influence of intake oxygen concentration (Figure 4.6) on oxidation of soot particulates and precursors. Also, there is an undisputed view, in the literature, that additional to the chemical kinetics, the air-fuel mixing process influences soot-formation and combustion over a wide range of engine operating conditions.

Lee et al (83) have shown that the soot particulate emission can be correlated in terms of the adiabatic flame temperature (T_f) and a turbulent mixing parameter involving engine speed (N), total fuel quantity injected (V_{fi}) and the rate of fuel injection (\dot{m}_f). The correlation is of the form

$$N^p \dot{m}_f^q V_{fi}^r e^{-\frac{E}{RT}} \quad (4.12)$$

where p , q and r are empirical constants and E is the activation energy. This suggests that in an Arrhenius type of rate equation which is widely used in existing Diesel engine soot oxidation models, the air-fuel mixing can be accounted for through a suitable mixing parameter in the pre-exponential term. If one considers after Magnussen (106), and Becker et al (104) that the soot burn up takes place in the fine structure of the turbulent eddy - the so called Kolmogorov structure, then it would be quite reasonable to assume that the soot burn out in these regions would indeed be on a molecular scale and therefore an equation such as that of Lee et al (52) would be applicable.

4.3 Proposed Model

Based on this concept the proposed model incorporates the effect of air-fuel mixing by modifying the Lee et al soot oxidation rate equation. Although the equation in its present form overestimates (when extrapolated in the region of high temperature) compared to other oxidation rate equations (Figure 4.5(b)), this seems to be the most appropriate in situations where the combustion takes place at a molecular level. Furthermore as will be discussed later, only a fraction of the small structure containing soot will actually burn up, so that this modification to the equation of Lee et al will result in burn up rates per unit mass comparable to the other data shown in Figure 4.5(b). Magnussen and co-workers (106, 107) have already suggested

that in turbulent systems the chemical reaction between oxygen-containing eddies and soot-containing eddies occurs when the reactants are mixed on a molecular scale at a sufficiently high temperature. In general, the large scale eddies (assumed to be of the order of the equivalent diameter of orifice, $L \sim 10^{-3}\text{m}$) break up into fine scale eddies (of the order of Kolmogorov length scale $\eta \sim 10^{-6}\text{m}$). This turbulent structure is represented in Figure (4.7). At any instant only a fraction ψ of the soot containing fine structure within the eddy will be burning. The fraction of the total fuel burning in the fine structure is simply the ratio of the local concentration of reacted fuel (m_{fb}) to the total fuel concentration ($m_{fu} + m_{fb}$) given by

$$\psi = \frac{m_{fb}}{m_{fu} + m_{fb}} \quad (4.13)$$

In terms of turbulent dissipation (ϵ) and the kinetic energy (k), Magnussen has expressed the mass fraction of the total fluid contained within the fine structures as

$$r^* = 9.7 \left(\frac{\nu \epsilon}{k^2} \right)^{\frac{3}{4}} \quad (4.14)$$

where ν is the kinematic molecular viscosity. Therefore, the term $r^*\psi$ will represent the mass fraction of the fine structure burned. Also, he defined the mass transfer between the fine structures and the surrounding large structure by

$$\dot{m} = 2 \frac{U^*}{L^*} r^* \quad (4.15)$$

where L^* is the characteristic length of the fine structure and U^* is its characteristic velocity. These quantities are given as

$$L^* = 1.43 \left(\frac{v^3}{\epsilon} \right)^{\frac{1}{4}} \quad (4.16)$$

and

$$U^* = 1.74 (v\epsilon)^{\frac{1}{4}} \quad (4.17)$$

In equation (4.14), the specific turbulent kinetic energy term can be expressed in terms of turbulence velocity u' as

$$k = u'^2 = (L\epsilon)^{2/3} \quad (4.18)$$

hence equation (4.14) becomes

$$r^* = 9.7 \frac{1}{L} \sqrt{\frac{v}{\zeta}} \quad (4.19)$$

where $1/\zeta$ is the measure of the mixing rate by which the fine structure breaks down and intermixes fuel and oxygen to the molecular level. This is represented as

$$\frac{1}{\zeta} \sim \left(\frac{\epsilon}{v} \right)^{\frac{1}{2}} \quad (4.20)$$

Dent (73) has calculated the turbulent energy dissipation rate (ϵ) in terms of fuel injection parameters for a quiescent chamber Diesel engine as

$$\epsilon = C \left(\frac{N}{\theta_{ip}} \right)^3 \left(\frac{V_{fi}}{A_o} \right)^2 \quad (4.21)$$

where C is a constant, N is engine speed, θ_{ip} is the injection period, V_{fi} is the fuel quantity (mm^3/cycle), A_o is the total orifice area.

He has also shown a correlation of the mixing rate with exhaust smoke for quiescent and swirl assisted engines.

Considering the Damkohler number for the fine structure soot burn up defined as $(\frac{R_{chem}}{R_{mix}})$ it is found that in the fine structure, kinetics seem to be controlling the burnout of soot because R_{chem} ($\sim 10^5 \text{ s}^{-1}$) $<$ R_{mix} ($\sim 10^6 \text{ s}^{-1}$) where

$$R_{chem} = \frac{6 C_s}{\rho_s d_s} q \quad (4.22)$$

$$R_{mix} = 1/\zeta \quad (4.23)$$

where C_s is the net soot concentration (kg/m^3), d_s is the average soot particle diameter (m), ρ_s is the density of soot (kg/m^3) and q is the surface reaction rate given by equation (4.4) of Lee et al.

The surface temperature of the soot particles reacting in the fine structures can be taken equal to the local adiabatic flame temperature (computed earlier from equations (2.17) - (2.19)) of the reacting eddies. At the finest Kolmogorov scale there is no oxygen gradient at the soot particle surface because of the high mixing rates in these regions as illustrated above from the Damkohler number.

This analysis suggested that the air fuel mixing can be accounted for in a kinetic rate equation of the soot oxidation. Although fuel burning and soot formation are considered on a gross basis, the soot burnout is assumed to occur in a fraction of the fine structure. The equation of Lee et al provides only for the gross oxidation rate of soot which appears to be a reason for overpredicting the oxidation rate. One can, therefore, consider the multiplication of the equation of Lee et al by ψr^* , to account for the reacting mass of the soot and

oxygen in the small structure. From the experience during this work, this seems a plausible assumption. The substitution of equation (4.4) in (4.22) derived from Lee et al and the multiplication of the fine structure burning fraction, the new soot oxidation equation thus takes the form

$$\frac{dS_c}{dt} = \frac{6.51}{\rho_s d_s} \frac{p_{O_2}}{T^2} \frac{m_s}{V_b} \exp\left(-\frac{39300}{RT}\right) r^* \psi \quad (\text{kg/m}^3 \cdot \text{s}) \quad (4.24)$$

where V_b is the burnt gas volume and m_s is the net soot mass available for oxidation.

Comparison of equation (4.12) suggested by Plee et al (83) as $N^p m^q V_{fi}^r \exp\left(-\frac{E}{RT}\right)$ with above soot oxidation rate equation indicates that the proposed modification brings the desired engine mixing parameter in the kinetic rate equation for soot oxidation through expression of r^* in terms of engine injection parameters which is

$$\frac{C}{d_o}, \left(\frac{N}{\theta_{ip}}\right)^{3/2} \left(\frac{V_{fi}}{A_o}\right)$$

Summary

In this model, the net soot release rate is given through soot formation and oxidation rate calculations. A summary of the equations used and the flow chart for the model is presented in Table 4.3 and Figure (4.8), respectively. The values of mean soot density and particle size are assumed equal to 2000 kg/m^3 and 250 \AA respectively. The value of mean particle size is in conformity with the findings of Vuk et al (108).

TABLE 4.3

Summary of Soot Formation and Oxidation Equations

PROCESS	EQUATIONS	REMARKS
Formation	<p>i) <u>Nuclei formation</u></p> $n_o = a_o \frac{P_{fu}}{T} \exp\left(-\frac{E_{sf}}{T}\right)$ $\frac{dn}{dt} = n_o + (f-g)n - g_o n N$ <p>ii) <u>Particle formation</u></p> $m_p = \frac{\pi}{6} d_s^3 \rho_s$ $\frac{dN}{dt} = (a-bN)n$ <p style="text-align: center;">(part/m³/s)</p> $S_f = \frac{dN}{dt} \cdot m_p$ <p style="text-align: center;">(kg/m³s)</p>	<p>m_p is the mass of a soot particle</p>
Oxidation	<p>i) <u>Soot oxidation</u></p> $\psi = \frac{m_{fb}}{m_{fb} + m_{fu}}$ $\frac{l}{\zeta} = \frac{C}{v^{\frac{1}{2}}} \left(\frac{N}{\theta_{ip}}\right)^{3/2} \left(\frac{V_{fi}}{A_o}\right)^2$ $r^* = \frac{9.7}{d_o} (v\zeta)^{\frac{1}{2}}$ $\dot{m} = \frac{23.6}{d_o} \left(\frac{v}{\zeta}\right)^{\frac{1}{2}}$ $S_o = \frac{6.51}{\rho_s d_s} \frac{P_{O_2}}{T^{\frac{1}{2}}} \frac{m_s}{V_b} \exp\left(-\frac{E_{so}}{T}\right) \cdot r^* \psi$ <p>ii) <u>Nuclei reduction</u></p> $\frac{dn_c}{dt} = \dot{m} r^* \psi \frac{\bar{n}}{C_{fu}} \bar{C}_{min}$	<p>\bar{C}_{min} is the minimum of fuel or oxygen concentration in fuel rich eddies. \bar{n} and C_{fu} represent the time mean values of the nuclei and fuel concentration</p>

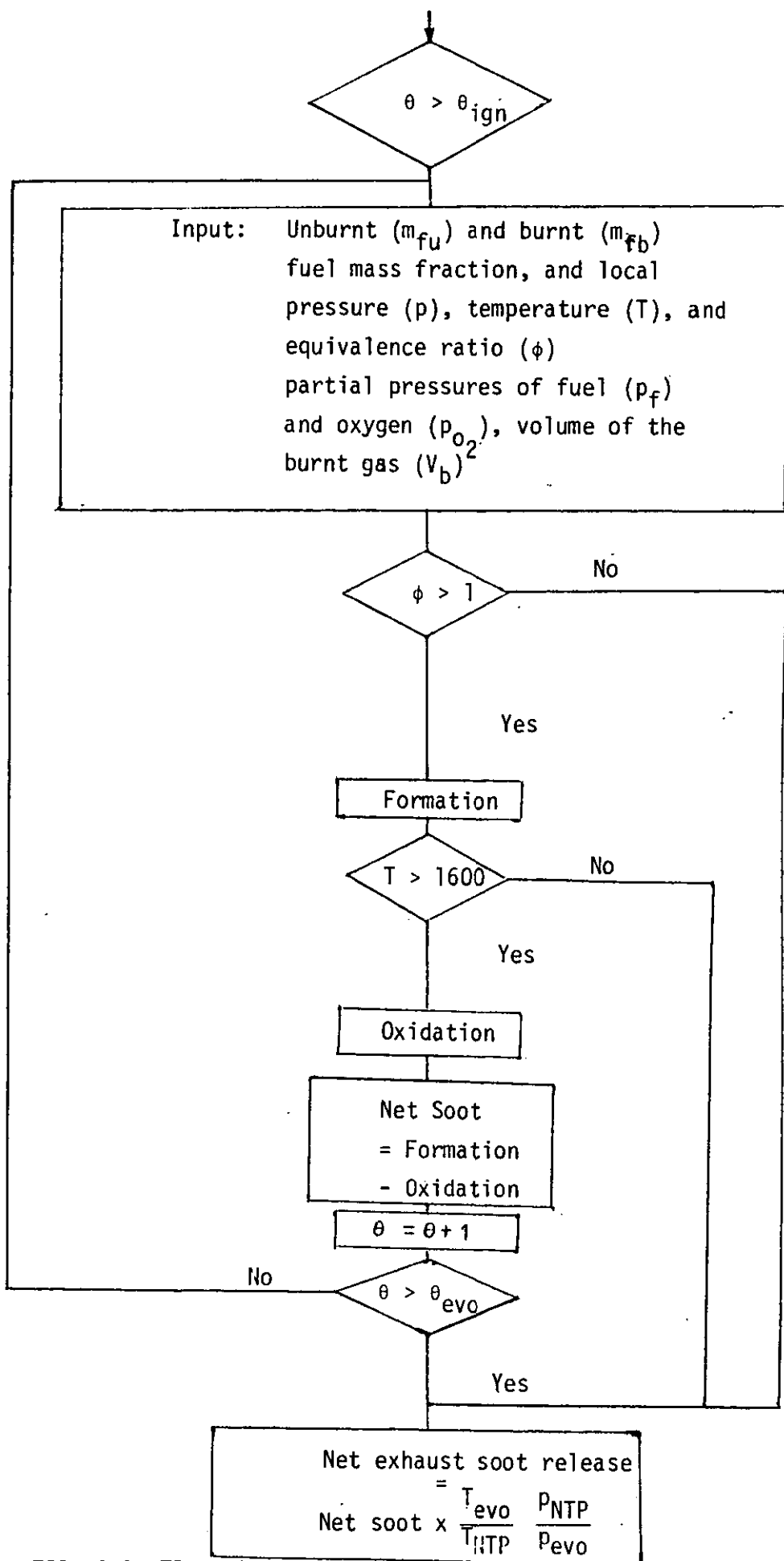


FIG. 4.8 Flow chart for the soot model

4.4 Calculation Procedure for the Net Soot Release

The net instantaneous soot from the engine exhaust is the result of soot formation and oxidation rates yielding

$$\dot{S}_{\text{net}} = \dot{S}_f - \dot{S}_o \quad (4.27)$$

where \dot{S}_f is the rate of soot formation and \dot{S}_o is the oxidation rate.

The soot formation occurs in rich regions (equivalence ratio greater than 1) of the jet and is calculated from the equations listed in Table 4.3.

The soot formation is assumed to occur in the whole eddy while oxidation takes place in the fraction of the fine structure. A uniform temperature is assumed to calculate the formation and oxidation rates at any instant. Plee et al (83) have already demonstrated that soot emission in diesel engines can be correlated with the stoichiometric flame temperature and hence it lends some support to the assumption of using the local adiabatic flame temperatures in computing soot formation and oxidation rates. The local flame temperature values reported in the work of Plee et al are of the order of 3000K. The maximum local temperatures computed in this work are of the same order.

The number of molecules contained in 1 kmole of gas is given by Avogadro's number ($\sim 6.02 \times 10^{26}$ molecules/kg mole). Therefore, the number of molecules contained in 1 m³ of gas may be expressed through equation of state as

$$N = 7.35 \times 10^{22} \frac{P}{T} \text{ molecules/m}^3 \text{ gas} \quad (4.28)$$

Using Avogadro's number in equation (4.28), the value of N_0 in equation (4.2) can be expressed in terms of the partial pressure of

fuel (p_{fu}) and temperature T as

$$N_o = 12.2 \times 10^{-5} M_{fu} \frac{P_{fu}}{T} \text{ (kg/m}^3\text{)} \quad (4.29)$$

Finally, equation (4.2) for the spontaneous rate of soot nuclei formation is expressed as

$$n_o = a_o \frac{P_{fu}}{T} \exp \left(- \frac{E_{sf}}{T} \right) \text{ (part/m}^3\text{/s)} \quad (4.30)$$

where a_o is the modified constant from Tesner. Its value is given in Table 4.4.

Also the value of other constants used in equations (4.1) - (4.3) are given in Table 4.4.

TABLE 4.4
Constants in Soot Nuclei and Particle Formation Equations (4.2 - 4.4) from Tesner et al (87)

constant	a	f-g	g_o	b	n_o	E_{sf} (Cal/mol)
value	10^5	10^2	10^{-15}	8.0×10^{-14}	7.254×10^{30}	9×10^4

The value of activation energy in the soot oxidation rate equation (4.24) is assumed equal to 39300 cal/mol following Lee et al (52). Also the soot oxidation is assumed to occur above a temperature of 1600K following Spalding (109).

The reduction in soot nuclei concentration follows the basis of Magnussen et al (107). - In terms of the instantaneous time-mean nuclei concentration (\bar{n}) and fuel concentration (\bar{C}_{fu}) values and the

mass transfer rate (\dot{m}) between surroundings and fine structures is written as

$$\frac{dn_c}{dt} = m \bar{c}_{\min} r^* \psi \frac{\bar{n}}{\bar{c}_{fu}} \quad (4.31)$$

where \bar{c}_{\min} is the smallest of \bar{c}_{fu} and \bar{c}_{o_2}/s , where \bar{c}_{o_2} is the local oxygen concentration and s is the stoichiometric constant.

The mixing time, and the net soot particle and nuclei concentrations at any instant are computed on the basis of the local jet volume. At the end of injection the volume occupied by the burned products and the entrained air in the engine cylinder is the basis of computing soot density. Note this volume is slightly less ($\approx 5\%$) than the cylinder volume at E.V.O.

4.5 Calculation of Exhaust Soot in Terms of Bosch Number

The net soot concentration at exhaust valve opening is reduced to NTP using the relationship

$$\dot{S}_{\text{net}} = \dot{S}_{\text{evo}} \frac{V_{\text{evo}}}{V_{\text{NTP}}} \quad (4.32)$$

where V_{evo} is the volume of burned mass at exhaust valve opening which is reduced to the corresponding volume at NTP (V_{NTP}).

This procedure is adopted to arrive at respective Bosch smoke number values for the exhaust soot for comparison of experimental and predicted results. The conversion of soot concentration to Bosch smoke number is obtained from the table given in reference (110).

In the computer simulation program subroutine S00T includes the above calculations for the soot emission.

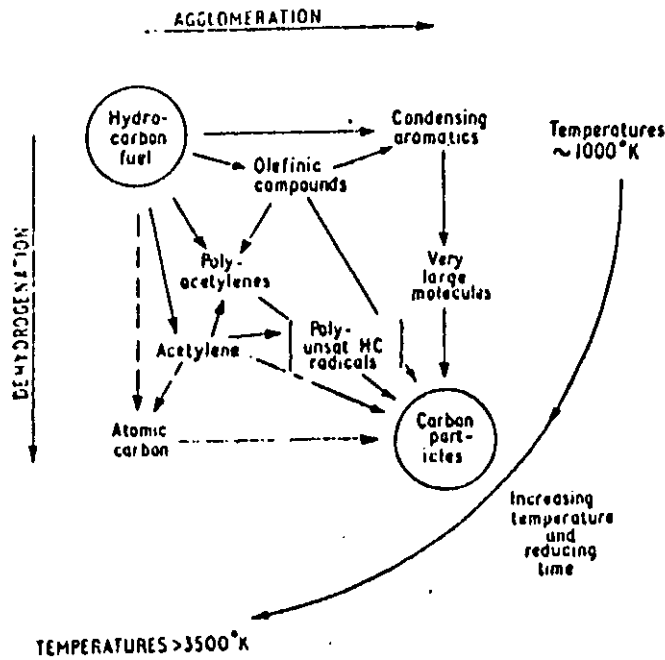


FIG. 4.1 Schematic of reactions involved in the formation of carbon from hydrocarbon fuels (80)

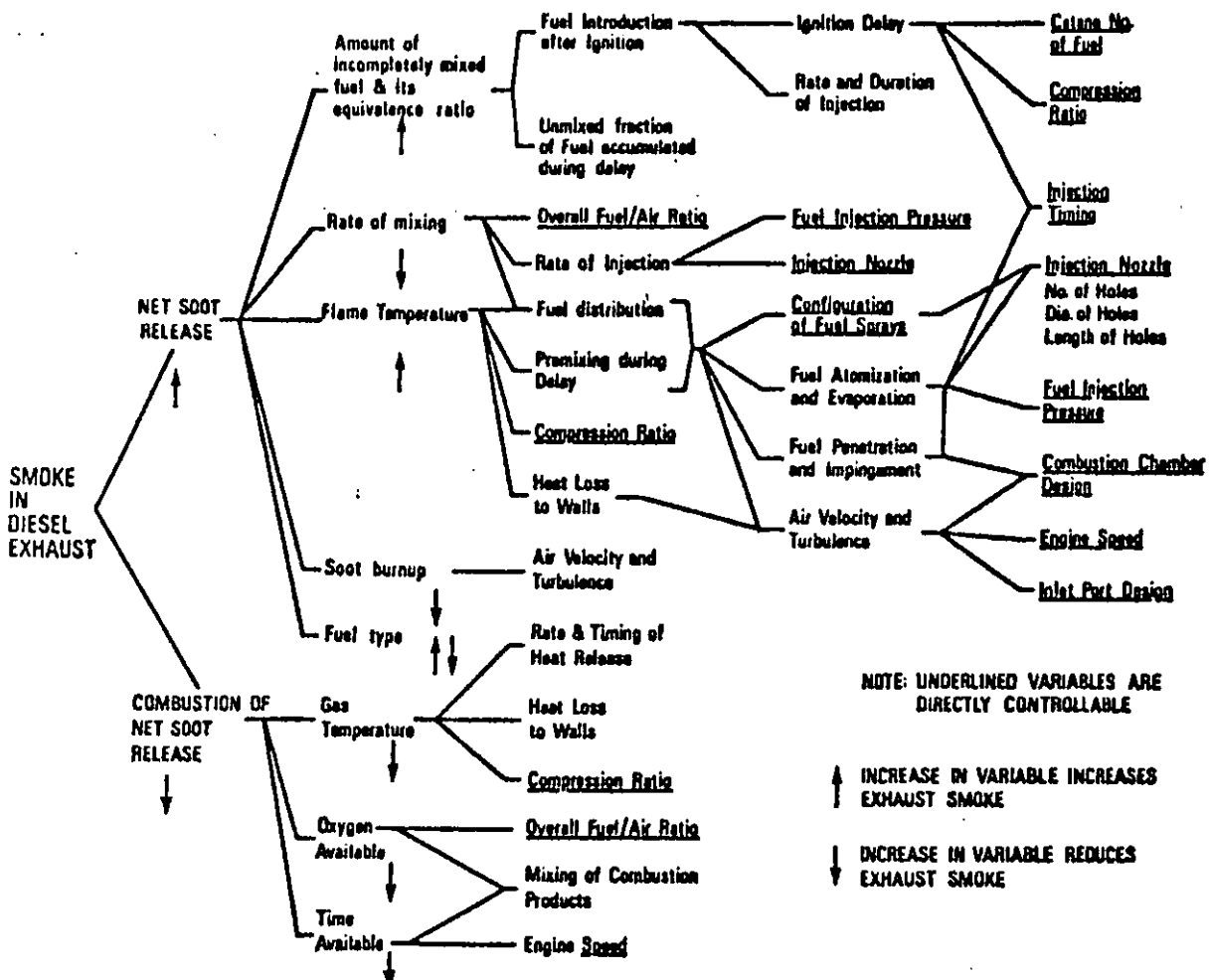


FIG. 4.2 Variables affecting diesel engine smoke (80)

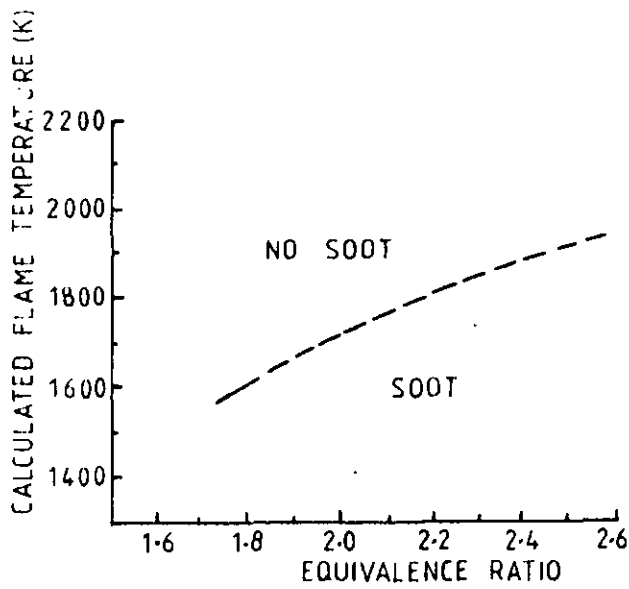


FIG. 4.3 Effect of equivalence ratio and flame temperature on soot formation (88)

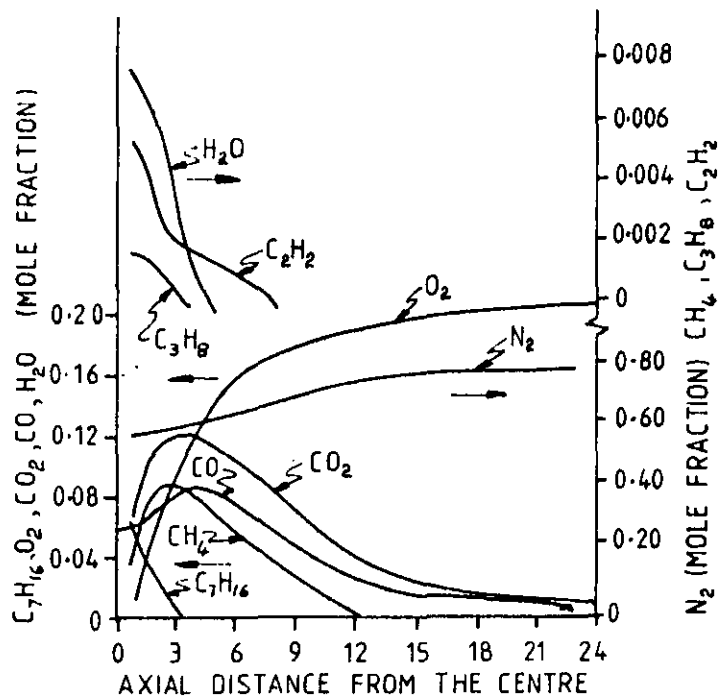
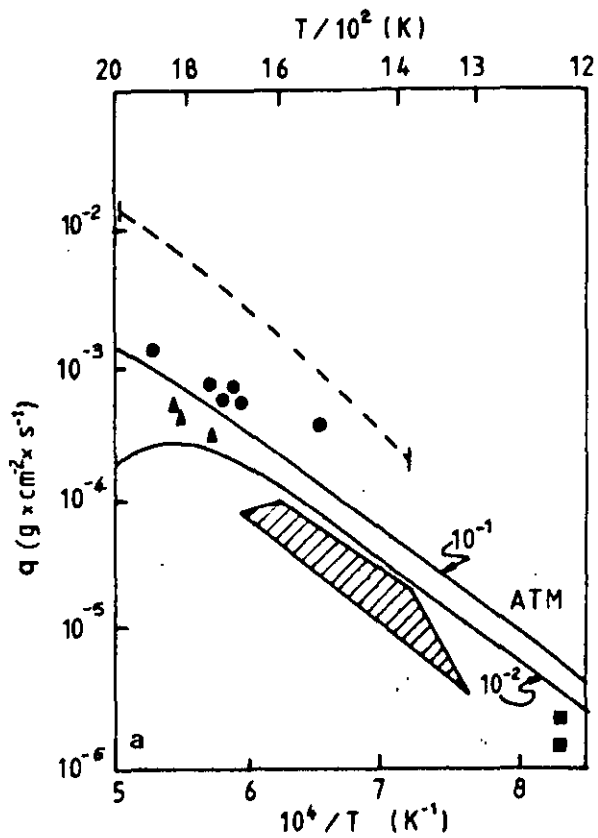


FIG. 4.4 Axial composition profiles in an envelope flame of n-heptane (95)



- □ ● Park and Appleton
 - ▲ ▴ Fenimore and Jones
 - - - Tesner and Tsibulvski
 - ////// Lee, Thring and Beer (LTB)
 - ⋯⋯⋯ LTB extended in higher temperature regions
 - ▭ LTB with mixing parameter $r^*\psi$
- $T \times 10^{-2}$ K

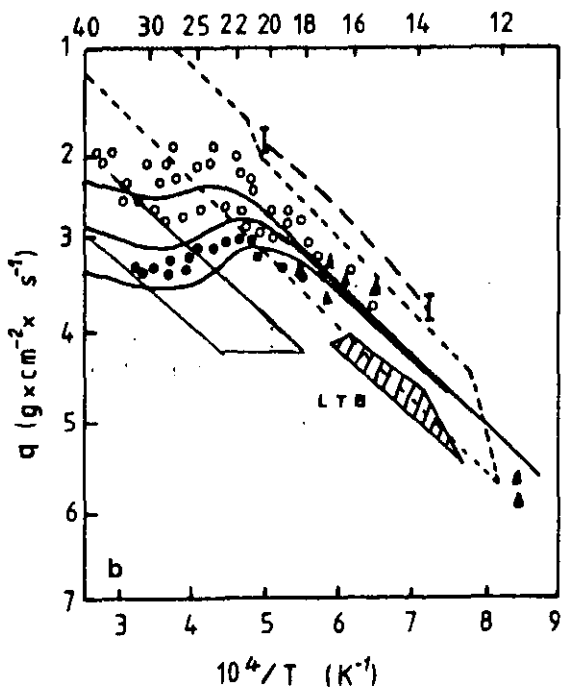


FIG. 4.5 Results of measurements of specific soot oxidation rate as a function of temperature (a) and the oxygen partial pressure (b) from reference (99)

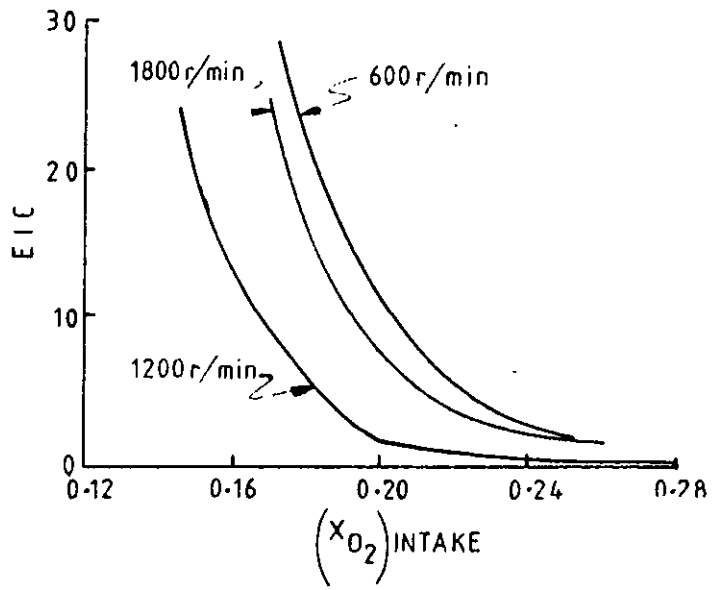


FIG. 4.6 Influence of intake oxygen concentration (83) on carbon index (EIC, soot emission index)

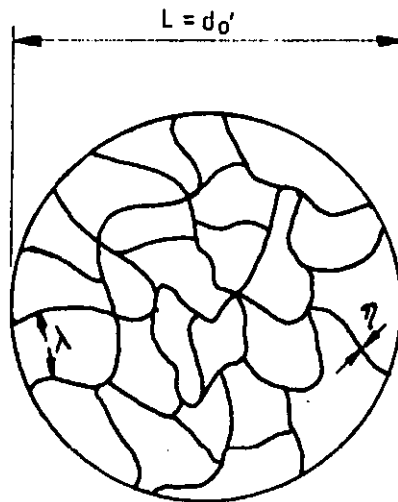


FIG. 4.7 Turbulent Structure

CHAPTER V

MODEL FOR SWIRL IN DIESEL ENGINES5.1 Introduction

The effect of swirl is of considerable importance in developing the high speed Direct Injection Diesel engine. The in-cylinder air motion assists the fuel injection process in the mixing of fuel and air and hence the engine combustion process. There have been successful attempts (111-114) to measure air motion inside the engine cylinder. However, very little has been achieved in terms of modelling. In many of the engine modelling studies (12, 13, 18, 19), the effect of swirl is accounted for quite implicitly by using empirical constants in entrainment equations or by changing the local concentration values (20), in an enhanced mixing assumption. The attempts of Adler and Lyn (10), and Whitehouse and Aburghers (39) in this direction are more involved, but both these studies used complicated sets of equations concerning mass, momentum, and energy conservation. The solution of these equations, therefore, is very cumbersome. The former study does not account for combustion and wall impingement effects, while the latter has incorporated the two zone combustion model (15) and the air entrainment calculation for the wall jet from literature of radial and parallel wall jets along with the spray trajectory calculations. A recent study of Sinnamon et al (115) has shown that an analytical spray model can be developed to calculate the penetration and trajectory of a spray in an engine combustion chamber with air swirl. Their model consists of solutions of integral continuity and momentum equations in a steady state gas jet with simplified assumptions.

Based on the assumptions of Sinnamon et al, a simple phenomenological approach for the modelling of swirl type engines is described below.

5.2 Physical Basis of the Model

5.2.1 Calculation of Swirl Ratio

The air swirl motion during the compression period is evaluated by applying the principle of conservation of momentum to the contents of the engine cylinder as described by Dent and Derham (113). Neglecting the effects of fluid friction, the rate of change of angular momentum of the solid body swirling flow can be written as

$$\frac{d}{dt} (I_c \omega_c) = 0 \quad (5.1)$$

therefore

$$I_c \omega_c = \text{constant} \quad (5.2)$$

where ω_c is the swirl and I_c is the moment of inertia during the compression period.

The moment of inertia of the cylinder contents, at any instant, for a deep bowl cylindrical combustion chamber concentric with the engine cylinder axis can be written as

$$I = \frac{m_t}{2} \left[\frac{\pi \left(\frac{D}{2}\right)^4 \frac{\lambda(\theta)}{V} + \left(\frac{d}{2}\right)^2}{\pi \left(\frac{D}{2}\right)^2 \frac{\lambda(\theta)}{V} + 1} \right] \quad (5.3)$$

where m_t is the trapped air mass in the cylinder, $\lambda(\theta)$ is the instantaneous stroke, d is the bowl diameter, D is the engine bore and V is the volume of the bowl.

During the induction period, equation (5.3) can approximately be written as

$$I = \frac{m_t}{2} \left(\frac{D}{2}\right)^2 \quad (5.4)$$

Since the angular momentum is constant during the compression period, $I_c \omega_c$ in equation (5.2) can be equated to the angular momentum of the cylinder contents at inlet valve closure (ω_0). Rearrangement of equations (5.2), (5.3), and (5.4) yields

$$\omega_c = \frac{\left(\frac{D}{2}\right)^2 \omega_0}{\pi \left(\frac{D}{2}\right)^4 \frac{\lambda(\theta)}{v} + \left(\frac{d}{2}\right)^2} \left[\frac{\pi \left(\frac{D}{2}\right)^2 \frac{\lambda(\theta)}{v} + 1}{\pi \left(\frac{D}{2}\right)^2 \frac{\lambda(\theta)}{v} + 1} \right] \quad (5.5)$$

Thus, knowing the intake swirl level (ω_0), the swirl during compression (ω_c) can be computed from the above relationship. In engines, the mean swirl at intake is represented by the swirl ratio defined as the ratio of swirl revolutions (N_s) to the engine revolutions (N), that is

$$SR = \frac{N_s}{N} \quad (5.6)$$

which is a known quantity. Invariably, the assumption of solid body rotation results in the following expression for the tangential velocity

$$u_{s\omega} = \omega r \quad (5.7)$$

where ω is angular velocity (rad/s) and r is the radial distance from the centre of the bowl. The general validity and acceptance of this assumption is demonstrated by various workers (17, 20, 116, 117).

5.3 Modifications in Quiescent Chamber Model

When fuel is injected in the presence of air motion in the engine cylinder, many features of the quiescent chamber analysis presented in Chapter II are altered, which include:

- i) Spray trajectory (spray penetration and deflection).
- ii) Air entrainment into the spray.
- iii) Wall impingement.
- iv) Turbulent mixing.

Modifications applied in the model for these features are described in this chapter.

5.3.1 Spray Trajectory

5.3.1.1 Penetration

Sinnamon et al have shown that the spray penetration distance predicted from their gas model primarily follow the penetration correlation of Chiu et al (27). The comparison of penetration results from the correlation of Chiu et al with those obtained from the correlation of Dent (used in this model) are shown in Figure 5.1. The predictions from these two correlations and the gas jet model of Sinnamon et al are in good agreement for the non-swirl case. This suggests that Dent's penetration equation can be applied with the modification suggested from the experimental studies of Chiu et al to incorporate the effect of swirl on penetration. In the presence of swirl, according to Chiu et al, the straight penetration decreases by an amount given by

$$\frac{S - S_{\omega}}{S} = 0.35 \left(\frac{S_{\omega} J_a}{d J_0} \right)^{0.44} \quad (5.8)$$

where S_w is the penetration in presence of swirl, d is the orifice diameter and J_a and J_o are the momenta of air and fuel jet respectively

$$J_a = \rho_o S_w^2 \omega^2 \quad (5.9)$$

and

$$J_o = \rho_f U_{jet}^2 \quad (5.10)$$

It is worth noting that the relationship developed by Chiu et al in its present form is applicable to central injection only.

5.3.1.2 Spray Deflection

Spray deflection results from the normal component of the air motion and the drag forces on the jet. Assuming an axisymmetric circular jet Sinnamon et al have described the following equation for the change in the direction of the jet centreline

$$\frac{d\theta}{d\ell} = \frac{2 U_t E_f}{r_{jet} U_m^2 R} + \frac{C_d U_n |U_n|}{\pi r_{jet} U_m^2 R} \quad (5.11)$$

where U_t and U_n are the tangential and normal components of the swirl velocity U_{sw} , r_{jet} is the jet radius, U_m is the jet centreline velocity, C_d is the drag coefficient, ℓ is the arc length of the jet, R is the integral defined in Appendix A after equation (A.13) and

$$E_f = \left(\frac{\rho_m}{\rho_a}\right)^{\frac{1}{2}} 2\pi r_{jet} [a_1 (U_m - U_t) + a_2 |U_n|] \quad (5.12)$$

where ρ_m is the density at the jet centreline.

Combining equations (5.8) and (5.11) in a vectorial approach, the position of the deflected jet is located in the engine cylinder. The parameters α_i ($i = 1,3$) and S_{ω_i} ($i = 1,3$) are the angles and coordinates of the jet centreline with respect to the three coordinate axes X, Y and Z respectively (Figure 5.3). The initial direction vector of the jet is known in terms of the position of the jet centreline with respect to the coordinate system.

The swirl velocity can be expressed in vectorial form as:

$$\overline{U_{S\omega_i}} = \overline{\omega_i} \times S_{\omega_i} \quad (5.13)$$

The suffix i in the analysis represents the x, y and z components of the vectorial quantity in question.

The swirl velocity is assumed to rotate about the cylinder axis and impinges on the jet at an angle θ_0 . Considering \overline{U}_{jet} and $\overline{U}_{S\omega}$ as the jet and air motion velocity vectors at any point A on the jet surface in an elementary plane containing these two vectors, the swirl velocity can be resolved in two components - one parallel to the jet velocity (called tangential component \overline{U}_t) and the other normal to the jet but in the elementary plane (called normal component, \overline{U}_n). These are obtained by writing

$$\overline{U}_t = (\overline{U}_{S\omega} \cdot \hat{t}) \hat{t} \quad (5.14)$$

and

$$\overline{U}_n = (\overline{U}_{S\omega} - \overline{U}_t) \quad (5.15)$$

The magnitude and direction of these velocity terms as required in equation (5.11) can easily be obtained from these vectorial equations. Also the arc length $d\ell$ is computed by

$$d\ell = \frac{dS_{\omega}}{\cos \alpha_0} \quad (5.16)$$

where α_0 is shown in Figure (5.3) and is assumed equal to zero at the start of computation. Subsequently, it is determined through the analysis of the jet deflection at each instant.

The change in the position of the jet tip under the effect of swirl is written vectorially as

$$d\vec{X}_j = d\vec{S}_{\omega_j} + \vec{S}_{\omega_j} d\theta \hat{n}_j \quad (5.17)$$

where \hat{n}_j is the unit vector normal to the plane of \vec{S}_{ω} .

5.3.1.3 Jet Width

Adler and Baron (118) have suggested a simple modification in the jet growth equation of Abramovich (46) used earlier in the quiescent engine case and given in equation (2.7) as

$$\frac{dr_{\text{jet}}}{d\ell} = 0.11 \frac{u_m}{(u_m + U_t)} \frac{\rho_{\text{jet}}}{(\rho_a + \rho_{\text{jet}})} \quad (5.18)$$

where u_m is the excess jet centreline velocity ($U_m - U_t$) and U_t is the tangential component of air velocity.

5.3.2 Air Entrainment

The entrainment in a deflecting jet is composed of two components:

- i) the entrainment due to the tangential component of the jet,
- ii) the entrainment due to the normal component.

Combining these two effects, Sinnamon et al (115) have expressed the entrainment equation in the following form:

$$\frac{d\dot{m}}{dx} = (\rho_m \rho_a)^{\frac{1}{2}} 2\pi r_{jet} [a_1 (U_m - U_t) + a_2 |U_n|] \quad (5.19)$$

where a_1 and a_2 are the axial and normal entrainment parameters, and ρ_m is the density at the jet centreline.

Also, similar relationships have been used by many other workers (119-121). These are listed in Table 5.1. The first two studies relate to engines and both of them give identical values of the axial entrainment parameter. This value is normally evaluated by reducing equation (5.19) to the non-swirl case and comparing it with entrainment equation (2.6) of Ricou and Spalding referred to in the quiescent chamber model. The value from the other two investigations seem too high. Also, there is considerable disagreement in the value of normal entrainment parameter a_2 .

When derived from the Ricou and Spalding equation, it is difficult to find how Sinnamon et al have arrived at the $(\rho_m \rho_a)^{\frac{1}{2}}$ term in their expression which instead should have been ρ_a as appearing in the equation of Rife and Heywood (119). In the present investigation the entrainment equation for the deflecting jet is used in the following form:

TABLE 5.1

List of Entrainment Equations for Deflecting Jet

Author(s)	Equation	Value of Constants		Remarks
		a_1	a_2	
1. Sinnamon et al (115)	$\frac{dm}{dx} = (\rho_m \rho_a)^{\frac{1}{2}} 2\pi r_{jet}$ [$a_1(U_m - U_t) + a_2 U_n $]	0.035	0.05	
2. Rife and Heywood (44,119)	$\frac{dm}{dx} = 2\pi r_{jet} \rho_a$ [$a_1(U_m - U_t) + a_2 U_n $]	0.035	0.19	
3. Kamotani and Greber (120)	$\frac{dm}{dx} = 2\pi r_{jet} \rho_a$ [$a_1(U_m - U_t) + a_2 U_n $]	0.07	0.32 0.182	$\frac{J_o}{J_a} = 15$ $\frac{J_o}{J_a} = 60$
4. Stoy and Benheim (121)	$\frac{dm}{dx} = 0.32\pi\rho \frac{A_{jet}}{C_{jet}}$ [$a_1(U_m - U_t) + a_2 U_n $] for circular jet			A is area and C is the cir- cumference of the jet
	$\frac{dm}{dx} = \pi\rho d_{jet}$ [$a_1(U_m - U_t) + a_2 U_n $]	0.08	0.354 0.32- 0.48	From Hirst From Woolers (123)

$$\frac{dm}{dx} = 2\pi r_{jet} \rho_a [0.035 (U_m - U_t) + 0.05 |U_n|] \quad (5.20)$$

5.3.3 Ignition Delay

The ignition delay equation of Hardenberg and Hase (71) used earlier has shown good correlation for the swirl engine data as shown in Figure 5.2.

5.3.4 Wall Impingement

At low swirl ratios, the possibility of the jet impingement on the wall exists. Hence, an analysis to establish the impingement and the entrainment in the wall region is essential. Although there is a large literature (64) available on wall jets, there was great difficulty experienced throughout this work in adopting any of the existing analysis, this is essentially due to three facts:

- i) The wall jet diameters considered in the literature are small compared to those found in the engine.
- ii) No literature dealt with the developing region of the wall jet.
- iii) Wall jet to co-flowing velocity ratios were $\gg 1$ in the literature compared to the engine case which is ≈ 1 .

The commencement of the jet impingement is decided by the relative position of the outer edge of the deflected jet with respect to the wall distance as shown in Figure 5.4. A preliminary attempt is made to characterise the wall jet by using the coaxial jet analysis of Forstall and Shapiro (43). According to them

$$\frac{U_x}{U_{jet} - U_s} = \frac{4 + 12 (U_s/U_{jet})}{(S_w/d_{ow})} \quad (5.21)$$

where U_x is the excess jet centreline velocity ($= U_m - U_s$) at S_w , U_{jet} is the velocity of the jet at the point of impingement and d_{ow} is the diameter of the jet at the wall established from the geometric consideration at that point, since

$$U_x = \frac{dS_w}{dt} \quad (5.22)$$

Substitution of equation (5.22) in (5.21) yields

$$\frac{S_w}{2} = 4 + 12 \left(\frac{U_s}{U_{jet}} \right) (U_{jet} - U_s) d_{ow} t + C$$

At $t = 0$, $S_w = 0$, giving $C = 0$.

Hence, wall penetration (S_w) can be expressed as

$$S_w = \left[\left\{ 1 + 3 \left(\frac{U_s}{U_{jet}} \right) \right\} (U_{jet} - U_s) (8 d_{ow} t) \right]^{\frac{1}{2}} \quad (5.23)$$

where t is the time from the instant of impingement.

Similarly, the jet width is obtained from results of Forstall and Shapiro as

$$\frac{b_{\frac{1}{2}}}{(d_{ow}/2)} = \left(\frac{S_w/d_{ow}}{4 + 12 \frac{U_s}{U_{jet}}} \right)^{\frac{1}{2}} \left(1 - \frac{U_s}{U_{jet}} \right) \quad (5.24)$$

The total width of the wall jet is assumed equal to three times the half width (b_2) which is in accord with the literature (65).

Morris and Dent (117) have shown that the fuel air-mixing process in a swirl engine can be approximated by assuming a steady state jet is injected into a steady air swirl flow. On this basis they defined a mixing parameter in terms of the ratio of the jet momentum flux (J_o) to the flow momentum flux (J_a).

Dent (124) has arrived at an expression for the wall jet entrainment using the concentration data of Morris (45) in terms of the total air momentum (G_a) to the jet momentum (G_o) represented as

$$G_a = \rho_a U_a^2 R H \quad (5.25)$$

$$G_o = \rho_{jet} U_{jet}^2 A_o \quad (5.26)$$

where R is the bowl radius, H is the bowl depth and A_o is the nozzle orifice area. This yields an equation from Figure (5.5) which has the form:

$$AFR + 1 = 2.58 \left(\frac{S_w}{d_o'} \right) \quad (5.27)$$

where d_o' is the equivalent orifice diameter. This equation is used to compute the air entrainment in the wall region of the co-flowing jet.

5.3.5 Turbulent Mixing

There is a pronounced effect of swirl on the turbulent mixing and hence the turbulent mixing rate computed from the jet energy in

case of quiescent chamber engine needs modification. The effect of swirl and squish motion on the turbulent mixing rate needs to be accounted for. Using hot wire anemometry Brandl et al (125) have measured the turbulent velocity in the Direct Injection Diesel engine for various port designs and injection timings. By using their data, a correlation is obtained between mixing rate $\frac{1}{\tau} (= 3.87 \frac{U'}{\lambda})$ and the mean air swirl velocity (ω). Figure 5.6 shows such a plot and the relationship obtained from these can be represented as

$$\frac{1}{\tau_{S\omega}} = 9.627 \omega \quad (5.28)$$

The effect of this mixing rate in conjunction with the mixing rate due to jet energy dissipation given in equation (2.55) is considered in parallel such that

$$\frac{1}{R_{mix}} = \frac{1}{R_{swirl}} + \frac{1}{R_{jet}} \quad (5.29)$$

where R_{swirl} and R_{jet} are the mixing rates due to swirl and the jet respectively. They are represented by inverse of their respective mixing time expressions resulting in

$$\tau = \tau_{swirl} + \tau_{inj} \quad (5.30)$$

Apart from these modifications, the evaporation calculation in the presence of swirl requires consideration of relative velocity at each point. This is included through calculation of Re in terms of local excess velocity ($U - U_t$) given by modifying equation (2.8) to the form

$$\frac{U - U_t}{U_m - U_t} = (1 - Y_p^{3/2})^2 \quad (5.31)$$

where $U_m - U_t$ is the excess centreline velocity.

In general, the swirl analysis proceeds in terms of the value of the excess velocity. The other features of the model remain the same as described in Chapter II.

The swirl scheme is incorporated in the computer model through subroutines SWIRL and DEFL. They provide for the calculation of swirl levels and spray trajectory at any instant. However, the other modifications described above are introduced in the program at appropriate places.

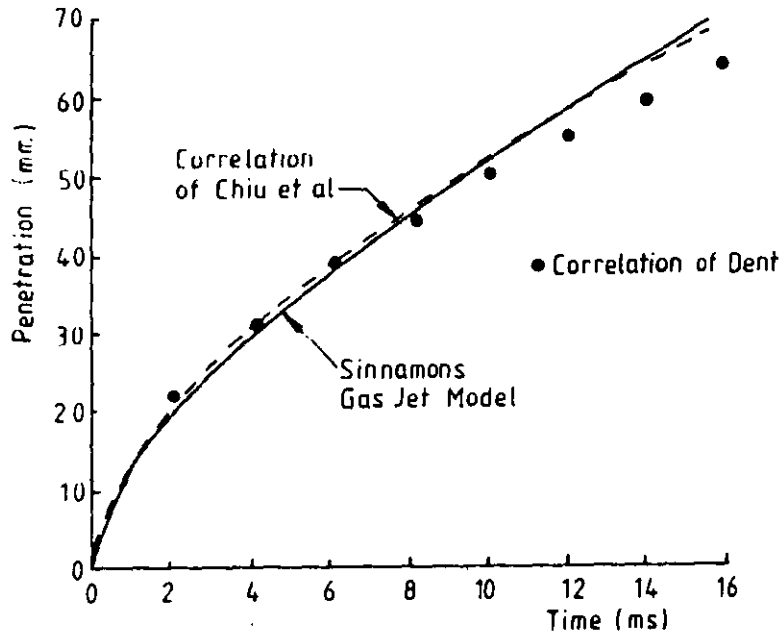


FIG. 5.1 Comparison of penetration relationship of Chiu et al, Dent, and Sinnamons et al gas jet model for non-swirl case

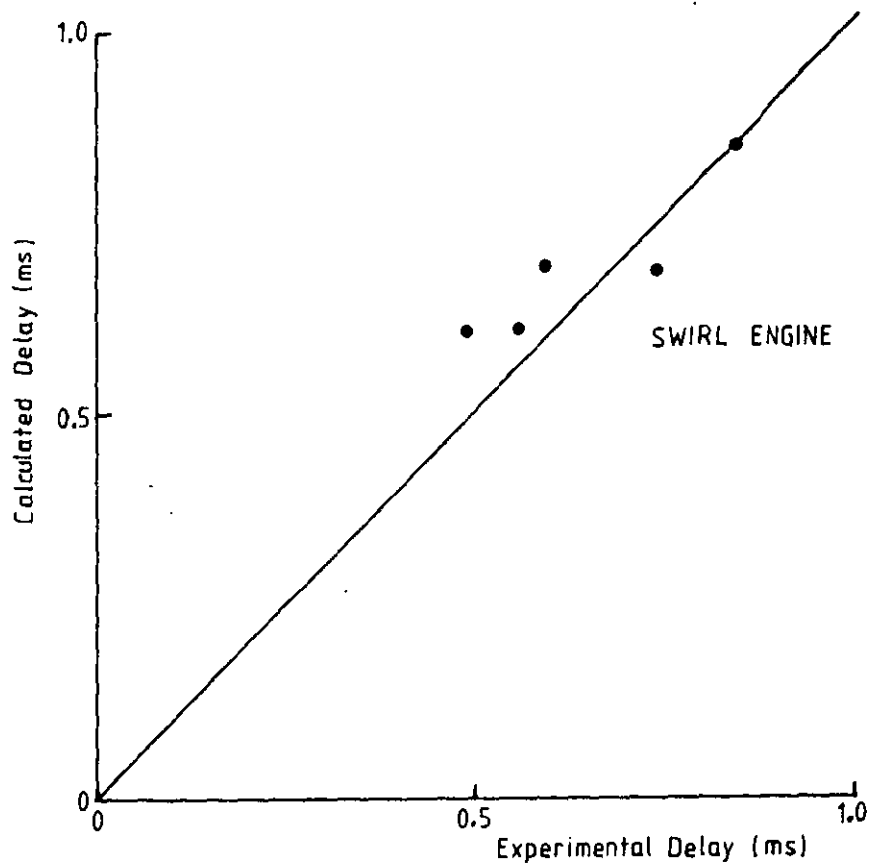


FIG. 5.2 Ignition delay correlation data

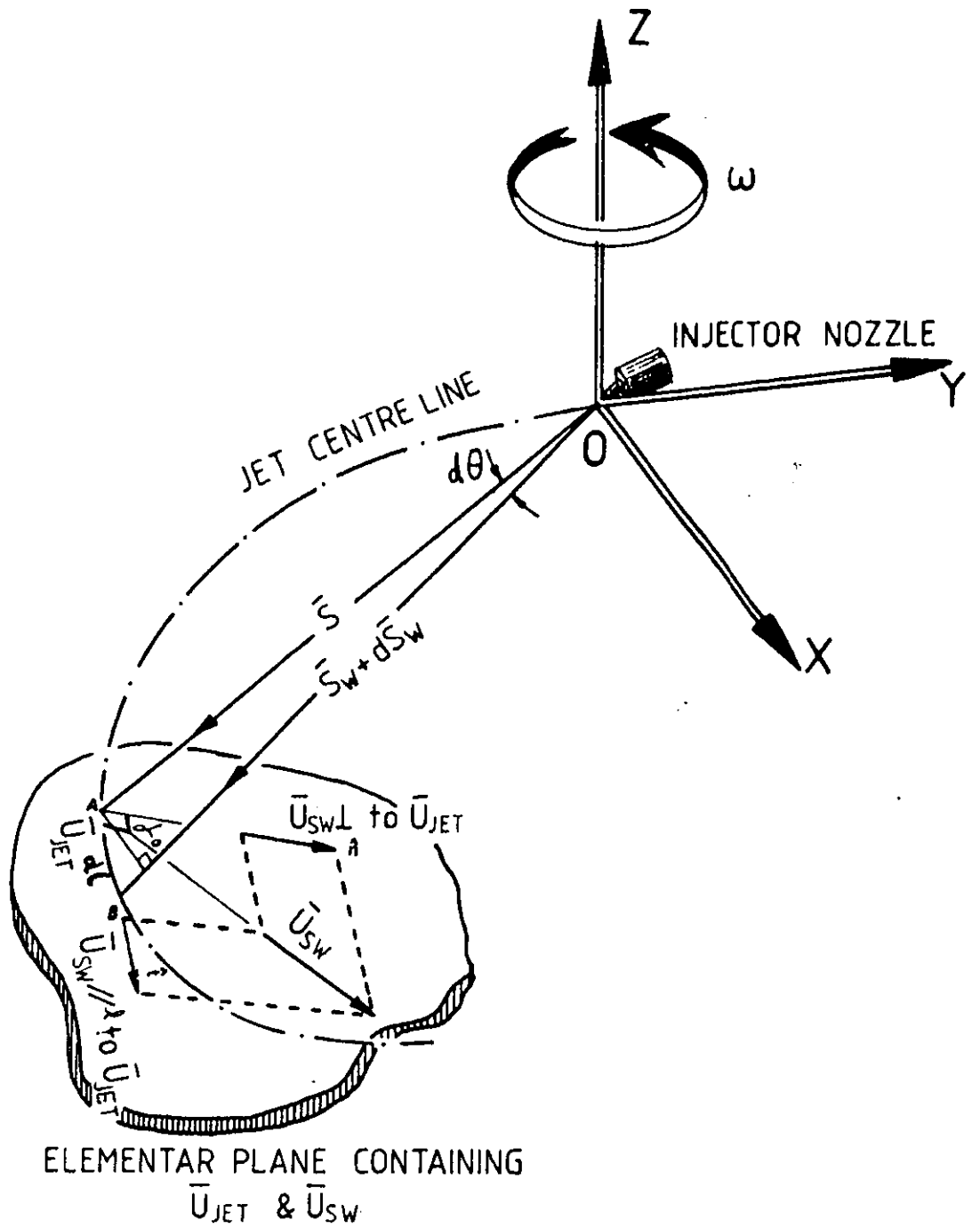


FIG. 5.3 Schematic of spray deflection in presence of swirl

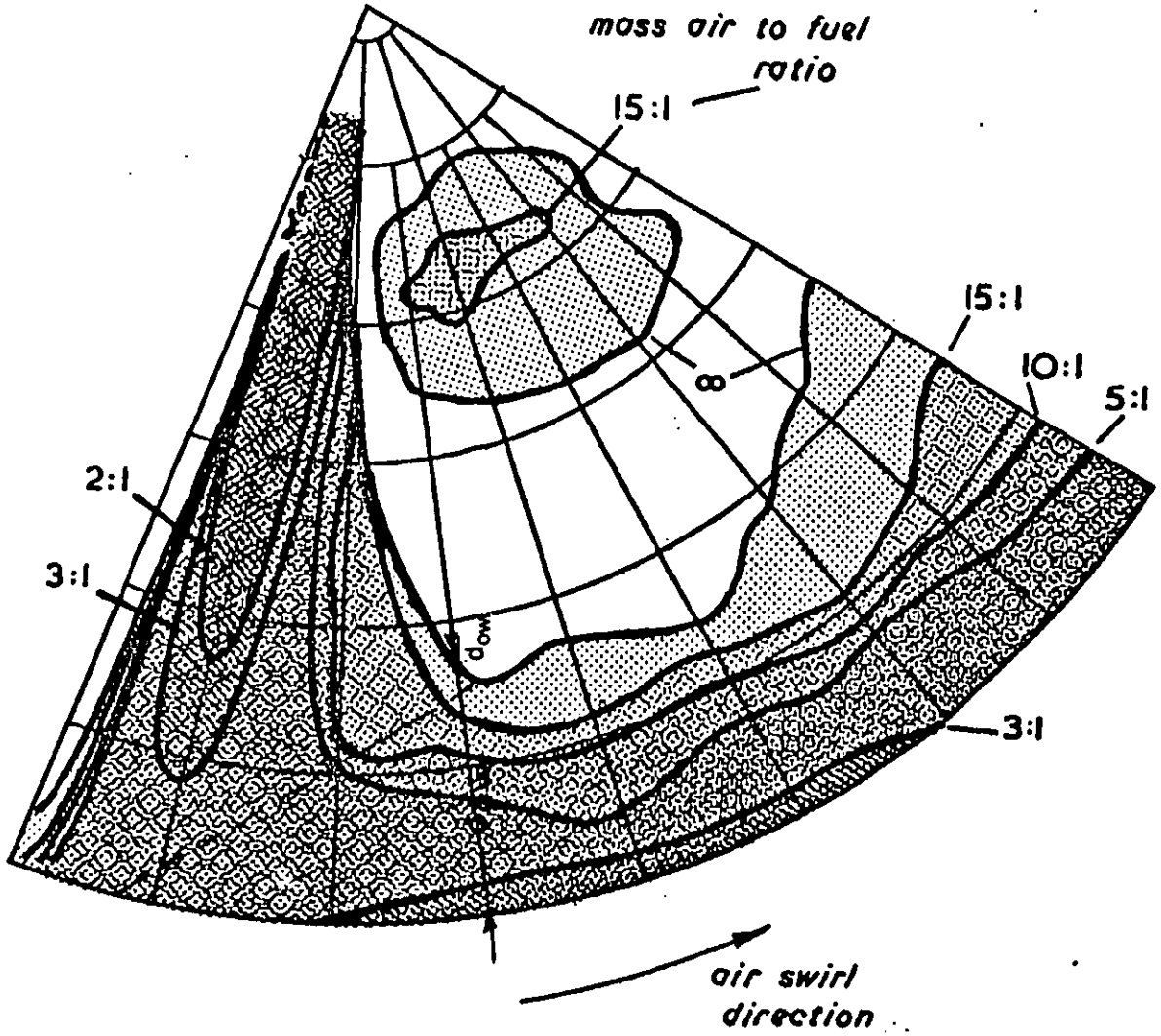


FIG. 5.4 Gas jet simulation (45) of the fuel spray in presence of swirl. (Nozzle size; 1 hole x 0.35 mm dia)

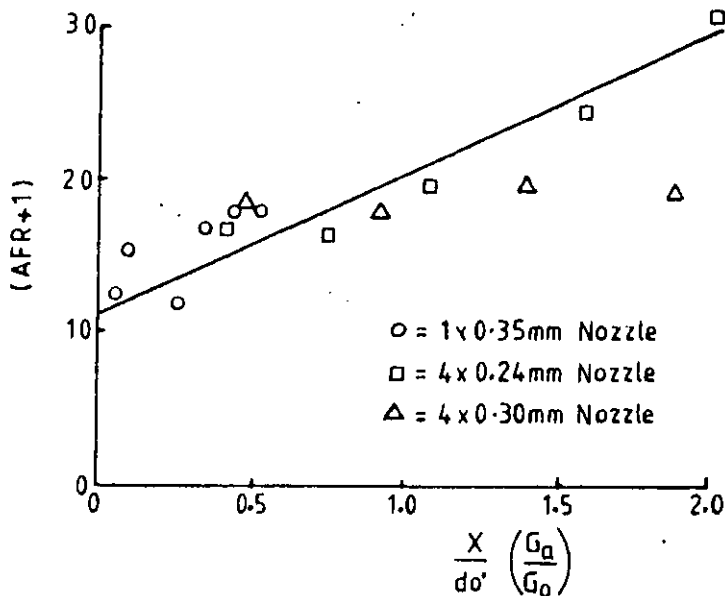


FIG. 5.5 Entrainment correlation for coflowing jet in the wall region. (Reference Dent (124))

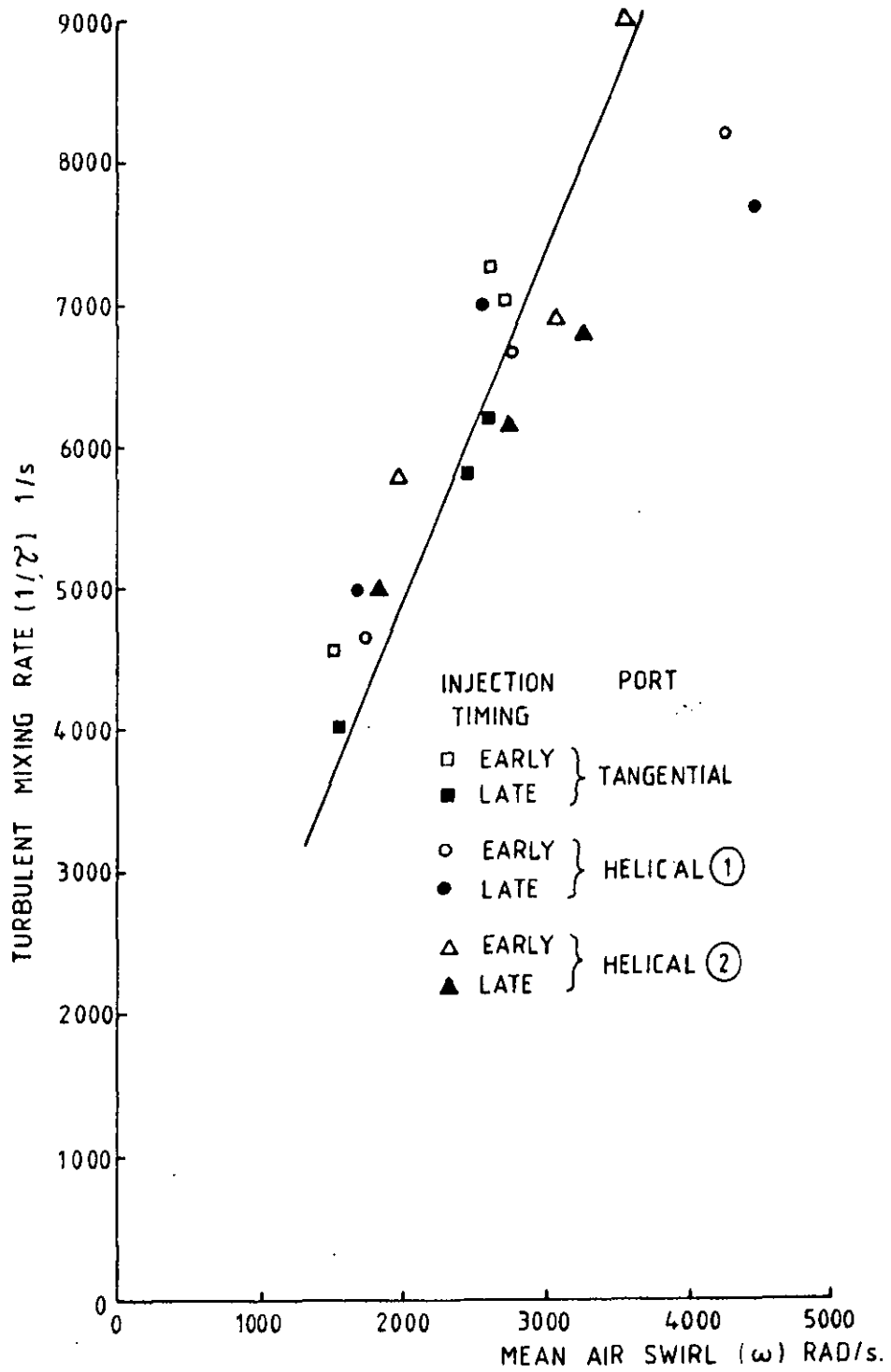


FIG. 5.6 Correlation of turbulent mixing rate with mean air swirl velocity

CHAPTER VI
RESULTS AND DISCUSSION

6.1 Quiescent Chamber Diesel Engine

6.1.1 Results

The main outputs from the model as a function of crank angle are the cylinder pressure, rate of energy release, air entrainment and mixing rate, mass fraction of fuel vaporised, mass of fuel burnt, mean jet and total trapped charge temperatures, heat transfer rate from the gaseous charge, and the soot formation oxidation and release rates.

The comparison of measured cylinder pressure diagrams taken from a single cylinder engine (refer to Appendix F for specifications) with model predictions for various test conditions are shown in Figures (6.1) - (6.8). The test conditions are listed in Table 6.1.

The plots relating other output variables for Set A of the listed data sets are given in Figures (6.9) - (6.13). A typical plot of radial temperature distribution in the jet is included in Figure (6.14).

On the entrainment diagram, points 1, 2 and 3 indicate changes in the flow regime,

- 1 - free to wall jet transition
- 2 - interaction of adjacent wall jet flows, and
- 3 - onset of turbulent mixing following end of injection.

These points are shown on Figure (6.10) to indicate their position in all entrainment diagrams.

Sets F, G and H are at low load and idling conditions. Figures (6.6) - (6.8) represent the corresponding cylinder pressure diagrams.

TABLE 6.1

Test Conditions for Single Cylinder Quiescent Chamber D.I. Diesel Engine

Test Condition \ Data Set	A	B	C	D	E	F	G	H
Engine Speed (rpm)	1300	1900	1300	1300	1300	1300	1900	700
Injection Timing ($^{\circ}$ ATDC)	-18	-10	-10	-24	-16	1	0	1
Injection Duration ($^{\circ}$ CA)	24	28	24	30	30	7	10	5
Fuelling Rate (mm^3/cycle)	142.3	142.3	142.3	191.6	191.6	20	20	20
Intake pressure (bars)	1.19	1.25	1.19	1.57	1.57	1.125	1.125	1.125
Intake Temperature (K)	333	333	333	333	333	350	350	350

Results for sets B and H are included in Figures (6.15)-(6.21).

Figures (6.22) - (6.25) show the results for a parametric study to test the effects of injection scheduling based on conditions of set A.

6.1.2 Discussion

In general the agreement between predicted and experimental pressure data is good. The results are obtained within an accuracy of about ten percent. However at low load and idling conditions, the model tends to underpredict during the expansion. It was found necessary to increase the entrainment constant in equation (2.6) to a value of 0.7 instead of 0.32 to ensure adequate entrainment during the delay period. There is some justification for the use of a higher entrainment constant from the results of Ricou and Spalding (42) who have shown that this constant increases in the transition Reynolds number region for the orifice flow. For the idling and low load cases considered, the Reynolds number are of the order of 8000 and 11000 respectively which are well within the transition region for the jet flow. However this cannot account for the factor of 2 increase in the entrainment constant. It is likely that assumptions concerning the quasi-steady nature of the flow and the simple nature of the droplet distribution model are limiting features.

At low loads and highly retarded timings, it is found that the ignition delay correlation of Hardenberg and Hase (71) was inadequate. The reason for the deviation from Hardenberg and Hase's correlation is likely to be in the use of a mean polytropic index to compute average pressure and temperature during the delay period which occurs in compression in general. Its evaluation in the expansion stroke will cause an error.

The air entrainment rate has a pronounced effect on the fuel evaporation rate during the delay period. This fact is responsible for the first peak in the heat release and will be effected significantly by the injection timing and fuelling rate. Advanced injection timing increases the delay and hence has a higher first peak.

The strong effect of the wall jet flow on air entrainment is apparent in entrainment diagrams (Figures 6.10 , 6.16) at high loads. Also, the assumption of entrainment reducing to that for the free jet once adjacent wall jets interact can be seen by a flat region followed by a dip in these diagrams towards the end of the injection. It would appear that the reduction in entrainment is too severe due to the assumption made, as it is likely that the wall jet entrainment will be reduced by recirculation rather than being eliminated completely by the assumption made here. However, the analysis as presented does highlight the role of injection timing on jet interaction and hence reduced air entrainment into the spray for a longer period of the fuel injection process. This feature is further sensitive to the tail region of the injection diagram. For low load and idling cases, these features are absent due to very short injection periods.

The turbulent mixing mechanism appears to characterise the combustion process following injection in a reasonable manner. The strong relationship between the entrainment-mixing and the energy release diagrams, Figures (6.9) - (6.10), are confirmed. It is noted here that approximately 50 percent of the total energy transfer in the closed period of the cycle is due to the turbulent mixing. Similar trend is observed in Figures (6.15-6.16) & (6.18-6.19).

The results concerning droplet evaporation appear to be consistent with the findings of Kamimoto et al (54) in that the mass fraction of vapour formed lags the injected fuel mass fraction by about 2°CA . However, the model discussed here shows a slower vaporisation rate in the early period of injection which is consistent with a low mass transfer number B in the absence of combustion, and also the inhibiting effect of air saturation on vaporisation during the period when air entrainment is low. However, during combustion there is no possibility for vaporisation to be inhibited by a saturation condition because the gas state conditions (temperature and pressure) are far removed from a saturated vapour state. The burned fraction curves in Figures (6.11) , (6.17)

for the high load case show that at fixed crank positions the mass fraction of vapour burned is significantly less than the vapour present (evaporated mass fraction), this implies long residence times before combustion, an important factor in soot formation.

In the idling and low load cases, because of the lower injection velocities and lower temperatures due to retarded timing, the vaporisation rate is slower and the vapour mass fraction curve in Figure (6.20) lags the injected mass fraction curve by about 10°CA . Now combustion promptly consumes the available vapour.

The net energy release curves were computed from algebraic summation of the rate of change of internal energy of the air charge and jet, the work done and the heat loss to the cylinder walls, the work done being calculated from the computed pressure diagrams. The oscillatory form of the early period of the diagrams is due to the time required by the regions which have burned within the limits of inflammability, to once again attain a flammable mixture condition. This feature is reflected in the output of this model.

The results of computation of temperature profiles in the free and wall jet regions are shown in Figure (6.14). Curves (1) and (2) are for periods before combustion has commenced. The flattening of the profile (2) due to entrainment of hot surrounding air into the jet is apparent. Curves (3) and (4) show the effect of combustion in the free jet region. The high temperatures (approximately 3000K) near the stoichiometric concentration contours within the jet correspond closely to the Adiabatic Flame Temperature for the conditions prevailing in the engine. The corresponding integrated mean temperature is of the order of 2300K which is of the same order as measurements made by Kamimoto et al (126) and Flynn et al (127). The broadening of regions coming within the flammability limits as air entrainment increases, cause combustion to occur

nearer to the centreline of the jet and hence the 'peakiness' of the temperature profiles is reduced. This can be seen in the difference between curves (3) and (4). The same features can be seen in the wall jet curve (5) being representative for this region.

In Figure (6.12), the mean charge and jet temperatures show close similarity in magnitude and variation with crank angle position with the experimental measurements of Kamimoto et al (126). Figure (6.21) for the idling and low load conditions show a rapid decrease in the jet temperature during the expansion stroke, resulting from the highly retarded condition of the fuel injection. This feature is important in understanding poor combustion behaviour under light load and idling. However, the peaky heat release curve is attributed to the atomisation of fuel being assumed to be too fine. Knights (49) correlation for SMD is as likely as not to be based on medium to high fuelling rates and therefore efficient injection processes. At low load fuel injection is usually poor and the resulting atomisation coarse.

To test this assumption a parametric study of the effects of SMD on energy release rate and jet temperature was undertaken, these results are shown in Figures (6.26) - (6.27) and lend support to the argument for poor atomisation put forward.

The magnitude of peak heat flux appears to be of the right order when compared against measured data of Oguri and Inaba (128), at approximately the same speed and load conditions.

The model was used to test its sensitivity to changes in injection scheduling which is important for noise and emission control. Figures (6.22) - (6.25) indicate that the model is capable of responding to this type of variation. The stepped injection schedule produces a lower peak pressure, and a reduced and delayed peak in the energy release, this is primarily caused by the lower entrainment and vaporisation rates at fixed crank angle positions.

6.2 Soot Results

The soot results for the data set A-E of Table 6.1 are shown in Figure (6.28). The experimental value of exhaust Bosch number is plotted against the calculated value using the model. The correlation shows some scatter around the mean line. However, the trends in the variation of exhaust smoke with injection timing, exhaust gas recirculation (EGR), speed and load follow the experimental data trends of Yu and Shahed (129) plotted in Figure (6.28) and also tabulated in Table 6.2. It should be noted that EGR has been simulated in the model by reducing the reactive (oxygen) component in the cylinder charge and increasing the nitrogen component by a corresponding amount.

TABLE 6.2

Comparison of Experimental Exhaust Bosch Number with the Model Predictions

Data Set	EGR = 0.0		EGR = 0.1		EGR = 0.2	
	Expt	Model	Expt	Model	Expt	Model
A	1.1	2.35	2.6	2.9	6.0	4.0
B	3.5	6.0	5.8	6.5	8.4	7.5
C	3.3	3.6	5.7	4.45	8.5	5.4
D	0.7	1.0	1.5	1.15	3.6	1.8
E	1.9	1.6	8.9	1.8	6.4	3.85

With retarded injection timing, the smoke level increases. This is due to lower temperatures in the cylinder with retarded conditions because of heat release occurring later in the expansion stroke (Figure 6.15). Similar trends follow with increase in EGR (Figure 6.29). The soot formation rate is considerably higher at higher engine speed than the corresponding oxidation rate giving a higher soot release. The higher formation rate is probably due to higher fuelling levels, and the poor oxidation due to the lower temperatures associated with a retarded timing of 10° btdc (Figure 6.30). The

plots of soot formation, oxidation and release for various data sets are included in Figures (6.31)-(6.35). The temporal variation of soot in the diesel engine is found to be similar to that in flames. This fact was confirmed by Hiroyasu et al (130). They also found that soot formation occurs predominantly during the mid-combustion period where fuel is rich but most of it burns out during the latter part of the combustion period where fuel lean conditions persist. Similar trends are obtained in the present study. The peak soot concentration seems to occur at the end of injection period in most cases. According to a parametric study on data sets C and E found that the twenty percent increase in injection pressure reduces the exhaust smoke Bosch number from 3.6 to 1.6 and 1.6 to 1.06 respectively. This change is mainly due to the increase in temperature.

The model at present has shown quite consistent results on the basis of the assumptions used. A recent soot modelling work of Ahmad et al (85) has shown some success in using a turbulent mixing soot combustion model developed by Magnussen (107) in conjunction with Tesner's formation scheme. They showed quite reasonable predictions for high pressure spray flames. In this area more work needs to be done to reach more exact quantitative prediction of soot.

6.3 Effect of Swirl

The results from a high speed Direct Injection Diesel engine are shown in Figures (6.36)-(6.41). The detailed engine specification is given in Appendix F and the test conditions of the results are included in Table 6.3. The data set is for three speeds (1100, 1700 and 2400 rpm) and two injection timings. The agreement of the cylinder pressure with experimental results are quite good for 1100 and 2400 rpm cases. However, due to lack of an adequate wall jet analysis, for the impinging jet, the 1700 rpm data are not adequately predicted. It was found necessary to alter the point of jet impinge-

TABLE 6.3

Test Conditions for High Speed Direct Injection Diesel Engine

Test Condition \ Data Set	S1	S2	S3	S4	S5	S6
Engine speed (rpm)	1100	1100	1700	1700	2400	2400
Injection timing ($^{\circ}$ ATDC)	-10.5	-0.5	-9.5	-2.5	-15.5	-7.0
Injection duration ($^{\circ}$ CA)	12	12	15	15	21	20
Fuelling rate (mm^3/cycle)	75.0	76.8	75.3	74.88	74.6	75
Intake pressure (bars)	0.977	0.977	0.977	0.977	0.977	0.977
Intake temperature (K)	298	298	298	298	298	298
Mean intake swirl ratio	2.06	2.06	2.06	2.06	2.06	2.06

ment from the centre line (curve 1) at 1100 rpm to the leading edge of the jet (curve 2) at 2400 rpm. The data for 1700 rpm was found from Figure (6.38) to need adjustment of the impingement point to somewhere between the values used for 1100 and 2400 rpm, but it was decided not to make this adjustment because of lack of time.

Plots of other variables for set S1 are shown in Figures (6.42)-(6.45).

The predictions from the soot model for the above data set indicate a qualitative trend only. In adopting the soot model described for the quiescent chamber case, one modification is needed. The mixing rate used in evaluating r^* is calculated on the basis of the composite effects of the mixing rates due to swirl and injection processes respectively as indicated earlier. These rates are considered in parallel, and are characterised by equations (2.55) and (5.28).

Table 6.4 shows the results of soot predictions at 1100 rpm. These results provide a trend for injection timings.

TABLE 6.4

Comparison of Soot Predictions with the Experimental Results Obtained for High Speed Direct Injection Engine at 1100 rpm

Data Set	Exhaust Bosch Number	
	Experiment	Model
S1	4	5.95
S2	3.7	4.64

More work needs to be done in this direction.

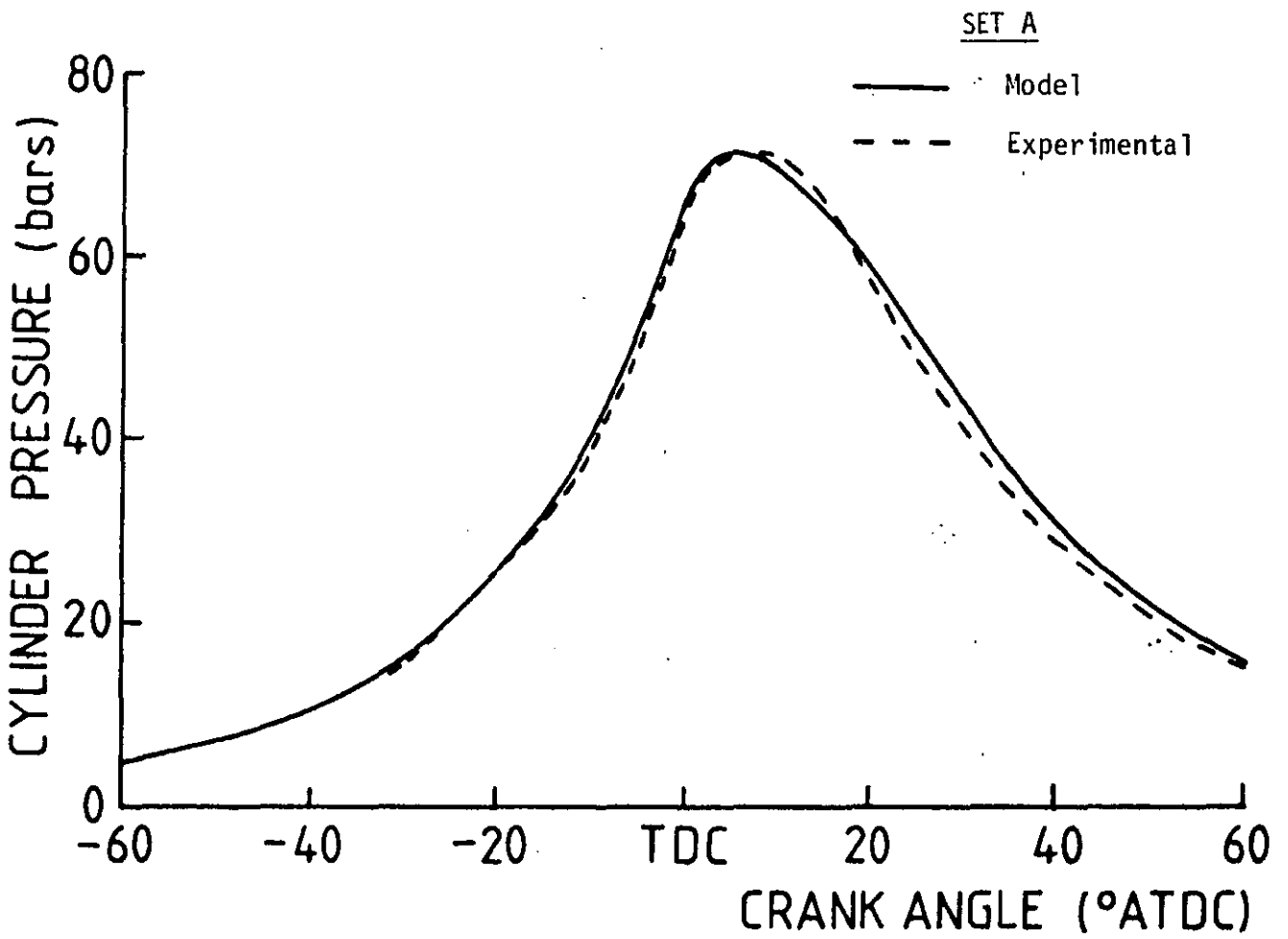


FIG. 6.1 Cylinder pressure diagram (High load; fuel quantity = 142.3 mm³, Engine speed = 1300 rpm, Injection timing = 18° btdc)

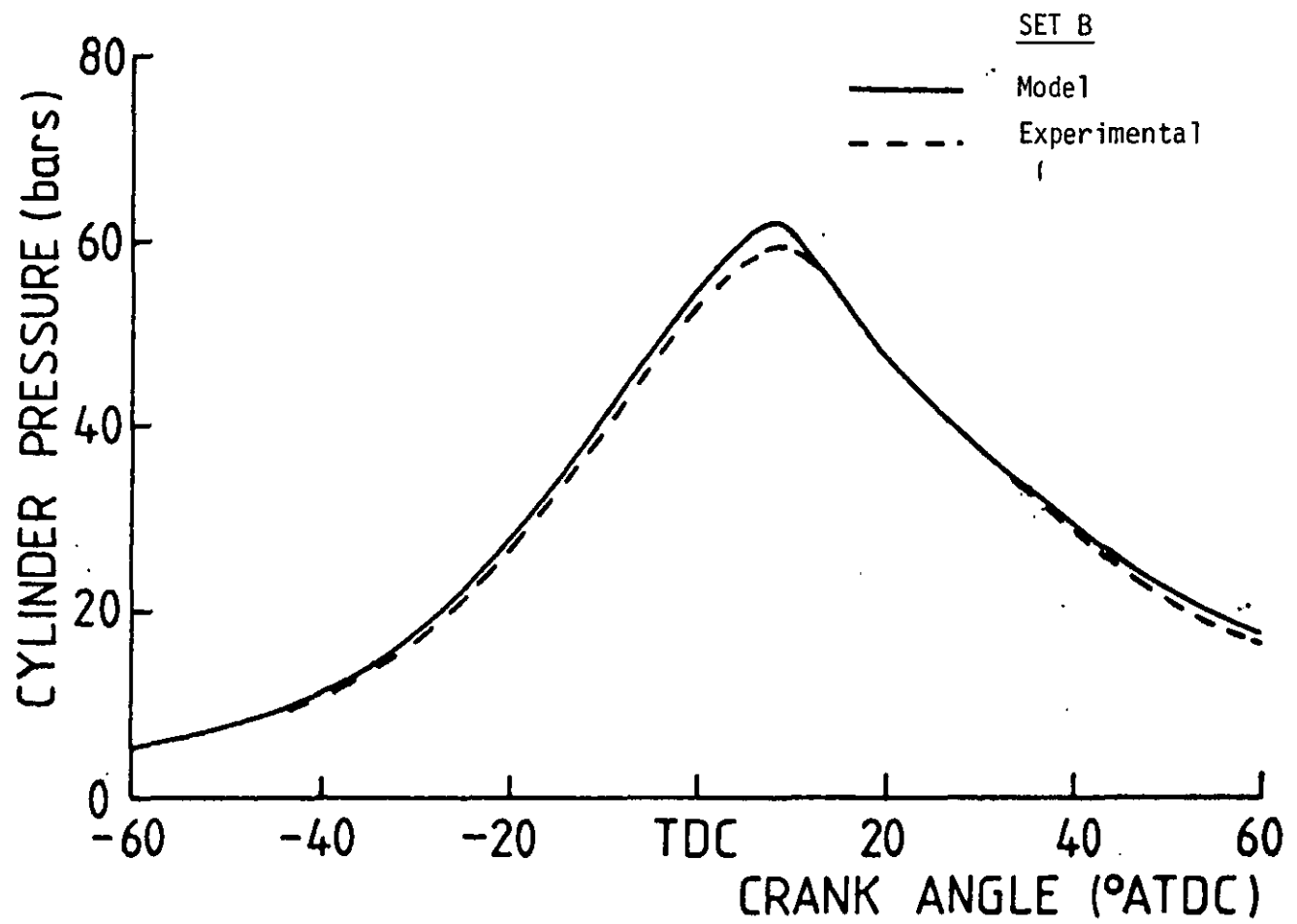


FIG. 6.2 Cylinder pressure diagram (High load, retarded injection timing: fuel quantity = 142.3 mm³, Engine speed = 1900 rpm, Injection timing = 10° btdc)

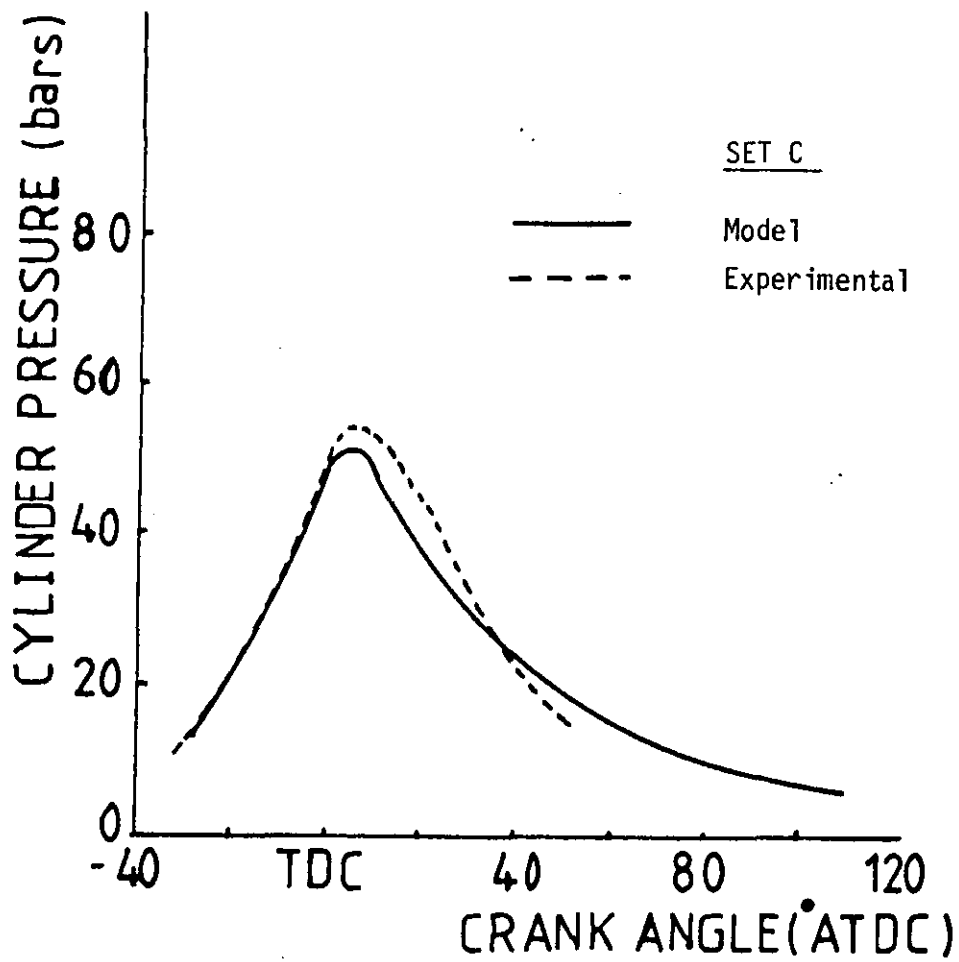


FIG. 6.3 Cylinder pressure diagram (High load, retarded injection timing: fuel quantity = 142.3 mm³, Engine speed = 1300 rpm, Injection timing = 10° btdc)

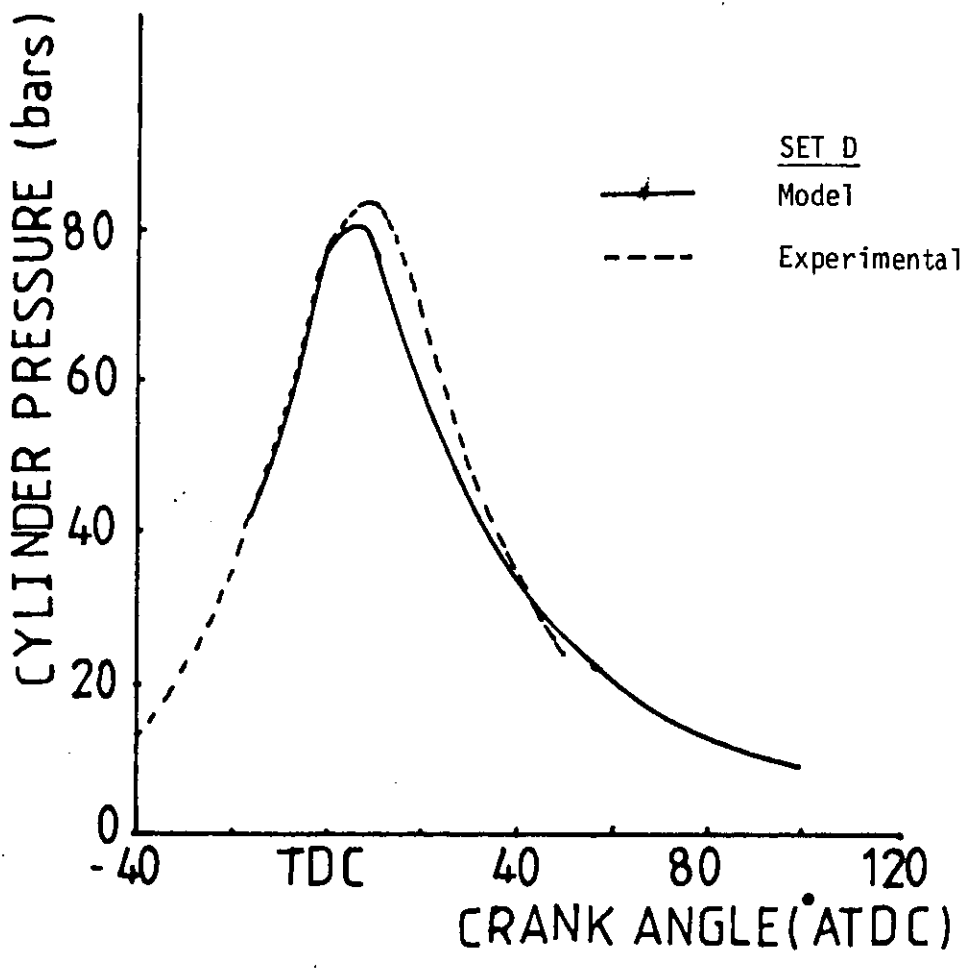


FIG. 6.4 Cylinder pressure diagram (High load: fuel quantity = 191.6 mm³, Engine speed = 1300 rpm, Injection timing = 24° btdc)

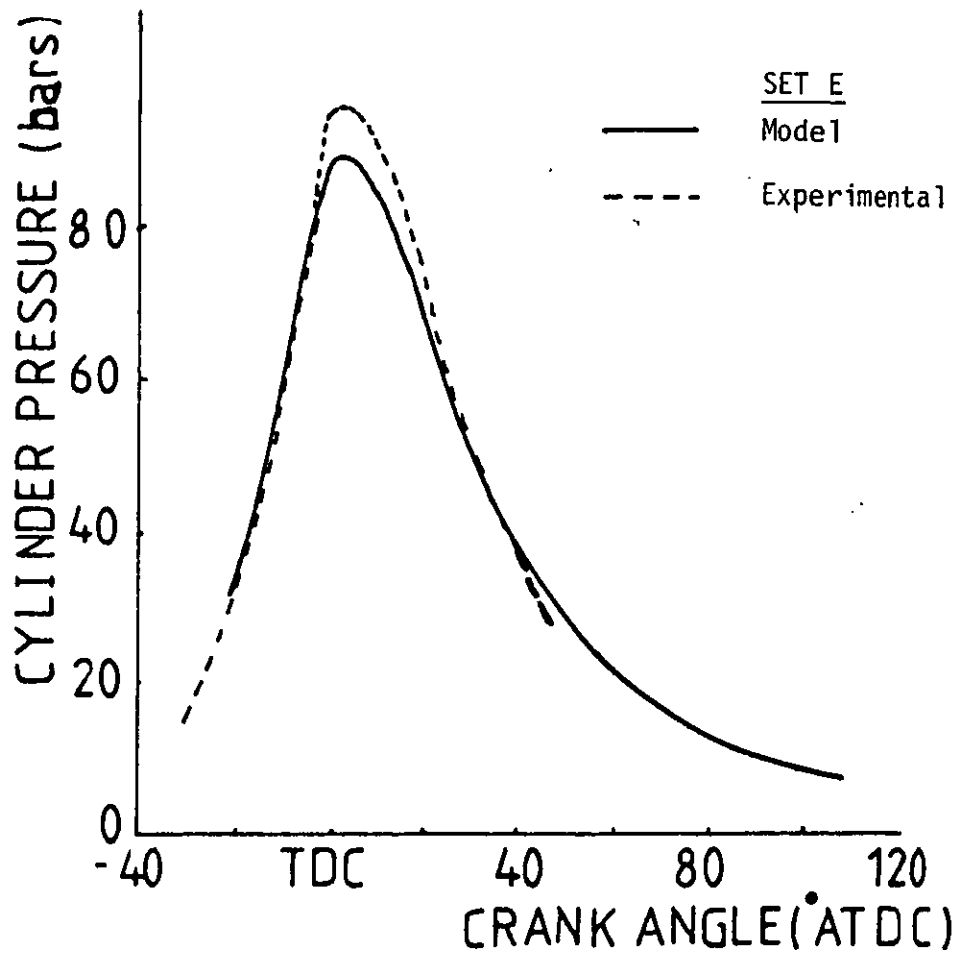


FIG. 6.5 Cylinder pressure diagram (High load, retarded injection timing: fuel quantity = 191.6 mm³, Engine speed = 1300 rpm, Injection timing = 16° btdc)

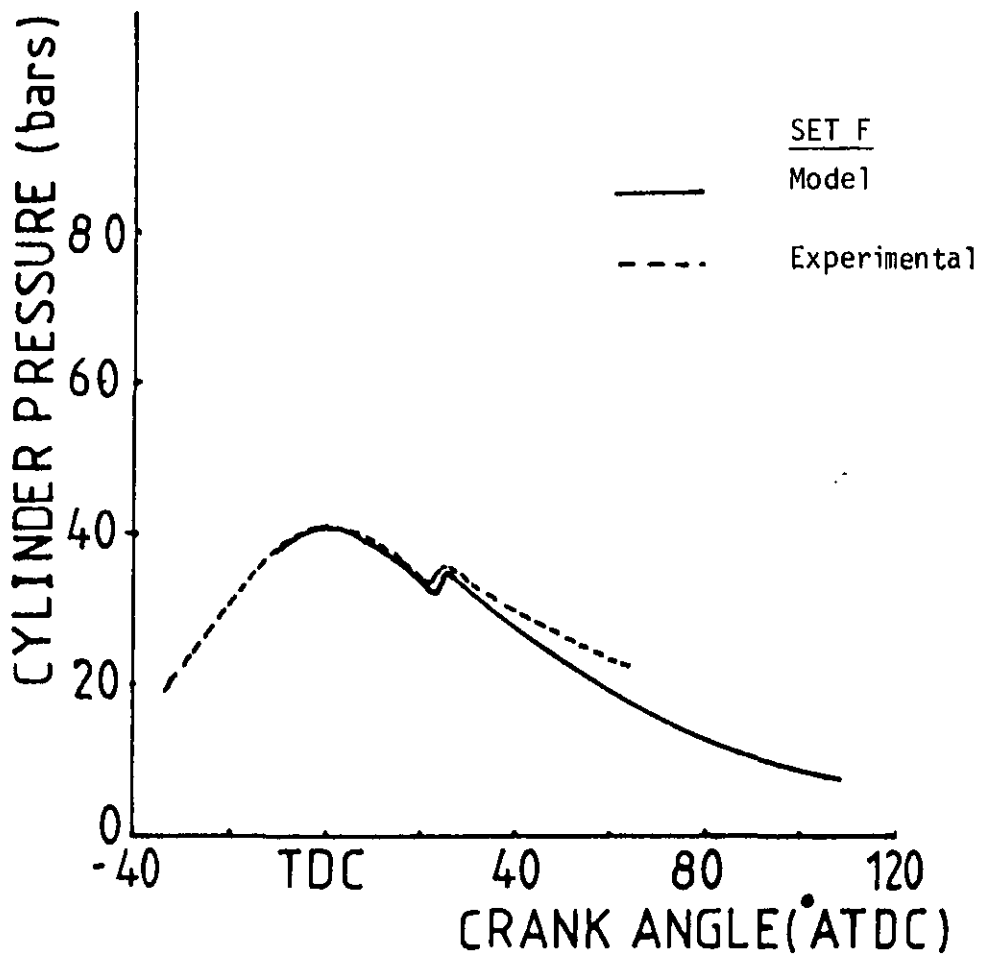


FIG. 6.6 Cylinder pressure diagram (Low load: fuel quantity = 20 mm³, Engine speed = 1300 rpm, injection timing = 1° atdc)

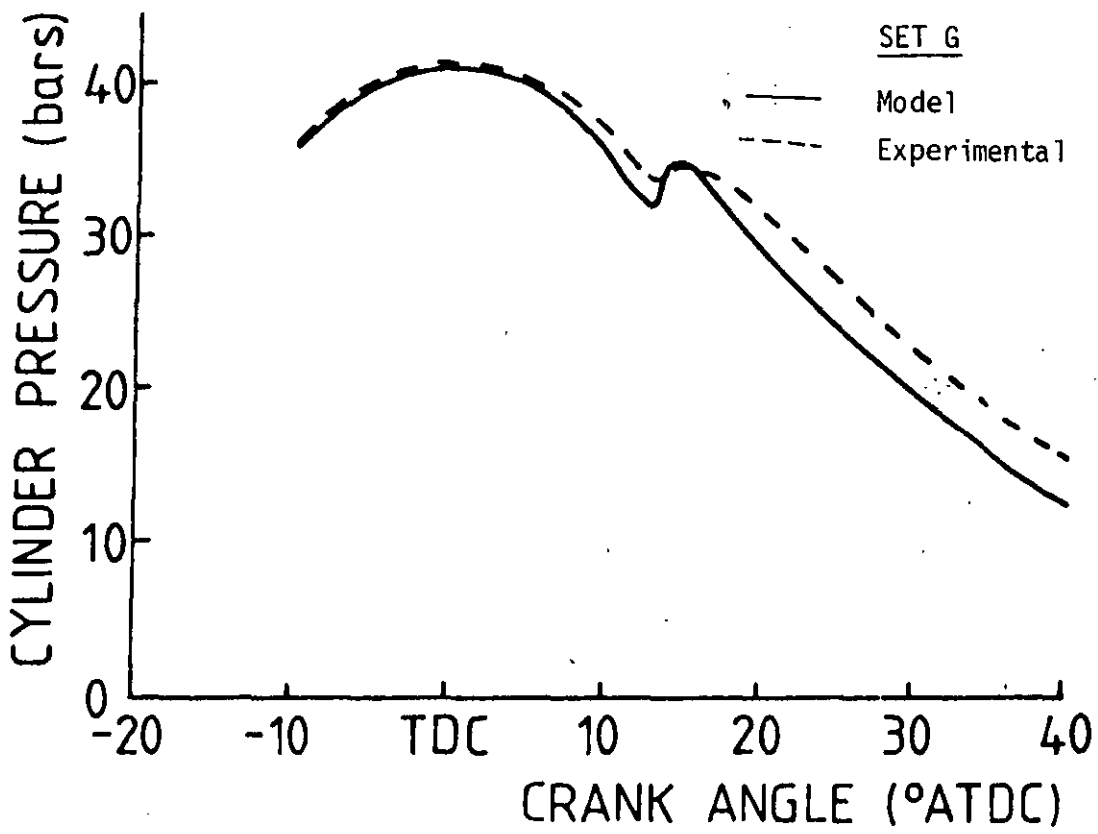


FIG. 6.7 Cylinder pressure diagram (Low load: fuel quantity = 20 mm³, Engine speed = 1900 rpm, Injection timing = TDC)

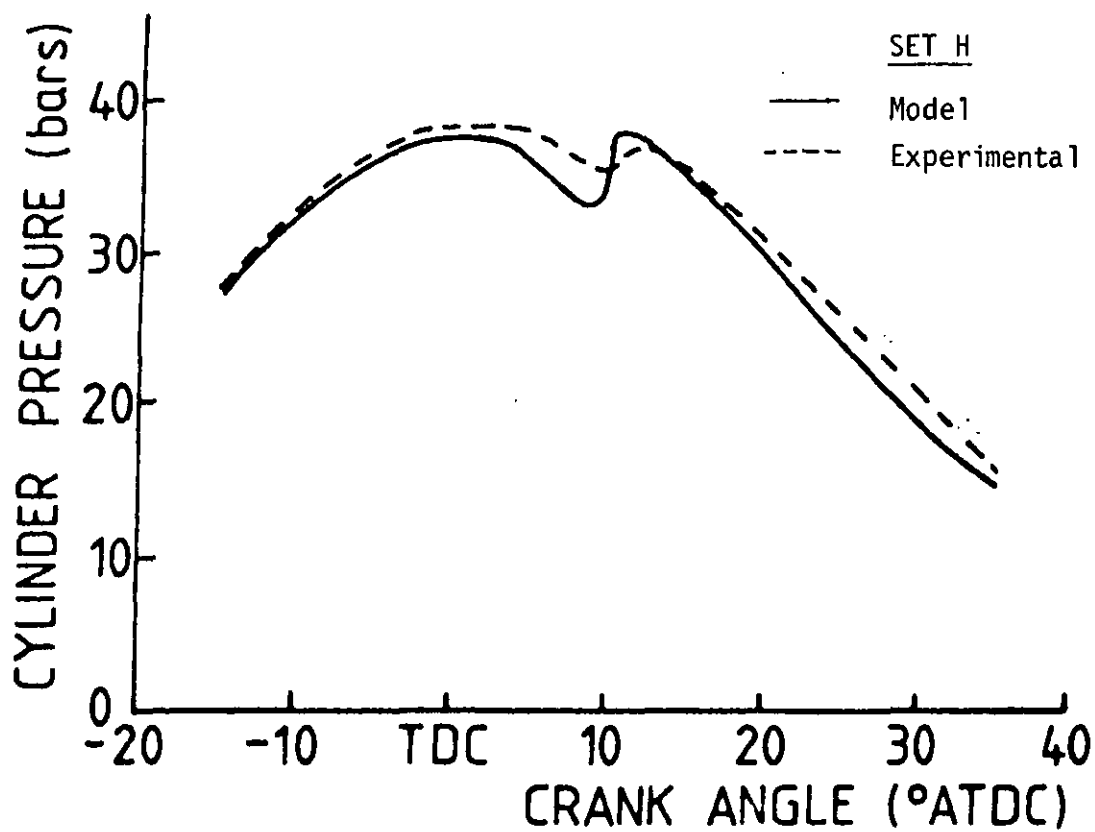


FIG. 6.8 Cylinder pressure diagram (Idling: Fuel quantity = 20 mm³, Engine speed = 700 rpm, Injection timing = 1° atdc)

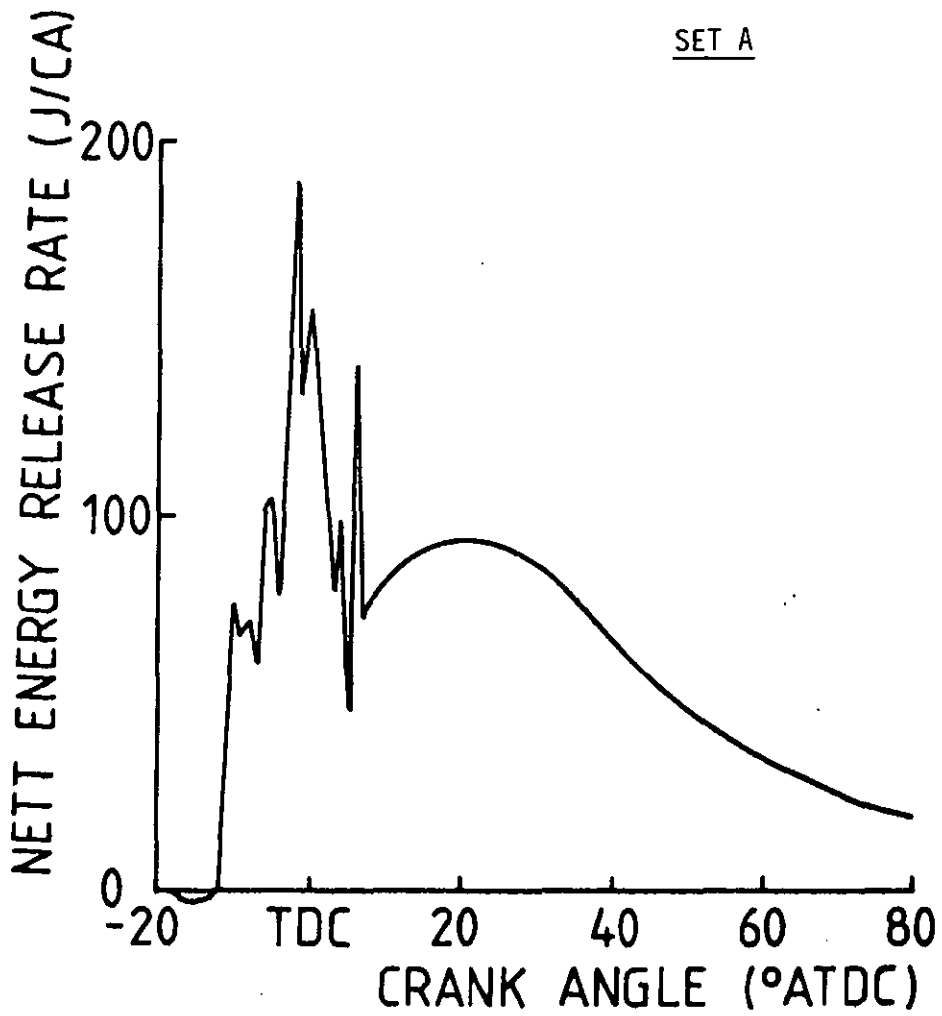


FIG. 6.9 Nett energy release rate (High load: fuel quantity = 142.3 mm^3 , Engine speed = 1300 rpm, Injection timing = 18° btdc)

SET A

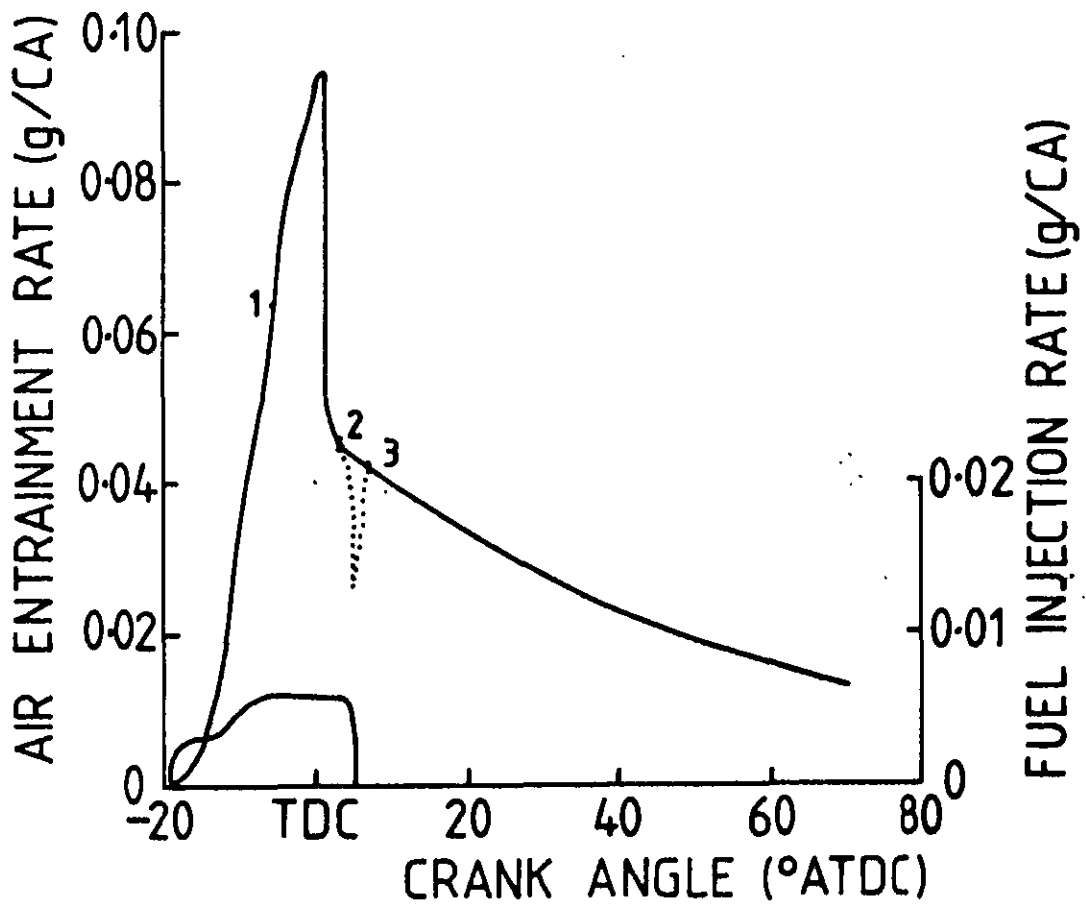


FIG. 6.10 Air entrainment and fuel injection rates
(High load: fuel quantity = 142.3 mm³, Engine speed = 1300 rpm, Injection timing = 18° btdc)

SET A

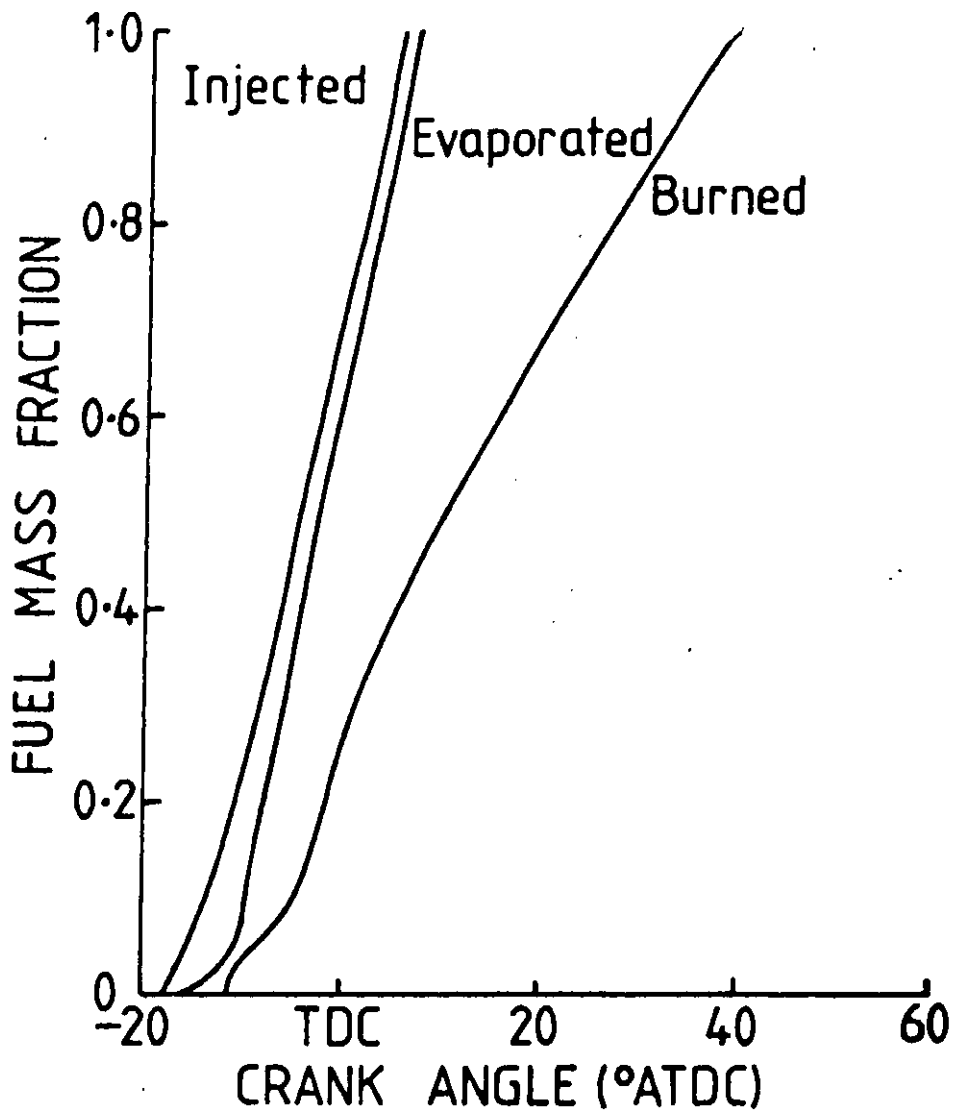


FIG. 6.11 Fuel mass fractions injected, evaporated and burned (High load: Fuel quantity = 142.3 mm^3 , Engine speed = 1300 rpm, Injection timing = 18° btdc)

SET A

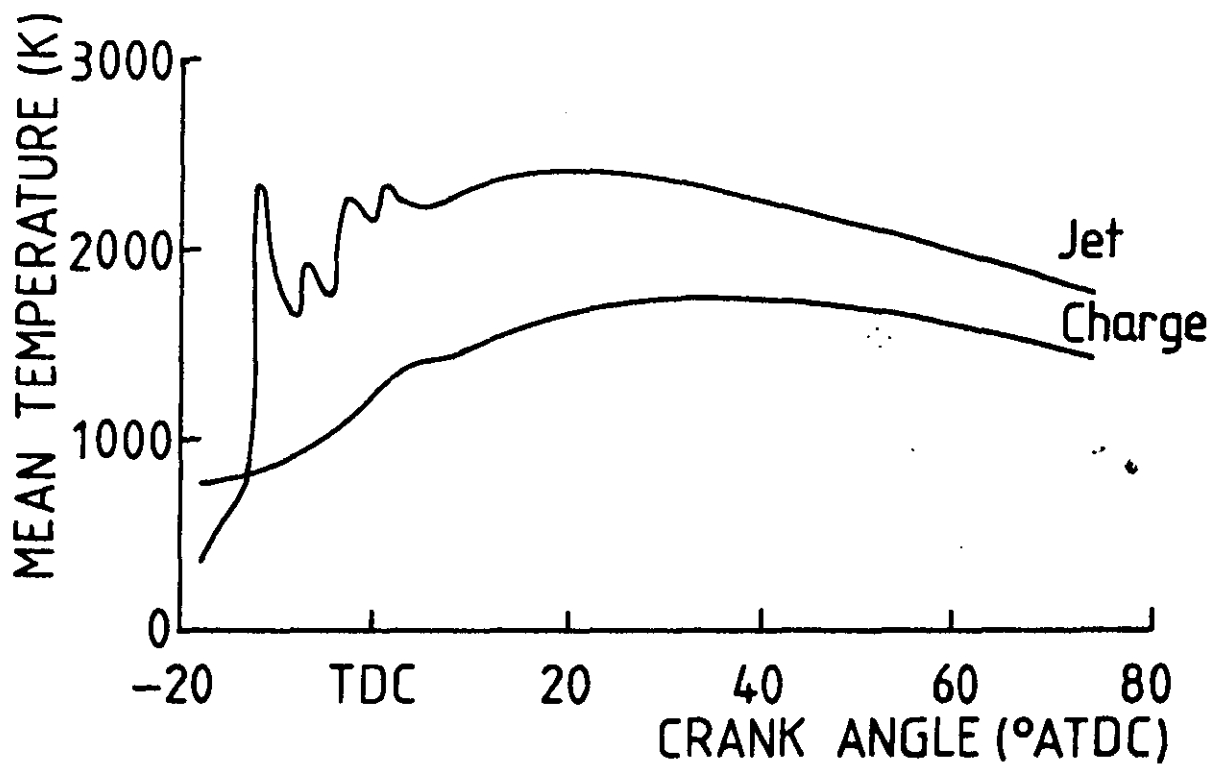


FIG. 6.12 Mean temperature diagram (High load: Fuel quantity = 142.3 mm^3 , Engine speed = 1300 rpm, Injection timing = 18° btdc)

SET A

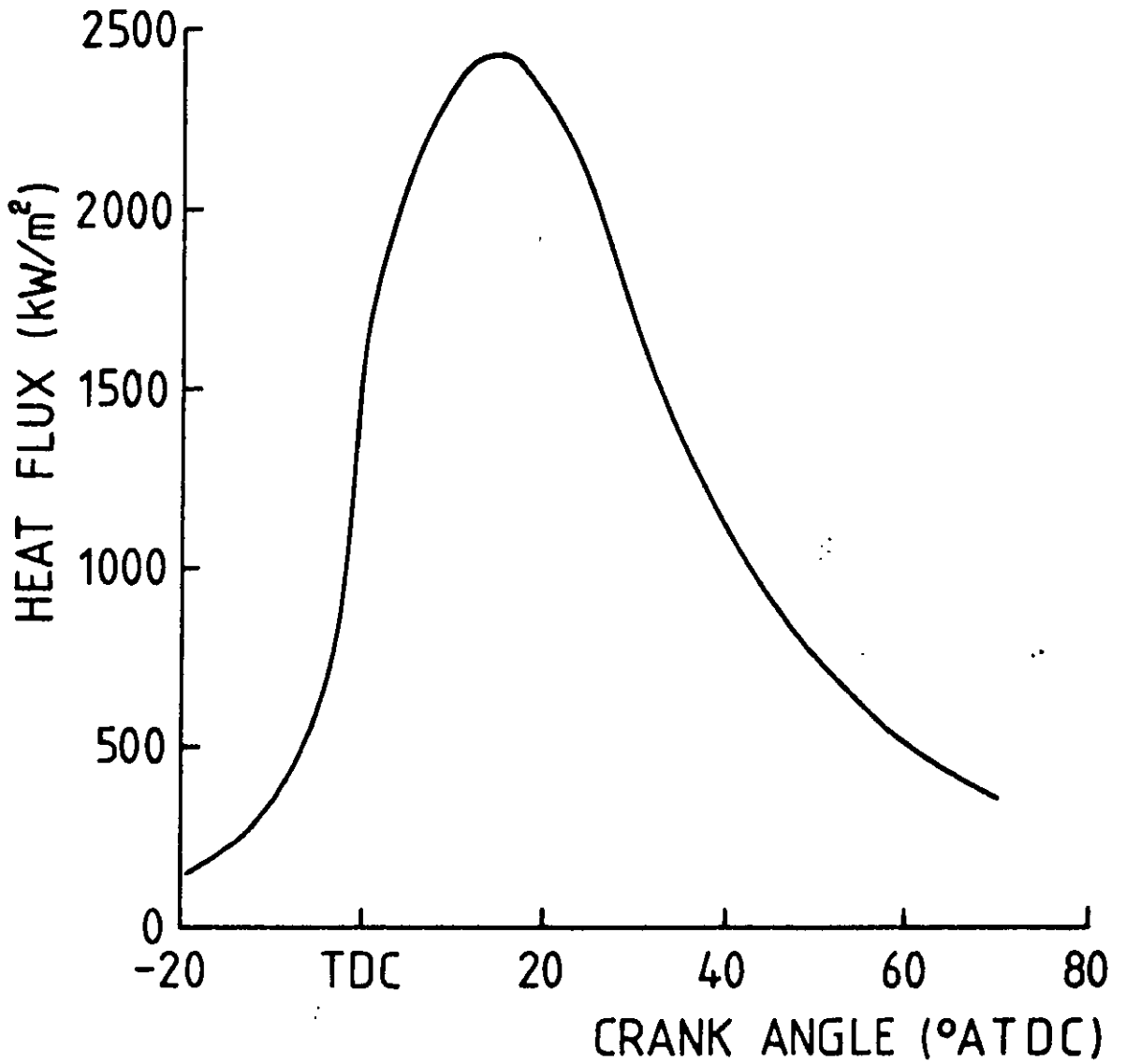


FIG. 6.13 Heat flux diagram (High load: fuel quantity = 142.3 mm³, Engine speed = 1300 rpm, Injection timing = 18° btdc)

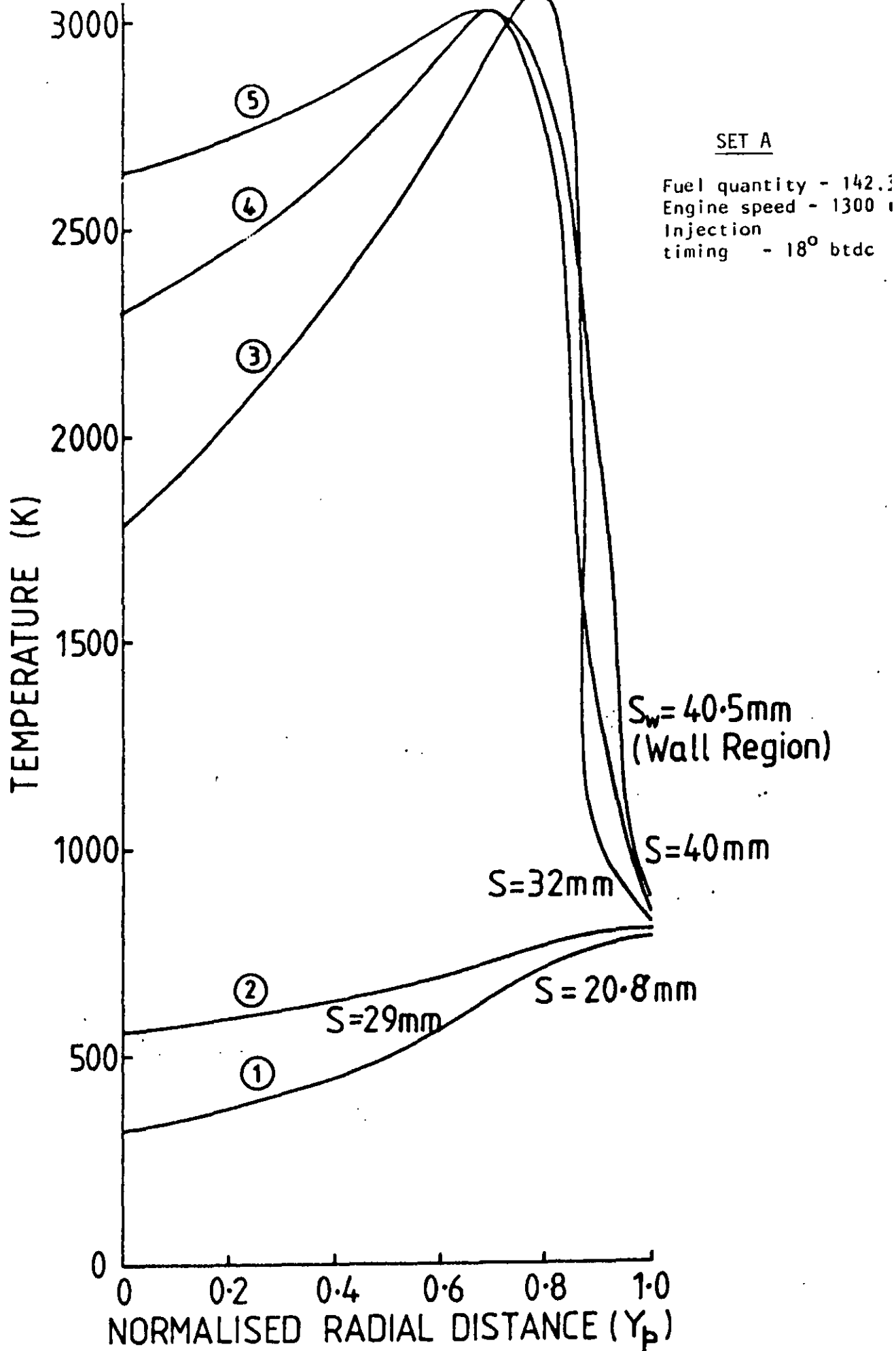


FIG.6.14 Typical radial temperature distribution in the spray (High load)

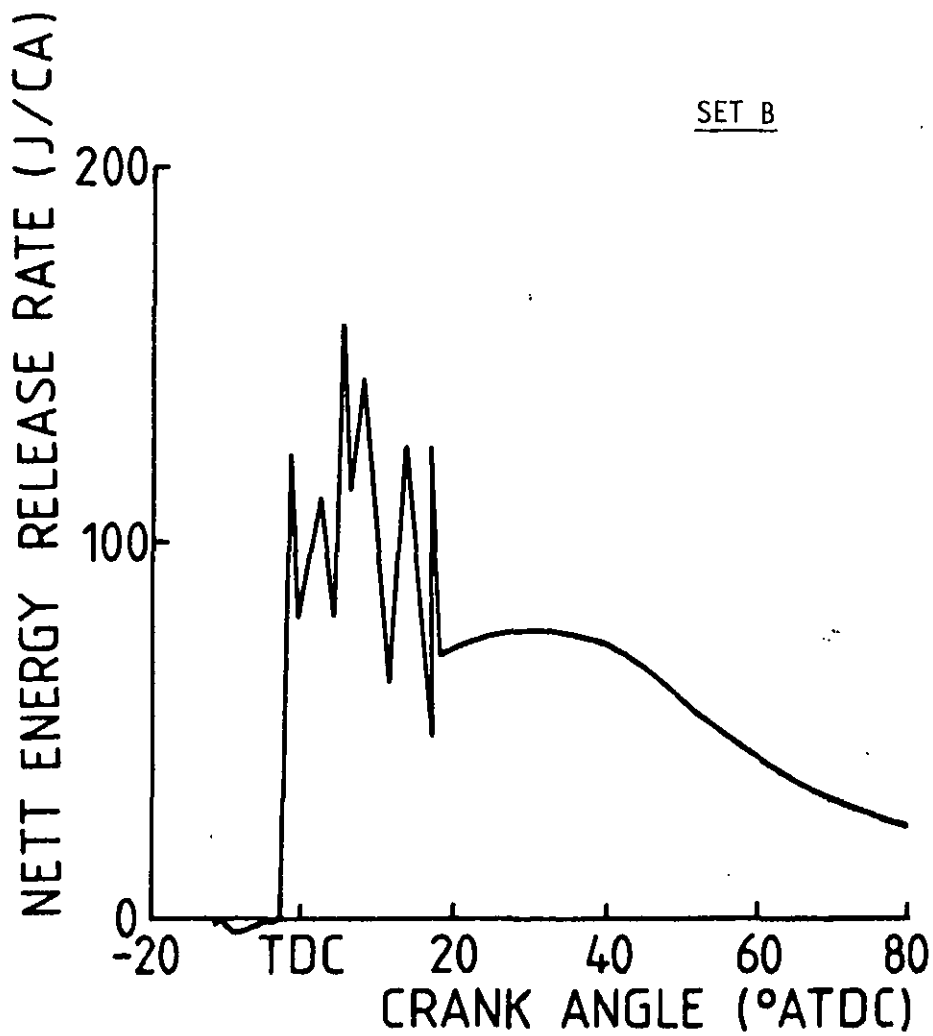


FIG. 6.15 Nett energy release rate (High load, retarded injection timing: Fuel quantity = 142.3 mm^3 , Engine speed = 1900 rpm, Injection timing = 10° btdc)

SET B

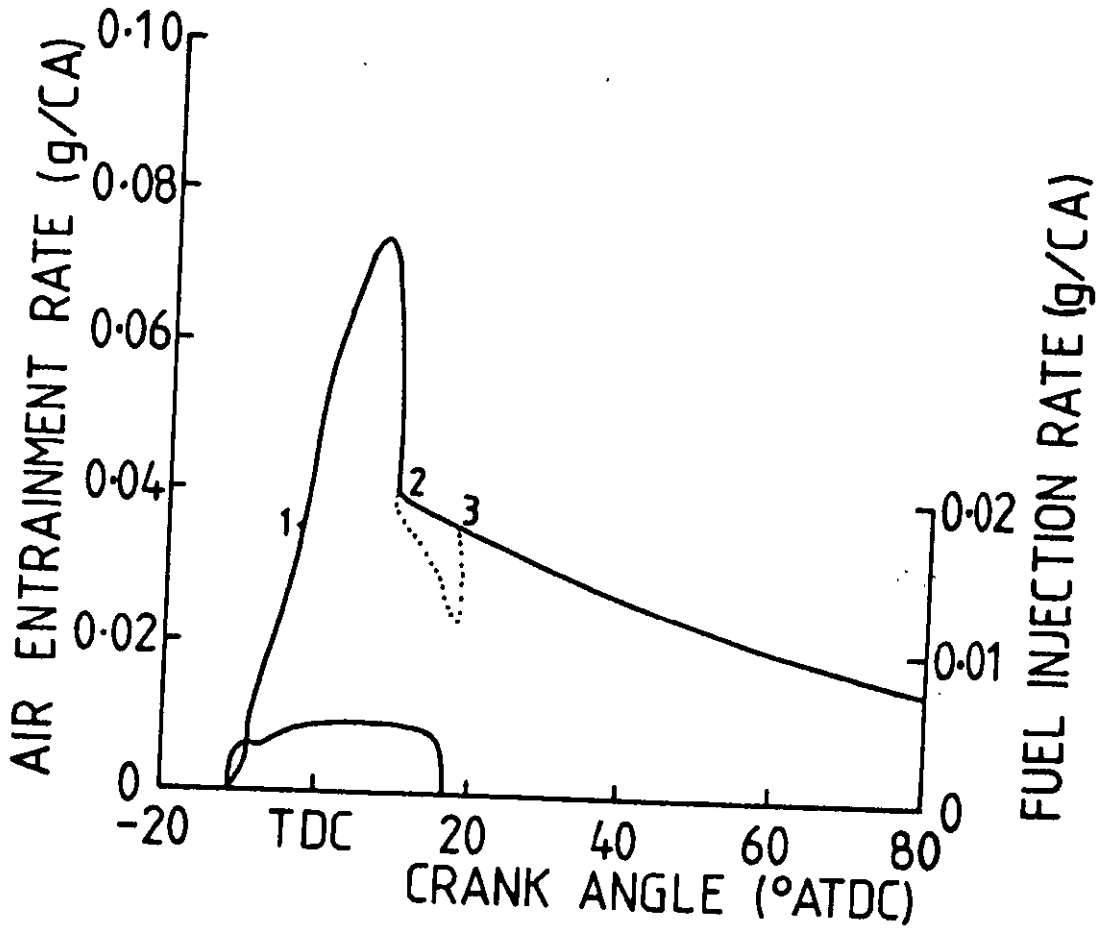


FIG. 6.16 Air entrainment and fuel injection rates (High load, retarded injection timing: Fuel quantity = 142.3 mm^3 , Engine speed = 1900 rpm, Injection timing = 10° btdc)

SET B

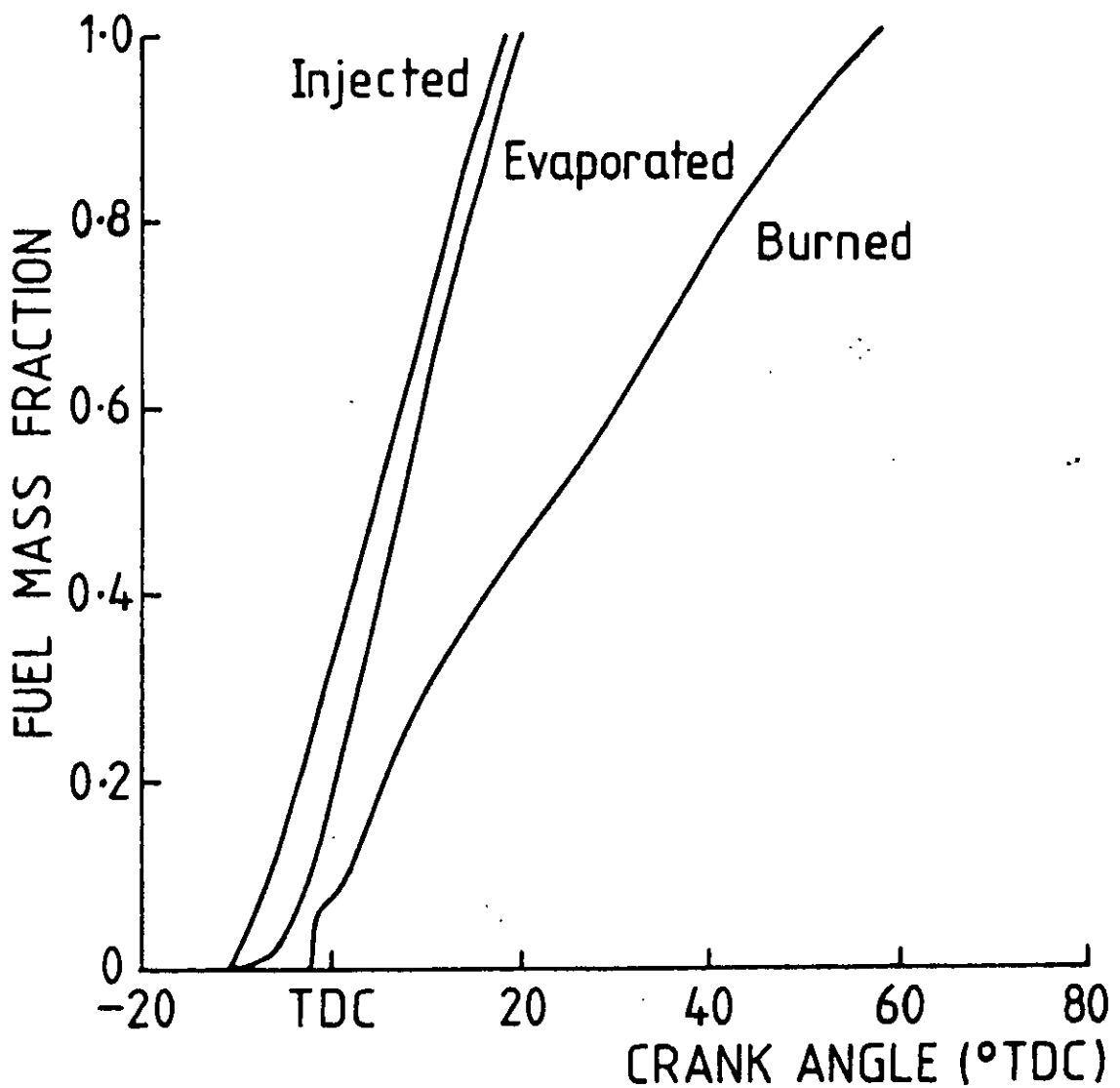


FIG. 6.17 Fuel mass fractions injected, evaporated and burned (High load, retarded injection timing: Fuel quantity = 142.3 mm³, Engine speed = 1900 rpm, Injection timing = 10° btdc)

NETT ENERGY RELEASE RATE (J/C)

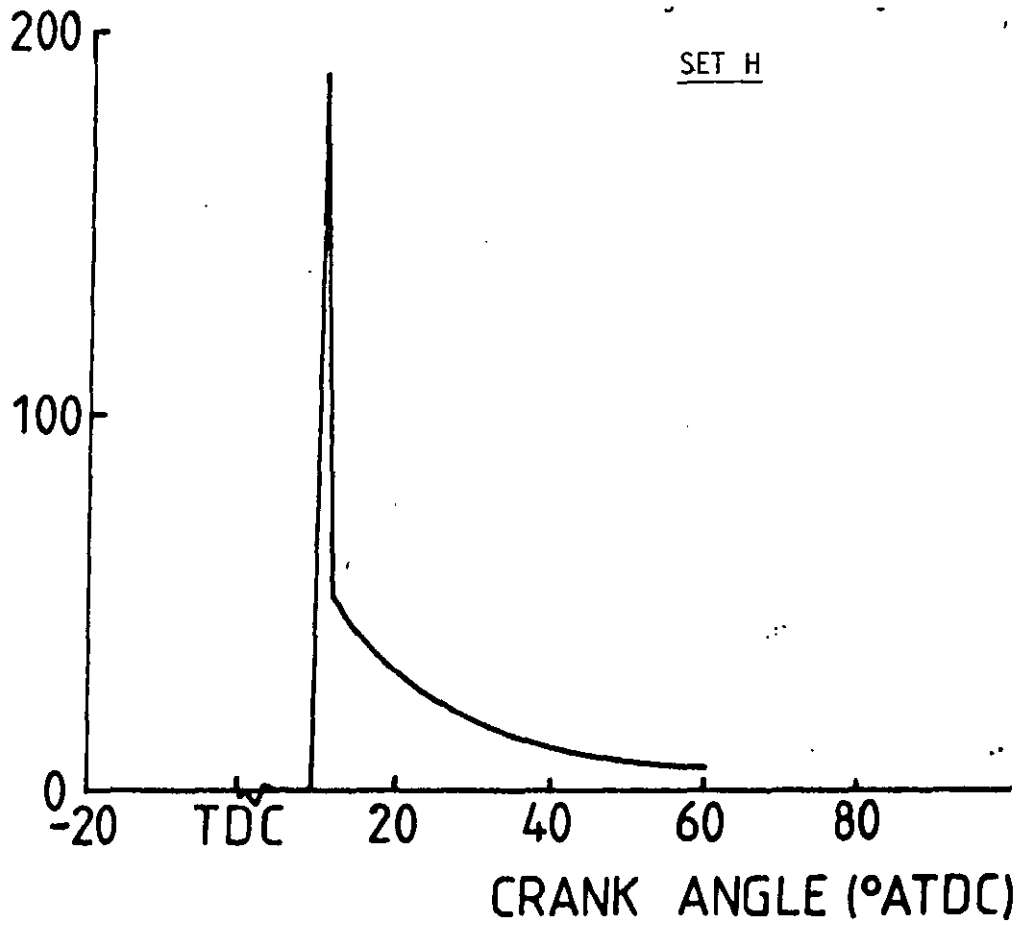


FIG. 6.18 Nett energy release rate (Idling; Fuel quantity = 20 mm^3 , Engine speed = 700 rpm, Injection timing = 1° atdc)

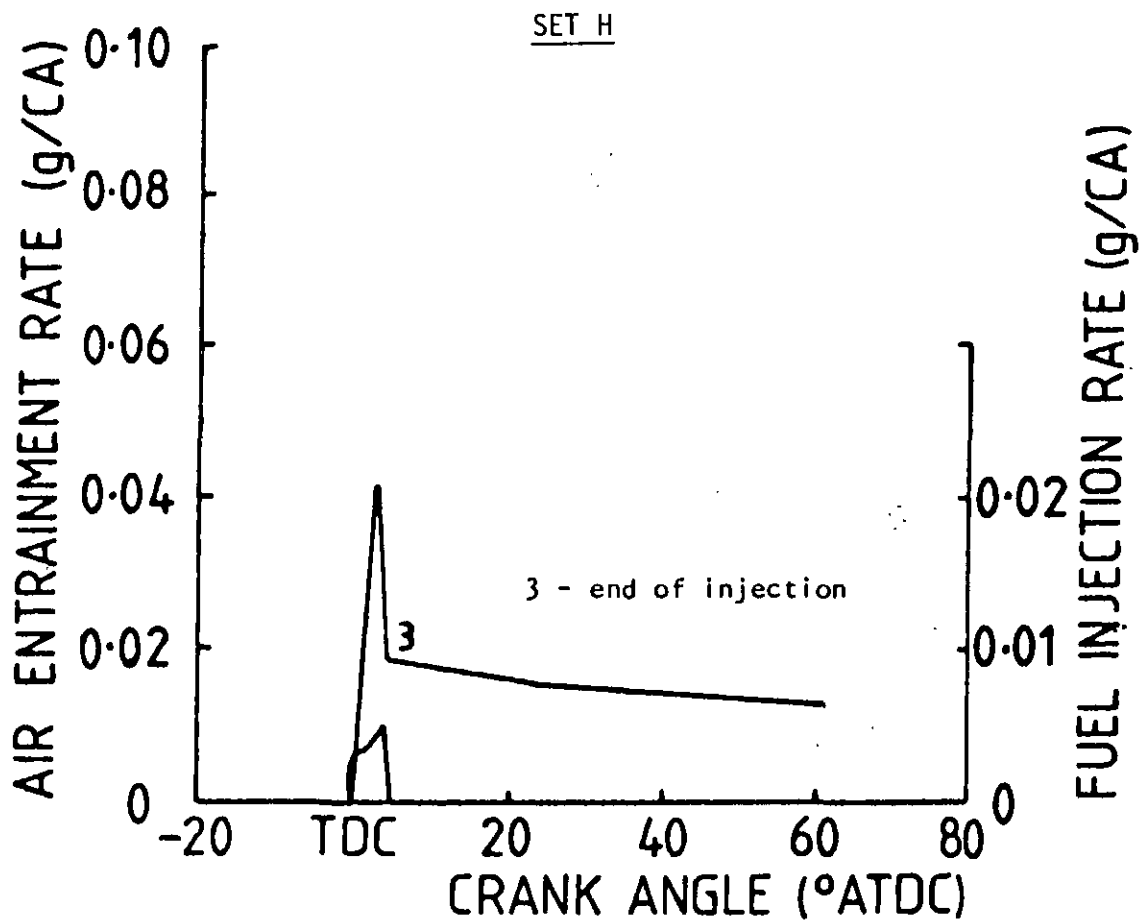


FIG. 6.19 Air entrainment and fuel injection rates (Idling: Fuel quantity = 20 mm^3 , Engine speed = 700 rpm, Injection timing = 1° atdc)

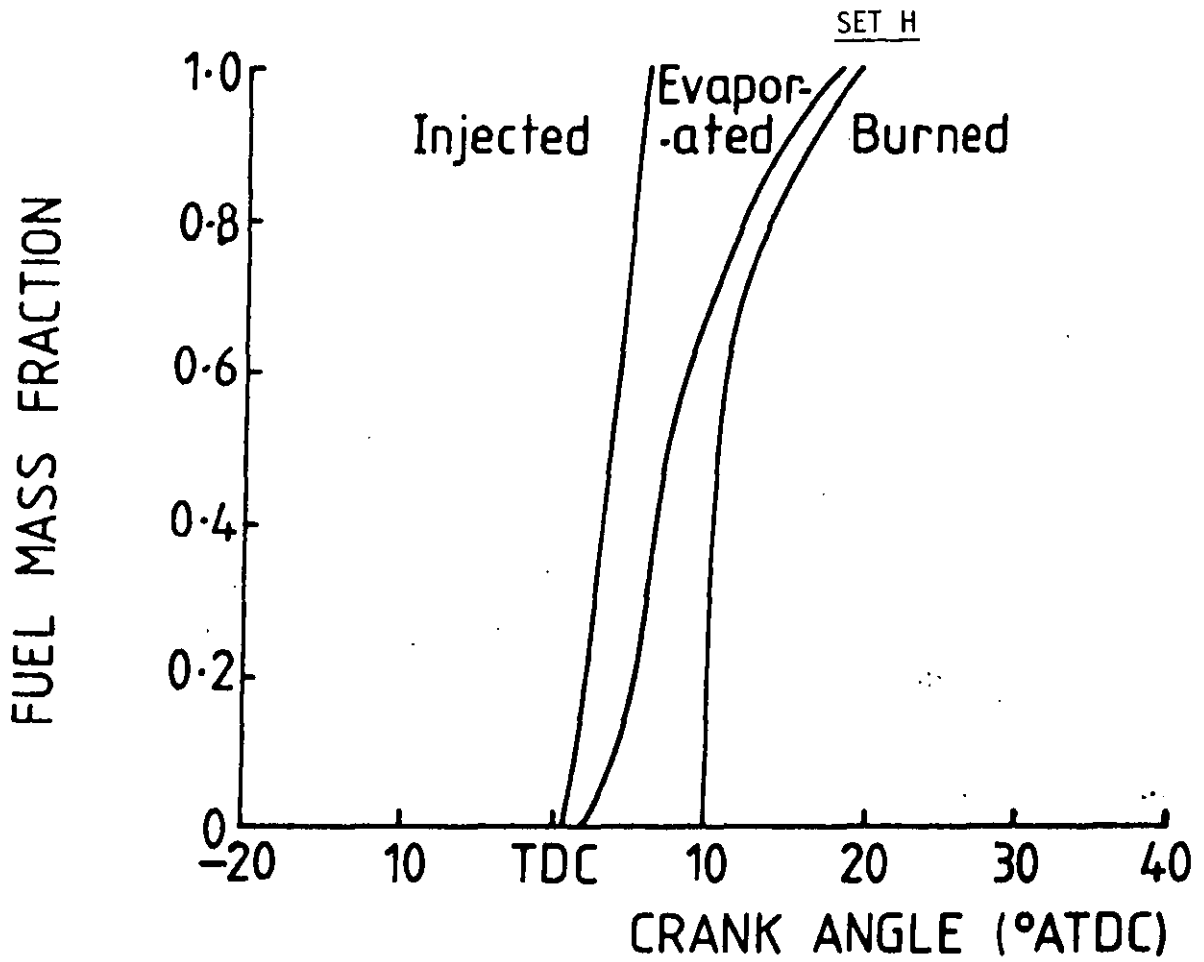


FIG. 6.20

Fuel mass fractions injected, evaporated and burned (Idling: Fuel quantity = 20 mm³, Engine speed = 700 rpm, Injection timing = 1° atdc)

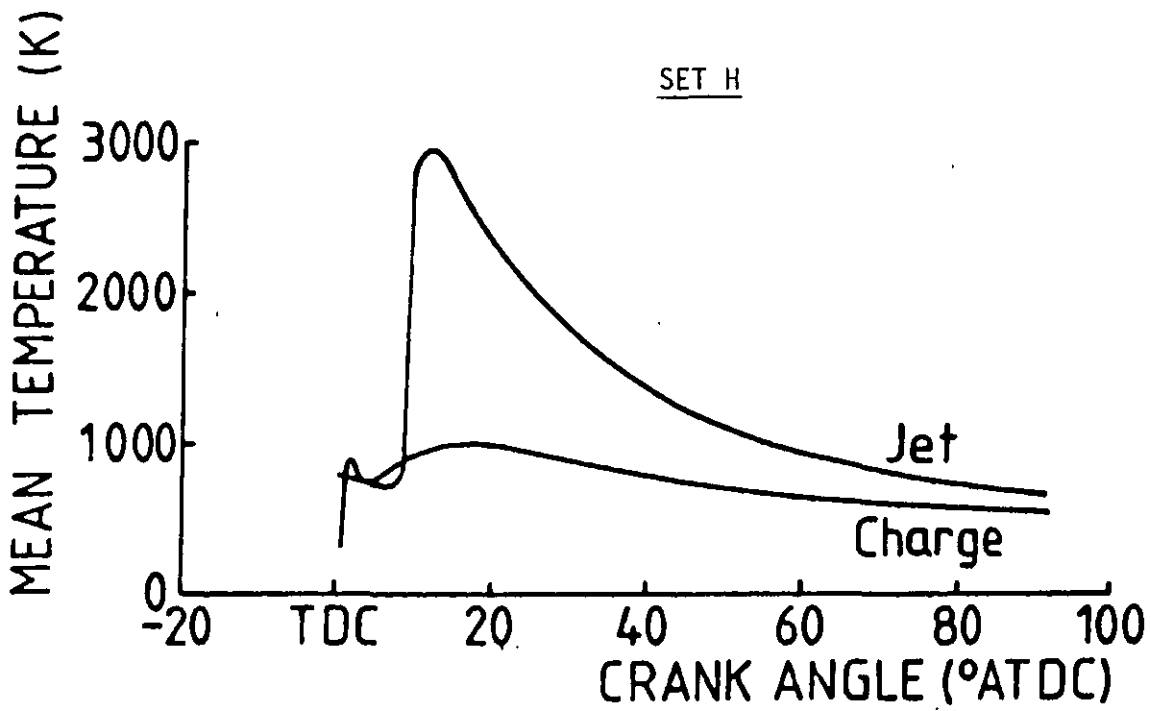


FIG. 6.21 Mean temperature diagram (Idling: Fuel quantity = 20 mm³, Engine speed = 700 rpm, Injection timing = 1° atdc)

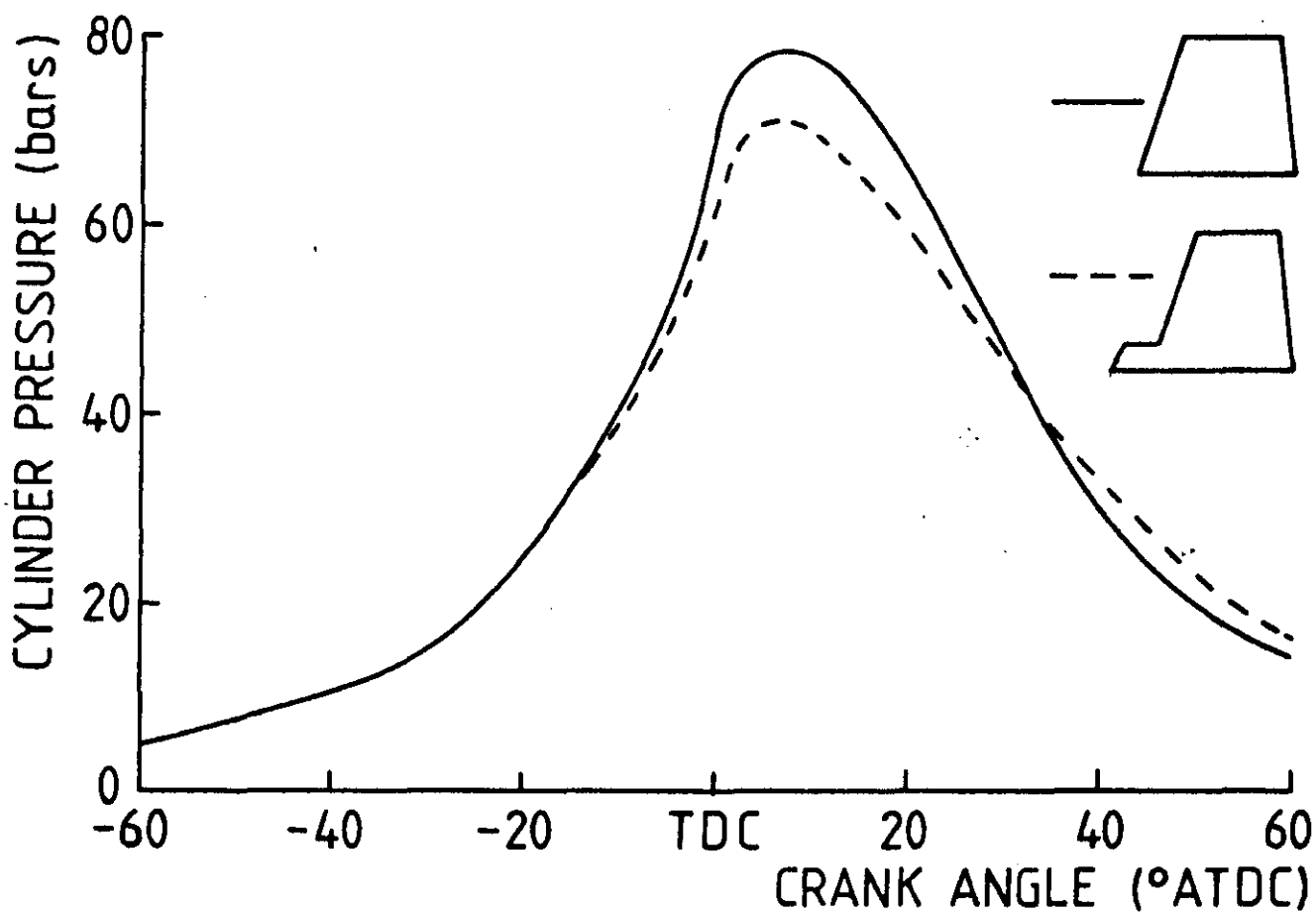


FIG. 6.22 Effect of injection scheduling on cylinder pressure with reference to set A (High load: Fuel quantity = 142.3 mm^3 , Engine speed = 1300 rpm, Injection timing = 18° btdc)

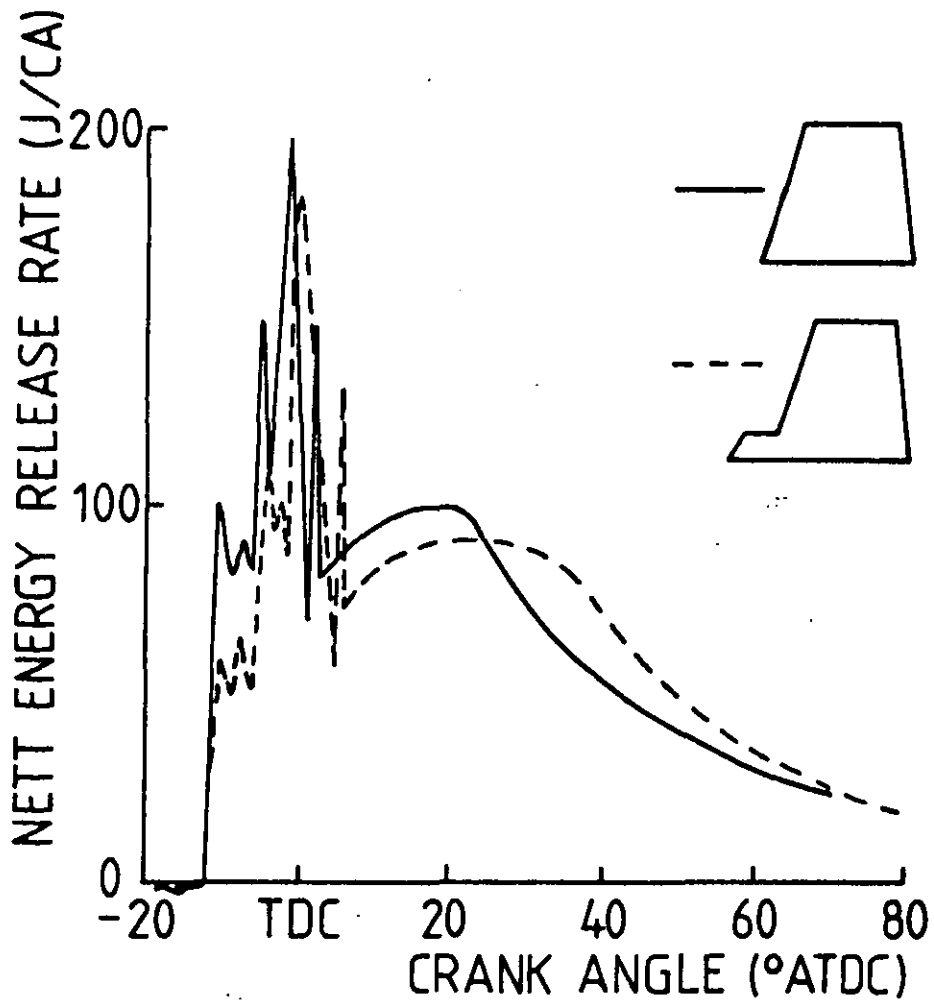


FIG. 6.23 Effect of injection scheduling on nett energy release rate with reference to set A

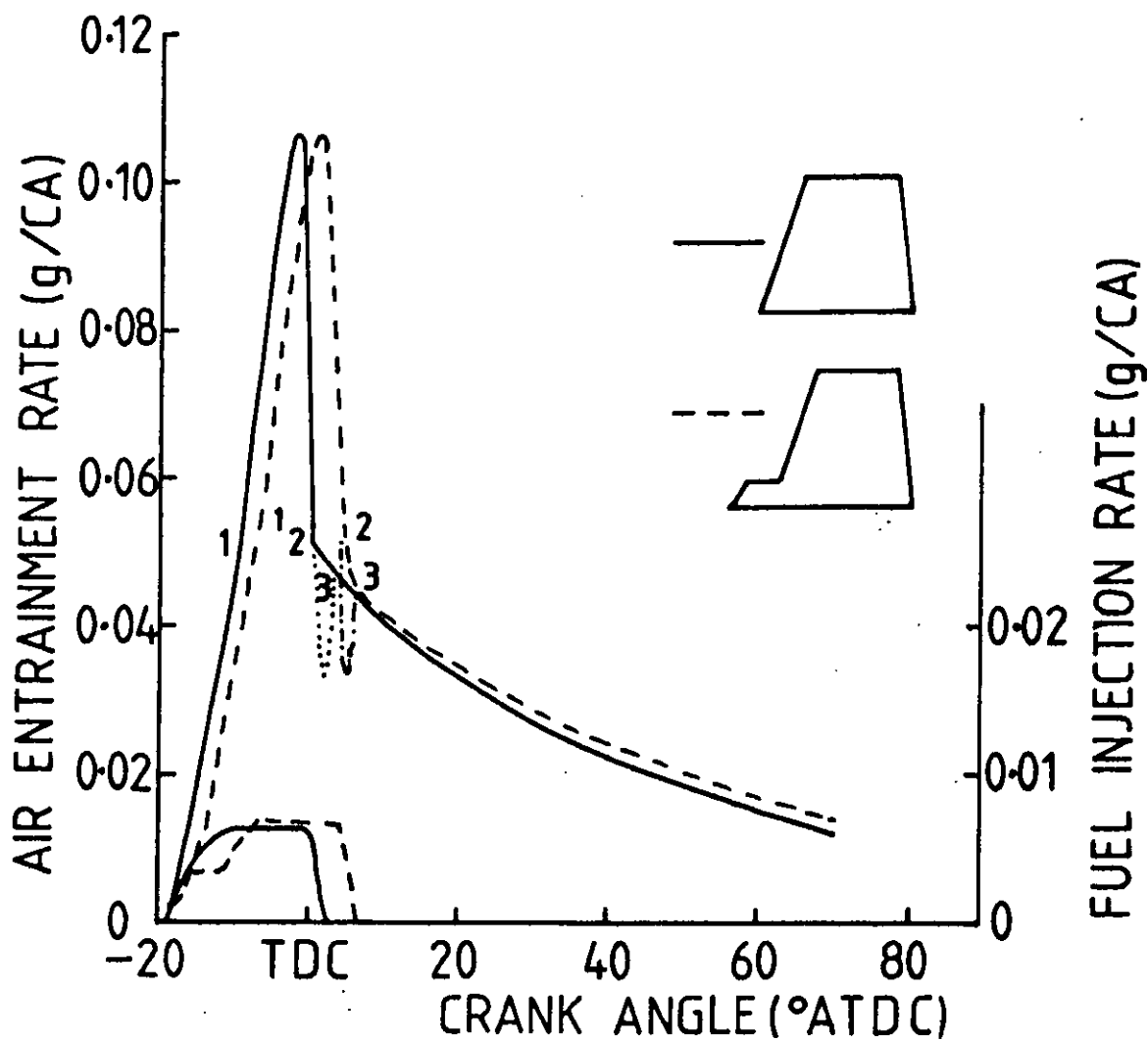


FIG. 6.24 Effect of injection scheduling on air entrainment and fuel injection rates with reference to set A

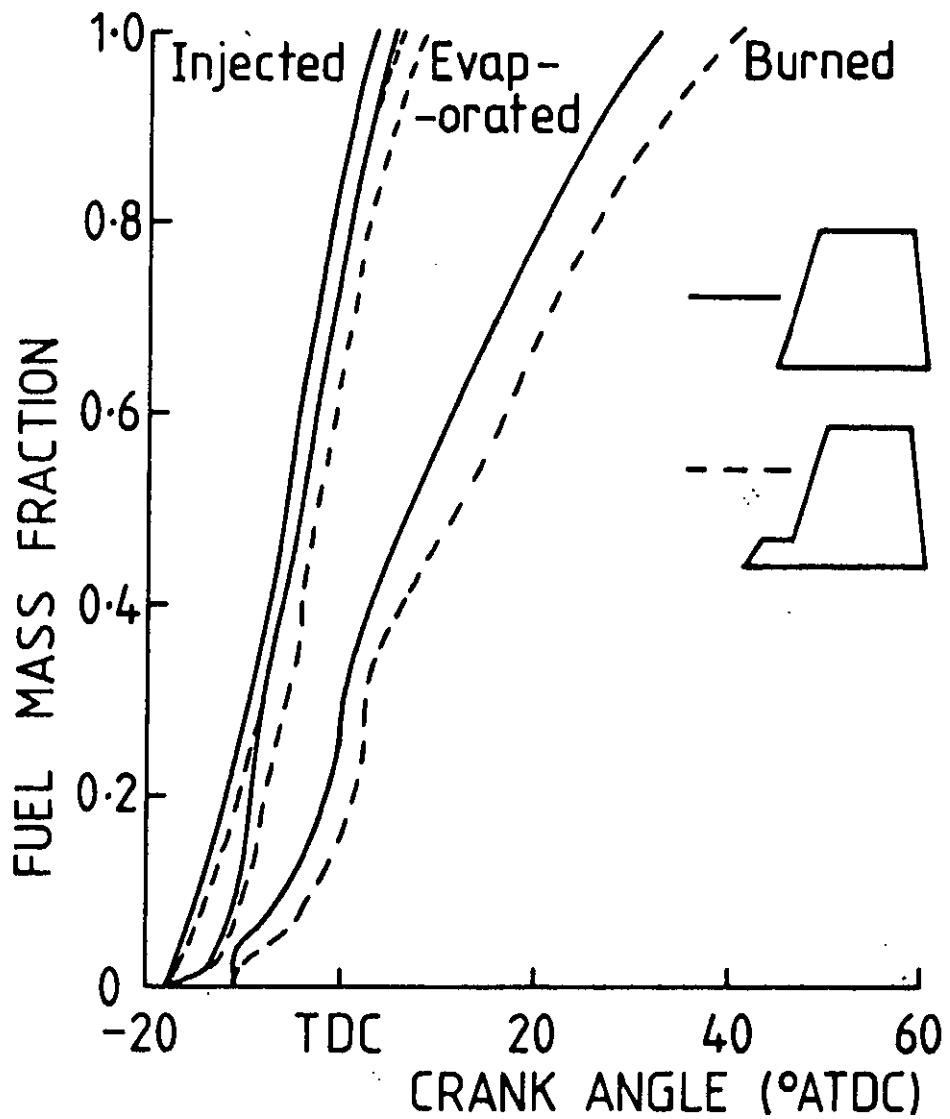


FIG. 6.25 Effect of injection scheduling on fuel mass fractions injected, evaporated and burned with reference to Set A

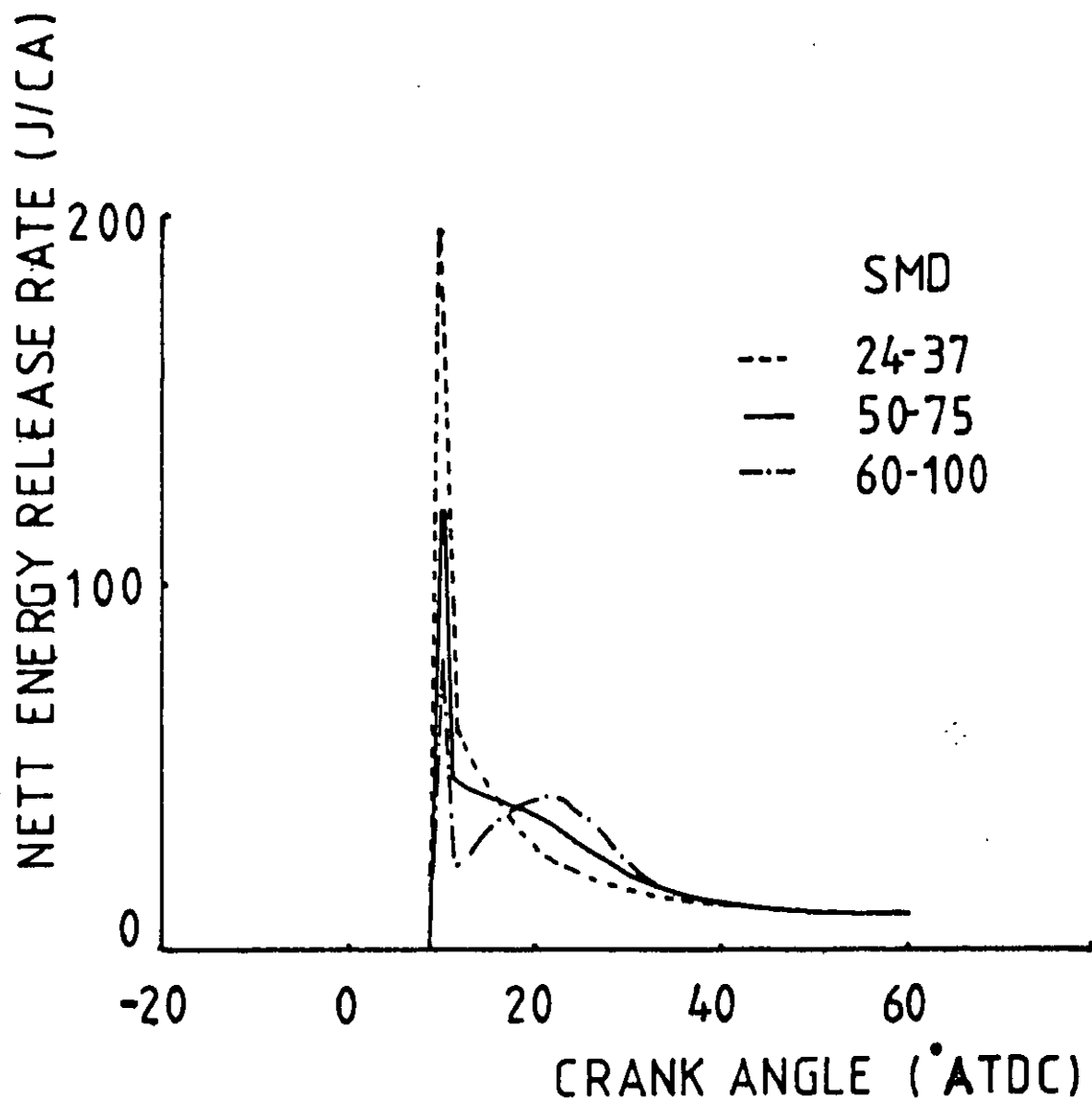


FIG. 6.26 Effect of SMD on nett energy release rate at idling (Set H)

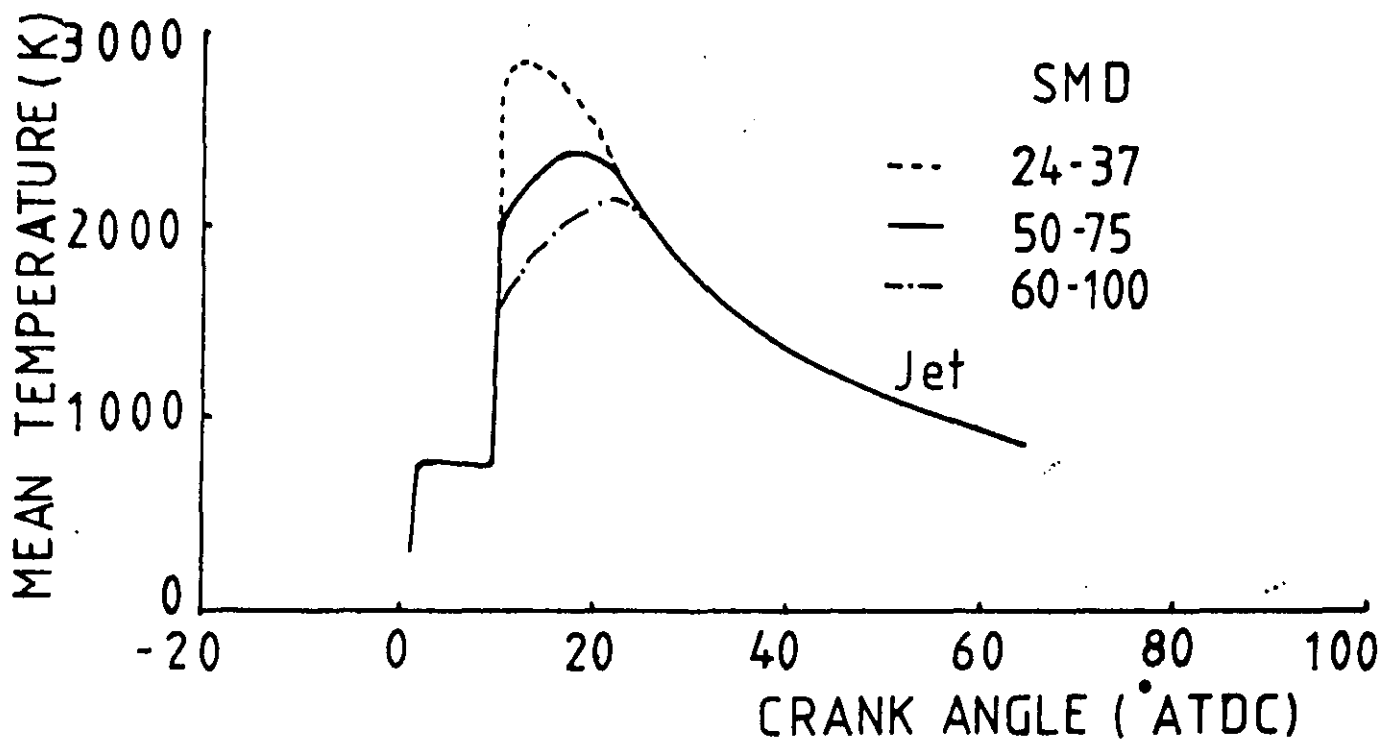


FIG. 6.27 Effect of SMD on mean jet temperatures at idling (Set H)

EGR=0.0	0.1	0.2	Speed	Fuel Quantity	Timing
△	▲	▲	1300	142.3	-18
○	⊙	●	1300	142.3	-10
□	◻	■	1300	191.6	-24
◇	◊	◆	1300	191.6	-16
▽	▼	▼	1900	142.3	-10

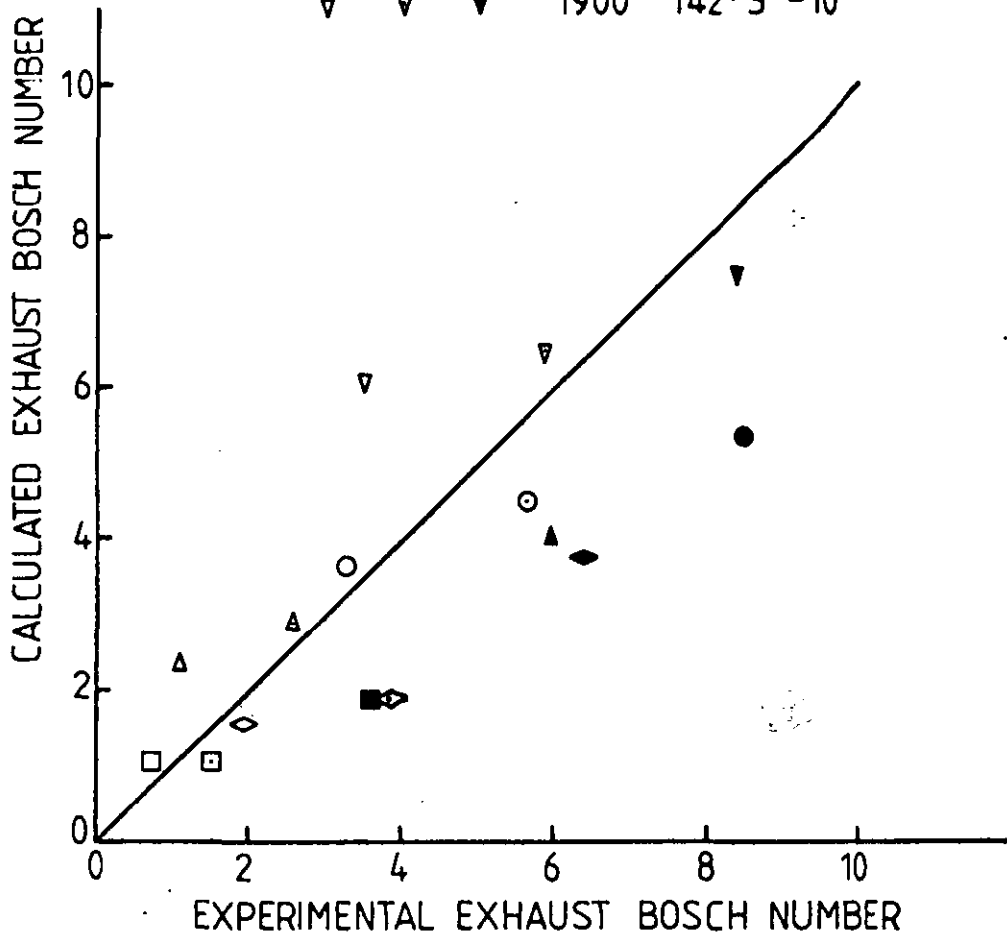


FIG. 6.28 Experimental exhaust Bosch number versus calculated values for quiescent chamber engine

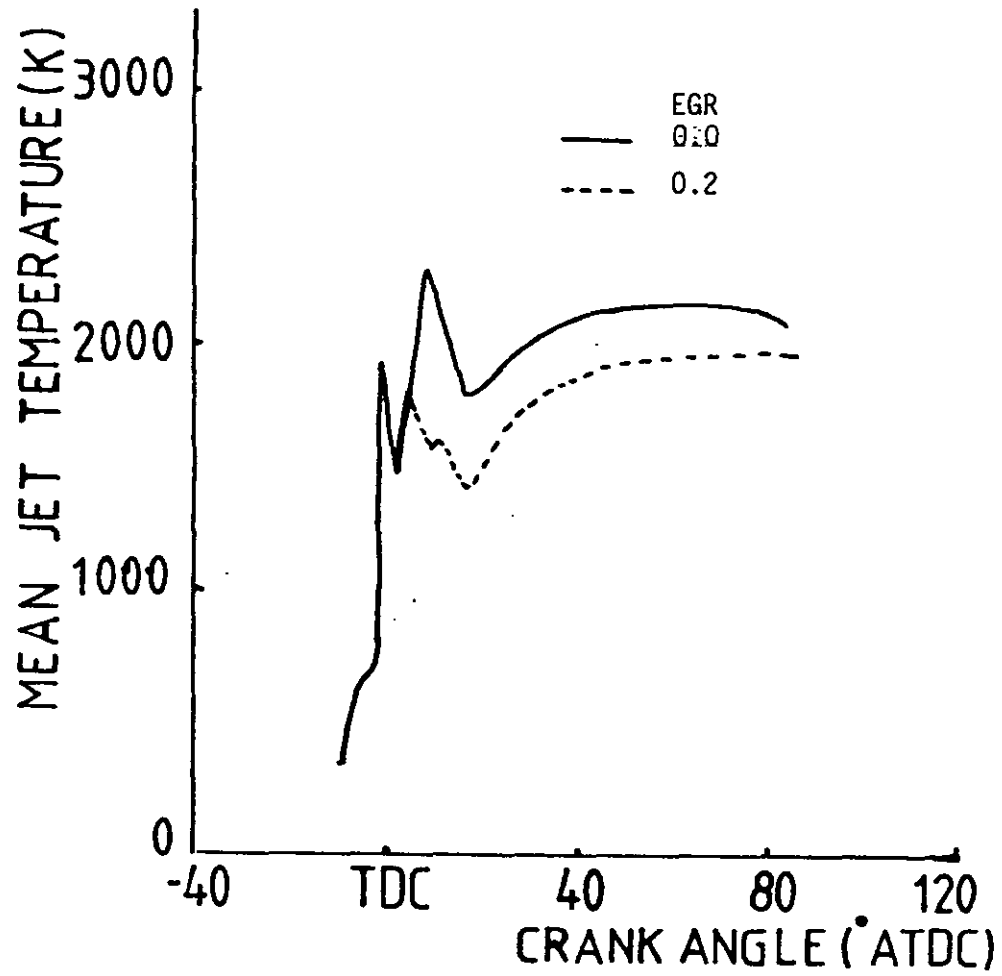


FIG. 6.29 Effect of exhaust gas recirculation on mean jet temperature with reference to set B

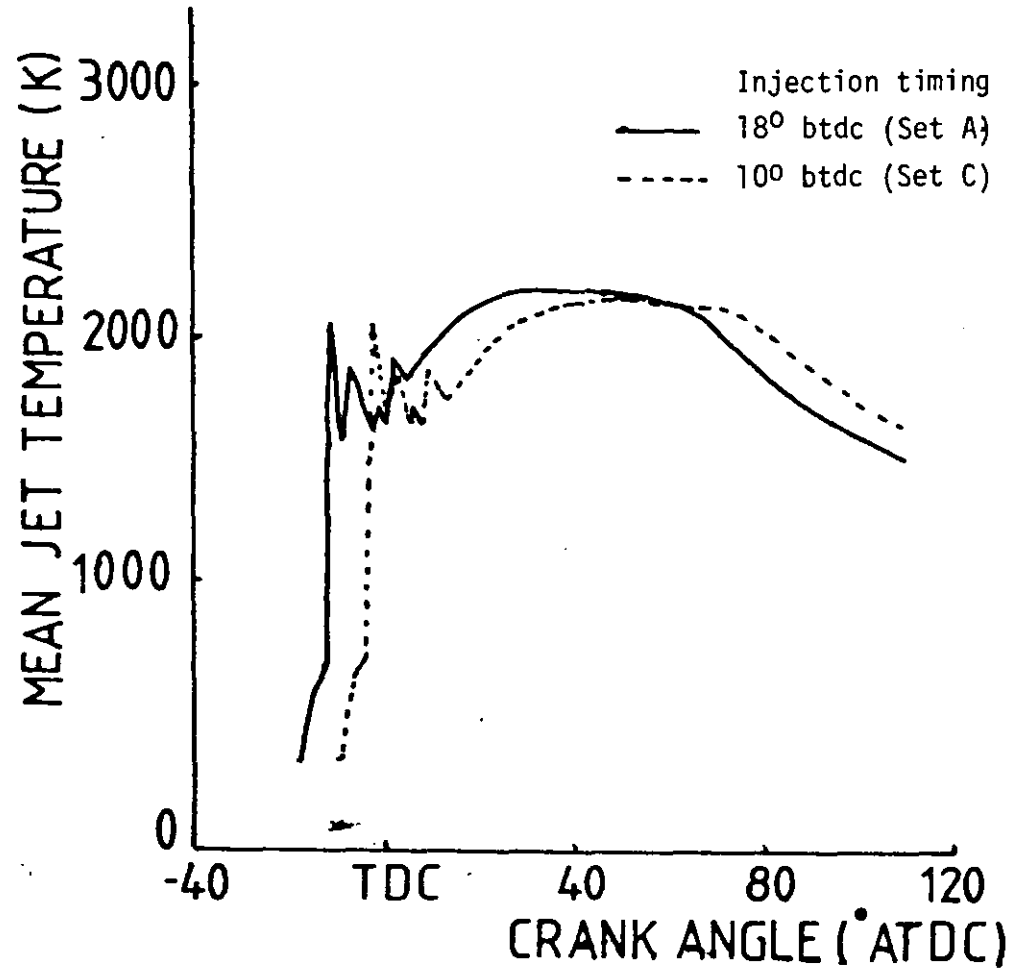


FIG. 6.30 Effect of injection timing on mean jet temperature

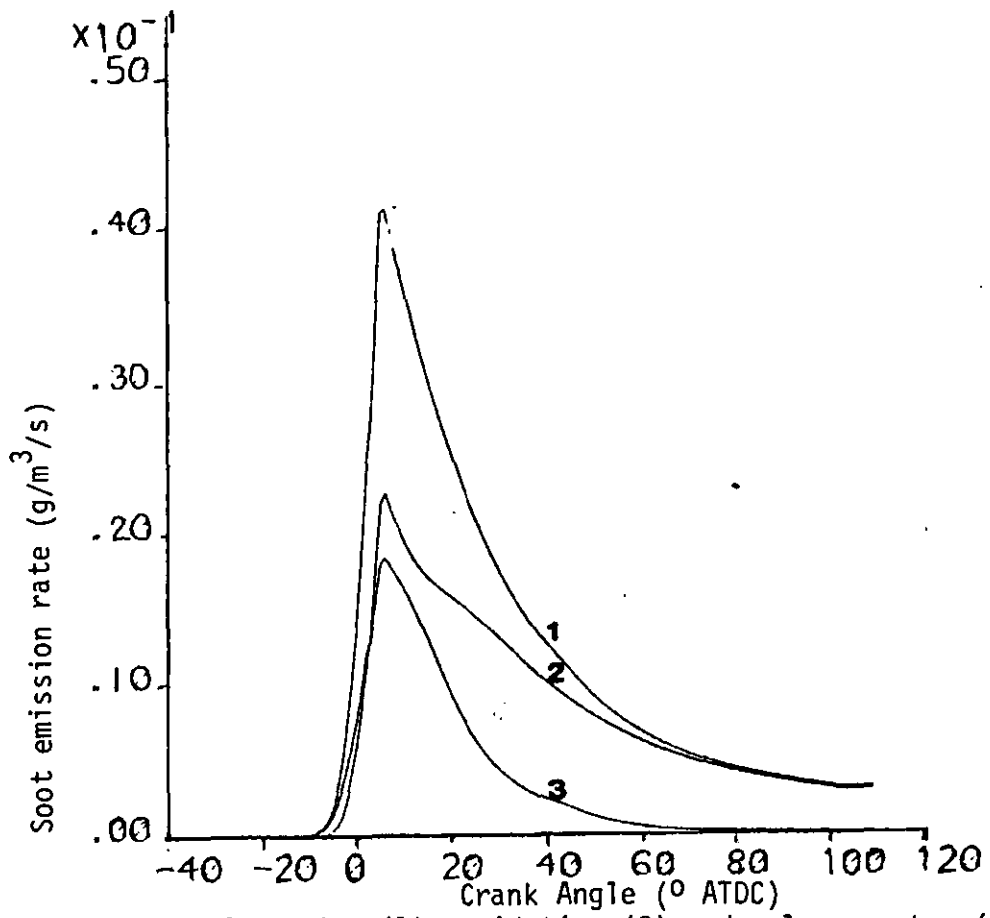


FIG. 6.31 Soot formation (1), oxidation (2) and release rates (3) for Set A

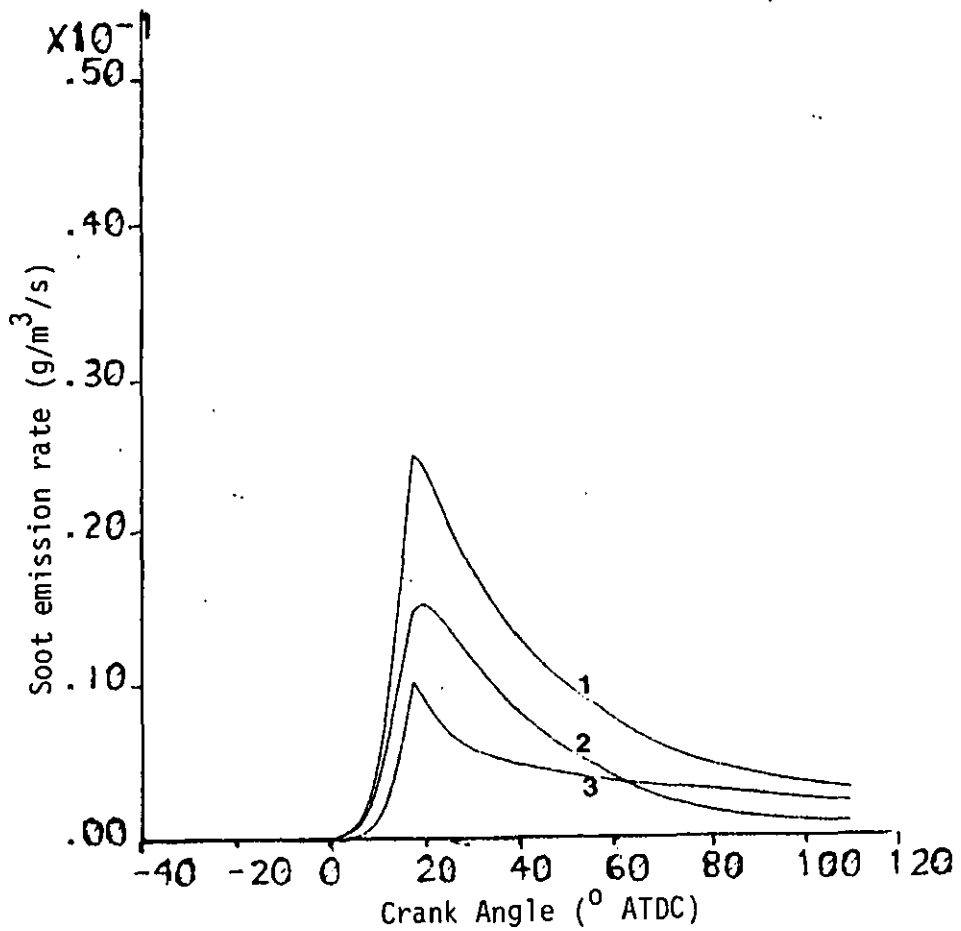


FIG. 6.32 Soot formation (1), oxidation (2) and release rates (3) for Set B

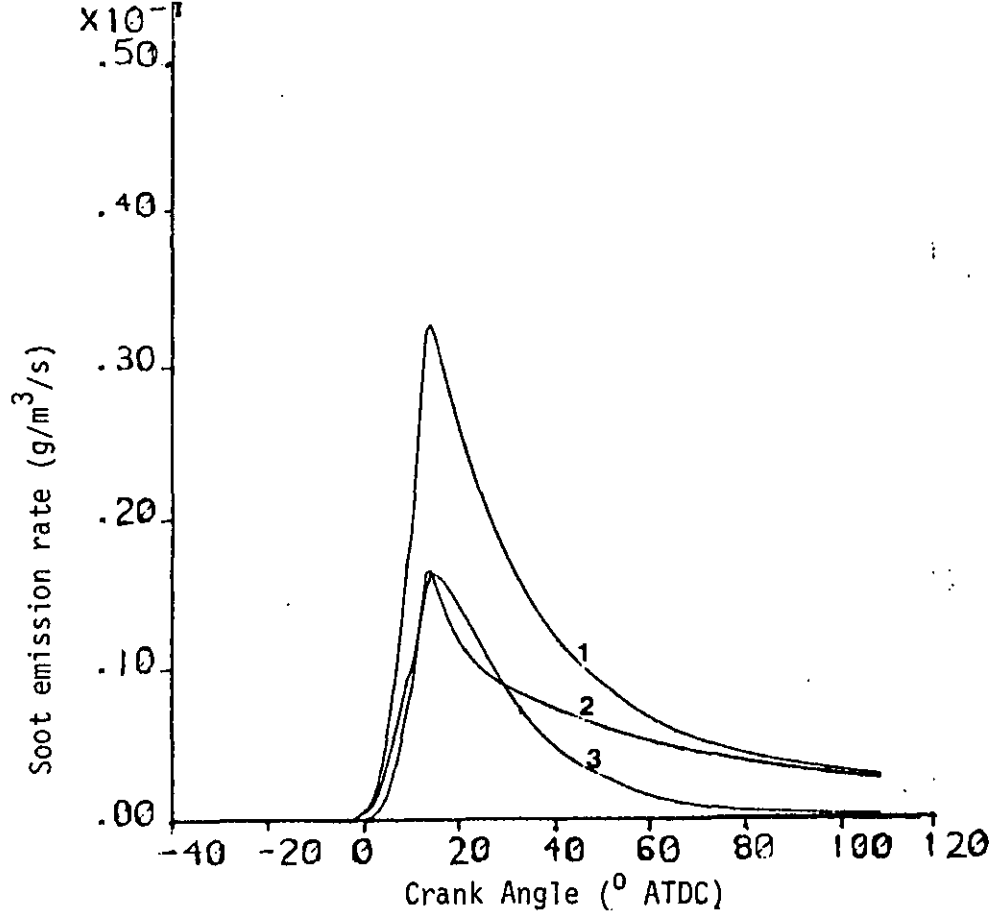


FIG. 6.33 Soot formation (1), oxidation (2) and release rates (3) for Set C

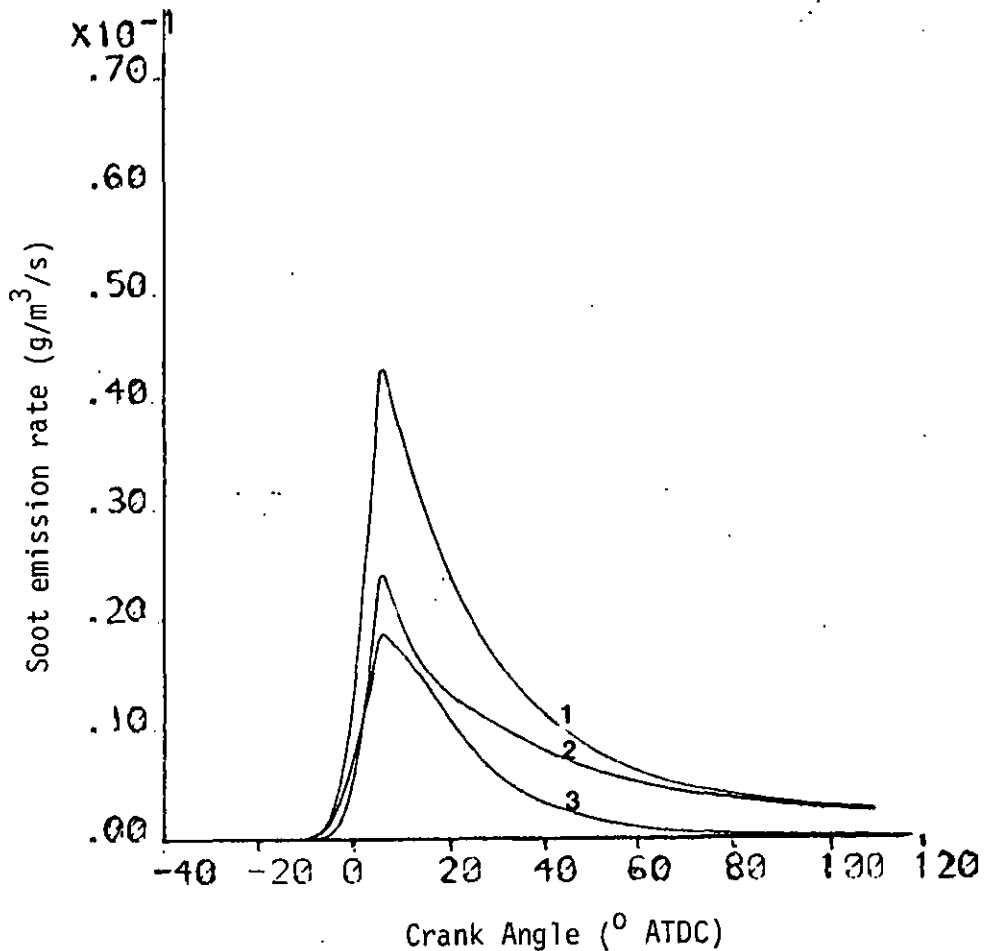


FIG. 6.34 Soot formation (1); oxidation (2) and release rates (3) for Set A with EGR = 0.1

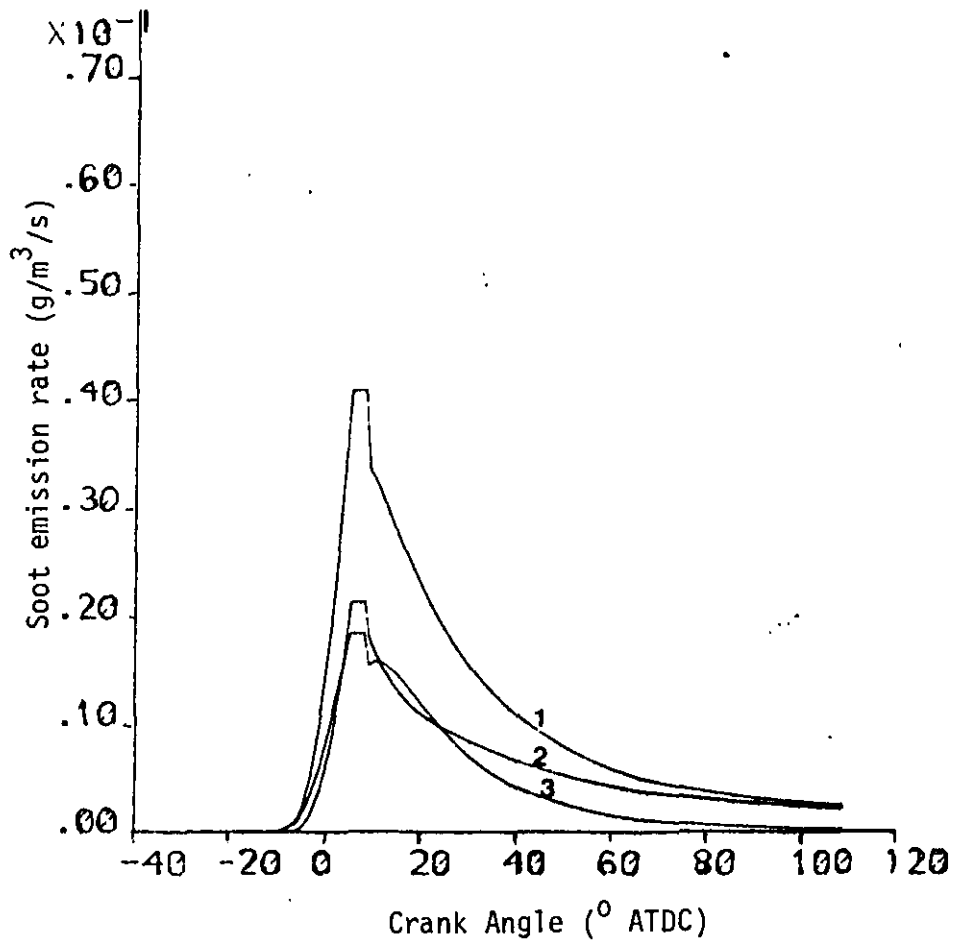


FIG. 6.35 Soot formation (1), oxidation (2), and release rates (3) for Set A with EGR = 0.2

Engine speed = 1100 rpm

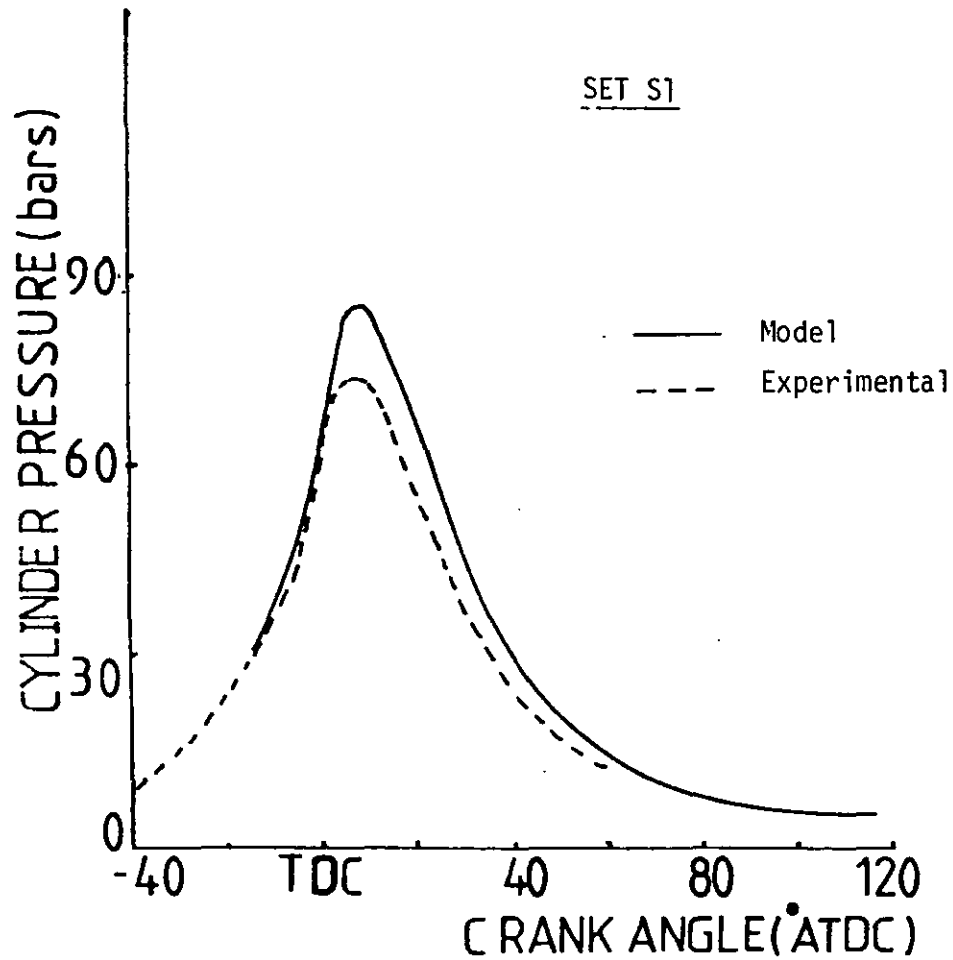


FIG. 6.36 Cylinder pressure diagram (Swirl Engine; High load: Fuel quantity = 75 mm^3 , Injection timing = 10.5° btdc)

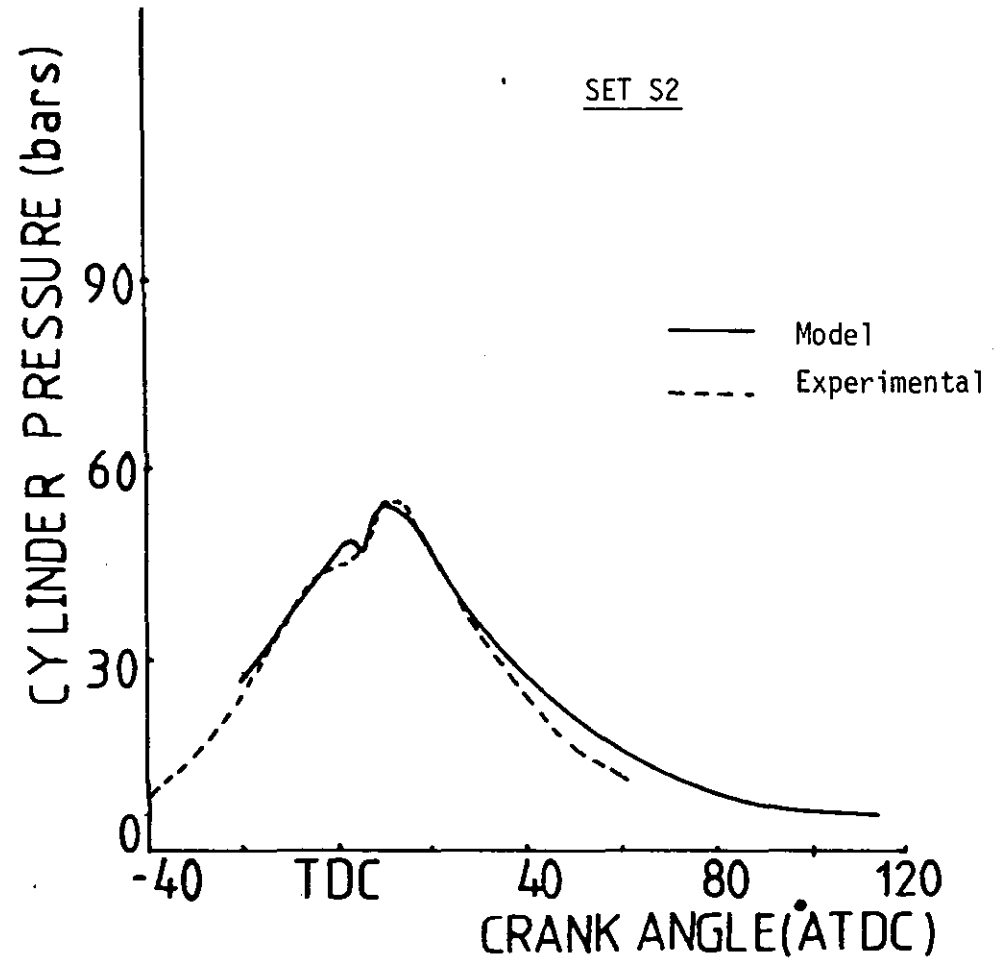


FIG. 6.37 Cylinder pressure diagram (Swirl Engine, High speed, retarded injection timing: Fuel quantity = 76.8 mm^3 , Injection timing = 0.5° btdc)

Engine speed = 1700 rpm

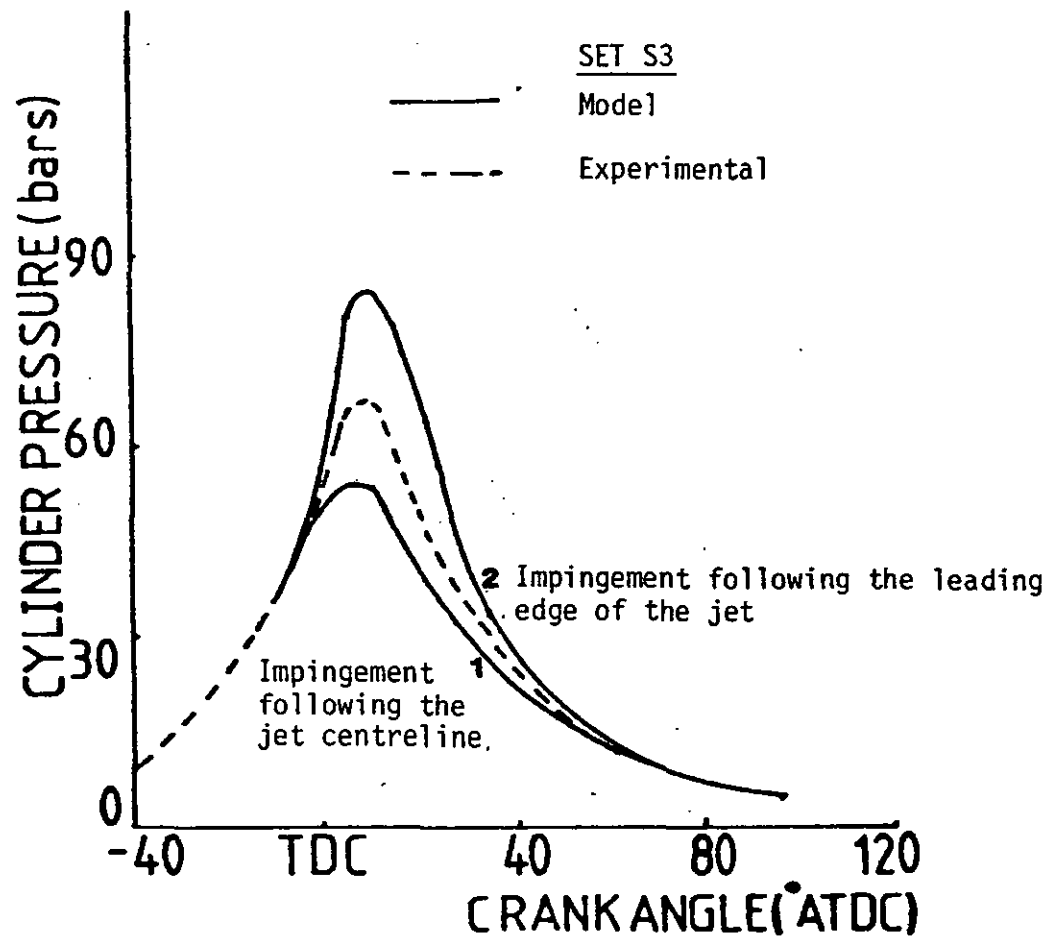


FIG. 6.38 Cylinder pressure diagram (Swirl engine; High load: Fuel quantity = 75.3 mm^3 , Injection timing = 9.5° btdc)

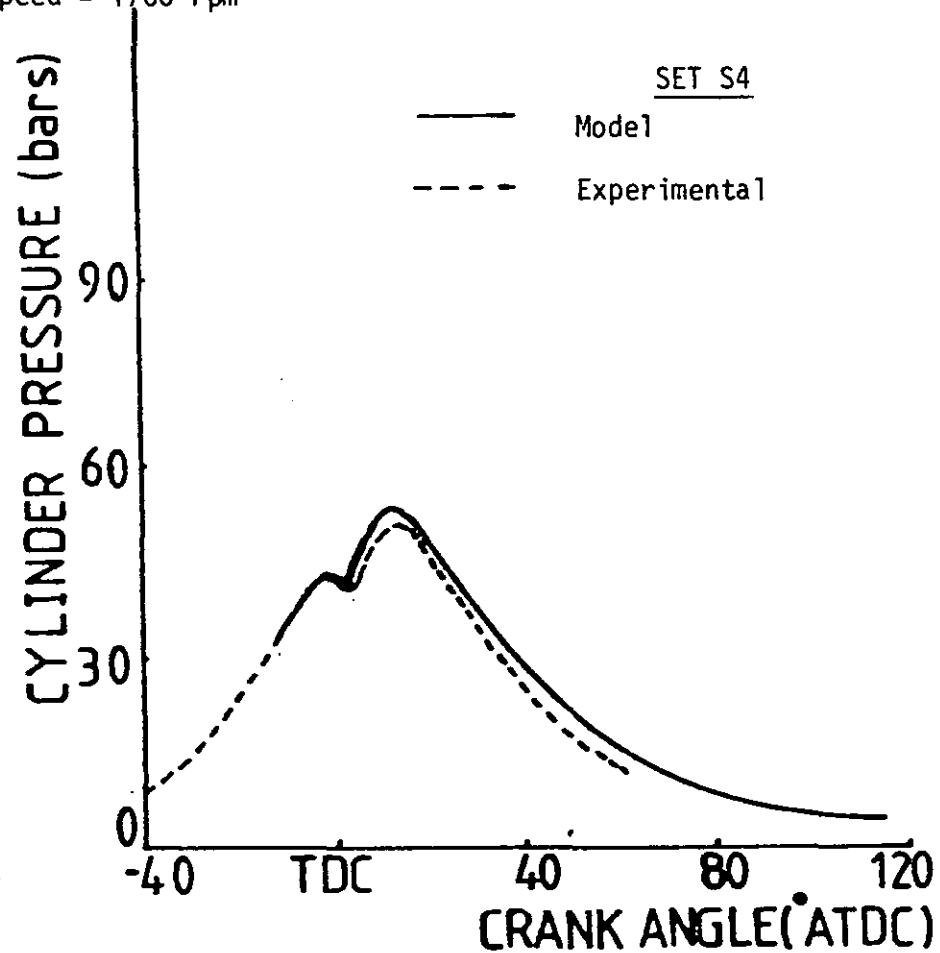


FIG. 6.39 Cylinder pressure diagram (Swirl engine, High load, retarded injection timing: Fuel quantity = 74.9 mm^3 , Injection timing = 2.5° btdc)

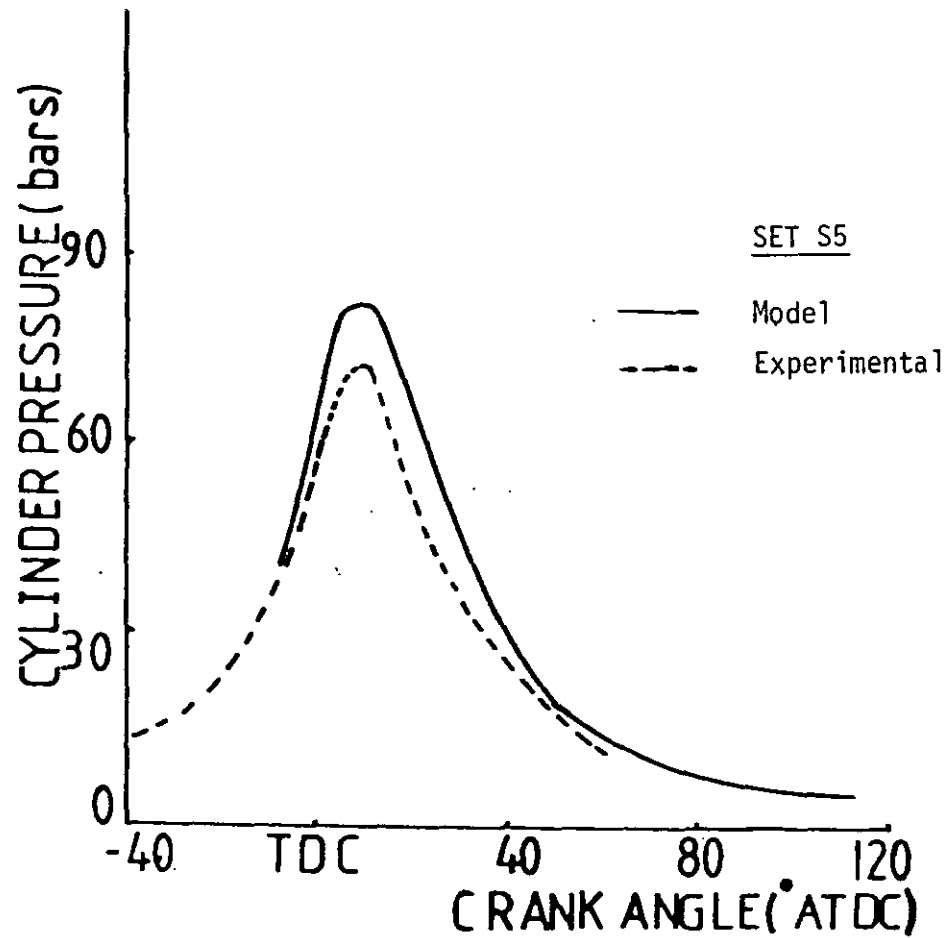


FIG. 6.40 Cylinder pressure diagram (Swirl engine, High load: Fuel quantity = 74.6 mm^3 , Injection timing = 15.5° btdc)

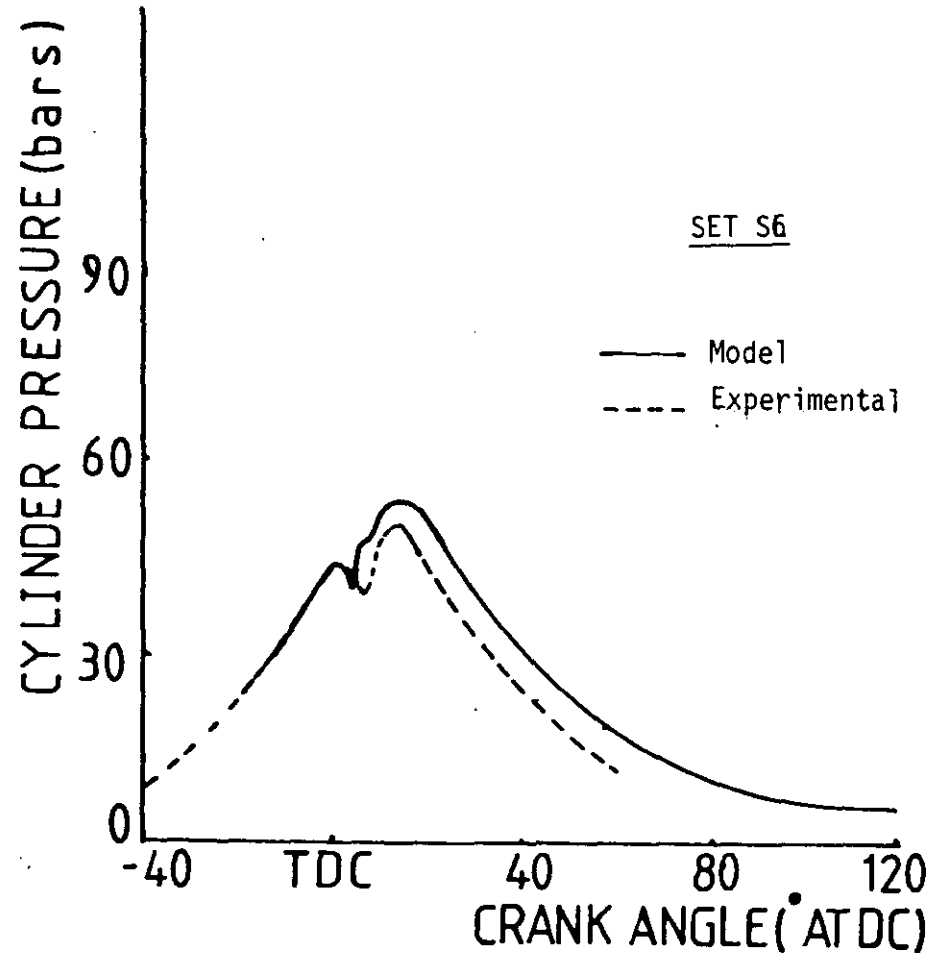


FIG. 6.41 Cylinder pressure diagram (Swirl engine, High load, retarded injection timing: Fuel quantity = 75 mm^3 , Injection timing = 7.0° btdc)

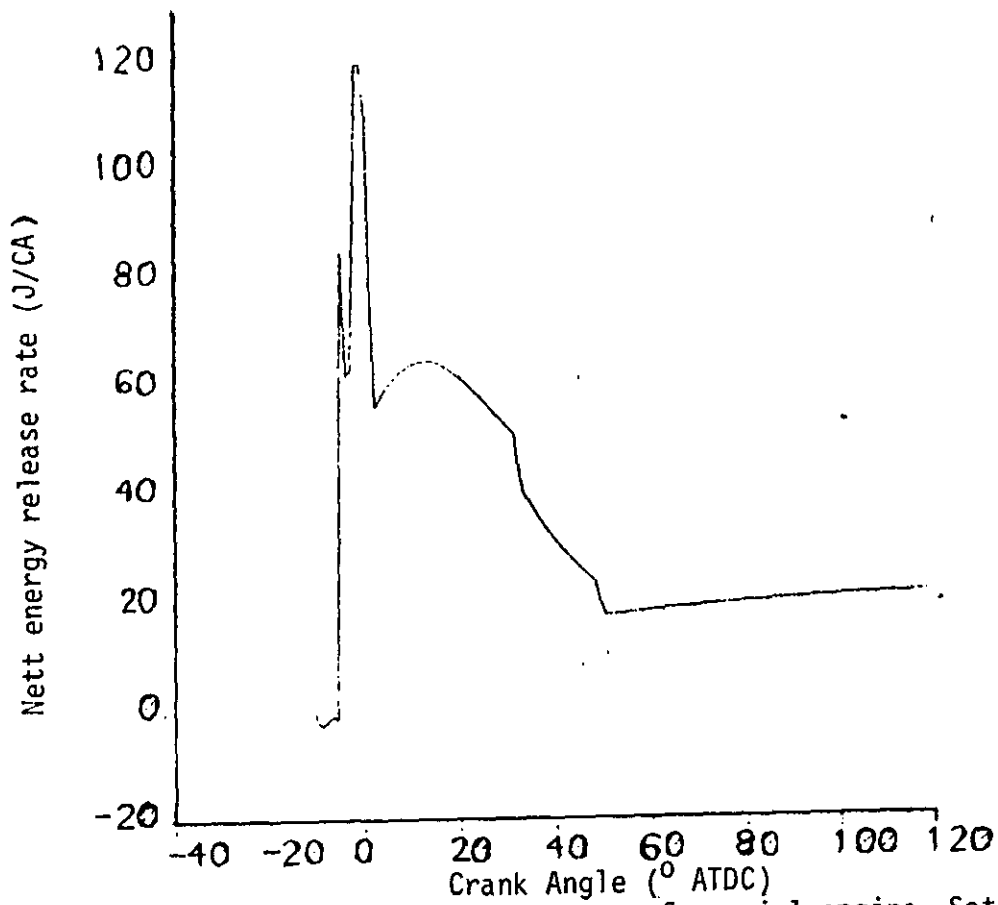


FIG. 6.42 Nett energy release rate for swirl engine, Set S1

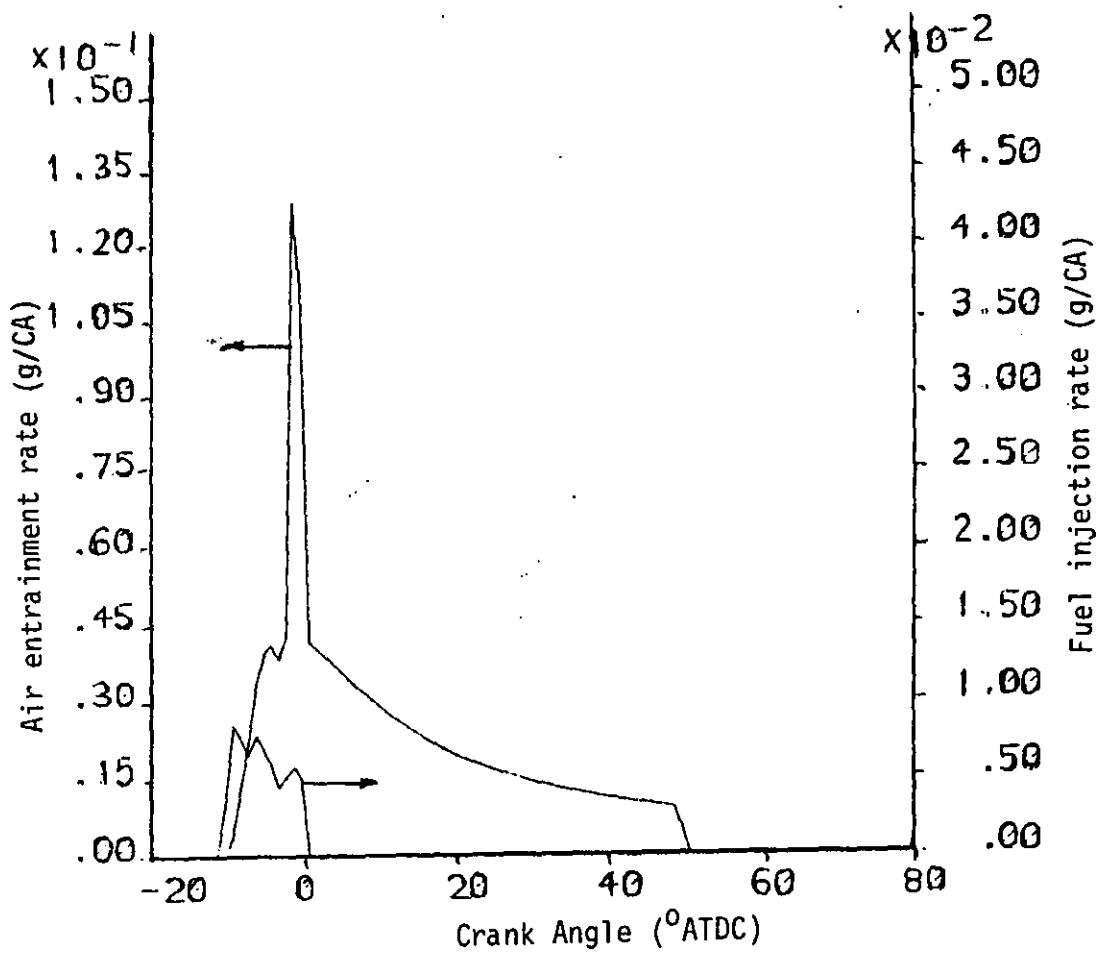


FIG. 6.43 Air entrainment and fuel injection rates for swirl engine, Set S1

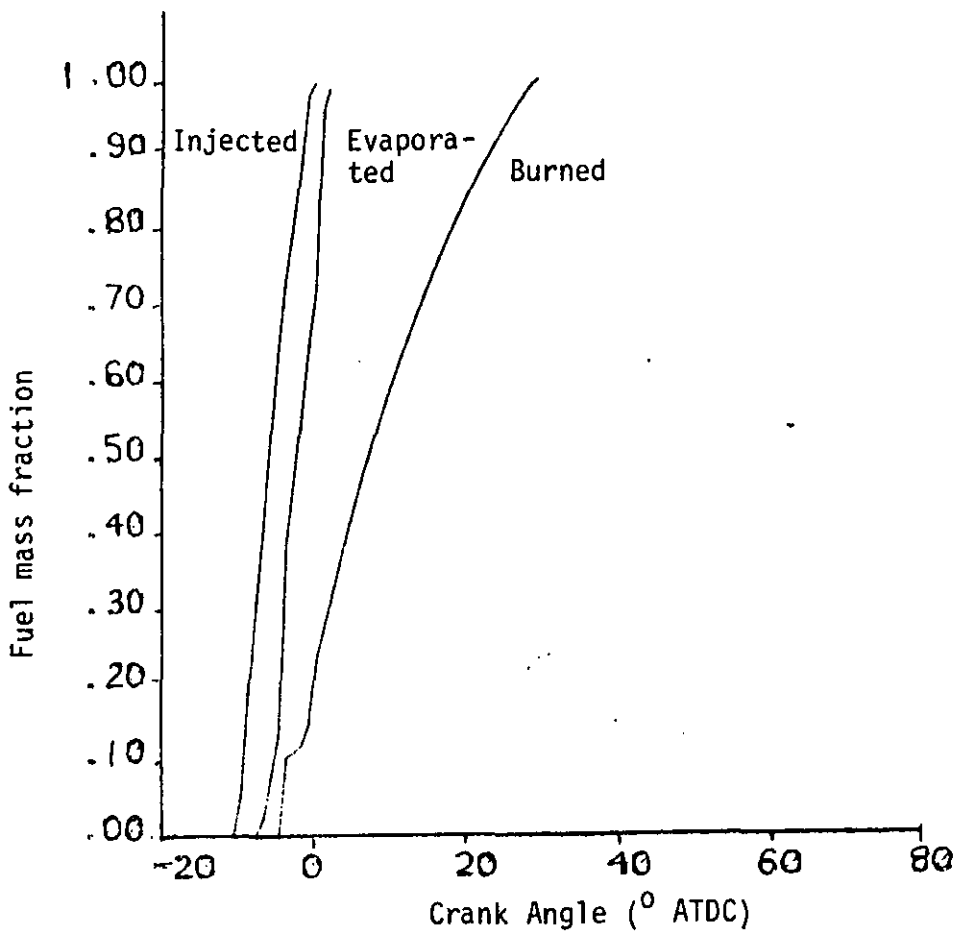


FIG. 6.44 Fuel mass fractions injected, evaporated and burned for swirl engine, Set S1

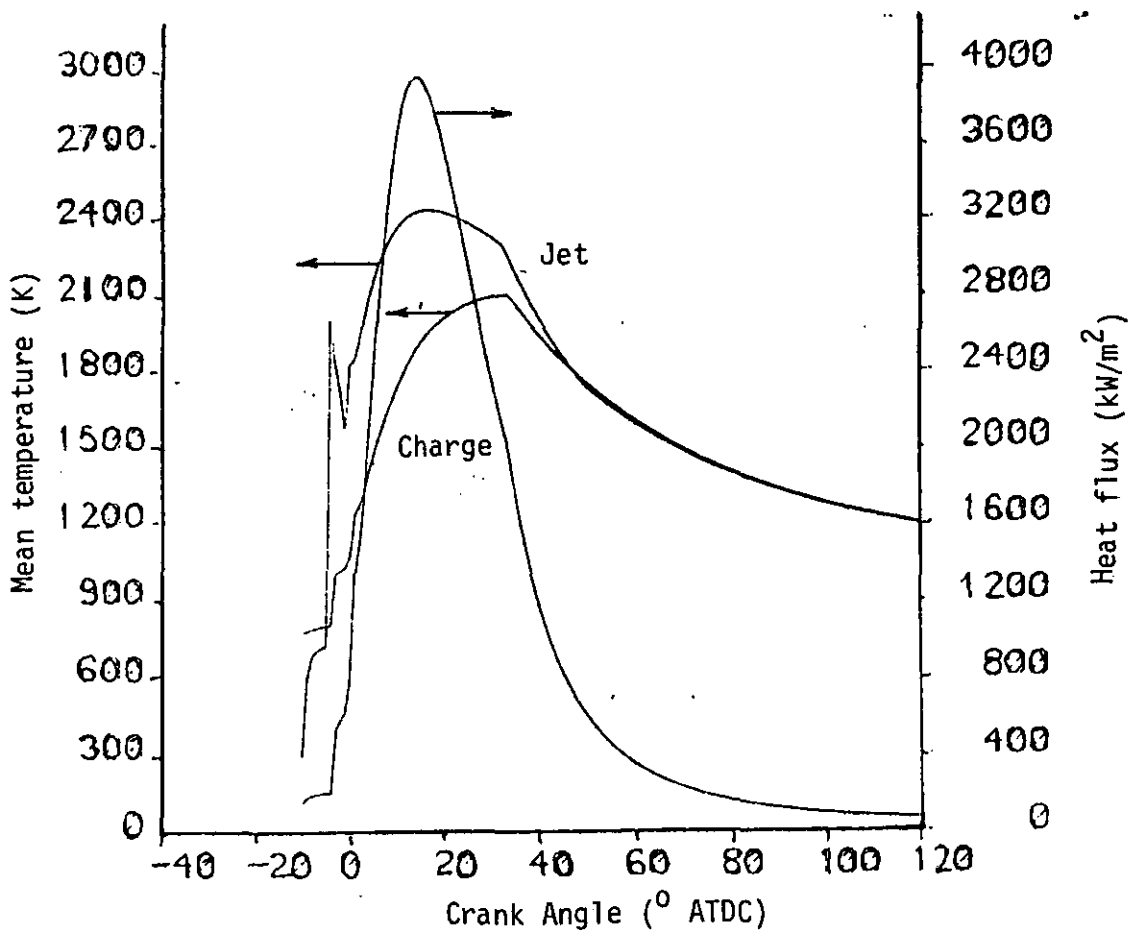


FIG. 6.45 Mean temperature and heat flux diagram for swirl engine, Set S1

CHAPTER VII

CONCLUSION AND FUTURE WORK

7.1 Conclusion

In general the modelling of the quiescent chamber engine in regard to combustion, performance parameter prediction and smoke emission, has been adequately demonstrated in this thesis. Some areas for further work are discussed later.

The modelling of the high swirl direct injection Diesel engine has only been partially successful, primarily due to lack of time to develop a suitable analysis/empirical relationship for the wall jet development. The soot model appears to yield the right trends in some cases, and further work needs to be done in this area. From the results obtained a better description of the wall jet behaviour will in all probability improve the soot prediction because of changes in the air entrainment and hence oxidation process.

7.2 Future Work

In the quiescent chamber model better characterisation of the combustion mechanism can be incorporated to account for vitiation of the burning regions with combustion product thereby reducing the combustion temperatures.

A better description of wall jet interaction to produce higher entrainment rates than presently estimated, needs some consideration. However, this is not a major point.

A better description of the SMD for low load prediction is necessary for effective prediction in these cases.

The soot model appears to have the correct features with regard to formation and oxidation. However this must be considered as empirical at the present time. Adjustment of local combustion temperature will upset the critical balance between the formation and oxidation mechanisms. A possible approach is that of Magnussen (107), where large and small scale structures are assigned their own temperatures.

The work on swirl presented here must be considered as preliminary in nature. However, the major area for further investigation certainly appears to be the impingement and wall jet development.

REFERENCES

1. Heywood, J B *'Engine Combustion Modelling - An Overview'*, Combustion Modelling on Reciprocating Engines (Ed. Mattavi, J N and Amann, A), Plenum Press, 1980.
2. Bracco, F V *'Introducing a New Generation of More Detailed and Informative Combustion Models'*, SAE Trans. Vol. 84 (paper No. 751187), 1975.
3. HaseIman, L C
Westbrook, C K *'A Theoretical Model for Two-Phase Fuel Injection in Stratified Charge Engines'*, SAE Trans. Vol. 87 (paper No. 780318), 1978.
4. Gosman, A D
Johns, R J R *'Computer Analysis of Fuel-Air Mixing in Direct-Injection Engines'*, SAE Trans. Vol. 89, (paper No. 800091), 1980.
5. Butler, T D
Cloutman, L D
Dukowicz, J K
Ramshaw, J D *'Towards a Comprehensive Model for Combustion in a Direct Injection Stratified Charge Engine'*, Combustion Modelling in Reciprocating Engines, (Ed. Mattavi, J N and Amann, A) Plenum Press, 1980.
6. Lyn, W T *'Study of Burning Rate and Nature of Combustion in Diesel Engines'*, Ninth Symposium (International) on Combustion, 1963.
7. Borman, G L *'Mathematical Simulation of Internal Combustion Engine Processes and Performance Including Comparisons with Experiments'*, PhD Thesis, University of Wisconsin, USA, 1964.

8. Whitehouse, N D
Way, R *'Rate of Heat Release in Diesel Engines and its Correlation with Fuel Injection Data'*, Proc. IMechE, Vol. 184, 1969-70.
9. Shipinski, J
Myers, P S
Uyehara, O A *'A Spray Droplet Model for Diesel Combustion'*, Proc. IMechE, Vol. 184, 1969-70.
10. Adler, D
Lyn, W T *'The Evaporation and Mixing of a Liquid Fuel Spray in a Diesel Air Swirl'*, Proc. IMechE, Vol. 184, 1969-70.
11. Grigg, H C
Syed, M H *'The Problem of Predicting Rate of Heat Release in Diesel Engines'*, Proc. IMechE, Vol. 184, 1969-70.
12. Bastress, E K
Chung, K M
Dix, D M *'Models of Combustion and Nitrogen Oxide Formation in Direct and Indirect Injection Compression-Ignition Engines'*, SAE paper No. 719053, 1971.
13. Khan, I M
Greeves, G
Probert, D M *'Prediction of Soot and Nitric Oxide Concentrations in Diesel Engine Exhaust'*, Symposium on Pollution Control in Transport Engines, IMechE, London, Nov. 1971.
14. Shahed, S M
Chiu, W S
Yumlu, V S *'A Preliminary Model for the Formation of Nitric Oxide in Direct Injection Diesel Engines and its Application on Parametric Studies'*, SAE Trans. Vol. 82 (paper No. 730083), 1973.
15. Whitehouse, N D
Sareen, B K *'Prediction of Heat Release in a Quiescent Chamber Diesel Engine Allowing for Fuel-Air Mixing'*, SAE Paper No. 740084, 1974.

16. Shahed, S M
Chiu, W S
Lyn, W T *'A Mathematical Model of Diesel Combustion'*,
IMEchE Conference on Combustion in Engines,
Cranfield, July 1975.
17. Hodgetts, D
Shroff, H D *'More on the Formation of Nitric Oxide in
a Diesel Engine'*, IMechE Conference on Com-
bustion in Engines, Cranfield, July 1975.
18. Hiroyasu, H
Kadota, T *'Models for Combustion and Formation of
Nitric Oxide and Soot in Direct Injection
Diesel Engines'*, SAE Trans. Vol. 85 (paper
No. 760129), 1979.
19. Kau, C J
Tyson, T J
Heap, M P *'Study of Oxides of Nitrogen and Carbon
Formation in Diesel Engines - Final Report'*,
EPA-460/3-76-008-a, March 1976.
- ... 20. Meguerdichian, M
Watson, N *'Prediction of Mixture Formation and Heat
Release in Diesel Engines'*, SAE Trans.
Vol. 87 (paper No. 780225), 1978.
21. Austen, A E W
Lyn, W T *'Relation Between Fuel Injection and Heat
Release in a Direct-Injection Engine and
the Nature of the Combustion Processes'*,
Proc. IMechE, Automobile Division, Vol. 3,
1960-61.
22. McAulay, K J
Wu, T
Chen, S K
Borman, G L
Myers, P S
Uyehara, O A *'Development and Evaluation of the Simula-
tion of the Compression-Ignition Engine'*,
SAE Trans. Vol. 74 (paper No. 650451), 1966
23. Schweitzer, P H *'Oil Sprays'*, Auto. Engrs, 1938.

24. Khan, I M
Greeves, G
Wang, C H T
'Factors Affecting Smoke and Gaseous Emissions from Direct Injection Engines and a Method of Calculation', SAE Trans. Vol. 82 (paper No. 730169), 1973.
25. Wilson, R P (Jr)
Waldeman, C H
Muzio, L J
'Foundation for Modelling NO_x and Smoke Formation in Diesel Flames', Final Report for Phase 1, EPA-460/s-74-002-a, January 1974.
26. Blumberg, P N
Lavoie, G A
Tabaczynski, R J
'Phenomenological Models for Reciprocating Internal Combustion Engines', Progress in Energy and Combustion Science, Vol. 5, Pergamon Press, 1979.
27. Chiu, W S
Shahed, S M
Lyn, W T
'A Transient Spray Mixing for Diesel Combustion', SAE Trans. Vol. 85 (paper No. 760128), 1976.
28. Oz, I H
'Calculation of Spray Penetration in Diesel Engines', SAE Trans. Vol. 78 (paper No. 690254), 1969.
29. Hiroyasu, H
Kadota, T
Arai, M
'Supplementary Comments: Fuel Spray Characterisation in Diesel Engines', Combustion Modelling in Reciprocating Engines (Ed. Mattavi, J N and Amann, A), Plenum Press, 1980.
30. Woschni, G
'A Universally Applicable Equation for Instantaneous Heat Transfer Coefficient in the Internal Combustion Engine', SAE Trans. Vol. 76, (paper No. 670931), 1967.
31. Lee, K B
Thring, M W
Beer, J M
'On the Rate of Combustion of Soot in a Laminar Soot Flame', Combustion and Flame Vol. 6, 1962.

32. Patrick, M A *'Experimental Investigation of the Mixing and Penetration of a Round Turbulent Jet Injected Perpendicularly into a Transverse Stream'*, Transactions Institution of Chemical Engineers, Vol. 45, 1967.
33. Dent, J C *'A Basis for the Comparison of Various Experimental Methods for Studying Spray Penetration'*, SAE Trans. Vol. 80 (paper No. 710571), 1971.
34. Kadota, T
Hiroyasu, H
Oya, H *'Spontaneous Ignition Delay of a Fuel Drop-let in High Pressure and High Temperature Gaseous Environments'*, Bulletin of the JSME, Vol. 19, 1976.
35. Tsao, K C
Myers, P S
Uyehara, O A *'Gas Temperature During Compression in Motored and Fired Diesel Engines'*, SAE Trans. Vol. 70, 1962.
36. Lyn, W T
Valdmanis, E *'The Effects of Physical Factors on Ignition Delay'*, Proc. IMechE, Vol. 181, 1966.
37. Annand, W J D *'Heat Transfer in the Cylinders of Reciprocating Internal Combustion Engines'*, Proc. IMechE, Vol. 177, 1963.
38. Glauert, M B *'The Wall Jet'*, J. Fluid Mech, Vol. 1, 1956.
39. Whitehouse, N D
Abughres, S M *'Calculation of Fuel-Air Mixing in a Diesel-Engine with Swirl for the Purpose of Heat Release Prediction'*, IMechE Conference on Combustion in Engines, Cranfield, July 1975.

40. Lichtarowicz, A
Duggins, R K
Markland, E
'Discharge Coefficients for Incompressible Non-Cavitating Flow Through Long Orifices', J. Mechanical Engineering Science, Vol. 7, 1965.
41. Hay, N
Jones, P L
'Comparison of the Various Correlation for Spray Penetration', SAE Paper No. 720776, 1972.
42. Ricou, F P
Spalding, D B
'Measurements of Entrainment by Axisymmetrical Turbulent Jets', J. Fluid Mechanics, Vol. 11, 1961.
43. Forstall, W
Shapiro, A H
'Momentum and Mass Transfer in Coaxial Gas Jets', J. Applied Mechanics, Vol. 17, 1950.
44. Rife, J
Heywood, J B
'Photographic and Performance Studies of Diesel Combustion with a Rapid Compression Machine', SAE Trans. Vol. 74 (paper No. 740918), 1974.
45. Morris, C J
'The Modelling of Fuel Dispersion and Concentration in Direct Injection Diesel Engines', PhD Thesis, Loughborough University, 1975.
46. Abramovich, G N
'The Theory of Turbulent Jets', The MIT Press, Mass., 1963.
47. Thring, M W
Newby, M P
'Combustion Length of Enclosed Turbulent Jet Flames', Fourth Symposium (International) on Combustion, 1952.
48. Spalding, D B
'Combustion and Mass Transfer', Pergamon Press, Oxford, 1979.

49. Knight, B E *'Communication on the Performance of a Type of Swirl Atomizer'*, Proc. IMechE, Vol. 169, 1955.
50. Simmons, H C *'The Correlation of Dropsizes Distributions in Fuel Nozzle Sprays - Part I: The Drop-Size/Volume Fraction Distribution'*, J. Engineering Power, July 1977.
51. Simmons, H C *'The Correlation of Dropsizes Distributions in Fuel Nozzle Sprays - Part II: The Drop-Size/Number Distribution'*, J. Engineering Power, July 1977.
52. Lee, D W *'The Effect of Nozzle Design and Operating Conditions on the Atomization and Distribution of Fuel Sprays'*, NACA Report 425, 1932.
53. Retel, R *'Contribution a L'etude de L'injection dans Les Moteurs Diesel'*, Publications Scientifiques et Techniques du Ministere de l'air, Paris, 1938.
54. Kamimoto, T
Matsuoka, S *'Prediction of Spray Evaporation in Reciprocating Engines'*, SAE Trans. Vol. 86, (paper No. 770413), 1977.
55. El Wakil, M M
Myers, P S
Uyehara, O A *'Fuel Vaporization and Ignition Lag in Diesel Combustion'*, SAE Trans. Vol. 64, 1956.
56. Ranz, W E
Marshall, W R *'Evaporation from Drops - Part II'*, Chem. Engineering Progress, Vol. 48, 1952.
57. Williams, A *'Combustion of Droplets of Liquid Fuels: A Review'*, Combustion and Flame, Vol. 21, 1973.

58. Spalding, D B *'Some Fundamentals of Combustion'*, Butterworths, London, 1955.
59. Bolt, J A
Saad, M A *'Combustion Rates of Freely Falling Fuel Drops in a Hot Atmosphere'*, Sixth Symposium, (International) on Combustion, 1957.
60. Kays, W M *'Convective Heat and Mass Transfer'*, McGraw Hill Book Company, New York, 1966.
61. Natarajan, R
Brzustowski, T A *'Some New Observations on the Combustion of Hydrocarbon Droplets at Elevated Pressures'*, Combustion Science and Technology, Vol. 2, 1970.
62. Dent, J C
Lakshminarayanan,
P A *'The Study of Transient Fuel Sprays Using Holographic Interferometry'*, Internal Report, Department of Mechanical Engineering, Loughborough University, October 1980.
63. Giralt, F
Chia, C J
Trass, O *'Characterization of the Impingement Region in an Axisymmetric Turbulent Jet'*, Ind. Engg., Chem. (Fundamentals), Vol. 16, 1977.
64. Rajaratnam, N *'Turbulent Jets'*, Elsevier, New York, 1976.
65. Era, Y
Saima, A *'An Investigation of Impinging Jets'*, (Experiments by Air, Hot Air and Carbon-dioxide), Bulletin of the JSME, Vol. 19, 1976.
66. Hertel, H *'Strömungsvorgänge beim Freien Hubstrahler'*, Luft Farttechnik, Vol. 8, 1962.

67. Wolfer, H H *'Ignition Lag in Diesel Engines'*, Translation Royal Aircraft Establishment, No. 358, 1950.
68. Sitkei, G *'Über den dieselmotorischen Zündverzögerung'*, M.T.Z. Jahrg, Vol. 6, 1963.
69. Stringer, F W
 Clarke, A E
 Clarke, J S *'The Spontaneous Ignition of Hydrocarbon Fuels in a Flowing System'*, Symposium on Diesel Engine Combustion, IMechE, London, April 1970.
70. Henein, N A *'Analysis of Pollutant Formation and Control and Fuel Economy in Diesel Engines'*, Pollutant Formation and Destruction in Flames, Progress in Energy and Combustion Science, (Ed Chigier, N A), Vol 1, Pergamon Press, 1976.
71. Hardenberg, H O
 Hase, F W *'An Empirical Formula for Computing the Pressure Rise Delay of a Fuel from its Cetane Number and from the Relevant Parameters of Direct-Injection Diesel Engines'*, SAE Trans. Vol 89, (paper No 790493), 1979.
72. Halstead, M P
 Pye, D B
 Quinn, C P *'Laminar Burning Velocities and Weak Flammability Limits Under Engine-Like Conditions'*, Combustion and Flame, Vol 29, 1974.
73. Dent, J C *'Turbulent Mixing Rate - Its Effect on Smoke and Hydrocarbon Emissions from Diesel Engines'*, Diesel Combustion and Emissions, SAE Publication P-86, (paper No 800092), 1980.
74. Spiers, H M *'Technical Data on Fuel'*, The British National Committee, World Power Conference, London, 1961.

75. Newhall, H K
Starkman, E S *'Thermodynamic Properties of Octane and Air for Engine Performance Calculations', Digital Calculations of Engine Cycles, Progress in Technology, SAE Vol 7, 1964.*
76. *'Selected Values of Properties of Hydrocarbons and Related Compounds', American Petroleum Research Project No 44, Thermodynamic Research Centre, Texas, 1981.*
77. Canada, G S
Faeth, G M *'Fuel Droplet Burning Rates at High Pressures', Fourteenth Symposium (International) on Combustion, 1973.*
78. West, C J (Ed) *'International Critical Tables - National Research Council of USA', McGraw Hill Book Co, New York, 1933.*
79. Watson, N
Janota, M S *'Development and Application of a Comprehensive Turbocharged Diesel Engine Model', Symposium of the Universities' I.C. Engines Group and Sponsored by the Science Research Council, Kings' College, London, 17-18 April 1980.*
80. Broome, D
Khan, I M *'The Mechanisms of Soot Release from Combustion of Hydrocarbon Fuels with Particular Reference to the Diesel Engine', IMechE Conference on Air Pollution Control in Transport Engines, London, November 1971.*
81. Lahaye, J
Prado, G *'Mechanisms of Carbon Black Formation', Chemistry and Physics of Carbon, Ed. by P L Walker, Jr, and P A Thrower, Marcel Dekker, Inc. 1978.*

82. Wagner, H Gg *'Soot Formation in Combustion'*, Seventeenth Symposium (International) on Combustion, 1979.
83. Plee, S L
Ahmad, T
Myers, J P
Siegla, D C *'Effects of Flame Temperature and Air-Fuel Mixing on Emission of Particulate Carbon from a Divided-Chamber Diesel Engine'*, General Motors Research Symposium, on Particulate Carbon Formation during Combustion, Warren, Michigan, October 1980.
84. Amann, C A
Stivender, D L
Plee, S L
MacDonald, J S *'Some Rudiments of Diesel Particulate Emissions'*, SAE Paper No 800251, 1980.
85. Ahmad, T
Plee, S L
Myers, J P *'Computation of Nitric Oxide and Soot Emissions from Steady Turbulent Spray and Jet Flames'*, General Motors Research Department, Report No. EN-231, November 1981.
86. Homann, K H *'Carbon Formation in Premixed Flames'*, Combustion and Flame, Vol. 11, 1967.
87. Tesner, P A
Snegiriova, T D
Knorre, V G *'Kinetics of Dispersed Carbon Formation'*, Combustion and Flame, Vol. 17, 1971.
88. Dyer, T M
Flower, W L *'A Phenomenological Description of Particulate Formation During Constant Volume Combustion'*, General Motors Symposium on Particulate Carbon Formation During Combustion, Warren, Michigan, October 1980.
89. McArragher, J S
Tan, K J *'Soot Formation at High Pressure: A Literature Review'*, Combustion Science and Technology, Vol. 5, 1972.

90. Macfarlane, J J
Holderness, F H
'Laboratory Studies of Carbon Formation in Fuel-Rich Flames at High Pressures,' Symposium on Diesel Engine Combustion Proceedings IMechE, Vol. 184, 1969-70.
91. Crookes, R J
Daie, S J
Janota, M S
Nazha, M A A
Sodha, M
'Soot and Gaseous Pollutant Formation in A Burning Fuel Spray in Relation to Pressure and Air/Fuel Ratio,' Internal Report, Queen Mary College, University of London, 1975.
92. Khan, I M
Wang, C H T
Langridge, B E
'Coagulation and Combustion of Soot Particles in Diesel Engines,' Combustion and Flame, Vol. 17, 1971.
93. Tesner, P A
Tsygankova, E I
Guilazetdinov, L P
Zuyev, V P
Loshakova, G V
'The Formation of Soot from Aromatic Hydrocarbons in Diffusion Flames of Hydrocarbon-Hydrogen Mixtures,' Combustion and Flame, Vol. 17, 1971.
94. Gollahalli, R S
Brzustowski, T A
'The Effect of Pressure on the Flame Structure in the Wake of a Burning Hydrocarbon Droplet,' Fifteenth Symposium (International) on Combustion, 1975.
95. Magnussen, B F
Hjertager, B H
'On Prediction of Soot Formation and Combustion in Turbulent Flames with Special Reference to a Free-Jet C_2H_2 Diffusion Flame,' Deuxieme Symposium Europeen sur la Combustion, Section Francaise du 'Combustion Institute', 1975.
96. Magnussen, B F
Hjertager, B H
'On Mathematical Modelling of Turbulent Combustion With Special Emphasis on Soot Formation and Combustion,' Sixteenth Symposium (International) on Combustion, 1977.

97. Tesner, P A
Tsibulevsky, A M *'Kinetics of Dispersed Carbon Gasification in Diffusion Flames of Hydrocarbons'*,
Combustion and Flame, Vol. 11, 1967.
98. Park, C
Appleton, J P *'Shock Tube Measurements of Soot Oxidation Rates'*, Combustion and Flame, Vol. 20,
1973.
99. Nagle, J
Stickland-Constable,
R F *'Oxidation of Carbon Between 1000-2000°C'*,
Proceedings of the Fifth Carbon Conference,
Vol. 1, 1962.
100. Fenimore, C P
Jones, G W *'Oxidation of Soot by Hydroxyl Radicals'*.
The Journal of Physical Chemistry, Vol. 71,
1967.
101. Page, F M
Ates, F *'The Oxidation of Soot in Fuel Rich Flames'*.
Symposium on Evaporation-Combustion of Fuel
Droplets, American Chemical Society, San
Francisco, August-September 1976.
102. Radcliff, S W
Appleton, J P *'Soot Oxidation Rates in Gas Turbine Engines'*,
Combustion Science and Technology, Vol. 4,
1971.
103. Magnussen, B F *'The Rate of Combustion of Soot in Turbulent Flames'*, Thirteenth Symposium (International) on Combustion, 1971.
104. Becker, H A
Yamazaki, S *'Soot Concentration Field of Turbulent Propane/Air Diffusion Flames'*, Sixteenth Symposium (International) on Combustion,
1977.

105. Prado, G P
Lee, M L
Hites, R A
Hoult, D P
Howard, J B
'Soot and Hydrocarbon Formation in a Turbulent Diffusion Flame', Sixteenth Symposium (International) on Combustion, 1977.
106. Magnussen, B F
Hjertager, B H
Olson, J G
Bhaduri, D
'Effects of Turbulent Structure and Local Concentrations on Soot Formation and Combustion in C_2H_2 Diffusion Flames', Seventeenth Symposium (International) on Combustion, 1979.
107. Magnussen, B F
'Modelling of Reaction Processes in Turbulent Flames with Special Emphasis on Soot Formation and Combustion', General Motors Symposium on Particulate Carbon Formation during Combustion, Warren, Michigan, October, 1980.
108. Vuk, C T
Jones, M A
Johnson, J H
'The Measurement and Analysis of the Physical Character of Diesel Particulate Emissions', SAE Trans. Vol. 85, (paper No. 760131), 1976.
109. Spalding, D B
'Conditions for the Stable Burning of Carbon in an Air Stream', Journal of the Institute of Fuel, 1953.
110. Dodd, A E
Holubecki, Z
'The Measurement of Diesel Exhaust Smoke'. The Motor Industry Research Association, 1965.
111. Fitzgeorge, D
Allison, J L
'Air Swirl in a Road-Vehicle Diesel Engine', Proc. Auto. Div. IMechE, Vol. 25, 1962-63.

112. Ohigashi, S
Hamamoto, Y
Tanabe, S *'Swirl - Its Measurement and Effect on combustion in a Diesel Engine'*, IMechE Conference on Air Pollution Control in Transport Engines, London, November 1971.
113. Dent, J C
Derham, J A *'Air Motion in a Four Stroke Direct Injection Diesel Engine'*, Proc. IMechE, Vol. 188, 1974.
114. Borgnakke, C
Davis, G C
Tabaczynski, R J *'Predictions of In-Cylinder Swirl Velocity and Turbulence Intensity for an Open Chamber Cup in Piston Engine'*, SAE Paper No. 810224, 1981.
115. Sinnamon, J F
Lancaster, D R
Stiener, J C *'An Experimental and Analytical Study of Engine Fuel Spray Trajectories'*, SAE Trans. Vol. 89, 1980, (Paper No. 800135).
116. Stock, D *'Untersuchungen der Gemischbildungs Zundund Verbrennungsvorgange eines direkteinspritzenden Diesel Motors'*, Doktor-Ingenieur Dissertation: Fakultat fur Maschinenwesen der Technischen Universitat, Verlin, July, 1970.
117. Morris, C J
Dent, J C *'The Simulation of Air Fuel Mixing in High Swirl Open Chamber Diesel Engines'*, Proc. IMechE, Vol. 190, 1976.
118. Adler, D
Baron, A *'Prediction of a Three-Dimensional Circular Turbulent Jet in Crossflow'*, AIAA Journal, Vol. 17, 1979.
119. Hoult, D
Weil, J C *'Turbulent Plume in a Laminar Cross Flow'*, Atmospheric Environment Vol. 6, Pergamon Press, 1972.

120. Kamotani, Y
Greber, I *'Experiments on a Turbulent Jet in a Cross Flow'*, AIAA Journal, Vol. 10, 1972.
121. Stoy, R L
Ben-haim, Y *'Turbulent Jets in a Confined Crossflow'*, Journal of Fluids Engineering, Trans. of the ASME, 1973.
122. Skifstad, J G *'Aerodynamics of Jets Pertinent to VTOL Aircraft'*, Journal of Aircraft, Vol. 7, 1970.
123. Wooler, P T
Burghart, G H
Gallagher, J T *'Pressure Distribution on a Rectangular Wing with a Jet Exhausting Normally into an Airstream'*, Journal of Aircraft, Vol. 4, 1967.
124. Dent, J C Unpublished work.
125. Brandl, F
Reverencic, I
Cartellieri, W
Dent, J C *'Turbulent Air Flow in the Combustion Bowl of a D.I. Diesel Engine and Its Effect on Engine Performance'*, SAE Trans. Vol. 88, (paper No. 790040), 1979.
126. Kamimoto, T
Aoyagi, Y
Matsui, Y
Matsuoka, S *'The Effects of Some Engine Variables on Measured Rates of Air Entrainment and Heat Release in a D.I. Diesel Engine'*, Diesel Combustion and Emissions, SAE Special Publication, P-86, (paper No. 800253), 1980.
127. Flynn, P
Mizusawa, M
Uyehara, O A
Myers, P S *'An Experimental Determination of the Instantaneous Potential Radiant Heat Transfer within an Operating Diesel Engine'*, SAE Trans. Vol. 81 (paper No. 720022), 1972.
128. Oguri, T
Inaba, S *'Radiant Heat Transfer in Diesel Engines'*, SAE Paper No. 720023, 1972.

129. Yu, R C
Shahed, S M
'Effects of Injection Timing and Exhaust Gas Recirculation on Emissions from a D.I. Diesel Engine', SAE Paper No. 811234, 1981.
130. Hiroyasu, H
Arai, M
Nakanishi, K
'Soot Formation and Oxidation in Diesel Engines', SAE Trans. Vol. 89, (paper No. 800252), 1980.

APPENDIX A

DETERMINATION OF CENTRELINE CONCENTRATION AND
VELOCITY AT ANY AXIAL POSITION

Centreline Concentration (f_m)

The local concentration at Y_p in equation (2.9) can be expressed as:

$$f = \frac{m_{fY_p}}{m_{aY_p} + m_{fY_p}} \quad (A.1)$$

where m_{fY_p} and m_{aY_p} are the masses of fuel and air at Y_p respectively.

The total mass of air entrained into the spray in the time the jet penetration is S is m_{aE} . This can be evaluated from equation (2.6) and expressed as a function of f over the whole jet radius r_j at S by the following relationship:

$$m_{aE} = 2 \int_0^{r_j} \frac{m_{fY_p} (1 - f)}{f} \quad (A.2)$$

On separating the terms of the right hand side, the above equation becomes:

$$m_{aE} = 2 \int_0^{r_j} \frac{m_{fY_p}}{f} - 2 \int_0^{r_j} m_{fY_p} \quad (A.3)$$

but

$$2 \sum_0^{r_j} m_f Y_p = m_f$$

and

$$f = f_m (1 - Y_p^{3/2})$$

where m_f is the total fuel mass injected up to that instant, therefore equation (A.3) becomes:

$$m_{aE} = 2 \sum_0^{r_j} \frac{m_f Y_p}{(1 - Y_p^{3/2}) f_m} - m_f \quad (\text{A.4})$$

Rearrangement of equation (A.4) yields:

$$f_m = \frac{2 \sum_0^{r_j} \frac{m_f Y_p}{(1 - Y_p^{3/2})}}{m_{aE} + m_f} \quad (\text{A.5})$$

Centreline Velocity (U_m)

Considering an axisymmetric two phase jet flow of fuel droplets with negligible relative velocity in the entrained air, the conservation equations at any section of the jet are written as:

Mass conservation for nozzle fluid

$$\dot{m}_f = \int_0^{A_{\text{jet}}} \rho_f U \, dA \quad (\text{A.6})$$

Momentum conservation for jet

$$G = \int_0^{A_{\text{jet}}} \rho U^2 dA \quad (\text{A.7})$$

where \dot{m}_f is the fuel mass flow rate and G is the momentum flux.

The initial momentum of the liquid jet is

$$G_0 = \dot{m}_{f_0} U_{\text{jet}} \quad (\text{A.8})$$

where \dot{m}_{f_0} is the mass flow rate and U_{jet} is the jet velocity at the nozzle respectively.

The total cross sectional area of the jet of radius r_{jet} at any section is A_{jet} . For any other radial position Y , the cross sectional area will be

$$A = \pi Y^2 \quad (\text{A.9})$$

Differentiating equation (A.9), yields

$$dA = 2 \pi Y dY \quad (\text{A.10})$$

In terms of normalised radial position $Y_p (= \frac{Y}{r_{\text{jet}}})$, equation (A.10) can be written as:

$$dA = 2 A_{\text{jet}} Y_p dY_p \quad (\text{A.11})$$

The mass and momentum equations (A.6) and (A.7) are written in normalised form by normalising concentration and velocity with corresponding centreline values as

$$\dot{m}_f = \rho_a A_{jet} U_m f_m P \quad (A.12)$$

and

$$G = \rho_a A_{jet} U_m^2 R \quad (A.13)$$

where P and R are integral constants, expressed as

$$P = 2 \int_0^1 \left(\frac{Y_p}{\beta}\right) \left(\frac{f}{f_m}\right) \left(\frac{U}{U_m}\right) dY_p$$

$$R = 2 \int_0^1 \left(\frac{Y_p}{\beta}\right) \left(\frac{U}{U_m}\right)^2 dY_p$$

Equating momentum to mass ratio at any instant to the value of the initial momentum to mass ratio, we obtain from

$$\frac{G}{\dot{m}_f} = \frac{G_0}{\dot{m}_{f_0}}, \quad (A.14)$$

and equation for centreline velocity in terms of centreline concentration and integral constants P and R

$$\bar{U}_m = \frac{U_m}{U_{jet}} = \frac{P}{R} \cdot f_m \quad (A.15)$$

where \bar{U}_m refers to the normalised centreline velocity.

Density Function (β)

For a mixture of air and fuel in liquid and vapour form, the total volume can be written as

$$V_t = V_{f\ell} + V_v + V_a \quad (\text{A.16})$$

where $f\ell$, v , a and t are suffixes for liquid fuel, vapour, air and total mixture respectively.

In terms of masses and density of these constituents, we can write equation (A.16) as

$$\frac{m_t}{\rho} = \frac{m_f}{\rho_f} + \frac{m_v}{\rho_v} + \frac{m_a}{\rho_a} \quad (\text{A.17})$$

Simplification of equation (A.17) for local density (ρ) of the mixture of liquid fuel, vapour and air components yields:

$$\frac{\rho_a}{\rho} = \frac{m_{f\ell}}{m_t} \frac{\rho_a}{\rho_{f\ell}} + \frac{m_v}{m_t} \frac{\rho_a}{\rho_g} + \frac{m_a}{m_t} \quad (\text{A.18})$$

But

$$\frac{m_f}{m_t} + \frac{m_v}{m_t} + \frac{m_a}{m_t} = 1 \quad (\text{A.19})$$

Therefore, substitution of (A.19) in (A.18) and further simplification gives:

$$\rho = \frac{\rho_a}{\left[1 - \left(\frac{m_{f\ell}}{m_t}\right)\left(1 - \frac{\rho_a}{\rho_{f\ell}}\right) + \frac{m_v}{m_t}\left(1 - \frac{\rho_a}{\rho_v}\right)\right]} \quad (\text{A.20})$$

The denominator in equation (A.20) is represented as:

$$\beta = \left[1 - \left(\frac{m_{f\ell}}{m_t}\right)\left(1 - \frac{\rho_a}{\rho_{f\ell}}\right) + \frac{m_v}{m_t}\left(1 - \frac{\rho_a}{\rho_v}\right)\right] \quad (\text{A.21})$$

where $\rho_{f\ell}$ is defined as the liquid fuel density and ρ_v is the fuel vapour density.

When $\frac{\rho_a}{\rho_v} \ll 1$ or $\frac{m_v}{m_t} \ll 1$ then (A.21) reduces to the form

$$\alpha = \left[1 - \frac{m_{f\ell}}{m_t}\left(1 - \frac{\rho_a}{\rho_{f\ell}}\right)\right] \quad (\text{A.22})$$

APPENDIX B
DROPLET-SIZE DISTRIBUTION

The radial droplet-size distribution is applied to the injected fuel volume (V_{fi}) through equation (2.22).

For any radial position change from Y_p to $Y_p + \Delta Y_p$, the normalised droplet diameter is considered to change from D_p to $D_p - \Delta D_p$.

The variation in the liquid fuel volume with respect to radial position Y_p in the element of volume ΔV_x and thickness Δx is expressed as:

$$\frac{d(V_{fi} Y_p)}{dY_p} = 2\pi r_j^2 Y_p \frac{\Delta x \rho f}{\rho_f} \quad (B.1)$$

where r_j is the jet radius, f is the local fuel mass concentration, ρ_f is the liquid fuel density and ρ is the local density expressed as:

$$\rho = \frac{\rho_a}{\alpha} \quad (B.2)$$

where

$$\alpha = \left[1 - \left(\frac{1 - \rho_a}{\rho_f} \right) f \right]$$

At $S = 0$, $f_m = 1$, hence from equation (2.9)

$$f = (1 - Y_p^{3/2}) \quad (B.3)$$

The volume fraction of injected liquid fuel is written as:

$$\frac{(dV_{fi} Y_p)}{V_{fi}} = \frac{2\pi r_j^2 Y_p \Delta x \rho_f}{[\int_0^1 2\pi r_j^2 Y_p \Delta x \rho_f dY_p]} \quad (B.4)$$

Using equation (B.2), equation (B.4) can be expressed as:

$$\frac{(dV_{fi} Y_p)}{V_{fi}} = \frac{(Y_p f/\alpha)}{[\int_0^1 (f/\alpha) Y_p dY_p]} \quad (B.5)$$

In evaluating the value of α , it is assumed that the effect of instantaneous air density variation on equation (B.5) during the injection period is small, because $\rho_a/\rho_f \ll 1$.

Since it is assumed that the total mass of injected fuel in various droplet sizes, ranging between the normalised limits of 0.082 and 3.0 are conserved over the total jet width.

Rearrangement and integration of equation (2.22) yields:

$$(1/V_{fi}) \int_0^{Y_p} (dV_{fi} Y_p / dY_p) dY_p = \int_{3.0}^{D_p} (dV_{cf} / dD_p) dD_p \quad (B.6)$$

In equation (B.4), the right hand side represents the cumulative droplet size/volume fraction given in equation (2.21). Therefore, the numerical solution of equation (B.6) gives discrete values of droplet diameter D_p for various radial positions Y_p ($0 < Y_p < 1$)

Selected discrete values are used as input data to the model. These values are shown in Figure 2.6 with a schematic of the radial distribution at $S = 0$.

APPENDIX C
EVALUATION OF MEAN THERMODYNAMIC
AND PHYSICAL PROPERTIES

The calculation of thermodynamic and transport properties of the working fluids in the engine cylinder is essential for the energy balance and the mass transfer analysis.

The local values of such properties of the component fluids and their mixtures are evaluated using the relationships and criteria enumerated below. The quantities evaluated include:

- i) internal energy,
- ii) mean specific heat,
- iii) density
- iv) enthalpy of vaporization,
- v) conductivity,
- vi) viscosity.

Internal Energy

The internal energy is expressed as:

$$u = C_v dT \quad (C.1)$$

where constant volume mean specific heat C_v for any fluid is computed based on the constant pressure specific heat C_p and the gas constant (R) values using relationships

$$C_v = C_p - R, \quad \text{for ideal gaseous substances}$$

and $C_v = C_p,$ for liquids.

Mean Specific Heat

The constant pressure specific heat for hydrocarbon fuel is computed from relations available in reference (74) as:

- i) mean specific heat of hydrocarbon fuel (liquid state)

$$C_{p_f} = \frac{(38692.0 + 53.585 T)}{\sqrt{\rho_f}} \quad (C.2)$$

- ii) mean specific heat of hydrocarbon fuel (vapour state)

$$C_{p_v} = (0.296285 + 0.000586T) (4000 - \rho_f) \quad (C.3)$$

where ρ_f is the fuel density at 293K and T is the local temperature in K.

The mean specific heat of air is represented in a polynomial form (75) as

$$C_{p_a} = \sum_{i=0}^5 Z_i T^i \quad (C.4)$$

Density

The density of pure hydrocarbon is evaluated in terms of reduced temperature and pressure, following the procedure of reference (76). According to this method, the density at any pressure and temperature is obtained from constants expressed as:

$$C = \sum_{i=0}^2 A_i T_r^i \quad (C.5)$$

where T_r is the reduced temperature ($= \frac{T}{T_c}$), T_c is the critical temperature and A_i are the coefficients given in terms of reduced pressure ($= \frac{P}{P_c}$) by the expression:

$$A_i = \sum_{i=1}^4 B_{0i} P_r^i \quad (C.6)$$

where B_{0i} are the coefficients, given in Table C.2. To reduce computation time, with optimum accuracy, only a few coefficients are used.

Thus, the density ρ_2 of any substance at a given pressure p , and temperature T , will be

$$\rho_2 = \rho_1 \frac{C_2}{C_1} \quad (C.7)$$

where C_2 is the constant determined at the given point T , and ρ_1 and C_1 are the density and the corresponding constant at a reference condition.

The pressure of 1 bar and temperature of 293K are chosen as reference for a liquid fuel while the critical point is the reference for the vapour phase.

Enthalpy of Vaporization

This is needed for determining the transfer number. Under high pressure, high temperature conditions the enthalpy of vaporization is a function of droplet temperature T_s . The enthalpy of vaporization for petroleum hydrocarbon is given by:

$$h_{fg_s} = 10^6 \frac{(354.1 - 0.3768 T)}{\rho_f} \quad (C.8)$$

where ρ_f is the fuel density at 293K.

This relationship is taken from reference (74).

Conductivity

Faeth and Olson (77) used the relationship for conductivity of fuel vapour as

$$k_{v_T} = k_v \frac{T}{T_b} \quad (C.9)$$

where k_v is the conductivity at normal boiling point T_b and T is the local temperature ($^{\circ}K$).

The conductivity of air (78) as a function of temperature T is given by

$$k_{a_T} = k_{T_0} \left(\frac{T_0 + C}{T + C} \right) \left(\frac{T}{T_0} \right)^{3/2} \quad (C.10)$$

where k_{T_0} is the value of conductivity of air at 1 atm and reference temperature T_0 (= 273K) and C is a constant having a value of 125.

Viscosity

Sherwood and Reid (76) express the viscosity of gaseous substances as a function of temperature T by the relationship:

$$\mu_T = \mu_{T_0} \left(\frac{T_0 + C_1}{T + C_1} \right) \left(\frac{T}{T_0} \right)^{3/2} \quad (C.11)$$

where, μ_{T_0} is the reference value of the viscosity at temperature T_0 and C_1 is the constant. The values of μ_{T_0} , T_0 and C_1 are chosen for calculation of fuel vapour and air viscosities and is explained in Table C3.

During evaporation and combustion calculations, the mean values of the physical properties of the system are evaluated following recommendations of reference (61). They suggest that the mean values depend on the droplet surface temperature T_s and the local temperature T calculated using equations (2.17) - (2.19).

The summary of the definition of the mean values of ρ , ν , C_p and k , used in the model, are shown in Table C4.

TABLE C.1

Values of coefficients of specific heat polynomials

	i = 0	1	2	3	4	5
Z_i	0.8857742E3	0.3731415E0	-.145183E-03	0.3133865E-07	-0.3534357E-11	0.1628437E-15

TABLE C.2

Values of coefficients of density polynomials

	i = 0	1	2
A_1 B_{0i}	1.6368	-0.04615	2.11380E-03
A_2 B_{0i}	-1.9693	0.21874	-8.0028E-03
A_3 B_{0i}	2.4638	-0.36461	12.8763E-03
A_4 B_{0i}	-1.5841	0.25136	-11.3805E-03

TABLE C.3
Constants for Viscosity

Substance	μ_{T_0}	T_0	C_1
Fuel vapour	Viscosity at value of critical temperature	Critical temperature	1.47 times the normal boiling point
Air	Value of viscosity at 1 atm & temperature T_0	273K	120

TABLE C.4
Definition of mean properties

Property	Evaporation	Combustion
ν and ρ	Value of surrounding gas at arithmetic mean temperature $\frac{1}{2}(T_s + T)$	Value of surrounding gas at weighted mean temperature $(0.25 T_s + 0.75 T)$
C_p and k	Mean of fuel vapour value at T_s and surrounding gas value at T	Mean of fuel vapour value at T_s and surrounding gas value at T

APPENDIX D

CALCULATION OF SHALLOW PISTON GEOMETRY

The total surface area (A_c) of the engine cylinder is computed from the overall engine dimensions, and the shape and instantaneous position of the piston. The procedure for a typical geometry shape is as follows:

For a shallow piston, the volume and area of the piston bowl is determined by splitting the half geometry of the piston into four simple geometric shapes, indicated as 1, 2, 3 and 4 in Figure D.1. The calculations for the individual sections are shown in Table D.1 with reference to the symbols used in the Figure D.1.

The surface area of the bowl (A_b) is written as

$$A_b = 2 \pi \bar{X} \ell_2 \ell_4 \quad (D.1)$$

where \bar{X} is the distance of the combined centroid from cylinder axis measured parallel to cylinder head and ℓ_2 and ℓ_4 are the lengths of the sectors in regions 2 and 4. These are given as:

$$\bar{X} = \frac{1}{A_{tot}} \sum_{i=1}^4 A_i X_i \quad (D.2)$$

but

$$A_{tot} = \sum_{i=1}^4 A_i$$

where A_i and X_i are the individual area and the x-coordinate of the four geometric regions,

$$\text{and} \quad l_2 = \frac{X_B}{\cos \alpha_2} \quad (\text{D.3})$$

$$l_4 = R_B \alpha_B \quad (\text{D.4})$$

The volume of the bowl is

$$V_b = 2 \pi \bar{X} A_{\text{tot}} \quad (\text{D.5})$$

The total cylinder area comprises of the four surfaces, the cylinder head (A_h), the side walls (A_w), the flat portion of the piston crown (A_p), and the piston bowl surface (A_b).

TABLE D.1

Geometry calculations for shallow piston

Section	Centroid		Area	Volume
	X	Y		
1	$\frac{X_B}{2}$	$\frac{h_1}{2}$	$h_1 \cdot X_B$	$\pi h_1 X_B^2$
2	$\frac{2}{3} X_B$	$h_1 + \frac{1}{3} X_B \tan \alpha_2$	$\frac{1}{2} X_B^2 \tan \alpha_2$	$\frac{2}{3} \pi X_B^3 \tan \alpha_2$
3 and 4 combined	$X_B + \frac{2}{5}(X_C - X_B)$	$\frac{3}{8}(h_1 + X_B \tan \alpha_2)$	$\frac{1}{2}(h_1 + X_B \tan \alpha_2)$ $(X_C - X_B)$ $+ \frac{R^2}{2}(\alpha_p - \sin \alpha_p)$ where: $\alpha_p = 2 \cos^{-1} \left(\frac{H}{R} \right)$ $H = \sqrt{R^2 - C^2}$ $C = \frac{1}{2} \sqrt{(h_1 + X_B \tan \alpha_2)^2 + (X_C + X_B)^2}$	-

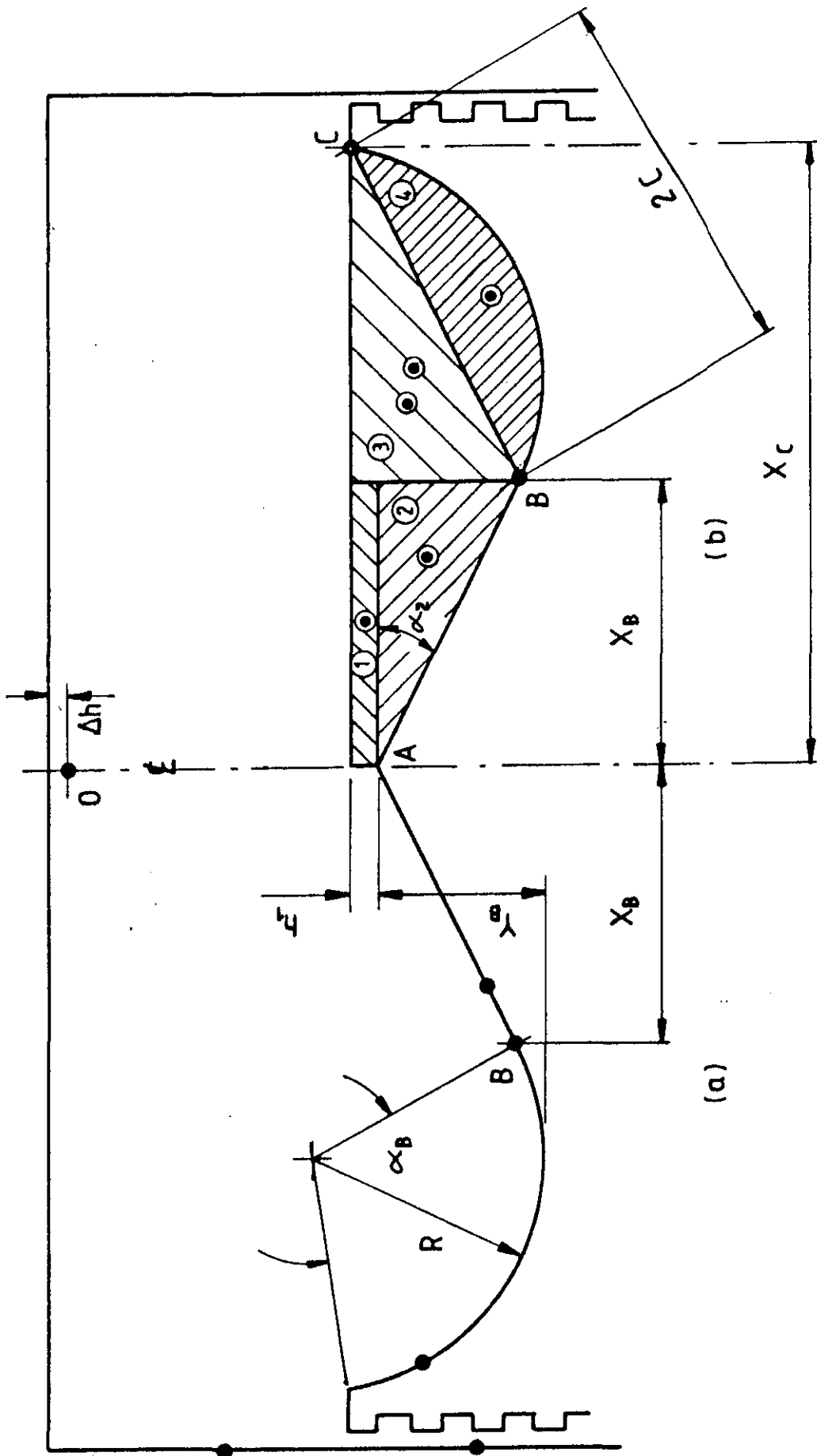


FIG. D1 Shallow Piston Geometry

APPENDIX E
MASS AND ENERGY BALANCE FORMULATION

Mass Balance

At any instant i , corresponding to crank position θ , the cylinder contents will constitute the following mass elements (see Figure 2.17).

- i) liquid fuel mass (m_l, m_{liq})
- ii) entrained air mass (m_a, m_{air})
- iii) fuel vapour mass (m_v, m_{vap})

along with the following additional mass elements included during combustion

- iv) burnt fuel mass ($m_{vb}, m_{vap,b}$)
- v) mass of air (i.e. oxygen) consumed during burning ($m_{ac}, m_{air,c}$)

where subscripts l, a, v, vb, ac are used for these mass elements distributed in each sector j and subscripts $liq, air, vap, vapb, airc$ represent the integrated values of the respective masses over the whole jet.

In a specific interval of time (say 1° CA), each mass element is altered by an amount dm .

If dm_{liq} is the total mass of fuel injected in the specified interval and dm_{air} is the corresponding mass of air entrained in the jet, then the mass of surrounding air, $m_{air,sr}$, will be reduced by an amount

$$dm_{air,sr} = -dm_{air} \quad (E.1)$$

The fuel mass is distributed in sectors as droplets sizes Δdp_j such that the mass of liquid fuel in droplets is

$$dm_{l_j} = \rho_f \left(\frac{\partial V_{c_f}}{\partial dp_j} \Delta dp_j \right) * dV_f \quad (E.2)$$

where V_{c_f} is the cumulative droplet-size/volume fraction distribution function and dV_{f_i} is the volume of fuel injected. Thus, the cumulative mass of liquid in arrays of droplets size will be

$$(m_{l_j})_{i+1} = (m_{l_j})_i + (dm_{l_j}) \quad (E.3)$$

For a few crank degrees after injection the droplet evaporation is considered to compute the mass of vapour formed as

$$dm_{v_j} = \dot{m}'' N_{p_j} A_{p_j} \Delta t \quad (E.4)$$

where N_{p_j} is the total number of droplets, A_{p_j} is the surface area of a droplet of specified size in that sector, Δt is the time interval and \dot{m}'' is the mass transfer rate, i.e.

$$\dot{m}'' = \frac{k \text{Nu}}{d_{p_j} C_p} \ln(1 + B) \quad (E.5)$$

where Nu is the Nusselt number and B is the transfer number. k and C_p are the thermal conductivity and specific heat respectively.

As soon as the ignition delay period is over, the burning of fuel vapour is considered for sectors within specified limits of inflammability ($\phi_1 < \phi_v < \phi_2$). The local equivalence ratio, ϕ_v , based on fuel vapour-air ratio is compared with the limits of inflammability ϕ_1 and ϕ_2 and the computation of burnt masses proceeds in the lean and rich regions of burning as follows:

i) Lean region ($\phi_v < 1$)

The mass of vapour burned in the fuel lean sector is

$$dm_{vb_j} = m_{v_j} \quad (E.6)$$

and the corresponding mass of air consumption for burning will be

$$dm_{ac_j} = dm_{vb_j} / s \quad (E.7)$$

Where s is the stoichiometric fuel-air ratio.

The available air dm_{a_j} is greater than dm_{ac_j} , then the liquid fuel mass in droplets of a particular sector are assumed to evaporate and burn instantaneously. The equivalence ratio ϕ_v is modified to a new value $\phi_{v_{new}}$ and the total fuel mass burnt in each lean sector is modified as

$$dm_{vb_j} = m_{v_j} + m_{l_{v_j}} \quad (E.8)$$

where

$$m_{\gamma v_j} = \begin{cases} m_{\gamma j} & ; \phi_{v_{new}} < 1 \\ (s m_{a_j} - m_{v_j}) & ; \phi_{v_{new}} > 1 \end{cases} \quad (E.9)$$

ii) Rich region ($\phi_v > 1$)

The mass of vapour burned in the fuel rich sector is

$$dm_{vb_j} = m_{a_j} \cdot s \quad (E.10)$$

and the corresponding mass of air consumed equals the total air available in the sector at that instant. Hence, in fuel rich burning regions some mass of fuel will be left unburned which is included in the next instant.

Since both lean and rich regions assume a stoichiometric combustion, the mass of combustion products will simply be:

$$dm_{cp_j} = dm_{vb_j} + dm_{ac_j} \quad (E.11)$$

Reference to Figure 2.17 will verify the mass elements in each sector.

After computing these masses in each sector, the total change in respective masses for the whole jet will be summed up as:

$$dm_{vap_b} = \sum_j dm_{vb_j} \quad (E.12)$$

$$dm_{air_c} = \sum_j dm_{ac_j} \quad (E.13)$$

$$dm_{comb_p} = \sum_j dm_{cp_j} \quad (E.14)$$

$$dm_{vap} = \sum_j dm_{v_j} \quad (E.15)$$

also
$$dm_{liq} = (dm_{liq_{inj}} - dm_{vap}) \quad (E.16)$$

and
$$dm_{air_{left}} = (dm_{air} - dm_{air_c}) \quad (E.17)$$

If there is any droplet mass left unevaporated; in any sector, then it is redistributed according to the redistribution procedure.

For the next instant the total integrated value of these mass elements in the whole jet is made available as:

$$(m_{liq})_{i+1} = (m_{liq})_i + dm_{liq} \quad (E.18)$$

$$(m_{air})_{i+1} = (m_{air})_i + dm_{air} \quad (E.19)$$

$$(m_{vap})_{i+1} = (m_{vap})_i + dm_{vap} \quad (E.20)$$

$$(m_{vapb})_{i+1} = (m_{vapb})_i + dm_{vapb} \quad (E.21)$$

$$(m_{air_c})_{i+1} = (m_{air_c})_i + dm_{air_c} \quad (E.22)$$

$$(m_{air,sr})_{i+1} = (m_{air,sr})_i + dm_{air,sr} \quad (E.23)$$

Energy Balance

Following the first law of thermodynamics the overall energy conservation equations for jet and surrounding fluids are written as

i) *Jet Fluids:*

$$[m_{air} C_{v_{air}} + m_{combp} C_{v_{combp}} + m_{vap} C_{v_{vap}} + m_{liq} C_{p_{liq}}]$$

$$dT_{jet} + pdV_{jet} = (u_{liq_0} - u_{vap}) dm_{vap} + (h_{air,sr} -$$

$$u_{air,jet}) dm_{air} + (u_{liq_0} - u_{liq_{jet}}) dm_{liq} + dQ_{rel} +$$

$$dQ_{tr_{jet}} \quad (E.24)$$

ii) *Surroundings:*

$$m_{air,sr} C_{v_{air}} dT - pdV_{jet} = (h_{air,sr} - u_{air,sr}) dm_{air,sr} - pdv_p +$$

$$dQ_{tr_{sr}} \quad (E.25)$$

Alongside these two energy conservation equations, the equations of state are written as

i) *Jet Fluids:*

$$(R_{combp} m_{combp} + R_{air} m_{air} + R_{vap} m_{vap}) dT_{jet} - pdV_{jet} -$$

$$V_{jet} dp = -(R_{air} dm_{air} + R_{vap} dm_{vap} + R_{combp} dm_{combp}) T_{jet} \quad (E.26)$$

ii) *Surroundings*:

$$\frac{dm_{\text{air,sr}}}{m_{\text{air,sr}}} + \frac{dT}{T} = \frac{dv_{\text{sr}}}{V} + \frac{dp}{p} \quad (\text{E.27})$$

where

$$dv_{\text{sr}} = dV_{\text{p}} - dV_{\text{jet}} \quad (\text{E.28})$$

dV_{p} is the change in cylinder volume due to piston motion, and u and h represent internal energy and enthalpy terms respectively with usual meaning of subscripts.

The procedure for calculating the thermodynamic properties is explained in Appendix C.

The following assumptions are made:

- i) the surroundings constitute air alone.
 - ii) the thermodynamic properties of the combustion products are the same as that of air.
 - iii) the temperature of the liquid fuel at the nozzle is equal to the inlet air temperature.
 - iv) the cylinder pressure is uniform throughout.
 - v) the instantaneous cylinder volume equals the sum of the surrounding and jet volumes, i.e.
- $$V = V_{\text{sr}} + V_{\text{jet}}$$
- vi) the initial jet temperature is equal to the temperature of liquid fuel.

Equations (E.24) to (E.27) contain four variables concerning changes in jet and surrounding conditions in the cylinder. These four variables are jet temperature and volume, and cylinder pressure and temperature represented by T_{jet} , V_{jet} , p and T respectively. The energy matrix formed from these equations is given in Figure E.1. This matrix is solved using Crout's factorization method applied to matrix equations of the type:

$$[A] [X] = [B].$$

$m_{air}C_{v,air} + m_{vap}C_{v,vap}$	p	0	0	dT_j	$(u_{liq} - u_{vap}) dm_{vap} + (h_{air, sr} - u_{air, jet})$
$+ m_{combp} + m_{liq} C_{p,liq}$					$\times dm_{air} + (u_{liq, 0} - u_{liq, jet}) dm_{liq}$
$R_{air} m_{air} + R_{vap} m_{vap}$	$-p$	$-V_{jet}$	0	dV_j	$- (R_{air} dm_{air} + R_{vap} dm_{vap} + R_{combp} dm_{combp})$
0	$-p$	0	$m_{air, sr} C_{v, air}$	dP	$= T_{jet}$
0	$\frac{1}{V}$	$\frac{1}{-p}$	$\frac{1}{T}$	dT	$(h_{air} - u_{air})_{sr} dm_{air, sr} - pdV_p +$
					$\frac{dQ_{tr, sr}}{V} - \frac{dm_{air, sr}}{m_{air, sr}}$

FIGURE E.1 Elements of Energy Matrix

APPENDIX F
ENGINE SPECIFICATIONS

Engine I

Engine type:	Single cylinder direct injection (quiescent) diesel engine
Bore:	0.140 m
Stroke:	0.1524 m
Connecting rod length:	0.3048 m
Compression ratio:	14.3:1
Speed:	1300 rev/min
Inlet valve closure:	133° btdc
Exhaust valve opening:	109° atdc

Injector specifications:

Number of holes:	8
Orifice diameter:	0.2032 mm

Engine II

Engine type:	Direct injection swirl type diesel engine
Bore:	0.120 m
Stroke:	0.120 m
Connecting rod length:	0.25 m
Compression ratio:	18.25:1
Speed:	1100-2400 rev/min
Inlet valve closure:	137 btdc
Exhaust valve opening:	126 atdc

Injector specifications:

Number of holes:	4
Orifice diameter:	0.34 mm

